ACTA GEOGRAPHICA SLOVENICA

GEOGRAFSKI ZBORNIK



2026
66
1

ACTA GEOGRAPHICA SLOVENICA

GEOGRAFSKI ZBORNIK

66-1

2026

ZNANSTVENORAZISKOVALNI CENTER
SLOVENSKE AKADEMIJE ZNANOSTI IN UMETNOSTI
GEOGRAFSKI INŠTITUT ANTONA MELIKA
•
RESEARCH CENTRE OF
THE SLOVENIAN ACADEMY OF SCIENCES AND ARTS
ANTON MELIK GEOGRAPHICAL INSTITUTE

ACTA GEOGRAPHICA SLOVENICA

GEOGRAFSKI ZBORNIK

66-1

2026

Založba ZRC

LJUBLJANA
2026

ACTA GEOGRAPHICA SLOVENICA

66-1
2026

ISSN: 1581-6613 (*Print edition/tiskana izdaja*)
ISSN: 1581-8314 (*Online edition/spletna izdaja*)
UDC: 91
2026, ZRC SAZU, Geografski inštitut Antona Melika

International editorial board/mednarodni uredniški odbor: Zoltán Bátori (Hungary), David Bole (Slovenia), Marco Bontje (the Netherlands), Mateja Breg Valjavec (Slovenia), Michael Bründl (Switzerland), Rok Ciglič (Slovenia), Špela Čonč (Slovenia), Lóránt Dénes Dávid (Hungary), Mateja Ferk (Slovenia), Matej Gabrovec (Slovenia), Matjaž Geršič (Slovenia), Maruša Goluža (Slovenia), Mauro Hrvatin (Slovenia), Ioan Ianos (Romania), Peter Jordan (Austria), Drago Kladnik (Slovenia), Blaž Komac (Slovenia), Jani Kozina (Slovenia), Matej Lipar (Slovenia), Dénes Lóczy (Hungary), Simon McCarthy (United Kingdom), Slobodan B. Marković (Serbia), Janez Nared (Slovenia), Cecilia Pasquinelli (Italy), Drago Perko (Slovenia), Florentina Popescu (Romania), Garri Raagmaa (Estonia), Ivan Radevski (North Macedonia), Marjan Ravbar (Slovenia), Aleš Smrekar (Slovenia), Vanya Stamenova (Bulgaria), Annett Steinführer (Germany), Mateja Šmid Hribar (Slovenia), Jure Tičar (Slovenia), Jernej Tiran (Slovenia), Radislav Tošić (Bosnia and Herzegovina), Mimi Urbanc (Slovenia), Matija Zorn (Slovenia), Zbigniew Zwolinski (Poland)

Editors-in-Chief/glavna urednika: Rok Ciglič, Blaž Komac (ZRC SAZU, Slovenia)
Executive editor/odgovorni urednik: Drago Perko (ZRC SAZU, Slovenia)

Chief editors/področni urednik (ZRC SAZU, Slovenia):
- *physical geography/fizična geografija:* Mateja Ferk, Matej Lipar, Matija Zorn
- *human geography/humana geografija:* Jani Kozina, Mateja Šmid Hribar, Mimi Urbanc
- *regional geography/regionalna geografija:* Matej Gabrovec, Matjaž Geršič, Mauro Hrvatin
- *regional planning/regionalno planiranje:* David Bole, Maruša Goluža, Janez Nared
- *environmental protection/varstvo okolja:* Mateja Breg Valjavec, Aleš Smrekar, Jernej Tiran

Editorial assistants/uredniška pomočnika: Špela Čonč, Jernej Tiran (ZRC SAZU, Slovenia)
Journal editorial system manager/upravnik uredniškega sistema revije: Jure Tičar (ZRC SAZU, Slovenia)

Issued by/izdajatelj: Geografski inštitut Antona Melika ZRC SAZU
Published by/založnik: Založba ZRC
Co-published by/sozaložnik: Slovenska akademija znanosti in umetnosti

Address/naslov: Geografski inštitut Antona Melika ZRC SAZU, Gosposka ulica 13, p. p. 306, SI – 1000 Ljubljana, Slovenija; ags@zrc-sazu.si

The articles are available on-line/prispevki so dostopni na medmrežju: http://ags.zrc-sazu.si
This work is licensed under the/delo je dostopno pod pogoji: Creative Commons CC BY-SA 4.0

Ordering/naročanje: Založba ZRC, Novi trg 2, p. p. 306, SI – 1001 Ljubljana, Slovenija; zalozba@zrc-sazu.si

Annual subscription/letna naročnina: 20 €
Single issue/cena posamezne številke: 12 €

Cartography/kartografija: Geografski inštitut Antona Melika ZRC SAZU
Translations/prevodi: DEKS, d. o. o., Živa Malovrh
DTP/prelom: SYNCOMP, d. o. o.
Printed by/tiskarna: CICERO, Begunje, d. o. o.
Print run/naklada: 250 copies/izvodov

The journal is subsidized by the Slovenian Research and Innovation Agency (B6-7614) and is issued in the framework of the Geography of Slovenia core research programme (P6-0101)/Revija izhaja s podporo Javne agencije za znanstvenoraziskovalno in inovacijsko dejavnost Republike Slovenije (B6-7614) in nastaja v okviru raziskovalnega programa Geografija Slovenije (P6-0101).

The journal is indexed also in/revija je vključena tudi v: Clarivate Web of Science (SCIE – Science Citation Index Expanded; JCR – Journal Citation Report/Science Edition), Scopus, ERIH PLUS, GEOBASE Journals, Current geographical publications, EBSCOhost, Georef, FRANCIS, SJR (SCImago Journal & Country Rank), OCLC WorldCat, Google Scholar, CrossRef, and DOAJ.

Design by/Oblikovanje: Matjaž Vipotnik

Front cover photography: Sečovlje Salt Pans at the Slovenian coast (photograph: SeanPavonePhoto, stock.adobe.com).
Fotografija na naslovnici: Sečoveljske soline na slovenski obali (fotografija: SeanPavonePhoto, stock.adobe.com).

ACTA GEOGRAPHICA SLOVENICA

ISSN: 1581-6613
UDC: 91
Number: 66-1
Year: 2026

Contents

Hasan BASRI, Tuti MUTIA, Abdul RASYAD, Ahmad TOHRI, Hanapi HANAPI, Muhamad ALI
The impacts of tourism on shifting mountain climbing ritual tradition in geopark Rinjani, Indonesia 7

Rok TURNIŠKI, Helena GRČMAN
Soils of the Dinaric karst in Slovenia: properties, pedogenesis and land use 21

Klemen COF, Uroš STEPIŠNIK, Manja ŽEBRE, Matej LIPAR
Hierarchical cluster classification and analysis of cirques in Slovenian Alps 39

Danijel DAVIDOVIĆ, Jure ČUŠ, Danijel IVAJNŠIČ
Land-use dynamics and grassland succession challenges in the Natura 2000 site Kras: The socioeconomic perspective 61

Zoltán BÁTORI, Kata FREI, Gábor LI, Orsolya VALKÓ, András VOJTKÓ, Csaba TÖLGYESI, Tünde FARKAS, Alida Anna HÁBENCZYUS, Ágnes TÓTH, László ERDŐS, Zsófia KRIVÁCS, Balázs DEÁK
Karstic microrefugia reflect diverse biogeographic affinities of vascular plant species 81

Boudjemline FOUZIA
Mapping and assessing forest fire severity using remote sensing indices: A case study of Tizi Ouzou, Algeria 99

Peter FRANTAR, Frank HERRMANN, Mišo ANDJELOV
National-scale water balance in Slovenia (1972–2024): Long-term trends and variability in water balance components 121

Juš GAŠPARIČ, Ana POTOČNIK BUHVALD, Dušan PETROVIČ
Satellite-based analysis of light pollution in Slovenia for the period 2013–2022 147

Entin HIDAYAH, Mokhammad Farid MARUF, Siti Norafida JUSOH, Joko WIDODO, Afif AMILUDDIN
Machine learning-based landslide susceptibility assessment for shallow landslide mitigation in the Gumitir Mountain Area, Indonesia 179

Acta geographica Slovenica, 66-1, 2026, 7–20

THE IMPACTS OF TOURISM ON SHIFTING MOUNTAIN CLIMBING RITUAL TRADITION IN GEOPARK RINJANI, INDONESIA

Hasan Basri, Tuti Mutia, Abdul Rasyad, Ahmad Tohri, Hanapi Hanapi, Muhamad Ali



MUHAMAD ALI

Mt. Rinjani, Lombok Indonesia.

DOI: https://doi.org/10.3986/AGS.13976
UDC: 338.48:796.52(594)
796.52:39(594)
Creative Commons CC BY-SA 4.0

Hasan Basri[1], Tuti Mutia[2], Abdul Rasyad[1], Ahmad Tohri[1], Hanapi Hanapi[1], Muhamad Ali[1]

The impacts of tourism on shifting mountain climbing ritual tradition in geopark Rinjani, Indonesia

ABSTRACT: This article aims to explore the tourism influence on the transformation of mountain climbing rituals. This study is a phenomenography centered on a mountain climbing ritual procession conducted by a guide named *Mangku*. Twenty participants, including *Mangku*, community leaders, mountain climbing guides, and local community, were interviewed, and their results were corroborated through the research of documentary materials and pertinent literature. Thematic data from Braun & Clark Framework were utilized to ascertain the tourism influence on spiritual value shifts, mountain climbing, and community engagement. It indicates that tourism diminishes the spiritual significance of indigenous mountain climbing rituals and reduces the societal role of the *Mangku*. The study advocates rules for preserving traditions, cultural education to uphold spiritual values, and sustainable environmental conservation.

KEYWORDS: Tourism, mountain climbing, ritual, tradition, Mount Rinjani, Indonesia

Vpliv turizma na spreminjanje ritualne tradicije plezanja v geoparku Rinjani na Indoneziji

POVZETEK: Namen članka je raziskati vpliv turizma na preoblikovanje ritualov plezanja v gorah. Študija je fenomenografija, osredotočena na ritualno procesijo plezanja po gorah, ki jo vodi vodnik *Mangku*. Intervjuirali smo dvajset udeležencev, med njimi *Mangkuja*, voditelje skupnosti, gorske vodnike in lokalno skupnost, rezultate pa potrdili z raziskavo dokumentarnega gradiva in literature. Tematski podatki iz okvira Braun & Clark so bili uporabljeni za ugotavljanje vpliva turizma na spremembe duhovnih vrednot, gorsko plezanje in vključevanje skupnosti. Kažejo, da turizem zmanjšuje duhovni pomen avtohtonih ritualov gorskega plezanja in zmanjšuje družbeno vlogo *Mangkuja*. Študija zagovarja pravila za ohranjanje tradicij, kulturno izobraževanje za ohranjanje duhovnih vrednot ter trajnostno varstvo okolja

KLJUČNE BESEDE: Turizem, plezanje, ritual, tradicija, gora Rinjani, Indonezija

The article was submitted for publication on November 7th, 2024.
Uredništvo je prejelo prispevek 7. novembra 2024.

[1] Universitas Hamzanwadi, Selong, Indonesia
hasanbasri@hamzanwadi.ac.id (https://orcid.org/0000-0002-2402-2795), abdulrasyad@hamzanwadi.ac.id (https://orcid.org/0000-0002-9552-1567), tohri@hamzanwadi.ac.id (https://orcid.org/0000-0003-4649-9719), hanapi@hamzanwadi.ac.id (https://orcid.org/0009-0004-2520-2482), muhamadali@hamzanwadi.ac.id (https://orcid.org/0000-0002-1158-2507)

[2] Universitas Negeri Malang, Malang, Indonesia
tuti.mutia.fis@um.ac.id (https://orcid.org/0000-0001-6589-914X)

1 Introduction

Mount Rinjani (hereafter Mt. Rinjani) had been a center of spirituality for the local community before the global tourism campaign. Mountains are regarded as sacred macrocosms symbolizing the balance between the physical, spiritual, and metaphysical dimensions that establish connections with individuals (Nuraini et al. 2023) as a microcosm. Traditional beliefs and rituals are significant in sustaining a harmonious relationship among humans, nature, and supernatural forces (Ween and Abram 2012; Høyem 2020). Processions and rituals on Mt. Rinjani are conducted by spiritual leaders commonly referred to as *Mangku* within the local community. *Mangku* holds significant responsibility in preserving traditions and customs transmitted across generations. In recent decades, the tourism industry has significantly impacted the region (Alamineh et al. 2023; Wu et al. 2023), particularly concerning the sustainability of local rituals and traditions, including mountain climbing activities. There is an initial ritual in mountain climbing ritual tradition in the form of reading the prayer for salvation and obeying customary rules known as *awik-awik*, which reflects local norms to preserve nature and social-spiritual harmony. This ritual is an essential part of mountain climbing activities to protect the mountain climbers from any form of danger while climbing. This practice is also witnessed before climbing the Himalaya peaks in Nepal (Nepal Traveller 2024) as well as other mountainous regions worldwide.

Mt. Rinjani is located on the island of Lombok, West Nusa Tenggara, Indonesia. Mt. Rinjani is situated between 80 18'18" and 80 32'19"S and 1160 21'30" and 1660 34'15" E (Siolemba Patiro et al. 2024). It is the second-highest active volcano with an altitude of 3,726 meters above sea level (Muntasib et al. 2019), making it the second-highest mountain in Indonesia after Mt. Kerinci in Sumatra. This mountain is part of the Rinjani-Lombok Geopark, which UNESCO recognizes as a geologically, ecologically, and culturally important area for sustainable development (Lee and Jayakumar 2021). This Geopark protects biodiversity and geology while supporting the local community's economy through sustainable tourism.

The accessibility of hiking due to high rainfall is influenced by the rainy season for safety reasons. In the dry season, the main popular hiking trails are through Sembalun and Senaru, which offer panoramic views and challenges for mountain climbers. The vegetation around Mt. Rinjani is very diverse and includes tropical rainforests, grasslands, and evergreen forests that dominate at certain altitudes. On the lower slopes, various tropical flora, such as orchids, palms, and typical mountain plants, grow. At higher altitudes, vegetation changes to plant species that are more resistant to cold temperatures and extreme conditions.

Mt. Rinjani is one of Indonesia's most in-demand mountain climbing destinations, attracting thousands of domestic and foreign tourists annually. This mountain climbing activity not only aims to enjoy Lake Segara Anak's natural beauty and panorama but also involves religious rituals for the local community, such as the traditional ceremony of Mulang Pakelem. This natural and cultural potential makes Mt. Rinjani a tourist destination and an essential place in environmental conservation and local culture.

As an increasingly popular tourist destination, Mt. Rinjani has undergone radical changes due to tourist visits, both domestic and international. Modernization that follows the flow of tourism contributes to economic progress (Paramati et al. 2017; Garau-Vadell et al. 2018; Li et al. 2018; Comerio and Strozzi 2019), creating jobs (Nair et al. 2015; Kantar and Svržnjak 2017) as well as increasing the income of local communities (Zhang and Gao 2016; Groizard and Santana-Gallego 2018; Pan et al. 2018). However, this modernization challenges the spiritual tradition that has long been an integral part of the Mt. Rinjani region. The increase in tourism that prioritizes physical, recreational, and commercial aspects, such as mountain climbing (Westskog et al. 2021) raises concerns about the loss of spiritual meaning in existing rituals. Rituals, such as *Ngasuh Gunung* (prayer offerings and embedding of local symbols commonly known as *Sembeq* for safety) and protecting mountain climbers from danger, as well as the *Jambeq Gunung* ritual practiced by traditional leaders to ask for blessings and maintain natural harmony, which were previously seen as sacred acts, are now beginning to be marginalized by the needs of the tourism industry, which prioritizes tourists' comfort and satisfaction.

Mangku's role as a ritual leader in mountain climbing encounters increasing pressure in this context. *Mangku* is responsible for leading ritual processions, such as special offerings and prayers; they maintain a spiritual relationship between the community and Mt. Rinjani, which many believe to be a sacred place (Crimmel 2003). These rituals, which usually involve offerings to ancestral spirits, are performed to pray for the safety and well-being of the mountain climbers and maintain the balance of nature. This tradition has been an important part of the spiritual life of the Sasak people (an ethnic group that lives on the island

of Lombok, where Mt. Rinjani is located) for centuries. The role of *Mangku* is very central to guiding activity, for example, providing an understanding of geographical and weather conditions that are indispensable in mountain climbing safety (Różycki and Dryglas 2014). However, with the development of the tourism industry, these rituals are increasingly losing their relevance for most mountain climbers, especially tourists from outside the region.

Today's main problem is the shift in spiritual values and mountain climbing rituals on Mt. Rinjani. The tourism industry places more emphasis on the physical and aesthetic aspects of mountain climbing (Westskog et al. 2021) without understanding the spiritual dimension contained in each traditional procession. Tourists, who are mostly interested in natural beauty and physical adventure, tend to ignore the rituals led by *Mangku*, even seeing them as part of a purely tourist attraction. This has led to the degradation of traditional values that should be maintained as an integral part of the cultural identity of the local community.

The change in views among the younger generation of the Sasak people further weakens the challenges *Mangku* faces in maintaining its spiritual role. The younger generation, who are more open to the influence of modernization and globalization (McKenzie 2019; Lin and Long 2020), is beginning to experience a shift in orientation from traditional spiritual values to more pragmatic economic values, which trigger social and cultural change as well (Stevens 1991). Traditional spiritual values emphasize the sacredness of nature through rituals and customary rules. Mountain climbing activity is a spiritual practice loaded with ecological awareness and cultural ethics. In the past, before climbing, mountain climbers always performed a prayer ritual at the entrance of the climb as a form of asking permission from the spirit of the mountain guard. They only brought enough refreshment, did not take anything from the forest, and maintained their attitude and speech during the journey, believing that the mountain was sacred. This practice reflects a high spiritual awareness of nature and is part of cultural ethics to maintain ecological balance. The correlation is robust because these values foster responsible behavior, preserve the environment, and make the mountain a sacred space.

On the other hand, the pragmatic economic value in modern climbing focuses more on exploiting mountains as a tourist commodity, where the main goal is financial gain through an increase in the number of tourists, guide services, entrance tickets, and other commercial activities. This orientation change often ignores sacred values; for example, mountain climbers violate customary prohibitions, litter, or climb without following the salvation prayer procession. Ritual processions that used to be carried out with great respect are now starting to be seen as something ancient in the context of the development of the times. As a result, *Mangku*'s role as the guardian of the community's spirituality began to be marginalized, and rituals that were once considered sacred were increasingly rarely carried out solemnly. In fact, rituals are an inseparable part of the culture (Richards 2018).

Research on the impact of tourism on the spiritual tradition of mountain climbing is still very limited (Shi et al. 2022), although attention to the influence of the tourism industry on the environment and economic impacts is increasing (Boyns and Luery 2015; Du et al. 2016; Azam et al. 2018; Comerio and Strozzi 2019; Nagaj and Žuromskaitė 2021). Studies of how tourism activities affect ritual practices and the sustainability of local traditions, especially those led by *Mangku*, are still understudied. This creates a knowledge gap that needs to be addressed immediately, given the importance of preserving spiritual traditions as part of an invaluable cultural heritage (Berkes et al. 2000). To address this gap, Interaction Ritual Theory (IRT) was in use introduced by sociologist Erving Goffman (1967). This theory focuses on the dynamics of social interaction (Wu et al. 2023) and how small rituals can shape individual identity and group cohesion. In this theory, social interaction is seen as a series of units that have certain components, such as shared presence, shared attention, and emotional resonance, that lead to group solidarity (Bargeman and Richards 2020; Johannessen and Collins 2024). This theory emphasizes that through interaction rituals, individuals can feel strong social bonds, reinforce social norms, and create deeper meaning in collective life.

This study, furthermore, seeks to examine the impact of tourism on the sustainability of local rituals and traditions on Mt. Rinjani. This research aims to significantly address the knowledge gap concerning the interplay between spiritual traditions and tourism while also offering practical recommendations for local communities and tourism stakeholders to preserve the sustainability of culturally significant traditions and rituals. In conclusion, the research question proposed was: How does tourism impact the mountain climbing ritual tradition (Sasak people) of Mt. Rinjani Geopark?

2 Literature review

Johannessen and Collins (2024) explain that IRT is a micro-sociological mechanism that explains how intense face-to-face interactions, which involve physical presence, shared attention, and synchronized emotion, can result in group solidarity, sacred symbols, moral standards, and emotional energy. IRT is the key to understanding social harmony as well as the dynamics of conflict, domination, and social transformation through »conflict rituals« that are also driven by collective emotional energy. In the context of mountain climbing involving local rituals and traditions, IRT offers a relevant framework of understanding to explain how interactions between tourists and local communities can shape unique and immersive experiences of mountain climbing.

The relevance of IRT in responding to the tourism phenomenon and its impact on local rituals and traditions can be seen in how tourism affects cultural sustainability. Through ritual interactions, traditional values can be conveyed and revived, but this also poses challenges, such as cultural commodification that may change the original meaning of the ritual (Cochrane 2009). If these rituals are repackaged or modified to meet tourists' expectations, they risk losing their spiritual essence and original meaning. The following is the research framework, as presented in Figure 1.

This theory contributes to filling a gap in tourism studies that have so far highlighted more the risk and physical aspects of climbing activities (Slentz and Chase 2003; Windsor et al. 2009; Lockwood and Sparks 2013; Gatterer et al. 2019). In this context, IRT is highly urgent because it is able to explain how ritual interaction in social infiltration not only strengthens local cultural values but also becomes a means of forming sustainable solidarity (Hausmann et al. 2011) between tourists and communities, thus making this theory a robust conceptual foundation in this paper.

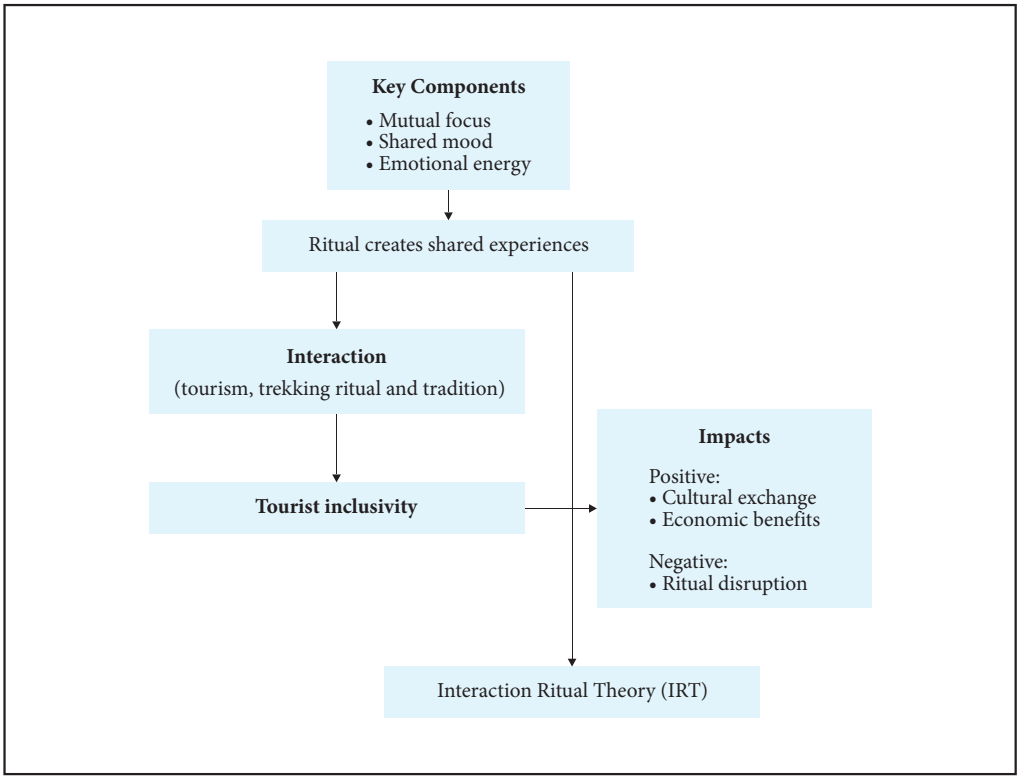


Figure 1: Research framework elaborated by authors.

3 Research methodology

3.1 Research design

This study uses a phenomenography approach to describe the phenomenon and current reality of mountain climbing rituals in Mt. Rinjani. Phenomenography is a research approach that has not been widely used in the field of tourism (Novais et al. 2018) although this approach has developed into various fields such as education (Marton 1981) and marketing (Lin and Niu 2011). According to Marton (1981), phenomenography is understood as a qualitative approach that tries to explore individual experiences in a content-oriented and relational way. Furthermore, Novais et al. (2018) explain that phenomenography focuses on the conception of certain aspects of reality that are generally recognized from empirical research, collective meaning rather than single meaning, and looking at phenomena from a second-order perspective of how phenomena are understood. The phenomenography is different from phenomenology, which focuses on decomposing meaning from the side of individual meaning (Barnard et al. 1999).

This approach was carefully selected as the focus of the study was to explore a deep understanding of the impact of tourism activities on the sustainability of local rituals and traditions. The phenomenography approach is particularly suitable in this context as it provides the flexibility to explore social, cultural, and spiritual aspects holistically through the perspectives of key actors, such as *Mangku*, local communities, indigenous leaders, and tour guides, to see how they understand and experience reality (Sandberg 2000). The approach was chosen because Mt. Rinjani is a unique site rich in spiritual traditions. To underpin this approach, IRT was applied to comprehensively explain the phenomena explored concerning the mountain ritual tradition in Geopark Rinjani, Indonesia. IRT also works to reveal how interaction rituals address the research aim explaining social norms, and the ritual sustainability from the perspective of traditions in the region of Mt. Rinjani, Lombok, Indonesia.

3.2 Sampling and data analysis

The data was collected from two main sources: primary and secondary data. Primary data were obtained through in-depth interviews and analysis of documentary materials related to the mountain climbing ritual procession. In-depth interviews were conducted with *Mangku*, other community leaders, the mountain climbing guide community, and representatives of the local community who were directly involved in the mountain climbing ritual on Mt. Rinjani. A number of questions were formulated to answer the two research questions listed in the following Table 1.

Table 1: Blueprint of interview.

	Questions
A.	Tourism impact on the mountain climbing ritual tradition in Mt. Rinjani
1.	What kinds of rituals are usually performed before or during the climb of Mt. Rinjani?
2.	How do tourists, both domestic and international, engage with this ritual tradition?
3.	Have you observed any changes in the way these rituals are performed since the growth of tourism in this area?
4.	In your opinion, are the spiritual values behind the rituals still understood and respected by mountain climbers today?
5.	How do local communities perceive the changes in ritual practices due to the presence of tourists?
6.	Are there any parts of the ritual that have been abandoned or replaced due to the influence of the tourism industry?
B.	Strategy proposed to preserve the mountain climbing ritual tradition of Mt. Rinjani
7.	What efforts have been made by traditional communities or spiritual figures such as *Mangku* to maintain the rituals?
8.	Are there any customary regulations (*awik-awik*) in place to govern how tourists interact with local traditions?
9.	What role does the government or tourism authorities play in supporting the preservation of mountain climbing rituals tradition?
10.	Are there any educational programs or awareness campaigns for tourists regarding the cultural and spiritual values of the area?
11.	In your opinion, what are the most effective strategies to ensure that ritual traditions are not lost as tourism continues to grow?
12.	Is there any collaboration between local communities, customary leaders, and tourism stakeholders to preserve the cultural values around Mt. Rinjani?

The judgment sampling technique was used to select participants who had deep knowledge and involvement in the spiritual traditions of the region. This technique was chosen because only individuals with specific insights into rituals and traditions can provide rich and relevant information for the purposes of this research.

The research participants comprised 20 participants, including three *Mangku*, four community leaders, and 13 others from the local community and mountain climbing guides (Table 2). Participants were selected based on their involvement in the ritual procession and their knowledge of the influence of tourism modernization on local traditions. Each participant was interviewed face-to-face in the area around Mt. Rinjani for 45 to 90 minutes. In addition to interviews, related documents were analysed and interpreted to strengthen the findings of how the mountain climbing ritual procession on Mt. Rinjani was carried out.

Secondary data were obtained from relevant literature, including previous studies related issued raised in the example of European mountains (Vidal-González and Sánchez 2019; Nowacki 2023) in other mountainous regions of Indonesia and other European regions, as well as tourism policy documents related to preserving culture and tradition in Mt. Rinjani. The collected data was analysed using thematic analysis proposed by (Braun and Clarke 2006). The first step was transcribing the interview results and interpreting the documentary materials, such as photos. Furthermore, the codes are grouped into several initial themes that are relevant to the two main research question, that is how does tourism impact the sustainability of the mountain climbing ritual tradition on Mt. Rinjani?

To answer the research question, themes such as the erosion of the sacred value of rituals (shifting spiritual values), the commercialization of mountain climbing, and the change in the role of *Mangku* were successfully identified. These themes were then reviewed to ensure they are coherent, clearly defined, and critically linked to relevant literature. These themes were categorized and compared with findings from the relevant literature. The validity of the data is ensured through a triangulation procedure, comparing them to each other to verify the consistency and relevance of the research results. Once the main themes have been identified and analysed, the researcher makes conclusions based on the patterns that appear in the data and relates them to the main research questions and the existing literature.

Table 2: Profile of participants (n=20).

Status	Sex	Number	Code
Mangku	Male	1	Mk1
Mangku	Male	1	Mk2
Mangku	Male	1	Mk3
Mountain climbing guide	Male	1	MCG1
Mountain climbing guide	Male	1	MCG2
Mountain climbing guide	Male	1	MCG3
Mountain climbing guide	Male	1	MCG4
Mountain climbing guide	Male	1	MCG5
Community leader	Male	1	CL1
Community leader	Male	1	CL2
Community leader	Male	1	CL3
Community leader	Male	1	CL4
Host-society	Female	1	HS1
Host-society	Male	1	HS2
Host-society	Female	1	HS3
Host-society	Male	1	HS4
Host-society	Female	1	HS5
Host-society	Male	1	HS6
Host-society	Female	1	HS7
Host-society	Male	1	HS8

4 Results

The rapid development of modern tourism has significantly impacted various aspects of local people's lives, including the continuity of their rituals and traditions. As one of Indonesia's most popular tourist destinations, Mt. Rinjani attracts thousands of tourists every year who are interested in its natural beauty and the physical challenges of its mountain climbing. Statistical data provided by Rinjani National Park (Figure 2) shows that the total number of tourist visits in 2024 was 80,109 people, while in 2025 the number decreased to 57,131 people due to nine-month visit record only. The highest visit in 2024 occurred in May with a total of 11,776 people, while in 2025 the peak visit was recorded in June with 11,759 people. In contrast, the lowest number of visits in 2024 occurred in December with 4,268 people, while in 2025 the lowest figure was in September with 6,693 people. When viewed from the monthly average, visits in 2024 will reach around 6,676 people, while in 2025 the monthly average increased to 9,522 people, although the data for 2025 only covered the period until September. These findings show that there were fluctuations in visit patterns influenced by seasonal factors and external dynamics relevant to tourism activities in the Mt. Rinjani region. However, behind the economic increase resulting from the tourism sector, local traditions that have long been part of the cultural identity of the Sasak people around the mountain face various challenges.

The most obvious impact of tourism on local traditions is the shift in ritual meaning and value. On Mt. Rinjani, the ritual led by *Mangku*, a spiritual leader who plays an important role in society, has sacred value. These rituals, such as offerings and prayers to seek protection and safety during the ascent, have been going on for centuries. However, with the increasing flow of tourists who mostly do not have a deep understanding of local traditions, the spiritual meaning of these rituals is further eroded. Tourists see these rituals more often as cultural attractions that can be displayed than as an integral part of the spiritual life

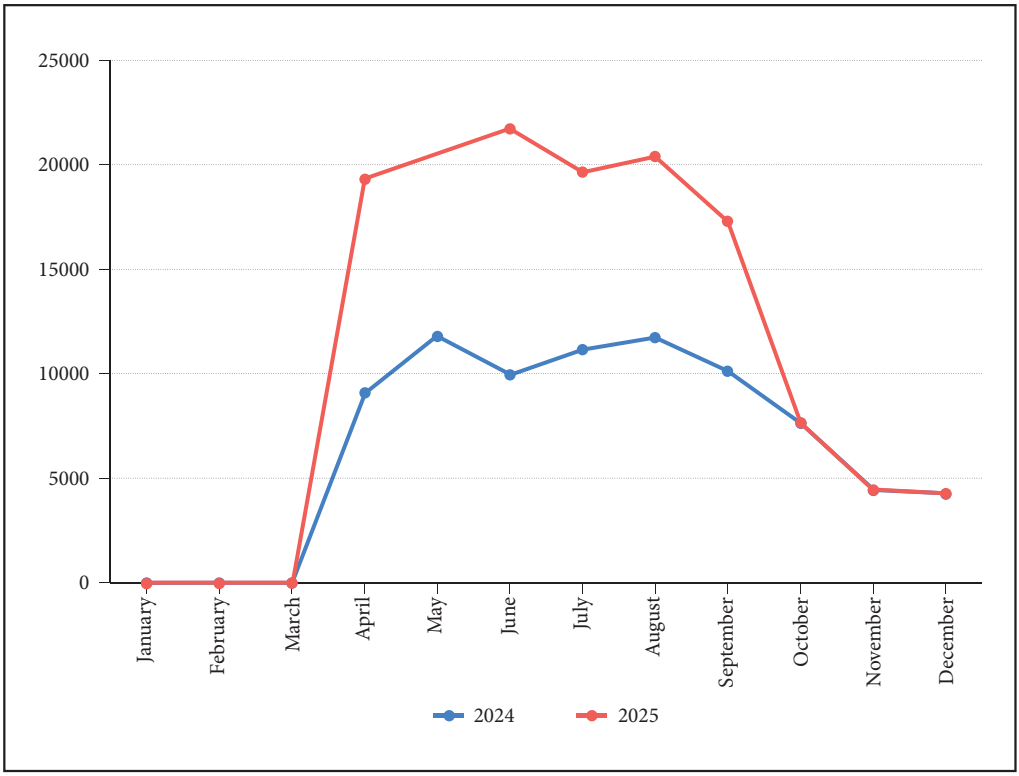


Figure 2: Mountain climbing visit in Rinjani National Park in 2024 and 2025.

of the Sasak people (HS3). As a result, the sacred value inherent in the ritual was degraded, and local communities began to feel that their rituals were no longer valued appropriately.

In addition, the modernization of tourism has also caused a change in the way people view and carry out rituals. The younger generation, who are more exposed to the current of modernization, are starting to abandon old traditions that are considered irrelevant in their lives. Pressure from the tourism sector that emphasizes economic benefits makes local communities prioritize commercial aspects rather than maintaining spiritual traditions. Many are more focused on developing mountain climbing services, accommodation, and other tourist facilities, while traditional rituals are beginning to be marginalized. This resulted in the loss of most of the values of the tradition that were once highly valued (MCG1).

The pressure from modern tourism also impacts *Mangku*'s role as a ritual leader. *Mangku*, who was once highly respected and served as a spiritual guardian, is now beginning to lose its influence in society. As more tourists come to enjoy the physical hike without regard for the spiritual aspect, *Mangku*'s role in leading the ritual becomes increasingly isolated. *Mangku* still leads some traditional processions, but community participation in these processions is diminishing, and the meaning of rituals that were once very important is now beginning to be seen as a mere formality. Tourists not involved in this ritual tend to ignore it, while younger locals are starting to see the role of *Mangku* as less relevant.

On the other hand, modern tourism also challenges environmental sustainability, an important part of traditional rituals on Mt. Rinjani. The rituals have always involved elements of nature conservation, where people believe that maintaining a harmonious relationship with nature is an essential part of their spiritual beliefs. However, increasing the number of tourists who do not always comply with customary rules and mountain climbing ethics causes environmental damage (Mk3). The increase in waste, destruction of vegetation, and the decline in water quality in the Mt. Rinjani area are problems that increasingly threaten the preservation of nature that has been preserved through local traditions. *Mangku* and the local community are experiencing difficulties maintaining this tradition of nature preservation during tourism modernization, which prioritizes economic growth over environmental preservation (Mk1).

Even so, the impact of modern tourism on the continuity of local rituals and traditions on Mt. Rinjani is not entirely devastating. Tourism also provides opportunities to promote and preserve traditions through interaction with tourists who are interested in local culture (CL3). Several tourism programs that aim to promote ecotourism and community-based tourism can play a role in maintaining a balance between tradition and modernization. With the right approach, modern tourism can be a means to introduce the spiritual and cultural values of the Sasak people to the outside world, as well as encourage tourists to appreciate local traditions more.

Overall, the impact of modern tourism on the continuity of local rituals and traditions on Mt. Rinjani is two-way. On the one hand, tourism has led to the degradation of spiritual meaning and shifted the important role of *Mangku* and local communities in preserving traditions. On the other hand, tourism also provides opportunities to protect and promote these traditions through a tourism approach that is more sensitive to local culture. The challenge ahead is how local communities, together with the government and tourism actors, can find a balance between tourism modernization and preserving traditions that have become the spiritual identity of the Sasak people around Mt. Rinjani.

5 Discussion

This study found that tourism activities on Mt. Rinjani significantly impact the sustainability of local trekking rituals and traditions in the Sasak community. On the one hand, the modernization of tourism has shifted the spiritual meaning contained in traditional rituals, especially due to the lack of appreciation from tourists who focus more on physical experience and recreation (Xuemei et al. 2024) than the spiritual meaning of trekking. In addition, the local younger generation is starting to abandon traditions that they consider archaic and less relevant to modern life. However, the study also identifies that preservation strategies such as community-based tourism development, regulations that support the preservation of traditions, and indigenous education for the younger generation can help maintain local traditions amid the modernization of the tourism industry.

Several studies on trekking and some related to local rituals have highlighted this issue closely. Although some studies only limit the study to the evaluation and challenges of trekking (Hillman 2019; Muntasib

et al. 2019), other studies agree with what was found in this study. An interesting thing, for example from the research of (Cochrane 2009) revealed that the impact of tourism on rituals and local traditions, particularly concerning sacred sites like Mt. Bromo, is perceived as mystical recognition. The author notes that tourism can lead to the commercialization of these sites, potentially altering their sacred atmosphere and affecting the authenticity of traditional rituals. Furthermore, the author discusses the potential degradation of rituals or local traditions due to tourism. It is mentioned that tourism at sacred sites, such as Mt. Bromo, brings management challenges and conflicts between different user groups, including worshippers and tourists. The influx of visitors can lead to commercialization and alterations to the environment that disturb the sacred atmosphere of these places. This often raises questions about authenticity and sustainability as the rituals might be modified or commodified to meet the expectations of tourists, which can undermine their original spiritual significance. Sacred site (mountains) is significantly affected by social and environmental change (Nyaupane et al. 2014).

In a non-Asian context, for example, trekking in the Himalayas represents a close connection between rituals, culture, and economy. The climbing path initially functioned as a pilgrimage route to a sacred location, where religious practices and traditional processions were combined with the spiritual experience of the mountain climbers (Nowacki 2023). On the other hand, this activity is a driver of the local economy through the services of guides, porters, accommodation, and the commercialization of expeditions that continue to grow (Pond et al. 2014). The complexity of accessibility including social, economic, and environmental factors also confirms that climbing is not just a physical activity, but part of a layered socio-economic system (Apollo 2017) that the majority of mountain destination managers globally shift from the sacredness of ritual to economic dominance.

Other findings show that tourism is closely related to spiritual values, for example, in rituals (Kim et al. 2013). Rituals play an important role in raising tourism's image through symbols and traditions. Visits to sacred sites and participation in local rituals help connect tourists with a destination's cultural heritage and create an authentic experience. Cooper et al. (2003) explained that performance rituals are the cause of improving the quality of education. There are value and experience from the ritual process that tourists can learn. Ritual performance also encourages customer intention to decide on a purchase. In addition, rituals encourage the preservation of local traditions, maintain the community's cultural identity, and provide economic benefits through sustainable tourism. However, it is important to maintain a balance so that the ritual is not degraded or over-commodified due to tourism pressures and that its spiritual meaning and authenticity are maintained.

Although this study contributes to filling the research gap on the impact of tourism activities on rituals, it has some limitations. The main limitation is that the focus is more on the supply perspective: local communities, especially traditional leaders, *Mangku*, local communities, and local trekking guides. This study has not explored in depth how tourists or outsiders, both in terms of their perception and experience of the rituals and customs on Mt. Rinjani, affect the sustainability of the tradition. It is very important to understand the tourist's perspective further because they are one of the main actors in the tourism industry that can contribute to preserving or eradicating local traditions. Further studies involving tourists can provide more holistic insights into how tourists view and appreciate local traditions and the impact of their interactions on the sustainability of rituals.

Another limitation of this study is that the approach used is qualitative, with interviews limited to several key informants, even though it is complete by digging for information from other sources such as documents and academic literature. Although this method provides a deep understanding of the role of *Mangku* and the dynamics of local traditions, this research may not fully represent the diversity of views and experiences of the Sasak people throughout the Mt. Rinjani region. Research with a larger sample size, using quantitative surveys or a mixture of qualitative and quantitative methods, can provide a more comprehensive picture of how local communities, including the younger generation, view the role of *Mangku* and their traditions during tourism modernization.

This research is also limited to the socio-cultural context without focusing on the environmental dimension. Although there is recognition that the traditions on Mt. Rinjani are closely related to nature conservation, the specific impact of tourism activities on the physical environment and how they affect the implementation of rituals have not been explained in detail in this study. Therefore, future research needs to combine socio-cultural analysis with studies on environmental impacts to provide a more thorough understanding of the sustainability of indigenous rituals on Mt. Rinjani. The study of how environmental damage

can affect local communities' spiritual practices and customs is very relevant, considering that Mt. Rinjani is a conservation area with a vulnerable ecosystem. Thus, while this study provides important insights into how tourism modernization affects local rituals and traditions in Mt. Rinjani, more in-depth studies are needed to explore other untapped dimensions, such as the perspective of tourists, the dynamics of the younger generation, and the interaction between environmental sustainability and ritual implementation. Future research is expected to make a deeper contribution to understanding how tradition and modernization coexist harmoniously in natural and cultural tourist destinations such as Mt. Rinjani.

6 Conclusion

This study seeks to examine the influence of tourism on the sustainability of local rituals and traditions in Mt. Rinjani, and to suggest strategies for preserving these traditions amid modernization. The research findings indicate that tourism activities in the Mt. Rinjani region significantly influence the rituals and beliefs of the local people. A primary influence is the transformation of spiritual values shown in the rituals conducted by *Mangku*, which are progressively marginalized by industrialization. Tourists frequently prioritize the physical and visual dimensions of trekking, neglecting the cultural and spiritual significance inherent to the Sasak people's way of life. Moreover, the economic demands of tourism compel many younger generations to forsake traditional practices in favour of a more pragmatic and profit-driven approach.

Nevertheless, the study indicates that opportunities remain to safeguard local traditions, particularly by incorporating cultural values into sustainable tourist management. Proposed initiatives encompass establishing community-based tourism, indigenous education for youth, and regulations safeguarding the spiritual values of local communities. This heritage may be preserved despite modernization by facilitating the active engagement of local communities, especially indigenous leaders like *Mangku*. Implementing ecotourism and cultural tourism strategies can facilitate the introduction of the spiritual values of the Sasak people to tourists, enabling a deeper appreciation of local traditions and contributing to their preservation.

ACKNOWLEDGEMENT: We thank the Center for Higher Education Funding and Assessment, Ministry of Higher Education, Science, and Technology of Republic of Indonesia for supporting the sponsorship of this project funding (BPI, PPAPT, LPDP).

RESEARCH DATA: For information on the availability of research data related to the study, please visit the article webpage: https://doi.org/10.3986/AGS.13976.

7 References

Alamineh, G. A., Hussein, J. W., Mulu, Y. E., Taddesse, B. 2023: The negative cultural impact of tourism and its implication on sustainable development in Amhara Regional State. *Cogent Arts & Humanities* 10-1. https://doi.org/10.1080/23311983.2023.2224597

Apollo, M. 2017: The true accessibility of mountaineering: The case of the High Himalaya. *Journal of Outdoor Recreation and Tourism* 17. https://doi.org/10.1016/j.jort.2016.12.001

Azam, M., Alam, M. M., Hafeez, M. H. 2018: Effect of tourism on environmental pollution: Further evidence from Malaysia, Singapore and Thailand. *Journal of Cleaner Production* 190. https://doi.org/10.1016/j.jclepro.2018.04.168

Bargeman, B., Richards, G. 2020: A new approach to understanding tourism practices. *Annals of Tourism Research* 84. https://doi.org/10.1016/j.annals.2020.102988

Barnard, A., McCosker, H. Gerber, R. 1999: Phenomenography: A qualitative research approach for exploring understanding in health care. *Qualitative Health Research* 9-2. https://doi.org/10.1177/104973299129121794

Berkes, F., Colding, J., Folke, C. 2000: Rediscovery of traditional ecological knowledge as adaptive management. *Ecological Applications* 10-5. https://doi.org/10.2307/2641280

Boyns, D., Luery, S. 2015: Negative emotional energy: A theory of the »dark-side« of interaction ritual chains. *Social Sciences* 4-1. https://doi.org/10.3390/socsci4010148

Braun, V., Clarke, V. 2006: Using thematic analysis in psychology. *Qualitative Research in Psychology* 3-2. https://doi.org/10.1191/1478088706qp063oa

Cochrane, J. 2009: Spirits, nature and pilgrimage: The »other« dimension in Javanese domestic tourism. *Journal of Management, Spirituality & Religion* 6-2. https://doi.org/10.1080/14766080902815130

Comerio, N., Strozzi, F. 2019: Tourism and its economic impact: A literature review using bibliometric tools. *Tourism Economics* 25-1. https://doi.org/10.1177/1354816618793762

Cooper, R., Groce, J., Thomas, N. D. 2003: Changing direction: Rites of passage programs for African American older men. *Journal of African American Studies* 7-3. https://doi.org/10.1007/s12111-003-1012-7

Crimmel, H. 2003: Trekking in the Seat of the Gods. *Organization & Environment* 16-3. https://doi.org/10.1177/1086026603256282

Du, D., Lew, A. A., Ng, P.T. 2016: Tourism and economic growth. *Journal of Travel Research* 55-4. https://doi.org/10.1177/0047287514563167

Garau-Vadell, J. B., Gutierrez-Taño, D., Diaz-Armas, R. 2018: Economic crisis and residents' perception of the impacts of tourism in mass tourism destinations. *Journal of Destination Marketing & Management* 7. https://doi.org/10.1016/j.jdmm.2016.08.008

Gatterer, H., Niedermeier, M., Pocecco, E., Frühauf, A., Faulhaber, M., Menz, V., Burtscher, J. et al. 2019: Mortality in different mountain sports activities primarily practiced in the summer season – A narrative review. *International Journal of Environmental Research and Public Health* 16-20. https://doi.org/10.3390/ijerph16203920

Goffman, E. 1967: Interaction ritual: Essays in face-to-face behavior. Pantheon Books.

Groizard, J. L., Santana-Gallego, M. 2018: The destruction of cultural heritage and international tourism: The case of the Arab countries. *Journal of Cultural Heritage* 33. https://doi.org/10.1016/j.culher.2018.06.005

Hausmann, C., Jonason, A., Summers-Effler, E. 2011: Interaction ritual theory and structural symbolic interactionism. *Symbolic Interaction* 34-3. https://doi.org/10.1525/si.2011.34.3.319

Hillman, W. 2019: Issues for women trekking in Nepal: '3 sisters adventure trekking' guides. *Journal of Sport & Tourism* 23-1. https://doi.org/10.1080/14775085.2019.1593226

Høyem, J. 2020: Outdoor recreation and environmentally responsible behavior. *Journal of Outdoor Recreation and Tourism* 31. https://doi.org/10.1016/j.jort.2020.100317

Johannessen, L. E. F., Collins, R. 2024. The future of interaction rituals: An interview with Randall Collins. *Theory and Society* 53. https://doi.org/10.1007/s11186-024-09587-y

Kantar, S., Svržnjak, K. 2017: Development of Sustainable Rural Tourism. *DETUROPE - The Central European Journal of Tourism and Regional Development* 9-1. https://doi.org/10.32725/det.2017.003

Kim, J., Kim, B., Park, S. 2013: The effects of tourism ritualization, ritual performance on tourist satisfaction. *Journal of Quality Assurance in Hospitality & Tourism* 14-3. https://doi.org/10.1080/1528008X.2013.802555

Lee, Y., Jayakumar, R. 2021: Economic impact of UNESCO Global Geoparks on local communities: Comparative analysis of three UNESCO Global Geoparks in Asia. *International Journal of Geoheritage and Parks* 9-2. https://doi.org/10.1016/j.ijgeop.2021.02.002

Li, K. X., Jin, M., Shi, W. 2018: Tourism as an important impetus to promoting economic growth: A critical review. *Tourism Management Perspectives* 26. https://doi.org/10.1016/j.tmp.2017.10.002

Lin, F., Long, C. X. 2020: The impact of globalization on youth education: Empirical evidence from China's WTO accession. *Journal of Economic Behavior & Organization* 178. https://doi.org/10.1016/j.jebo.2020.08.024

Lin, H. M., Niu, H. J. 2011: A Phenomenographic Approach for Exploring Learning Marketing Conceptions of Undergraduate Students. *Business and Economic Research* 1-1. https://doi.org/10.5296/ber.v1i1.829

Lockwood, N., Sparks, P. 2013: When is risk relevant? An assessment of the characteristics mountain climbers associate with eight types of climbing. *Journal of Applied Social Psychology* 43-5. https://doi.org/10.1111/jasp.12063

McKenzie, J. 2019: Introduction to the special issue: Globalization as a context for youth development. *New Directions for Child and Adolescent Development* 164. https://doi.org/10.1002/cad.20276

Marton, F. 1981: Phenomenography-describing conceptions of the world around us. *Instructional science* 10-2.

Muntasib, H. E. K. S., Nadhira, F., Meilani, R. 2019: Hazard management in tourism: A case study of the Senaru-Sembalun hiking trail, Mount Rinjani National Park, Indonesia. *Jurnal Manajemen Hutan Tropika* 25-3. https://doi.org/10.7226/jtfm.25.3.199

Nagaj, R., Žuromskaitė, B. 2021: Tourism in the era of Covid-19 and its impact on the environment. *Energies* 14-7. https://doi.org/10.3390/en14072000

Nair, V., Munikrishnan, U. T., Rajaratnam, S. D., King, N. 2015: Redefining rural tourism in Malaysia: A conceptual perspective. *Asia Pacific Journal of Tourism Research* 20-3. https://doi.org/10.1080/10941665.2014.889026

Nepal Traveller 2024: The significance of praying before climbing a mountain. *Blog post*.

Novais, M. A., Ruhanen, L., Arcodia, C. 2018: Destination competitiveness: A phenomenographic study. *Tourism management* 64. https://doi.org/10.1016/j.tourman.2017.08.014

Nowacki, M. 2023: Mountaineering in the Himalayas: A comprehensive analysis through a literature review and research profiling. *Polish Journal of Sport and Tourism* 30-4. https://doi.org/10.2478/pjst-2023-0019

Nuraini, C., Alamsyah, B., Novalinda, N., Sagala, P., Sugiarto, A. 2023: Planning with 'three-world structures': A comparative study of settlements in mountain villages. *Journal of Regional and City Planning* 34-1. https://doi.org/10.5614/jpwk.2023.34.1.4

Nyaupane, G. P., Lew, A. A., Tatsugawa, K. 2014: Perceptions of trekking tourism and social and environmental change in Nepal's Himalayas. *Tourism Geographies* 16-3. https://doi.org/10.1080/14616688.2014.942233

Pan, S. Y., Gao, M., Kim, H., Shah, K. J., Pei, S. L., Chiang, P. C. 2018: Advances and challenges in sustainable tourism toward a green economy. *Science of The Total Environment* 635. https://doi.org/10.1016/j.scitotenv.2018.04.134

Paramati, S. R., Alam, Md. S., Chen, C. F. 2017: The effects of tourism on economic growth and CO_2 emissions: A comparison between developed and developing economies. *Journal of Travel Research* 56-6. https://doi.org/10.1177/0047287516667848

Pond, M., Martin, B., Collins, E., Szolosi, A. M. 2014: Investigating climbing as a spiritual experience. *Journal of Outdoor Recreation, Education, and Leadership* 6-2. https://doi.org/10.7768/1948-5123.1262

Richards, G. 2018: Cultural tourism: A review of recent research and trends. *Journal of Hospitality and Tourism Management* 36. https://doi.org/10.1016/j.jhtm.2018.03.005

Różycki, P., Dryglas, D. 2014: Trekking as a phenomenon of tourism in the modern world. *Acta Geoturistica* 5-1.

Sandberg, J. 2000. Understanding human competence at work: An interpretative approach. *Academy of management journal* 07/1556383

Shi, D., Shan, Y., Zhao, Z., Zhang, S. 2022: Identification and influence of tourism rituals: Analysis of eye movement recognition of tourism images. *Journal of Hospitality & Tourism Research* 46-1. https://doi.org/10.1177/1096348021996783

Siolemba Patiro, S. P., Hendarto, K. A., Parmono, V. R., Wibowo, L. R., Suka, A. P., Abdurakhman, A., Pramusita, A. et al. 2024: Analyzing residents' preferences to ecotourism impacts using simple additive weighting: The case of Mount Rinjani National Park, Indonesia. *Forest Science and Technology* 20-1. https://doi.org/10.1080/21580103.2023.2284282

Slentz, T. C., Chase, M. A. 2003: Climbing Mount Everest a new challenge for physical education adventure education. *Journal of Physical Education, Recreation & Dance* 74-4. https://doi.org/10.1080/07303084.2003.10609201

Stevens, S. F. 1991: Sherpas, tourism, and cultural change in Nepal's Mount Everest Region. *Journal of Cultural Geography* 12-1. https://doi.org/10.1080/08873639109478419

Vidal-González, P., Sánchez, V. 2019: Hiking paths and intangible heritage: A quest for cultural roots. Cases in the province of Castellón, Spain. *Sport in Society* 22-12. https://doi.org/10.1080/17430437.2018.1551368

Ween, G., Abram, S. 2012: The Norwegian trekking association: Trekking as constituting the nation. *Landscape Research* 37-2. https://doi.org/10.1080/01426397.2011.651112

Westskog, H., Aase, T. H., Leikanger, I. 2021: The Norwegian trekking association: Conditions for its continued existence with new tourism patterns. *Scandinavian Journal of Hospitality and Tourism* 21-3. https://doi.org/10.1080/15022250.2021.1913219

Windsor, J. S., Firth, P. G., Grocott, M. P., Rodway, G. W., Montgomery, H. E. 2009: Mountain mortality: A review of deaths that occur during recreational activities in the mountains. *Postgraduate Medical Journal* 85-1004. https://doi.org/10.1136/pgmj.2009.078824

Wu, M. Y., Tong, Y., Li, Q., Wall, G., Wu, X. 2023: Interaction rituals and social relationships in a rural tourism destination. *Journal of Travel Research* 62-7. https://doi.org/10.1177/00472875221130495

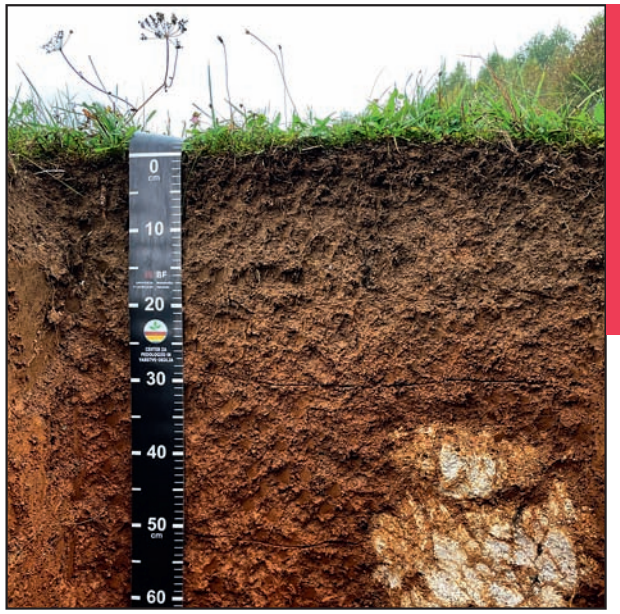
Xuemei, L., Wang, F., Huili, C., Jingwen, T. 2024: Development of an indicator system for evaluating risks in trekking tourism. *Leisure Sciences* 1-20. https://doi.org/10.1080/01490400.2024.2415941

Zhang, L., Gao, J. 2016: Exploring the effects of international tourism on China's economic growth, energy consumption and environmental pollution: Evidence from a regional panel analysis. *Renewable and Sustainable Energy Reviews* 53. https://doi.org/10.1016/j.rser.2015.08.040

Acta geographica Slovenica, 66-1, 2026, 21–38

SOILS OF THE DINARIC KARST IN SLOVENIA: PROPERTIES, PEDOGENESIS AND LAND USE

Rok Turniški, Helena Grčman



ROK TURNIŠKI

Luvisol developed over dolomite.

DOI: https://doi.org/10.3986/AGS.14434
UDC: 631.41:552.54(497.4-13)
332.362:631.4(497.4-13)
Creative Commons CC BY-SA 4.0

Rok Turniški[1], Helena Grčman[1]

Soils of the Dinaric karst in Slovenia: properties, pedogenesis and land use

ABSTRACT: The study evaluates the physical and chemical properties of soils developed on limestones and dolomites in the Dinaric karst of Slovenia. Statistical analysis of 257 soil profiles was performed to compare the properties of different soil types and to assess the impact of land use on soil characteristics. The predominant soil types in the area are Leptosols and Phaeozems, followed by Eutric Cambisols and Luvisols. Although these soils are chemically fertile, their agricultural potential is limited due to their variable depth, rocky surface, and lack of surface water. As a result, forests are the predominant type of land use. Land use influences soil processes and properties, as evidenced by the differences in soil pH, base saturation, cation exchange capacity and organic matter content.

KEYWORDS: soil, karst, carbonate parent material, Leptosols, Phaeozems, Cambisols, Luvisols

Tla dinarskega krasa Slovenije: lastnosti, pedogeneza in raba tal

POVZETEK: V raziskavi predstavljamo pregled fizikalnih in kemijskih lastnosti tal (prsti) na apnencih in dolomitih dinarskega krasa v Sloveniji. Izvedli smo statistično analizo 257 talnih profilov. Primerjali smo lastnosti glavnih talnih sistematskih enot in vrednotili vpliv rabe tal. Prevladujoča talna sistematska enota so rendzine, sledijo rjava pokarbonatna tla in izprana tla. Kljub ugodnim kemijskim lastnostim, ki kažejo na visoko rodovitnost, je njihova kmetijska raba omejena zaradi različne globine, površinske skalovitosti in pomanjkanja površinske vode. Zaradi teh omejitev je prevladujoča vrsta rabe tal na dinarskem krasu gozd. Raba tal vpliva na procese in lastnosti tal, kar se odraža v razlikah v pH, nasičenosti z bazičnimi kationi, kationski izmenjalni kapaciteti in vsebnosti organske snovi.

KLJUČNE BESEDE: tla/prst, kras, karbonatna matična podlaga, Leptosols, Phaeozems, Cambisols, Luvisols

The article was submitted for publication on April 25th, 2025.
Uredništvo je prejelo prispevek 25. aprila 2025.

[1] University of Ljubljana, Biotechnical Faculty, Ljubljana, Slovenia

rok.turniski@bf.uni–lj.si (https://orcid.org/0000–0002–0630–6620), helena.grcman@bf.uni–lj.si (https://orcid.org/0000–0003–0724–9151)

1 Introduction

The Dinaric karst region (Figure 1) covers almost one fifth of the territory of Slovenia (Zorn et al. 2020). It consists mainly of Triassic, Jurassic and Cretaceous limestones and dolomites (also named dolostones) (Dozet and Pleničar 2009; Knez and Kranjc 2009), which are considered very pure and contain only a small proportion of insoluble residues (Ogorelec and Rothe 1992; Pleničar and Dozet 1993; Gams 2004). The area is characterised by plateaus with intervening depressions and lowlands in which the karst poljes extend (Knez and Kranjc 2009). The pedogenesis of soils on limestone and dolomite, their productivity and land use have been studied since the middle of the 20th century. Early research on the Terra rossa of the Karst Plateau (SW Slovenia) by Sušin (1964) in the 1960s, for example, contributed significantly to the knowledge of soil properties associated with limestone bedrock. Meanwhile, Gregorič's (1965) doctoral thesis on soil genesis on the dolomites of the Dolenjska region attempted to clarify the origin of the reddish-brown Bt horizons and two-layer soil profiles. Sušin (1972) investigated the differentiation of clay content and colour variability in relation to pedogenesis. At the time, Lobnik (1978) studied the migration of manganese and the formation of manganese concretions and coatings on structural aggregates in Eutric Cambisols on dolomite. Overall, the soil research conducted supported the theory of polygenetic soil formation on carbonate bedrock (Gregorič 1965; Sušin 1972), which is widely accepted today (Costantini et al. 2018; Durn et al. 2023). As the exact pathways of formation remain a hotly debated topic, research into soil formation and development in karst environments remains relevant. This is demonstrated, for instance, by a recent study on the Divača karst (Zupančič et al. 2018), which highlighted the geochemical fingerprint of insoluble material in soils on different limestone formations and drew particular attention to other materials contributing to soil mass, including interbedded material, palaeosoils, and probably aeolian material. Improved analytical methods in the fields of geochemistry, minerals and micromorphology have recently triggered a new wave of soil research across the Dinaric karst region (Durn et al. 2021; Durn et al. 2023; Turniški et al. 2023). In the 1970s, soil scientists and agronomists began to investigate the productive potential of karst soils. Having identified their properties and spatial distribution, they evaluated the most suitable types of land use. Since the shallow depth and rocky nature of karst soils hindered ploughing, they emphasised the importance of these soils for livestock production, and, consequently, for protein supply, which was a major concern at the time. Stepančič (1972) also compared soils developed on limestone and dolomite. He concluded that soils on limestone were mainly covered by forest due to the rocky and cavernous relief associated with this type of bedrock. The rock-free surfaces of soils on dolomite, on the other hand, made them more suitable for agriculture. At the same time, Stritar (1972) focused on the land use of rendzinas formed on dolomite, while Ažnik (1975) studied their productive potential. Eutric Cambisols (slv. *rjava pokarbonatna tla*) on dolomite in the Lower Carniola (slv. *Dolenjska*) were studied by Stepančič (1972), and on the Karst Plateau (slv. *Kras*), the suitability of Terra rossa for viticulture was examined by Stepančič and Ažnik (1976). Stritar (1967) also investigated the agricultural value of soils associated with a specific forest type (slv. *steljnik*) consisting of silver birch (*Betula pendula*), common heather (*Calluna vulgaris*) and eagle fern (*Pteridium aquilinum*), which frequently occurs on the Luvisols (slv. *izprana tla*) of the White Carniola (slv. *Bela krajina*) in SE Slovenia. The most systematic and extensive soil survey was carried out between 1960 and 1990 to produce the Slovenian soil map at a 1:25,000 scale (Vidic et al. 2015).

Previous studies have focused on geographically narrower areas, whereas the aim of our research was to analyse the spatial distribution of soil types developed on limestone and dolomite in the Dinaric karst region, based on the comprehensive database of the digital soil map of Slovenia, and to provide an overview of their chemical and physical properties in relation to pedogenetic processes and human influences. Particular attention was paid to analysing soil properties that are important for agricultural use and to identifying significant differences between forest and agricultural topsoils that can be attributed to human activities.

2 Materials and methods

2.1 Study area

The study area covered the Dinaric karst of Slovenia (Figure 1), which is bounded in the north by the Julian Alps, the Lower Carniola Lowland (slv. *Dolenjsko podolje*), and the Sava River (Mihevc and Prelovšek 2010).

The predominant part of the Dinaric karst in Slovenia is influenced by a temperate continental climate with average annual precipitation ranging from 1300 to 2800 mm and average temperatures of the coldest month ranging from 0 to –3°C and of the warmest month from 15 to 20°C (Ogrin 1996). White Carniola is distinguished by lower average annual precipitation, ranging between 1200 and 1300 mm. The Mount Snežnik area is characterised by a low average temperature in the coldest month (below –3°C) and high annual precipitation ranging between 1600 and 3000 mm. In contrast, the Karst Plateau is characterised by generally higher temperatures, with the average temperature in the coldest month above 0°C and in the warmest month above 20°C, and average annual precipitation ranging between 1200 and 1700 mm (Ogrin 1996).

2.2 Source of data and analysis

The study is based on data from the Soil Map of Slovenia 1:25,000 (PK25) available from Soil Information System of the Infrastructure Centre for Soil and Environmental Sciences (TIS-ICPVO) provided by Biotechnical Faculty, University of Ljubljana (Infrastrukturni … 2023). The physical and chemical properties (Table 1) of the soils were analysed in the ICPVO laboratory following the standardised protocols described in Vidic et al. (2015). For the area of the Dinaric karst in Slovenia (Zorn et al. 2020), the pedocartographic units (PCUs) were exported from the PK25 attribute table and merged into a new data layer. The physical and chemical properties of 747 individual soil horizons from 257 soil profiles within the study area (Figure 1) were statistically evaluated using descriptive statistics to characterise the central tendency and variation of soil properties. Data processing was carried out using the statistical computing environment R v.4.2.3 (R Foundation … 2023). The package »aqp« (Beaudette et al. 2013) was used to plot the soil depth functions and »ggplot2« (Wickham 2016) was used to generate the texture triangles and mean plots.

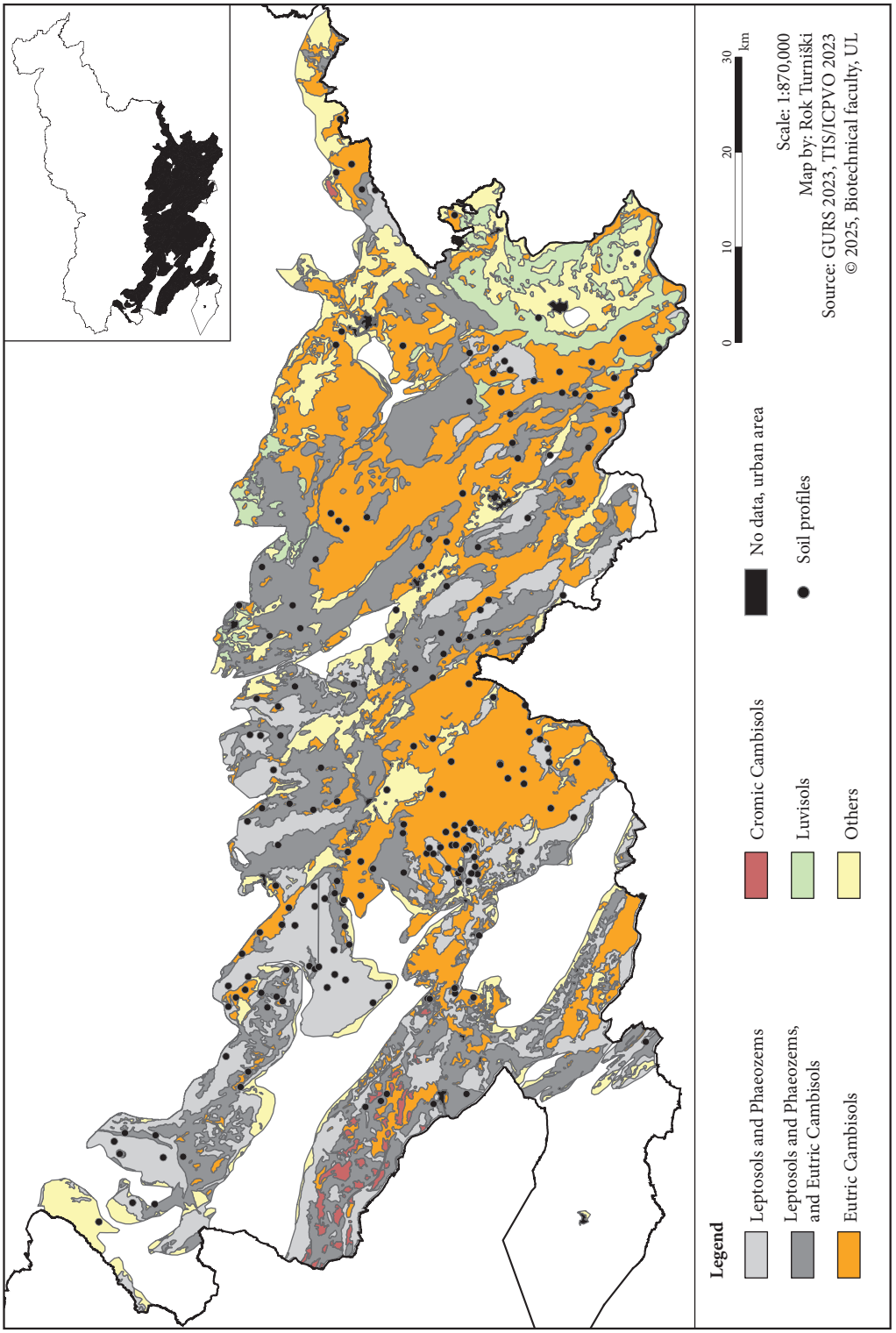
3 Results

On limestones and dolomites the main soil groups are Leptosols and Phaeozems (slv. *rendzina*) (42.7%), followed by Eutric Cambisols (slv. *rjava pokarbonatna tla*) (36.3%), Luvisols (slv. *izprana tla*) (6.7%), Rhodic

Table 1: Overview of analysed soil properties.

Variable	Description	Unit	Method
pH	Soil acidity	–	SIST ISO 10390: 2005: Soil quality – Determination of pH
Sand	Sand content	%	SIST ISO 11277: 2009: Determination of Particle Size Distribution in Mineral Soil Material. Method by Sieving and Sedimentation.
Silt	Silt content	%	
Clay	Clay content	%	
SOM	Soil organic matter	%	SIST ISO 14235: 1999: Soil quality – Determination of organic carbon by sulfochromic oxidation.
N	Total nitrogen	%	SIST ISO 11261: Soil quality – Determination of total nitrogen – Modified Kjeldahl method.
CN	Carbon-to-Nitrogen ratio	–	Calculated
CEC	Cation exchange capacity	$cmol_c\ kg^{-1}$	Burt 1992
Ca-sat	Calcium saturation	%	Calculated
Mg-sat	Magnesium saturation	%	Calculated
BS	Base saturation	%	Calculated
P_2O_5	Plant-available phosphorus	$mg\ kg^{-1}$	SIST-TS: Method AL (Egnér et al. 1960)
K_2O	Plant-available potassium	$mg\ kg^{-1}$	SIST-TS: Method AL (Egnér et al. 1960)

Figure 1: Soil map of the Dinaric karst of Slovenia 1:250,000 (modified) with locations of the analysed soil profiles. ► p. 25


Legend
Leptosols and Phaeozems
Leptosols and Phaeozems, and Eutric Cambisols
Eutric Cambisols
Cromic Cambisols
Luvisols
Others
No data, urban area
Soil profiles
0
10
20
30
km
Scale: 1:870,000
Map by: Rok Turniški
Source: GURS 2023, TIS/ICPVO 2023
© 2025, Biotechnical faculty, UL

Cambisols (slv. *rdečerjava tla*) (0.7%) and Nudilithic Leptosols (slv. *litosol*) (0.6%), which together account for 87% of all soils in the area (Figures 1 and 2, Table 2). Alternating with limestones and dolomites, various clastic consolidated or unconsolidated sedimentary rocks, such as Pleistocene (Markič 2009) and Pliocene (Bavec and Pohar 2009) sediments are also found, especially in alluvial plains and karst poljes, where different soil types have developed. The most common are Eutric Cambisols (slv. *rjava tla, evtrična*) (7.1%) and Dystric Cambisols (slv. *rjava tla, distrična*) (1.5%), followed by Gleysols (slv. *oglejena tla*) (1.4%), and Fluvisols (slv. *obrečna tla*) (0.7%). In the Lower Carniola, in the area of Novo mesto, Eutric Cambisols have developed on Pleistocene and Pliocene unconsolidated sediments, as well as on marlstones and marl sediments. Eutric Cambisols have also developed on karstic alluvial plains covered with clayey alluvial sediments, and on gravel deposits, and moraines. Hydromorphic soils are associated with a high water table. Gleysols (1.4%) occur on alluvial plains, while Stagnosols (0.4%) are more common on slopes. The combination of calcareous and non-calcareous rocks is also common. In the south of the Ljubljana region, dolomites alternate with siliceous shales, clays, siltstones and sandstones. Dystric Cambisols have developed on siliceous clastic sedimentary rocks. The characteristics of the most common soil groups developed on limestone and dolomite are presented in Table 2 and Figures 3 and 4.

Leptosols and Phaeozems are generally the shallowest soils. Their total profile depths varies from very shallow (a few cm) to about 60 cm. Rendzinas mostly have a silty to silty-clayey texture. They are rich in organic matter, especially in the Oa and Ah horizons (average C_{org} contents of 30% and 13%, respectively). Soils are mostly slightly acidic, with an average value of 6.3. The lowest pH values occur in Oa and Ah horizons. Leptosols and Phaeozems are eutric, with high average base saturation value of 75.8%. CEC values are high, with an average of 49 $cmol_c\ kg^{-1}$ soil. The content of plant-available phosphorus (P_2O_5) and potassium (K_2O) is low, with an average value of 62 mg $P_2O_5\ kg^{-1}$ and 155 mg $K_2O\ kg^{-1}$. The highest concentrations occurring in the O horizons, with an average values of 147 mg $P_2O_5\ kg^{-1}$ and 176 mg $P_2O_5\ kg^{-1}$, due to biocycling.

Eutric Cambisols differ in soil depth, generally ranging from 30 cm to 200 cm. The texture classes of Eutric Cambisols are mostly loam, silty clay loam, clay loam, and clay. Topsoils have the highest concentration of organic matter, especially Oa and Ah horizons (averages of 47% and 21.7%, respectively). Higher organic matter content is also characteristic of A (average 7.1%) and Ap (average 6.2%) horizons. The average CN ratio is 11. Organic matter content and CN ratio decreases with soil depth (Figure 4). Eutric Cambisols are in average moderately acidic with an average pH value of 5.7. The upper parts of soil profiles, rich with organic matter, are usually more acidic than the lower parts. Higher values in the lower BC horizons are a consequence of the contact with the carbonate parent material. Typical Eutric Cambisols have an average base saturation of 71%, whereas leached varieties show lower values, with an average of 48%. CEC values are relatively high, with an average value of 30 $cmol_c\ kg^{-1}$ soil. Similar to Leptopsols and Phaeozems the supply of available phosphorus and potassium in soils is low, with avarages 55 mg $P_2O_5\ kg^{-1}$ and 129 mg $K_2O\ kg^{-1}$. The higher contents of phosphorus and potassium are characteristic for Oa, Ah, and Ap horizons. In Oa and Ah horizons, high values (an average > 95 mg $P_2O_5\ kg^{-1}$ and > 200 mg $K_2O\ kg^{-1}$) result from biorecycling, while Ap horizons show the apparent influence of fertilizing (an average of 97 mg $P_2O_5\ kg^{-1}$ and 410 mg $K_2O\ kg^{-1}$).

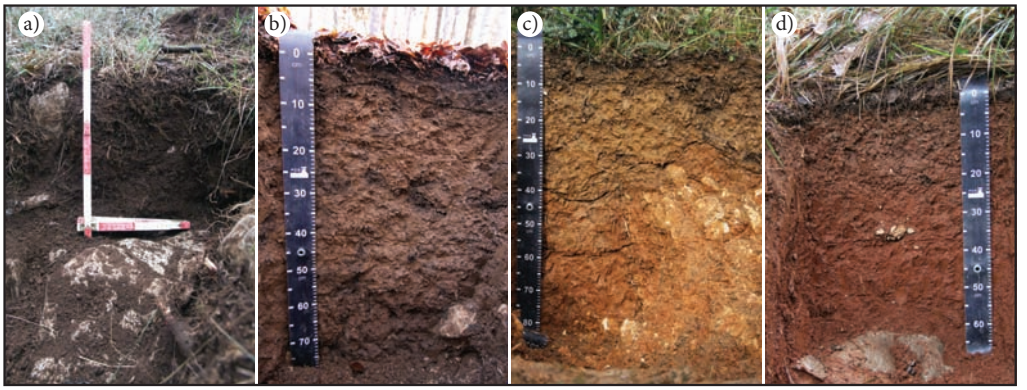
In some areas, mainly on the Karst Plateau, **Rhodic Cambisols** also occur, representing typical Mediterranean soils (Figure 2d). Similar to Eutric Cambisols, Rhodic Cambisols vary in soil depth. In concave geomorphological settings, like dolines, they are several metres thick. Generally, they are clay rich, with texture classes of silty clay loam, clay loam and clay. The SOM content is lower compared to Eutric Cambisols, with an average of 2.6%. The average CN of the soil is 11. Soils are moderately acidic. The average pH value (5.2) is lower compared to Eutric Cambisols, which also reflects in lower base saturation. Base saturation is the highest in the A (average 56.5%) and Ap horizons (average 83.1%), while the cambic Brz (rz comes from Latin residuum) and illuvial Bt horizons are more depleted, with an average value of 51.5%. E horizons in leached Rhodic Cambisols are dystric, which is also common in Bt. Similar to Eutric Cambisols, CEC values are relatively high, with an average of 32.2 $cmol_c\ kg^{-1}$ soil.

Luvisols are well-developed soils (Figure 2c), usually deeper than 70 cm. Their diagnostic feature is a pronounced texture differentiation between the upper (A, E) and lower (Bt) horizons. In the E horizon, which lies directly above the Bt horizon, the average clay content is 29.7%, and in the Bt horizon, 46.5%. In general, the A, E, and Bt horizons contain little sand (median < 12.6%) (Figure 3). SOM content decreases with depth; the topsoil under forest vegetation is rich in organic matter (the average SOM content in Oa/Ah

is 28%). The eluvial and illuvial horizons contain less than 2.5% SOM. The average pH value (5.2) is similar to Rhodic Cambisols, however the range is broader (2.9 to 6.9). Except for Oa/Ah and A horizons, the lowest pH values were detected in E horizons (average 4.6). The average pH value in Bt horizon is 5. The lower values of base saturation are noticeable in E horizons (32.7%), while values in Bt are higher (51.5%) (Table 3). The average CEC value is 27.6 $cmol_c\ kg^{-1}$. The supply of available phosphorus and potassium is very low, with average concentrations of 50 $mg\ kg^{-1}$ and 112 $mg\ kg^{-1}$, respectively.

Table 2: Properties of predominant soil groups in the Dinaric karst of Slovenia. For selected chemical soil properties, averages and ranges (in brackets) are presented. The area was calculated according to the Soil Map of Slovenia 1:25,000 (Infrastrukturni . . . 2023). The »/« symbol is not a classification rule but replaces the word »or«.

	Leptosols and Phaeozems	Eutric Cambisols	Luvisols	Rhodic Cambisols
Area (km^2)	2317.4	1970.2	362.1	30,7
Area (%)	42.7	36.3	6.7	0.7
Predominant lithology	limestone and dolomite			
Predominant natural vegetation	*Omphalodo-Fagetum, Lamio orvalae-Fagetum, Ostryo carpinifoliae-Quercetum pubescentis* (Karst Plateau)			*Ostryo carpinifoliae-Quercetum pubescentis*
Predominant land use	Forest			Forest/agricultural
n (soil profiles)	92	116	41	8
n (soil horizons)	183	375	163	26
Typical profile	Oa-C/R, Ah-C/R, A/Ap-C/R	Oa/Ah-A-B-C/R, Ah-B-C/R, A/Ap-B-C/R	Oa/Ah-E-B-C/R A/Ap-E-Bt-C/R	Oa/Ah-A-B-C/R, Oa/Ah-E-B-C/R, Ah/Ap-B-C/R
Typical depth (cm)	0–30	30–100	70–125	30–150
Typical texture	silty	silty to clayey	silty to clayey	clayey
pH	6.3 (3.6–7.4)	5.7 (3.6–7.6)	5.7 (3.6–7.6)	5.2 (3.7–7.2)
SOM (%)	16.2 (1.4–83.3)	6.4 (0.2–71.8)	6.9 (0.31–70.8)	4.5 (0.6–12.3)
N	0.58 (0.06–2.25)	0.40 (0.04–14.6)	0.60 (0.04–14)	0.22 (0.07–0.53)
CN	15.7 (9–40)	13.1 (1–38)	14.5 (1–100)	10.8 (5–16)
CEC ($cmol_c\ kg^{-1}$)	48.9 (21–124)	30.3 (10.7–76)	27.6 (13.4–99.9)	32.2 (16.7–45.9)
Base saturation (%)	75.8 (27.2–99.5)	63.5 (5.6–96.7)	42.9 (2.4–84.4)	54.2 (5.5–89.5)



ROK TURNIŠKI

Figure 2: Main soil types formed on limestones of the Dinaric karst a) Leptosol, b) Eutric Cambisol, c) Luvisol, and d) Rhodic Cambisol.

The comparison of soils developed on limestone and dolomite revealed clear differences in Ca and Mg saturation, reflecting the contrasting mineral composition of the parent material. Soils developed on limestone exhibit higher Ca saturation, whereas those formed on dolomite show markedly higher Mg saturation (Figure 5). However, no significant differences were observed in the other soil properties.

Forests cover as much as 72.5% of the area of the Dinaric karst (Ministry … 2021). Permanent grassland (15.5%) is the second most common type of land use in the area, while arable land and combined land use (i.e., agroforestry) lag behind with 2.3% and 1.3%, respectively. Land use affects some properties of the horizons, so in Table 3 we present mean values and ranges for the horizons according to forest (F) and agricultural (A) land use.

Forests promote the accumulation of organic matter in their uppermost organic horizons (Oi, Oe, Oa), with a high organic matter content in the Oa horizons (> 28.9%). The organic surface layers also show high CN ratios – on average 20.7, 19.9 and 26.9 in Leptosols/Phaeozems, Cambisols and Luvisols, respectively (Table 3). The high organic matter content is also reflected in a very high cation exchange capacity. The average CEC in the Oa/Ah horizons of the forest soils is 68.6, 52.5 and 51.5 $cmol_c\ kg^{-1}$ in Leptosols/Phaeozems, Cambisols and Luvisols, respectively. Forest soils typically exhibit lower pH values in the upper horizons than agricultural soils.

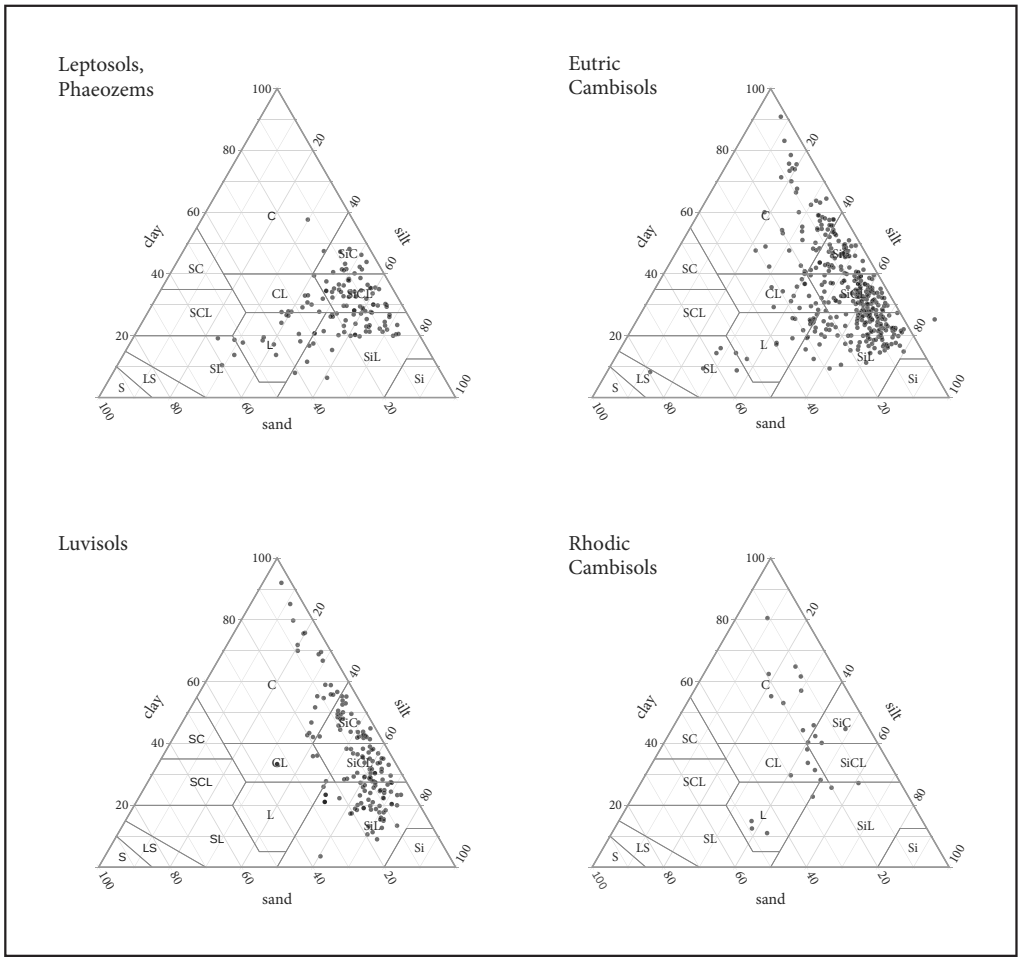


Figure 3: Soil texture of Leptosols and Phaeozems, Eutric Cambisols, Luvisols, and Rhodic Cambisols.

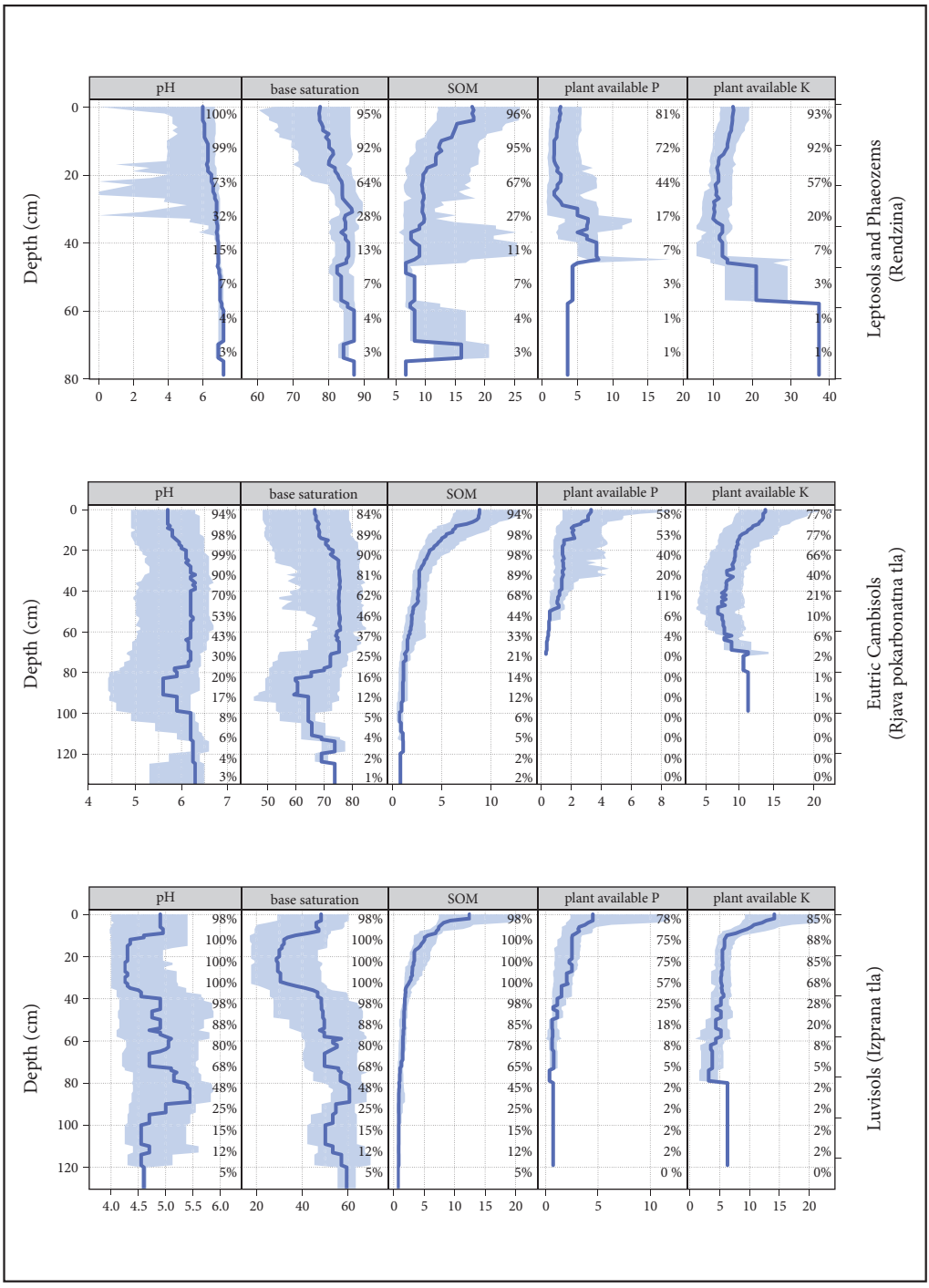


Figure 4: pH, base saturation (%), SOM (%), plant available phosphorus (mg kg^{-1}) and plant available potassium (mg kg^{-1}). The solid blue lines represent the median that is bounded by the 25th and 75th percentiles. The percentages along the right side of the depth axis describe the fraction of profiles that contributed to the computations.

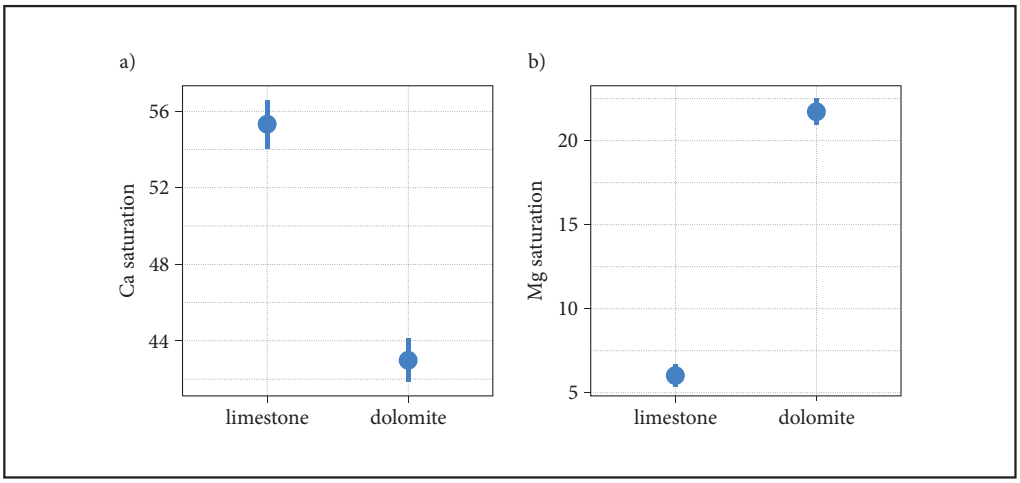


Figure 5: Mean values with standard errors for Ca saturation and Mg saturation in soils developed on limestone (n = 230) and dolomite (n = 139) in the Dinaric karst region.

4 Discussion

4.1 Pedogenesis on limestone and dolomite

The diversity of soils on limestone and dolomite is closely related to karst geomorphology (Stritar 1990; Turniški 2024). The main pedogenetic processes involved in soil development on carbonate rocks are organic matter accumulation, carbonate dissolution and leaching, and clay illuviation (Birkeland 1999). Soils begin to develop with the accumulation of organic matter when bare rock is covered by pioneer vegetation (Blume et al. 2016). Protection from erosion simultaneously promotes the accumulation of mineral weathering products. In the early stages, however, only a thin horizon with a high organic matter content can be recognised. These soils are classified as Nudilithic Leptosols. The organic matter is poorly decomposed (CN ratio > 25), especially at higher altitudes. Nudilithic Leptosols occur locally on very steep slopes where intense erosion processes prevent the accumulation of soil material.

As the humus accumulative horizon thickens, Leptosols and Phaeozems, the most common soil types in Slovenia's Dinaric karst, begin to develop. They are characterized by shallow profiles, consisting of only O and/or A horizons overlying the parent material. The contact with parent material influences soil pH and base saturation; both parameters are higher compared to more developed soil types, Cambisols and Luvisols. Due to their high organic matter content, the CEC is high, although the clay content is lower compared to Cambisols and Luvisols (Table 2, Figure 3). Leptosols and Phaeozems vary in thickness, content of organic matter, and the rate of organic matter decomposition. Organic matter accumulation is largely dependent on climatic conditions (Suhadolc and Črepinšek 2018). At higher altitudes, i.e., on the Snežnik Plateau, the Trnovo Forest Plateau (slv. *Trnovski gozd*), Mount Gotenica, the organogenic form of Leptosols and Phaeozems is common. This form can also be found in cold micro-locations at lower altitudes, especially on northern slopes. However, pure organogenic forms of Leptosols are rare, mainly occurring above 900 m.a.s.l. While closely associated with organo-mineral forms of Leptosols and Phaeozems, these soils tend to frequently alternate with Nudilithic Leptosols at higher altitudes. The most widespread forms of Leptosols and Phaeozems are organo-mineral soils with mull humus (Figure 2a), characterized by the accumulation and gradual mineralization of organic matter as their main soil-forming processes (Stepančič and Ažnik 1976). Predominantly they are found on limestone and dolomite, often in combination with more developed soil types, i.e., Eutric Cambisols; to a lesser extent, they are also present on carbonate gravels, moraines, and alluvial river deposits on karst poljes. A thin Brz horizon can sometimes be observed

Table 3: Chemical properties of the soil horizons within three main soil types of the Slovenian Dinaric karst. Data are shown for generalised horizons subdivided according to land use (A – agriculture, F – forest). Both mean values and ranges (in brackets) are presented.

Soil type	Soil horizon	Land use	pH –	SOM %	CN –	CEC $cmol_c\ kg^{-1}$	BS %
Leptosols and Phaeozems (slv. *rendzina*)	Oa/Ah	A	6.2 (5–7)	21.4 (15.3–30.3)	14.7 (11.2–20.2)	52.9 (43.4–74)	73.6 (48.3–89.8)
		F	6.0 (3.6–7.2)	30.5 (16.3–39.6)	20.7 (12.7–39.6)	68.6 (32.7–124)	73.4 (36.1–99.5)
	A	A	6.3 (4.8–7.4)	9.5 (2.2–14.9)	12.9 (9.4–20.9)	37.7 (24.6–58.1)	76.1 (49.2–91)
		F	6.4 (3.9–7.4)	9.3 (1.4–14.9)	16.2 (9.4–39.5)	43.2 (20.9–71.7)	75.1 (27.2–95.1)
	Ap	A	7.1 (7.0–7.2)	8.9 (3–8.6)	11.6 (9.2–15.1)	36 (29.3–39.5)	89.5 (86.5–91.6)
		F	–	–	–	–	–
Eutric Cambisols (slv. *rj. pokarbonatna tla*)	Oa/Ah	A	6.7 (6.4–7)	23.4 (16.8–30.6)	14.4 (11.1–17)	60.8 (44.2–76)	80.8 (75.8–87.2)
		F	5.2 (3.9–6.9)	28.9 (15.1–71.8)	19.9 (3.9–29.4)	52.5 (27.8–72.1)	54.2 (30.3–86.3)
	A	A	5.8 (4–7.6)	6.3 (1.3–13.2)	12 (1–19.8)	29.9 (16.3–61.3)	63.2 (12–93.9)
		F	5.5 (3.6–7.3)	7.6 (1.8–14.2)	16.8 (6.7–38.1)	31.9 (14.6–52.7)	61.4 (7.7–96.4)
	Ap	A	6.1 (5.2–6.9)	4.9 (2.6–10.8)	10.1 (6.7–14.9)	23.8 (13.9–35.7)	68.5 (38.3–87.4)
		F	–	–	–	–	–
	B	A	5.9 (3.8–7.6)	2.1 (0.2–10)	9.6 (1–18.7)	24.8 (10.7–46.7)	66.2 (17–96.7)
		F	5.5 (3.7–7.2)	3.2 (0.3–10.7)	13.9 (2.5–26.7)	29.1 (14.2–44.9)	63.1 (5.6–90.2)
Luvisols (slv. *izprana tla*)	Oa/Ah	A	–	–	–	–	–
		F	4.3 (2.9–6.5)	33.7 (15.4–70.8)	26.9 (15.5–100)	51.5 (41.6–99.9)	39.2 (15.3–71.7)
	A	A	5.5 (3.8–6.6)	8.1 (4.4–13.3)	12.4 (0.3–16.3)	27.8 (22.2–37.2)	54.2 (15.9–80.9)
		F	4.7 (3.3–6.8)	7.1 (3.2–12.7)	18.1 (14.1–24.6)	26.4 (17.3–36)	35.6 (6.5–83.5)
	Ap	A	4.7 (4.3–5.1)	5.9 (3.3–7.2)	11.8 (10.1–14.3)	24.3 (18.2–27.5)	33.9 (29.2–39.7)
		F	–	–	–	–	–
	E	A	5.1 (3.9–6.5)	2.8 (0.8–6.4)	9.3 (1–18.7)	19.6 (15.2–28.9)	45.9 (19.6–73)
		F	4.2 (3–6.5)	3.7 (0.7–9.9)	15.6 (5.4–28.3)	22.0 (13.4–43.1)	24.9 (3.8–70.4)
	Bt	A	5.1 (4–6.7)	1.3 (0.5–3.1)	8.4 (1–13.7)	24.3 (14.8–40)	53.9 (20–84.4)
		F	4.9 (3.8–6.9)	2.1 (0.3–5.4)	11.9 (2.6–19.8)	27.2 (13.9–46.8)	50.3 (2.4–82.8)

between A horizon and the underlying parent material, indicating further soil evolution. Such a transitional soil type, mainly found on less steep slopes or in limestone pockets and fissures, is named brown rendzina (Prus et al. 2015). The soil surface of Leptosols and Phaeozems on limestone is usually rocky, which gives a characteristic appearance to the karst landscape (Gams 2004). Most of the evaluated soils of this type also contain skeletal or rock debris. In contrast to the rendzinas on limestone, the rendzinas on dolomite can be found on unweathered rock and loose dolomitic sands. Due to the specific weathering of dolomite (Zupan Hajna 2014), these soils do not exhibit surface rockiness; nevertheless, they often contain coarse fragments within the soil matrix.

Eutric Cambisols are characterized by the presence of a cambic horizon (Brz), which is thought to have initially formed by the accumulation of insoluble residue of limestone and dolomite (Figure 2b; Vidic et al. 2015). However, following the advances in the development of pedogenetical models for this soil type (Duchaufour 1982), Stepančič and Lobnik (1985) described these soils as relict and undergoing polycyclic genesis. Additions of different allochthonous material (i.e., interbedded material, paleosoils, eolian dust), as well as polycyclic genesis were further discussed in investigations of Zupančič et al. (2018) and Turniški et al. (2023). Throughout the geological periods, soil material was translocated and resedimented, covering dolines, terraces and plateaus in some places with a blanket several meters thick. Often, we can find relict Brz horizons remaining in the subcutaneous channels and scallops of the chemically weathered bedrock and in larger depressions between the plateaus, where water erosion failed to remove them completely (Stepančič and Lobnik 1985). Pedogenetic processess, i.e., decarbonation and eluvial-illuvial processes, result in lower pH and base saturation in comparison with Leptosols and Phaeozems (Table 2). The Slovenian soil classification recognizes two subtypes: typical and leached (illuvial, luvic). The differences between the two are reflected in additional differentiation of soil material. Typical Eutric Cambisols show no apparent signs of eluviation, while the illuvial subtype shows textural differentiation in the profile; higher clay content in lower part of the profile and lower pH and base saturation in the upper part of the profile (Figure 3). The skeletal content in the soil differs depending on the parent material; Eutric Cambisols on limestone contain individual rounded rock fragments, while those on dolomite have a higher content of smaller and sharp-edged rock fragments. Eutric Cambisols occur throughout the Dinaric karst, most often on flats and at the middle altitudes on less steep slopes within the pockets and fissures in the local bedrock, alternating with Leptosols and Phaeozems. In such instances, the depth of the soil varies greatly within short distances and surface rockiness is very common (Ciglič et al. 2012).

Among Cambisols developed on limestone and dolomite, a distinct subgroup is represented by Rhodic Cambisols. These soils, known also as Terra rossa, are characterized by a reddish colour (5YR to 10R), which serves as an important diagnostic feature. It reflects the intensity of rubification, i.e., the preferential formation of hematite over goethite, which takes place in a Mediterranean climate (Schwertmann et al. 1982). The dominant theory of its genesis explains Terra rossa as a relict polycyclic soil, initially formed by the weathering of limestones in warm, dry climate conditions, resulting in clayey material rich in iron and aluminium oxides (insoluble residue) (Durn et al. 2023; Torrent et al. 2023). During the Pleistocene, the material was exposed to strong water and wind erosion, so it has been preserved mainly in caves, dolines and pockets, and fissures within the weathered bedrock (Stepančič 1978). However, the origin of the red residues and the evolution of this soil type are still debated (Liu et al. 2013). In Slovenia two subtypes of Rhodic Cambisols are known: »*kremenica*« (from Slovenian *kremen*, quartz) and »*ilovka*« (from Slovenian *ilovica*, clay) (Sušin 1964). The presence of chert skeleton in the soil determines the »*kremenica*« subtype, which forms on the Upper Cretaceous limestone containing chert nodules and sheets (Jurkovšek et al. 2013). The other form is »*ilovka*«, a clayey soil with or without a low chert skeleton content. Due to the presence of chert skeleton, »*kremenica*« has a higher sand content (average 21.6%) compared to »*ilovka*« (average 14.1%). The Rhodic Cambisols generally show evidence of illuvial processes.

In environments with higher precipitation rates, eluvial-illuvial processes play an important role in pedogenesis. The most evident process is the vertical translocation of clay, leading to the formation of an argic horizon. Luvisols are mainly found on plains protected from erosion and colluvial processes (Turniški and Grčman 2018). However, when they form in pockets and fissures on steeper slopes, Luvisols can also alternate with Eutric Cambisols, Leptosols and Phaeozems (Turniški 2024). Many Luvisols are also found on the Pliocene and Pleistocene sediments in the White Carniola (Turniški and Grčman 2018). In general, Luvisols consist mainly of clay and silty particles (Turniški and Grčman 2018). The average ratio of

clay in the illuvial horizon (Bt1) to that of the coarser-textured eluvial horizon is 1.6. Due to eluviation, Luvisols have lower average pH (4.7) and base saturation values (42.9%) compared to Leptosols, Phaeozems and Eutric Cambisols (Table 2). In general, Luvisols are poor in base cations. Due to their leaching into the lower horizons, the upper part of the Luvisols is usually dystric (base saturation < 50%). Higher values in the Bt horizons (Figure 4, Table 3) result from the accumulation of base cations and/or the influence of the carbonate parent material (Turniški et al. 2023). In some cases, higher concentrations of base cations in Oa/Ah and A horizons are due to biocycling (Čirič 1984). Sudden textural changes between the upper and lower horizons in some soil profiles indicate the presence of two-layered soils (Turniški et al. 2023), which are probably due to the aforementioned geological processes of material displacement during the Pleistocene. Distinguishing between originally related parent materials is challenging, but Turniški et al. (2023) suggested using element ratios to indicate different sources of soil material. The geochemical composition of the parent material is reflected in soil properties, as clearly evidenced by the differences in the proportions of Ca and Mg on the soil exchange complex between soils developed on limestone and dolomite. Since Ca plays a key role in the formation and stability of soil structural aggregates, differences in morphological characteristics could also be expected. However, such differences could not be evaluated within the framework of the soil map database.

4.2 Land use and human impact on soil properties

The favourable chemical properties of the soils on limestone and dolomite (Table 2) indicate their fertility and provide a solid basis for agriculture. The high cation exchange capacity (Table 2) reflects the high organic matter content in the O and A horizons and the high clay content in the B horizons. Both properties enable good retention of nutrients and water. The high content of base cations, i.e., calcium, magnesium and potassium, adsorbed on the soil colloids serves as a source of important plant nutrients (Weil and Brady 2017). A stable polyhedral soil structure allows water to percolate through the soil, which means that water stagnation rarely occurs in the soils despite the high clay and silt content. However, the initial neutral pH decreases in the subsequent stages of soil development due to the dissolution of carbonates and leaching (Turniški et al. 2023; see Table 2). This acidification would most likely have been buffered in cultivated areas through liming with carbonate-containing materials, which would have increased the pH value in the soil.

A large part of the Dinaric karst area has been classified as areas with natural or other specific constraints relevant for agricultural land use. This was demonstrated by additional soil surveys, mapping and soil analyses (Prus et al. 2017). The three main limitations to agricultural land use in the region are the shallow depth of the soils, their stoniness, and the karst geomorphology (Ciglič et al. 2012; see Figures 6a and 6b). Deeper soils only occur in alluvial plains and flats, in smaller and larger depressions such as dolines, poljes, and uvalas, and in subcutaneous cracks, channels, and scallops (Slabe and Hong 2009). Such karst forms act as traps for both aeolian (Sauro et al. 2009; Zupančič et al. 2018) and colluvial material (Gaiffe and Bruckert 1985), leading to the development of deep soils. For example, soils in dolines are often thicker with relatively silty upper horizons (Turniški 2024) and such soils provide favourable conditions for potential cultivation. Historically, some of these dolines were adapted for cultivation, also in the case of semicovered karst (Gams and Gabrovec 1999). The bottoms of dolines were levelled, and in some cases, additional soil material from the surroundings was added, creating a surface suitable for ploughing. In such cases, the properties of the original soils were altered, most notably in terms of soil depth. However, due to the limitations in the available data, it was not possible to assess systematic differences in the physical and chemical properties of these soils.

The vast majority of Leptosols and Phaeozems are covered by forest. The high proportion of stones and boulders on the surface of these soils generally prevents large-scale clearing or mowing and limits land use mainly to grazing. However, mowing is possible only in areas where stones have been systematically removed or where their presence on the soil surface is negligible. The few arable areas in the region are mainly associated with Eutric Cambisols or Luvisols. The relationship between soil properties and land use is a dynamic, two-way system (Verheyen et al. 2001). Agricultural land use alters the properties of the topsoil and influences various pedogenetic processes in the soil (see Table 3 and Figure 7). As shown in Figure 7, there are differences in pH, base saturation, CEC and organic matter content between forest and agricultural soils. In particular, the agricultural topsoils have a higher pH and base saturation than



BOŠTJAN MEDVED KARNIČAR, ROK TURNIŠKI

Figure 6: a, b) shallow soil with subsurface rockiness (hidden rockiness) and distinct epikarst forms, c) typical karst landscape with agricultural terraces on dolomite.

the forestry topsoils, with values of 5.9 and 65.7% compared to 5.5 and 59.3% (Figure 7). Conversely, organic matter content and CEC are lower in agricultural topsoils than in forest soils (Figure 7). This trend is expected as both ploughing and nitrogen fertilisation favour the mineralisation of organic matter, especially in the Oa and Ah horizons where organic matter is not stably bound to the mineral soil fraction (Blume et al. 2016). Agriculture also modifies the expression of eluvial-illuvial processes, with liming, fertilisation and ploughing obscuring the contrast between the eluvial E and illuvial Bt horizons (Table 3).

The use of fertilisers in the Dinaric karst region has not been intensive. As demonstrated in Figure 7, the content of plant-available phosphorous in the local topsoils remains low, on average less than 50 mg kg^{-1} soil, regardless of soil use. Phosphorous availability could be further reduced by its adsorption to iron oxides and aluminium hydroxides (Blume et al. 2016) (Figure 3). The content of plant-available potassium is naturally higher (140 mg kg^{-1}), originating from primary silicates and clay minerals. Further, the plant-available potassium content of agricultural topsoils is higher than that of forest soils. Rather than being associated with fertilisation, such high values are most likely correlated with the lower organic matter content and consequently higher mineral soil content of ploughed soils.

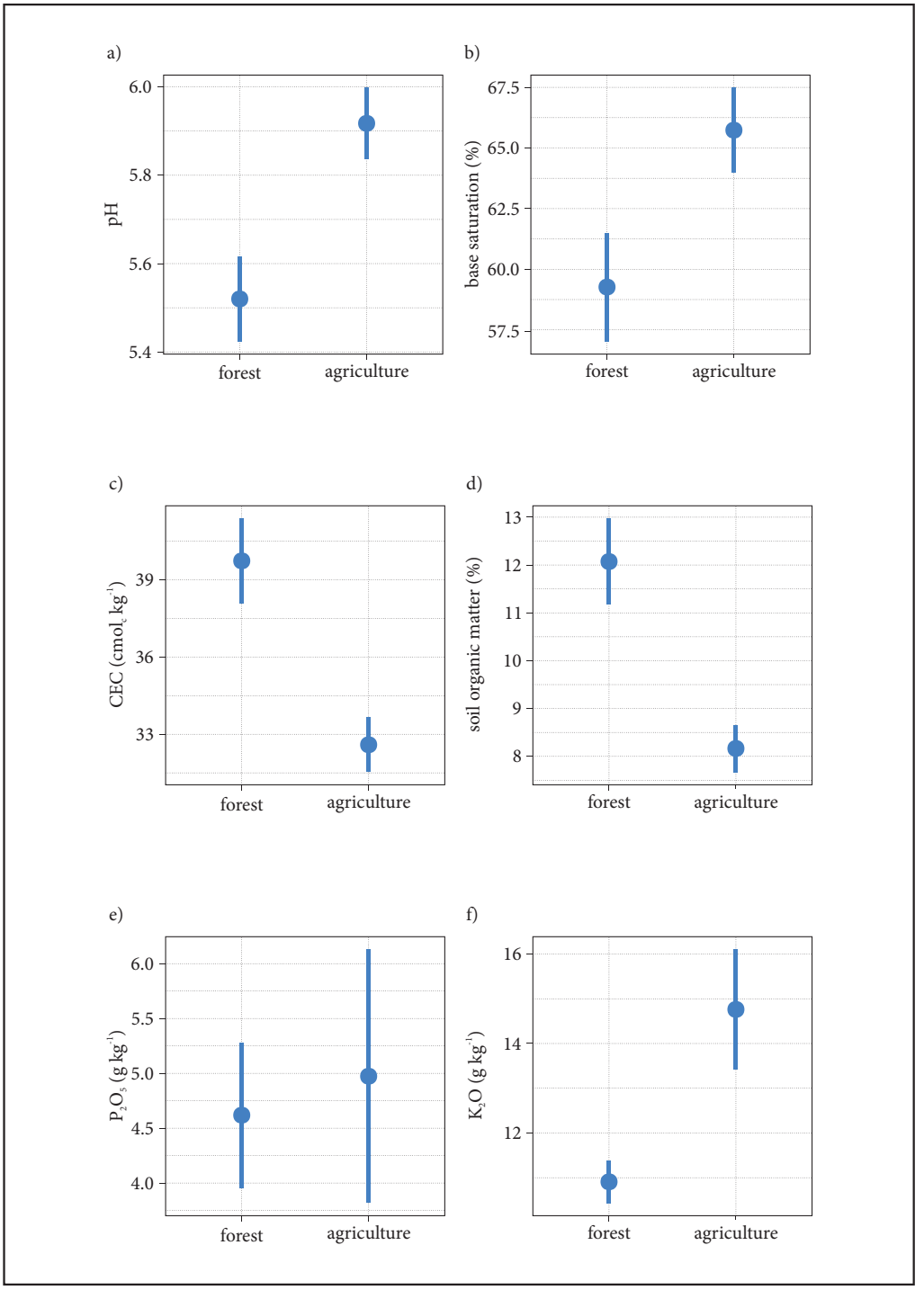


Figure 7: Mean values with standard errors for pH, base saturation, CEC, soil organic matter, plant-available phosphorous, and plant-available potassium in topsoils at 0–30 cm depth under forest (n = 131) and agricultural land (n = 121) in the Dinaric karst region.

5 Conclusion

The formation and development of soils is a complex spatio-temporal phenomenon involving various pedogenetic factors and processes. In the Dinaric karst region, the distinct chemical and physical weathering of limestone and dolomite affects the physiochemical properties of local soils. The variations in the depth and stoniness of the soils are mainly caused by the local sub-surface and surface topography, including variations in elevation, slope and exposure, which in turn influence the microclimate and the movement of water and soil masses on the slope. In places where mineral material accumulates, eluvial-illuvial processes are favoured under the influence of high precipitation, leading to the formation of argic horizons. The interplay of all these factors has contributed to the formation of the three predominant regional soil types: Leptosols and Phaeozems, Eutric Cambisols and Luvisols, which differ in their suitability for agriculture and other ecosystem services. A systematic review of the soil map database also revealed certain limitations in assessing the role of karst geomorphology in soil characteristics. To achieve a better understanding of these relationships, as well as to determine the extent and nature of anthropogenic influences on soil development, further research is required.

ACKNOWLEDGEMENT: This study was supported by the ARIS research program »Agroecosystems« (P4–0085) and the Infrastructure centre for soil and environmental protection (ARIS I0–0022–0481–06).

RESEARCH DATA: For information on the availability of research data related to the study, please visit the article webpage: https://doi.org/10.3986/AGS.14434.

6 References

Ažnik, M. 1975: Pomen fizikalno-kemičnih analiz tal za ocenjevanje produktivnih sposobnosti tal. *Report*. Biotehniška fakulteta UL.

Bavec, M., Pohar, V. 2009: Quaternary. In: The Geology of Slovenia. Geološki zavod Slovenije.

Beaudette, D. E., Roudier, P., O'Geen, A. T. 2013: Algorithms for quantitative pedology: A toolkit for soil scientists. *Computers & Geosciences* 52. https://doi.org/10.1016/j.cageo.2012.10.020

Blume, H. P., Brümmer, G. W., Fleige, H., Horn, R., Kandeler, E., Kögel-Knabner, I., Kretzschmar, R. et al. 2016: Scheffer/Schachtschabel soil science. Springer. https://doi.org/10.1007/978–3–642–30942–7

Birkeland, P. W. 1999: Soils and geomorphology. Oxford University Press.

Burt, R. (ed.) 1992: Soil survey laboratory methods manual. Soil survey investigations report No. 42, Version 2.0. *Report*. United States Department of Agriculture, Natural Resources Conservation Service.

Ciglič, R., Hrvatin, M., Komac, B., Perko, D. 2012: Karst as a criterion for defining areas less suitable for agriculture. *Acta geographica Slovenica* 52–1. https://doi.org/10.3986/AGS52103

Costantini, A. C. E., Carnicelli, S., Sauer, D., Priori, S., Andreetta, A., Kadereit, A., Lorenzetti, R. 2018: Loess in Italy: Genesis, characteristics and occurrence. *Catena* 168. https://doi.org/10.1016/j.catena.2018.02.002

Čirič, M. 1984: Pedologija. Svjetlost.

Duchaufour, P. 1982: Pedology – Pedogenesis and classification. George Allen & Unwin.

Dozet, S., Pleničar, M. 2009: Splošni uvod v mezozoik. In: Geologija Slovenije. Geološki zavod Slovenije.

Durn, G., Perković, I., Stummeyer, J., Ottner, F., Mileusnić, M. 2021: Differences in the behaviour of trace and rare-earth elements in oxidizing and reducing soil environments: Case study of Terra Rossa soils and Cretaceous palaeosols from the Istrian peninsula, Croatia. *Chemosphere* 283. https://doi.org/10.1016/j.chemosphere.2021.131286

Durn, G., Perković, I., Razum, I., Ottner, F., Škapin, S., Faivre, S., Beloša, L. et al. 2023: A tropical soil (Lixisols) identified in the northernmost part of the Mediterranean (Istria, Croatia). *Catena* 228. https://doi.org/10.1016/j.catena.2023.107144

Egnér, H., Riehm, H., Domingo, W. R. 1960: Investigations on the chemical soil analysis as a basis for assessing the soil nutrient status II. Chemical extraction methods for phosphorus and potassium determination. *Kungliga Lantbrukshügskolans Annaler* 26.

Gaiffe, M., Bruckert, B. 1985: Analyse des transports de matieres et des processus pedogenetiques impliques dans les chaines de sols du karst Jurassien. In: Soils and geomorphology. *Catena supplement* 6. Catena Verlag.

Gams, I., Gabrovec, M. 1999: Land use and human impact in the Dinaric karst. *International Journal of Speleology* 28–1. https://doi.org/10.5038/1827–806X.28.1.4
Gams, I. 2004: Kras v Sloveniji v prostoru in času. Založba ZRC.
Gregorič, V. 1965: Nastanek tal na triadnih dolomitih. *Ph.D. thesis*. Univerza v Ljubljani.
Infrastrukturni center za pedologijo in varstvo okolja (ICPVO), Biotehniška fakulteta, Univerza v Ljubljani 2023: Pedološka karta Slovenije 1 : 25.000. *1:25,000 map*.
Jurkovšek, B., Cvetko Tešović, B., Kolar-Jurkovšek, T. 2013: Geologija krasa. Geološki zavod Slovenije.
Knez, M., Kranjc, A. 2009: Karst. In: The geology of Slovenia. Geološki zavod Slovenije.
Lobnik, F. 1978: Dinamika mangana v nekaterih rjavih pokarbonatnih tleh v Sloveniji. *Ph.D. thesis*. Univerza v Ljubljani.
Markič, M. 2009: Pliocene and Plio-quaternary. In: The Geology of Slovenia. Geološki zavod Slovenije.
Mihevc A., Prelovšek M. 2010: Georaphical position and general overview. In: Introduction to the Dinaric karst. Inštitut za raziskovanje krasa ZRC SAZU. https://doi.org/10.3986/9789612541989
Ministry of Agriculture, Forestry and Food 2021: Grafični podatki RABA za celo Slovenijo. *Dataset*.
Ogorelec B., Rothe P. 1992: Mikrofazies, Diagenese und Geochemie des Dachsteinkalkes und Hauptdolomits in Süd-West-Slowenien. *Geologija* 35. https://doi.org/10.5474/geologija.1992.005
Ogrin, D. 1996: Podnebni tipi v Sloveniji. *Geografski vestnik* 68.
Pleničar M., Dozet S. 1993: Contribution to the knowledge of Upper Cretaceous beds in Kočevje and Gorski Kotor Area (NW Dinarides). *Geologija* 36. https://doi.org/10.5474/geologija.1994.008
Prus, T., Kralj, T., Vrščaj, B., Zupan, M., Grčman, H. 2015: Slovenska klasifikacija tal. *Guidelines.* Biotehniška fakulteta.
Prus, T., Turniški, R., Zupan, M. 2017: Preveritev podatkov pedološke karte na terenu za območja z omejenimi možnostmi za kmetijsko dejavnost v Sloveniji v okviru izvedbe reforme OMD 2017. *Report.* Biotehniška fakulteta.
R Foundation for Statistical Computing, R Core Team 2023: R: A language and environment for statistical computing (4.2.3). *Computer software*.
Sauro, U., Francese, R., Ferrarese, F., Miola, A., Mozzi, P., Rondo, G.Q., Trombino, L., Valentini, G. 2009: Doline fills – Case study of the Faverghera Plateau (Venetian Pre-Alps, Italy). *Acta Carsologica* 38–1. https://doi.org/10.3986/ac.v38i1.136
Slabe, T., Hong, L. 2009: Significant subsoil rock forms. In: Karst Rock Features: Karren Sculpturing. Založba ZRC. https://doi.org/10.3986/9789610502968
Stepančič, D. 1972: Morfološke in pedodinamske značilnosti rendzine na dolomitu. *Report*. Biotehniška fakulteta.
Stepančič, D., Ažnik, M. 1976: Talne preiskave vinogradniških površin pri Komnu na Krasu. *Report*. Biotehniška fakulteta.
Stepančič, D. 1978: Poročilo o pedološkem pregledu kmetijskega zemljišča pri Brestovici na Krasu. *Report*. Biotehniška fakulteta.
Stepančič, D., Lobnik F. 1985: Komentar k listu Ljubljana. Biotehniška fakulteta.
Schwertmann, U., Murad, E., Schulze D. G. 1982: Is there Holocene reddening (hematite formation) in soils of axeric temperate areas? *Geoderma* 27–3. https://doi.org/10.1016/0016–7061(82)90031–3
Stritar, A. 1967: Novi putovi kultiviranja i promjene u tlu Belokranjskih vriština. *Zemljište i biljka* 16.
Stritar, A. 1972: Raba in izkoriščanje rendzine na dolomitu. *Report*. Biotehniška fakulteta.
Stritar, A. 1990: Krajina, krajinski sistemi; Raba in varstvo tal v Sloveniji. Partizanska knjiga.
Suhadolc, M., Črepinšek Z. 2018: Temperaturna odvisnost razgradnje opada v tleh travnikov v zaraščanju. *Acta agriculturae Slovenica* 111–1. https://doi.org/10.14720/aas.2018.111.1.18
Sušin, J. 1964: Doprinos k poznavanju terra rosse v Slovenskem primorju. *Ph.D. thesis*. Univerza v Ljubljani.
Sušin, J. 1972: Teksturna diferenciacija in barvna različnost pokarbonatnih rjavih izpranih tal. *Zbornik Biotehniške fakultete Univerze v Ljubljani* 19.
Torrent, J., Pfeiffer M., Ibánez, J. J. 2023: Soils from a warm-temperate semi-tropical ecozone (Mediterranean) with humid winter months. In: Encyclopedia of Soils in the Environment (Second Edition). Elsevier. https://doi.org/10.1016/B978–0–12–822974–3.00048–3
Turniški, R., Grčman, H. 2018: Izprana tla v Sloveniji: pedološke lastnosti, prostorska razporeditev in klasifikacija. *Acta agriculturae Slovenica* 111–1. http://doi.org/10.14720/aas.2018.111.1.12

Turniški, R., Grčman, H., Zupan, M. 2022: Understanding the »acric« Illuvial soils in Slovenian soil classification in relation to Acrisols. *Geoderma Regional* 29. https://doi.org/10.1016/j.geodrs.2022.e00522

Turniški, R., Zupančič, N., Grčman, H. 2023: Geochemical evidence of illuvial processes in clay-rich soils on limestones in a humid temperate climate. *Geoderma* 429. https://doi.org/10.1016/j.geoderma.2022.116266

Turniški, R. 2024: Geokemične in mineralne lastnosti tal kot kazalniki eluvialno-iluvialnih procesov in izvora tal na apnencih. *Ph.D. thesis*. Univerza v Ljubljani.

Verheyen, K., Bossuyt, B., Hermy, M., Tack, G. 2001: The land use history (1278–1990) of a mixed hardwood forest in western Belgium and its relationship with chemical soil characteristics. *Journal of Biogeogeography* 26–5. https://doi.org/10.1046/j.1365–2699.1999.00340.x

Vidic, N. J., Prus, T., Grčman, H. Zupan, M., Lisec, A., Kralj, T., Vrščaj, B. et al. 2015: Soils of Slovenia with soil map 1:250,000. European Commission Joint Research Centre (JRC), Publications Office of the European Union. https://doi.org/10.2788/88750

Weil, R. R., Brady, N. C. 2017: The nature and properties of soils. Pearson.

Wickham, H. 2016: ggplot2: Elegant Graphics for Data Analysis, Second edition. Springer-Verlag.

Zorn, M., Ferk, M., Lipar, M., Komac, B., Tičar, J., Hrvatin, M. 2020: Landforms of Slovenia. In: The Geography of Slovenia: Small But Diverse. *World Regional Geography Book Series*. Springer. https://doi.org/10.1007/978–3–030–14066–3_3

Zupan Hajna, N. 2014: Nepopolno raztapljanje karbonatnih kamnin v kraških jamah Slovenije. Založba ZRC. https://doi.org/10.3986/9789612546724

Zupančič, N., Turniški, R., Miler, M., Grčman, H. 2018: Geochemical fingerprint of insoluble material in soil on different limestone formations. *Catena* 170. https://doi.org/10.1016/j.catena.2018.05.040

Acta geographica Slovenica, 66-1, 2026, 39–59

HIERARCHICAL CLUSTER CLASSIFICATION AND ANALYSIS OF CIRQUES IN SLOVENIAN ALPS

Klemen Cof, Uroš Stepišnik, Manja Žebre, Matej Lipar



URO̍ STEPIŠNIK

The cirque under Mount Mangrt, Julian Alps.

DOI: https://doi.org/10.3986/AGS.14012
UDC: 551.435.42(497.4)(234.3)
Creative Commons CC BY–SA 4.0

Klemen Cof[1], Uroš Stepišnik[1], Manja Žebre[2], Matej Lipar[3]

Hierarchical cluster classification and analysis of cirques in Slovenian Alps

ABSTRACT: This paper presents a morphometry-based classification of cirques in Slovenia in the southeast European Alps. The classification was performed using a hierarchical cluster analysis and verified using ANOVA, Kruskal-Wallis, Watson's U^2 and Chi-square tests. 86 Slovenian cirques were categorized into five cirque types. Type 1, 2, 3 and 5 cirques indicate a formation by high-altitude (1800–2000 m) glaciers under varying conditions and on varied aspects (NNW, W, SE, E). Type 4 cirques indicate a formation by low-altitude (1500–1800 m) glaciers in areas of marginal glaciation on northeast aspects. This classification provides a rapid and consistent method of partitioning new cirque populations and offers a preliminary insight into the cirque population and palaeoclimate properties of Slovenia.

KEYWORDS: glacial geomorphology, cirques, hierarchical cluster analysis, analysis of variance, Slovenia, southeast European Alps

Hierarhično razvrščanje in analiza krnic v slovenskih Alpah

POVZETEK: V članku je predstavljena klasifikacija slovenskih krnic v jugovzhodnih evropskih Alpah na osnovi morfometričnih podatkov. Klasifikacija je bila izvedena s hierarhično metodo razvrščanja in nato preverjena z analizo variance ter testi Kruskal-Wallis, Watsonov U^2 in Hi-kvadrat. 86 slovenskih krnic je bilo razdeljenih v pet krniških tipov. Krniške tipe 1, 2, 3 in 5 so oblikovali ledeniki na visokih nadmorskih višinah (1800–2000 m) pod različnimi pogoji in na različnih ekspozicijah (SSZ, Z, JV, V). Krniški tip 4 so oblikovali ledeniki na nižjih nadmorskih višinah (1500–1800 m) na območjih robne poledenitve na severovzhodnih ekspozicijah. Klasifikacija nudi hitro in dosledno metodo deljenja novih krniških populacij in nudi prvi vpogled v krniško populacijo in paleopodnebne razmere v Sloveniji.

KLJUČNE BESEDE: glacialna geomorfologija, krnice, hierarhična metoda razvrščanja, analiza variance, Slovenija, jugovzhodne evropske Alpe

The article was submitted for publication on November 28th, 2024.
Uredništvo je prejelo prispevek 28. novembra 2024.

[1] University of Ljubljana, Faculty of Arts, Ljubljana, Slovenia
[2] Geological Survey of Slovenia, Ljubljana, Slovenia
[3] Research Centre of the Slovenian Academy of Sciences and Arts, Ljubljana, Slovenia

cof.nagrand@gmail.com (https://orcid.org/0009–0003–7478–6050), uros.stepisnik@gmail.com (https://orcid.org/0000–0002–8475–8630), manja.zebre@geo–zs.si (https://orcid.org/0000–0001–6772–2866), matej.lipar@zrc–sazu.si (https://orcid.org/0000–0003–4414–0147)

1 Introduction

Former mountain glaciers and their responses to past climate changes are valuable analogues for predicting how modern glacial environments may respond to future climate change (Knight and Harrison 2014). However, reconstructing former mountain glaciers to draw conclusions about past environmental conditions is a challenging task, especially when the glacial source area relationship is not straightforward (Carr and Coleman 2007). Cirques, however, tend to have a very well-defined glacial area and have often been used as palaeoenvironmental proxies based on their morphology and morphometry, particularly in remote and inaccessible regions where other proxies may be limited or non-existent (e.g., Evans 2006b; Barr and Spagnolo 2013; Barr and Spagnolo 2015; Barr et al. 2017).

Cirques are concave hollows formed by glacial erosion with gently sloping floors bounded upstream by an arcuate steep headwall. Downstream they often have a reverse slope called a cirque threshold (Barr and Spagnolo 2015). The cirque floor is often overdeepened under the altitude of the cirque threshold (Evans 1997). Cirques typically form beneath mountain ridges at elevated altitudes (Evans 2006a), preferring shaded poleward aspects unless other factors (e.g., precipitation, bedrock, winds, weathering and chemical denudation) compensate for increased ablation due to exposure to solar radiation (Evans and McClean 1995; Coleman et al. 2009; Barr et al. 2017; Steinemann et al. 2020). It is specified that for a feature to be classified as a cirque, it should have headwall slopes exceeding 35° and floor slopes less than 20° in at least some sections (Evans and Cox 1974).

Cirques form mainly during the early and late stages of glaciation when glaciers are confined to their cirques (Barr and Spagnolo 2015) and when the equilibrium lines are located at the altitudes of cirque floors, leading to maximized subglacial erosion and the development of overdeepened cirques (Mitchell and Montgomery 2006). During glacial maxima, equilibrium line altitudes (ELAs) fall below the altitude of cirque floors and the glacial ice within cirques either becomes frozen to its bed or flows down valley into glacial troughs – both cases mean a reduction in subglacial erosion and a shift towards shallower cirques (Barr and Spagnolo 2015; Dixon et al. 2016).

Classification partitions data into distinct subgroups according to shared characteristics (Gareth et al. 2013). Historically, the classification of cirques has been predominantly based either on morphological characteristics (e.g., Penck 1905; Vilborg 1984; Evans and Cox 1995) or key geomorphic processes (e.g., Evans and Cox 1974). However, these earlier classifications relied heavily on the subjective judgement of researchers to properly apply to new cirque populations. They required each new cirque to be examined in detail to determine its origin and underlying geomorphic processes before it could be classified, thus limiting the practicality of these classifications. A cirque classification based on morphometric variables would allow for rapid, objective, and automatic differentiation of entire cirque populations.

The aim of this paper is to create such a statistically verifiable cirque classification based on key morphometric cirque variables. Slovenia was used as the study area because its distinct cirque shapes indicate a good degree of segmentation in the population to test the classification on. At the same time, Slovenia's cirque population has yet to be systematically explored, which makes classification an essential first step in determining the existing cirque types and focusing field work into the most typical cirques of each type. It helps in determining the feasibility of various field analyses for individual cirque types and will allow for a systematic and thorough analysis of the factors that influenced the formation of Slovenia's cirque population.

2 Material and methods

2.1 Regional setting

Slovenia is located in a unique geographical position at the junction of the European Alps, the Pannonian Basin, the Dinaric Alps and the Mediterranean Sea (Perko et al. 2021), creating a diverse climate across its mountainous regions. The southwestern areas of Slovenia are influenced by a moderate Mediterranean climate, while the northwestern mountainous regions experience a mountain climate. This climate is marked by winter temperatures below –3°C and summer temperatures below or slightly above 10°C, depending on altitude (Komac et al. 2020; Ogrin et al. 2023). The mountainous region is composed mainly of limestones

and dolomites which are mostly a combination of Upper Triassic rocks of the Julian Carbonate Platform to the north and Mesozoic rocks of the Slovenian Basin to the south. The eastern parts of the Karawanks are partially comprised of Palaeozoic limestones, sandstones, and flysch shales. Many valleys and basins are covered by Quaternary carbonate deposits of glacial, fluvial and colluvial origin. The Periadriatic fault crosses the northeast part of the Kamnik-Savinja Alps while the Julian Alps are intersected by the Sava, Ravne and Idrija faults from north to south (Hrvatin et al. 2020).

Despite having relatively low altitudes compared to the other parts of the Alps, several mountainous regions of Slovenia (the Julian Alps, the Karawanks and the Kamnik-Savinja Alps) were glaciated during the last glacial maximum (LGM) (Figure 1). Large glaciers formed in the Soča and Sava valleys as well as the Bohinj basin in the Julian Alps. The reported ELAs using the toe-to-headwall altitude ratio method for these three glaciers were between 1090 m a.s.l. and 1280 m a.s.l. and the glaciers extended to altitudes as low as 500 m a.s.l. with a thickness of up to 700 m (Ferk et al. 2017; Hughes et al. 2021). Several smaller valleys in all three mountain ranges were glaciated while a smaller ice cap formed on the Kanin Plateau in the west. Cirques formed at higher altitudes of all three mountain ranges (Bavec 2001; Stojilković et al. 2013). The two Dinaric plateaus Snežnik in the south and Trnovski gozd in the west of Slovenia were also glaciated, and there is evidence of marginal glaciation in the Pohorje Hills in the northeast (Natek 2007; Žebre et al. 2013; Žebre and Stepišnik 2016; Kodelja et al. 2018). Due to a high intensity of postglacial erosion and denudation, many glaciogenic forms and sediments have been eroded or redeposited. Additionally, very few of the moraines have been dated. This makes the present knowledge of the LGM ice position in Slovenia inconclusive (Bavec and Verbič 2004; Hughes et al. 2021).

2.2 Detection of cirques

The process of cirque detection was conducted manually in the ESRI ArcGIS Pro software, using three data sources: high-resolution Lidar surface data (1 m × 1 m) from the Slovenian Environment Agency (2015),

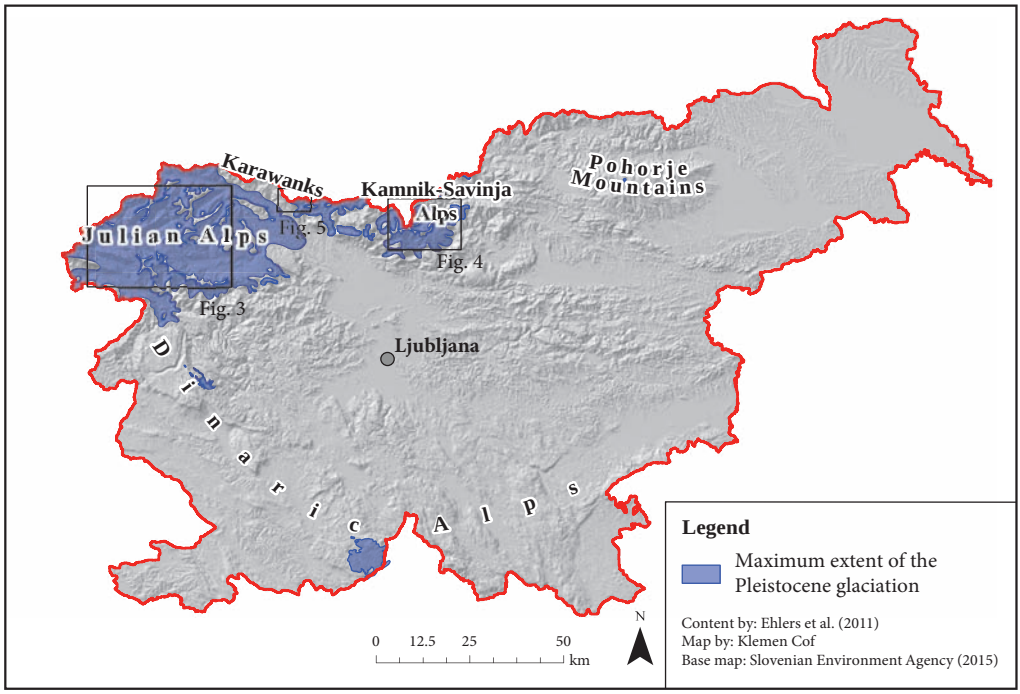


Figure 1: The maximum extent of the Pleistocene glaciation in Slovenia. Source of data: Ehlers et al. (2011); Slovenian Environment Agency (2015).

along with digital elevation models (DEMs) at resolutions of 5 m × 5 m and 12.5 m × 12.5 m provided by the Surveying and Mapping Authority of the Republic of Slovenia (2016a; 2016b). From the Lidar dataset, shaded relief was derived to enhance the visualization of topography, while the DEMs facilitated the extraction of slope and surface closure information (both plan and profile views). To mitigate data anomalies, the 5 m × 5 m DEM was smoothed using a 3 × 3 cell low pass filter. The 5 m × 5 m DEM was used over Lidar data for extracting slope data since the latter is too precise and more suited to small-scale analyses of individual cirques as opposed to broader analyses of cirque populations. Similarly, the 12.5 m × 12.5 m DEM was used for plan and profile closure extraction as the 5 m × 5 m data was too detailed to distinguish major ridges and gulleys. The following variables were used in the detection:

- Location: landforms at altitudes above 1100 m a.s.l. and relatively close to mountain ridges were considered, since cirques typically form only at the highest altitudes along mountain tops and ridges and since regional ELAs were reported at altitudes of 1090–1280 m a.s.l. (Ferk et al. 2017);
- Shape: in accordance with the definition, this research took into consideration concave landforms with a steep wall arcing around a flat floor that was open down-valley. Landforms with a height or diameter of less than 100 m were excluded as nivation hollows or niche glaciers (Evans and Cox 1974; Singh et al. 2011; Barr and Spagnolo 2015; Gutiérrez and Gutiérrez 2016);
- Slope: landforms with minimal floor slopes under 20° and maximal headwall slopes above 31–35° were considered. Gentler floor slopes are typical for cirques developed by a rotationally flowing glacier while headwall slopes steeper than talus slopes are indicative of more intense glacial erosion. Steeper headwall slopes separate cirques from nivation hollows. 26.6° was chosen as the slope threshold between headwalls and floors (Evans and Cox 1974; Evans 2006a; Barr and Spagnolo 2015);
- Plan and profile curvature: useful for accurate delineation of cirque extents. Where thresholds were absent, plan curvature was used to identify the spurs of the headwall to define the downward extent. Where profile closure did not show a clear upward extent, it was extended up to the cirque's overlying ridges. Landforms with a plan closure of less than 90° were excluded as nivation hollows (Hughes et al. 2007; Ardelean et al. 2013; Barr et al. 2017; Spagnolo et al. 2017).

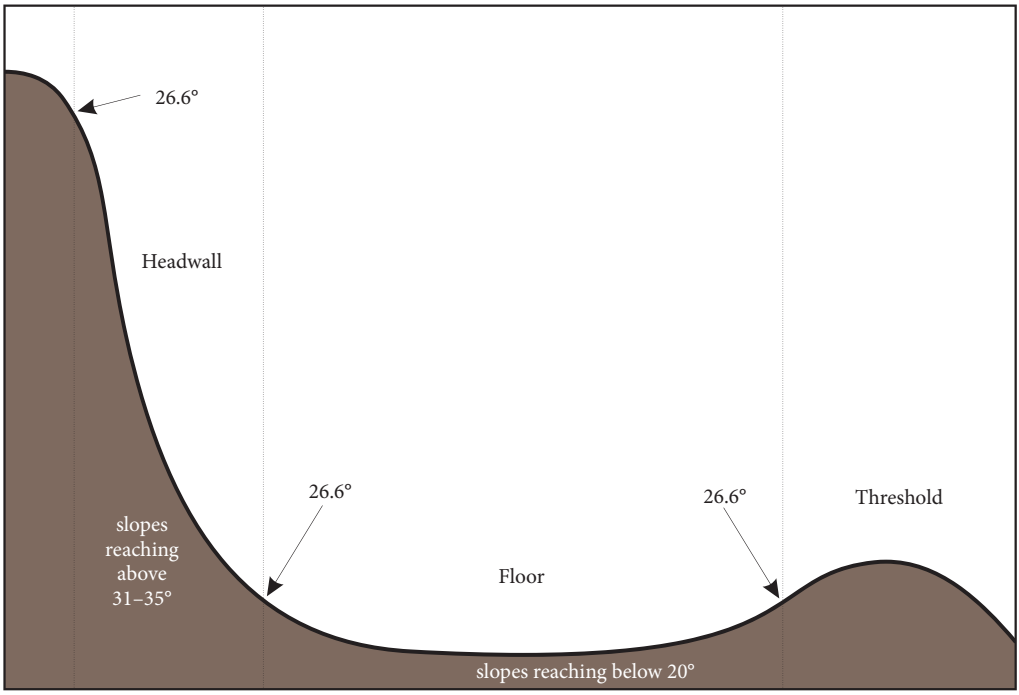


Figure 2: Schematic of a typical cirque's cross section.

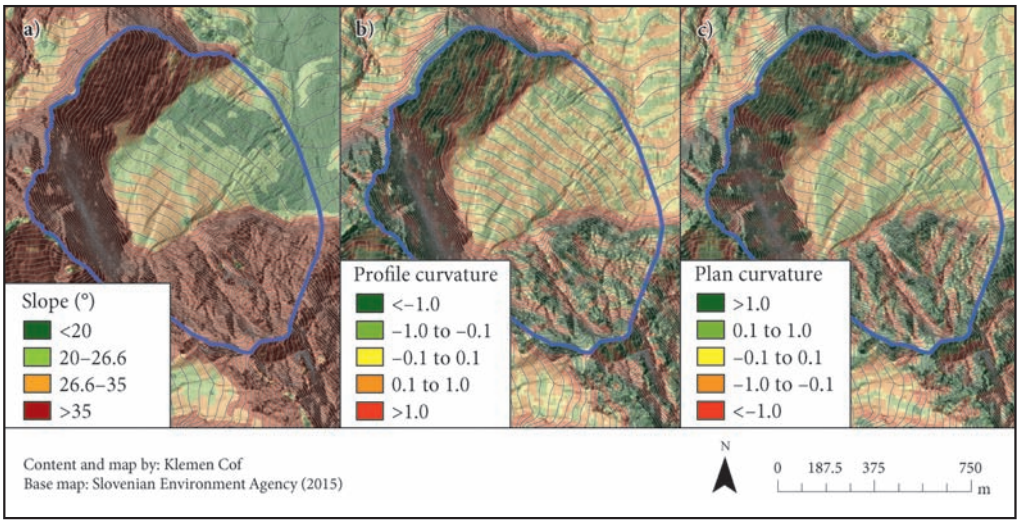


Figure 3: Example of cirque floor delineation. (A) Reclassified slope data and 20 m contours help delineate the cirque floor/headwall boundary. (B) Reclassified profile curvature data helps delineate the upward extent. (C) Reclassified plan curvature data helps delineate the spurs of the headwall.

Cirque delineation also involved separating the cirques into their respective cirque floors, headwalls, and thresholds based on their slopes (Figure 2) as well as the calculation of cirque threshold midpoints using the »Generate points along lines« function in ArcGIS. Figure 3 shows how various variables were used in the delineation of a sample cirque.

2.3 Morphometric analysis

For the analyses of the detected cirques, 14 morphometric variables were calculated, utilizing both manual techniques and the automated toolbox provided by Spagnolo et al. (2017). Table 1 shows the variables and their methods of calculation.

2.4 Classification

To classify the cirques a hierarchical cluster analysis was performed using the IBM SPSS Statistics 21 software, which was also used for many of the statistical analyses in the research. Hierarchical clustering does not require a predetermined number of clusters (Gareth et al. 2013), but is an exploratory method whose results require further validation (IBM 2021). Variables were standardized into Z scores to equalize the impact of variables with different value ranges (Zhenhua 2011).

Multiple sets of variables that cover key variables of cirques (see chapter 2.3) were entered into the analysis in a way that would enable the resulting classification to differentiate between cirques according to those variables (Barr and Spagnolo 2015). To properly include median axis aspect into the classification, its values were transformed into Cartesian coordinates using sine and cosine components (Mardia and Jupp 1999). All variables were standardized into Z scores and checked for collinearities using collinearity diagnostics (minimal variance inflation factors and condition indices). Several clustering methods (between-groups, within-groups, nearest neighbour, furthest neighbour, Ward's) were used for each set of variables (Gareth et al. 2013). A method was discarded if its dendrogram contained classes with only 1–3 cases at the first or second possible cut-off point, otherwise a range of 3–6 potential solutions was derived from the dendrogram and used to generate cluster membership for that clustering method.

Table 1: Calculated morphometric variables.

Morphometric variable	Method of calculation	Reference
Minimum floor altitude	Minimum of altitude values for all cirque pixels	Spagnolo et al. (2017)
Length (L) [a]	The length of the cirque median axis	Spagnolo et al. (2017)
Width (W)	The length of the line perpendicular to the median axis at its midpoint	Spagnolo et al. (2017)
Height (H)	Difference between maximum and minimum altitude	Spagnolo et al. (2017)
L/W ratio	Ratio between length and width	Barr and Spagnolo (2015)
L/H ratio	Ratio between length and height	Barr and Spagnolo (2015)
W/H ratio	Ratio between width and height	Barr and Spagnolo (2015)
Cubic size [b]	$\sqrt[3]{LWH}$	Evans (2006a)
Perimeter (O)	ArcGIS function »Perimeter length«	Spagnolo et al. (2017)
Circularity [c]	O/O_c	Aniya and Welch (1981)
Median axis slope [d]	arctan(Amp/L)	Evans and Cox (1995)
Median axis aspect	Bearing of the cirque median axis	Mîndrescu and Evans (2014)
Plan closure [e]	$360° - (\gamma_{max} - \gamma_{min})$	Hughes et al. (2007); Spagnolo et al. (2017)
Profile closure [f]	$\beta_{max} - \beta_{min}$	Hughes et al. (2007)

[a] A line that connects the cirque threshold midpoint with the top of its headwall and separates the cirque into two parts with an equal surface area. [b] Where L is the length, W the width and H the height of the cirque. [c] Where O is the cirque perimeter and Oc is the perimeter of a circle with the same surface area as the cirque. [d] Where Amp is the altitude range of the median axis and L its length. [e] Where γ_{max} and γ_{min} are the maximum and minimum aspect of the cirque headwall measured towards the cirque centroid at the mean cirque altitude. [f] Where β_{max} is the maximum slope of the cirque headwall and β_{min} the minimum slope of the cirque floor.

2.5 Analysis of variance

Each obtained classification was analysed for the statistical significance of the differences between its classes using the analysis of variance (ANOVA). This analysis has four assumptions: the variables used are on an interval or ratio scale, the variances within the groups are equal and the data for individual groups are independent from one another and normally distributed within each category (Rogerson 2001; IBM 2022). Normality of distribution in all groups was tested using the Kolmogorov-Smirnov statistical test while homogeneity of variances between groups was tested using the Levene test (Rogerson 2001; Field 2013).

Variables were not transformed to satisfy the assumptions of this analysis in order to preserve interpretability, but due to its robustness the ANOVA was still used since some of the assumptions can be violated (Field 2013). For variables with a normal distribution and no homogeneity of variances, the ANOVA's F-test was replaced with the more robust Welch F-test and followed up with the Games-Howell post hoc test, which accounts for both uneven category sizes and heterogenous variances (IBM 2022). For variables with non-normal distributions a non-parametric Kruskal-Wallis test was performed instead since ANOVA is sensitive to violations of the normality of distribution assumption in the case of very unequal group sizes (Field 2013). The omnibus tests were followed up by pairwise comparisons: the Games-Howell post hoc test if the Welch F-test was applied and the Dunn post hoc test with Bonferroni correction if the Kruskal-Wallis test was applied.

2.6 Circular statistics

Circular data were analysed using the R package 'circular' (Agostinelli and Lund 2025; R Foundation … 2025). To analyse circular data across classes, mean directions (φ) and mean resultant lengths ($\bar{R}$) were calculated. The mean directions were assessed for statistical significance using the Rayleigh test (Fisher 1993; Mardia and Jupp 1999). To test for differences between mean directions, the Mardia-Watson-Wheeler test was applied first (Batschelet 1981), followed by pairwise comparisons using the Watson's U^2 test (Watson 1962) with Stephens' correction (Stephens 1970) and Holm-Bonferroni correction, to control for familywise error (Holm 1979). Both tests assume continuous circular distributions and a lack of ties between samples (Batschelet 1981).

2.7 Chi-square tests

Two categorical variables were also analysed: the presence of a cirque threshold and lithology. For both, the Pearson Chi-square test was used to determine potential correlations between cirque type membership and the variable values. The main assumptions of the analysis are: the variables used are categorical, all the observations are independent from one another, each unit can belong to only one cell in the contingency table and the expected count of at least 80% of the cells in the contingency table must be equal to or greater than 5 with no single cell having an expected count of less than 1 (Field 2013). If the last assumption was violated, the Fisher exact test was interpreted instead due to its accuracy with small samples (Fisher 1922). To assess the strength of statistically significant correlations Cramer's V was used (Field 2013). Cirque thresholds were identified using the ArcGIS function »Fill« and the 12.5 m × 12.5 m DEM since it is more hydrologically accurate than its 5 m × 5 m counterpart (Surveying and Mapping Authority of the Republic of Slovenia 2016b). Lithological data were obtained from a version of the lithostratigraphic map made by the Geological Survey of Slovenia (2007) and modified by Hrvatin (2016).

3 Results

3.1 Detection of cirques

Using the predetermined slope and closure thresholds and adhering to the known data on glaciation locations, a total of 86 cirques were manually delineated for the purpose of this research. In the Slovenian part of the Julian Alps (Figure 4), two larger groups of cirques can be observed, one on the ridge between the

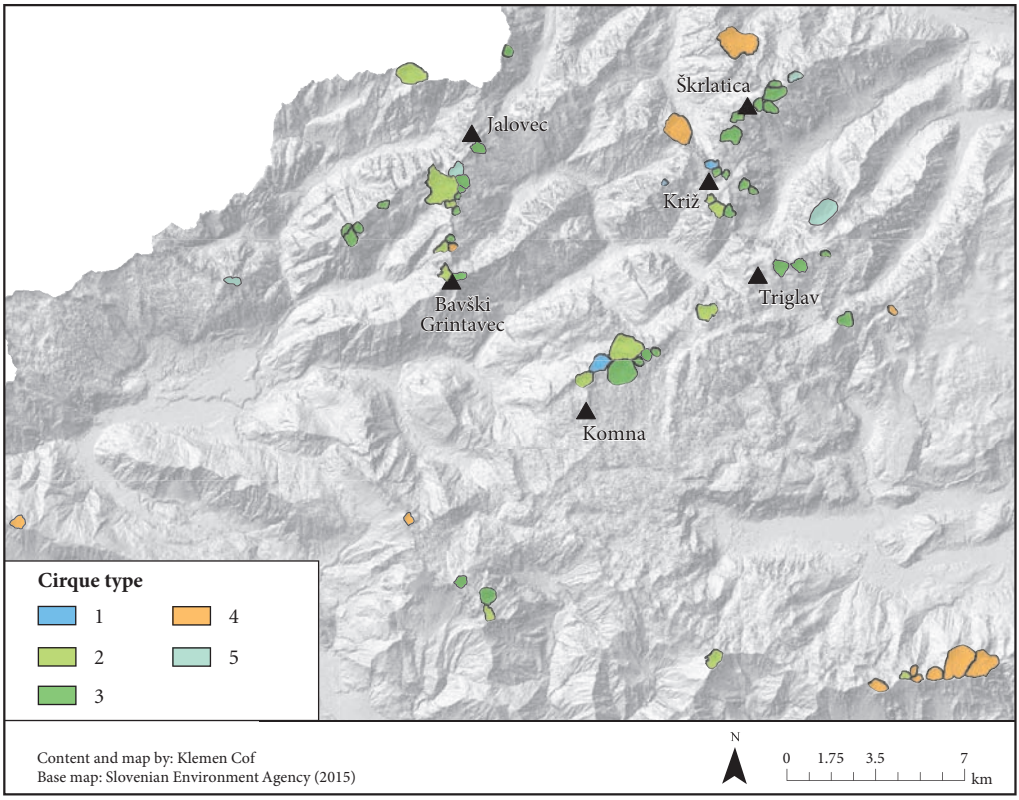


Figure 4: Spatial distribution of cirque types in the Slovenian part of the Julian Alps. See Figure 1 for location in Slovenia.

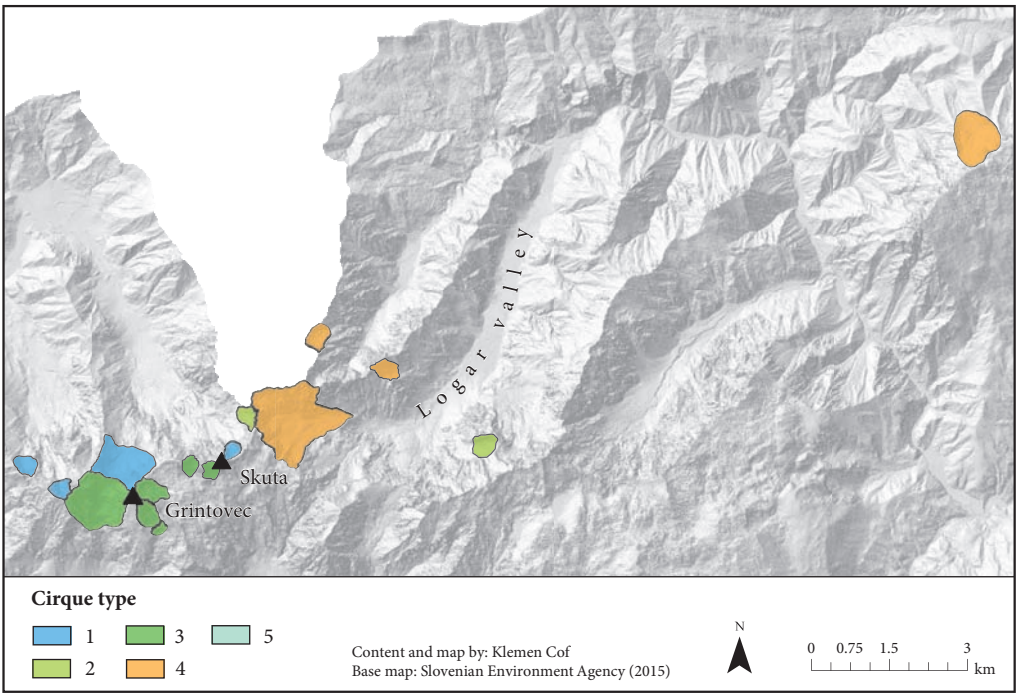


Figure 5: Spatial distribution of cirque types in the Kamnik-Savinja Alps. See Figure 1 for location in Slovenia.

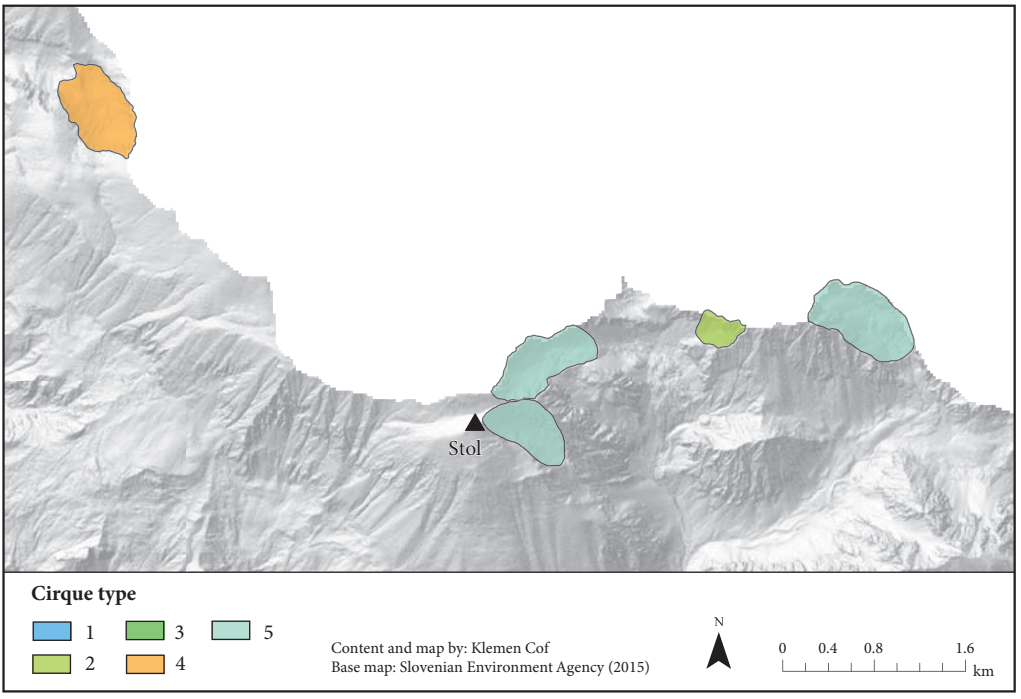


Figure 6: Spatial distribution of cirque types in the Slovenian part of the Karawanks. See Figure 1 for location in Slovenia.

peaks of Mount Bavški Grintavec and Mount Jalovec, and one scattered across the Škrlatica, Križ and Triglav plateaus and the northern fringes of the Komna Plateau. In the Kamnik-Savinja Alps, the cirques are mainly located underneath the peaks of Mount Grintovec and Mount Skuta with a few in the upper reaches of the Logar Valley (Figure 5). In the Slovenian part of the Karawanks, the cirques are located underneath several mountain ridges around Mount Stol (Figure 6). The information about cirque types in Figures 4 through 6 is presented in the subsequent chapter.

3.2 Classification

In the presented classification five cirque variables were used: minimum cirque floor altitude, L/W ratio, median axis slope, the sine and cosine Cartesian coordinates of median axis aspect, and plan closure, resulting in a total of six variables with an insignificant amount of collinearity.

The presented classification was performed using the Ward's Linkage clustering method. From the dendrogram several cut-off points were selected with the one resulting in 5 cirque types yielding the best results. The numbers of cirques in each cirque type across the population and in individual mountain ranges are shown in Table 2. Figures 4 through 6 show the spatial distribution of various cirque types across the Slovenian mountainous regions.

Table 2: Number of cirques of each cirque type in the population and individual mountain ranges, obtained with the presented classification.

Cirque type	Total population	Julian Alps	Kamnik-Savinja Alps	Karawanks
1	7	3	4	0
2	16	13	2	1
3	39	33	6	0
4	17	12	4	1
5	7	4	0	3

3.3 ANOVA

For the presented classification, the means of the following variables were analysed using ANOVA: minimum cirque floor altitude, L/W ratio, L/H ratio, cubic size, circularity, median axis slope, plan closure, and profile closure. Four variables (»Minimum floor altitude,« »L/W ratio,« »Median axis slope« and »Plan closure«) had unequal variances while the other four showed a non-normal distribution between cirque types.

Tables 3 and 4 show the initial results of the two types of ANOVA performed, indicating statistically significant differences at the 0.05 level between cirque types in most variables except for cubic size and profile closure.

Table 5 displays the variable means for all cirque types. A graphical display in the form of box whisker diagrams is shown in Figure 7. The results show that type 4 cirques vary significantly from all other types in terms of minimum floor altitude with mean differences of over 250 m. On average, type 3 cirques have minimum floor altitudes that are over 100 m higher than any other type, though that difference is only significant at the 0.05 level in relation to types 2 and 4. Type 3 also shows the greatest variability in minimum floor altitude. In terms of L/W ratio, type 5 stands out with a significantly higher mean of 1.91 and an interquartile range showing minimal overlap with the other types. Conversely, type 1's mean L/W ratio of 0.78 is significantly lower than all other types, with tight clustering around the mean. The other cirque types' L/W ratios indicate roughly equidimensional planimetric forms. L/H ratios show a similar pattern, where type 1 exhibits a significantly lower and more tightly clustered mean than all other types. Type 5 varies significantly only from types 1 and 3. In terms of cubic size, no cirque type stands out significantly. All cirque types have a roughly equal circularity on average, despite the analysis indicating a significant difference

Table 3: Welch F-test results for the variables »Minimum floor altitude«, »L/W ratio«, »Median axis slope«, and »Plan closure«.

	Statistic[a]	df1	df2	Significance
Minimum floor altitude	21.000	4	21.000	**0.000***
L/W ratio	19.000	4	23.000	**0.000***
Median axis slope	26.000	4	23.000	**0.000***
Plan closure	6.000	4	24.000	**0.001***

[a] Asymptotically F distributed.
* There are statistically significant differences between two or more types at the 0.05 level.

Table 4: Kruskal-Wallis test results for the variables »L/H ratio«, »Cubic size«, »Circularity«, and »Profile closure«.

	Null Hypothesis	Significance	Decision
1	The distribution of L/H ratio is the same across cirque types	**0.000***	Reject the null hypothesis
2	The distribution of Cubic size is the same across cirque types	0.332	Retain the null hypothesis
3	The distribution of Circularity is the same across cirque types	**0.027***	Reject the null hypothesis
4	The distribution of Profile closure is the same across cirque types	0.652	Retain the null hypothesis

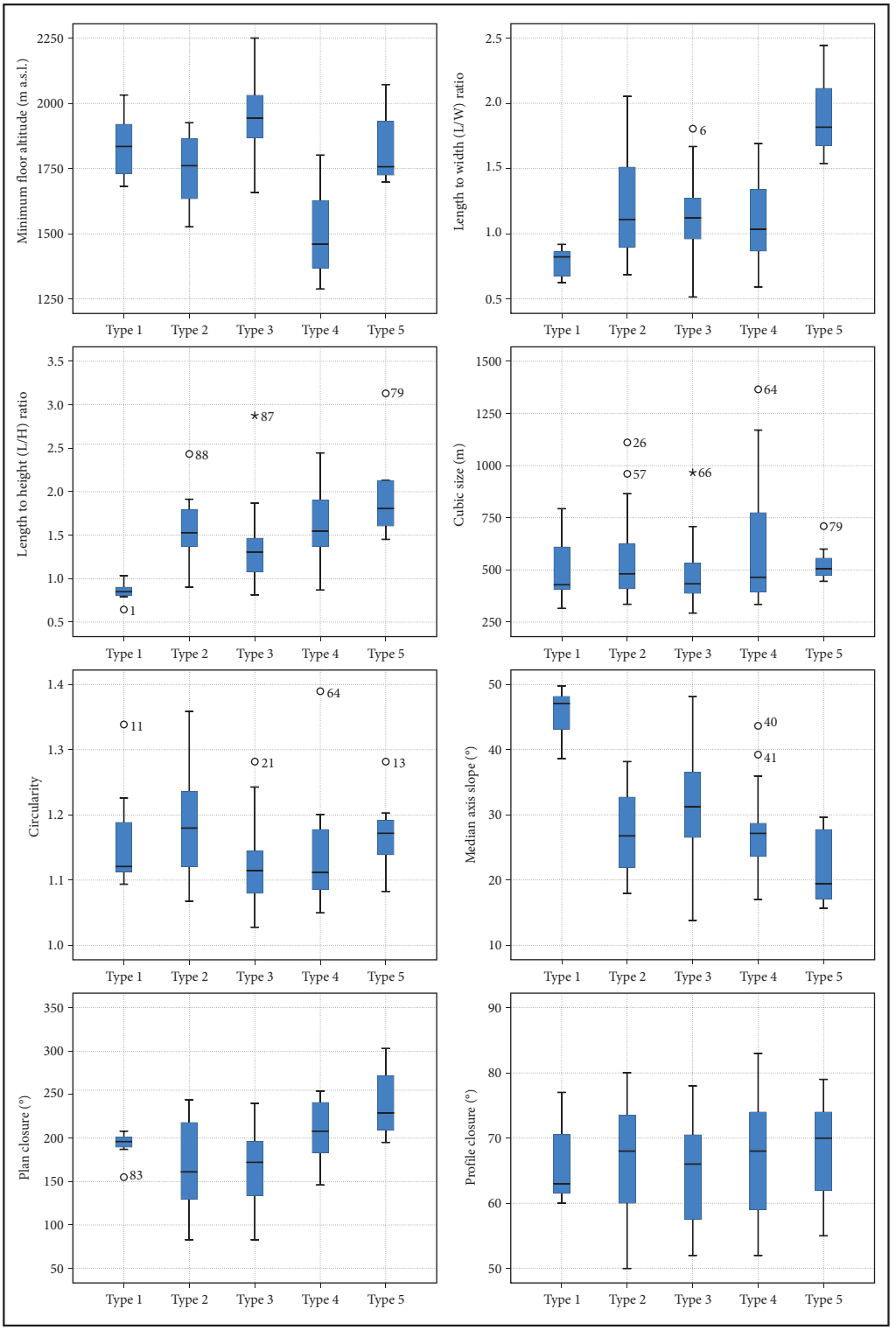
Asymptotic significances are displayed.
* There are statistically significant differences between two or more types at the 0.05 level.

Table 5: Variable means for all cirque types for the presented classification.

Variable	Type 1	Type 2	Type 3	Type 4	Type 5
Minimum floor altitude [m a.s.l.]	1903	1794	2033	1519	1900
Length to width (L/W) ratio	0.78	1.21	1.11	1.09	1.91
Length to height (L/H) ratio	0.85	1.55	1.32	1.62	1.98
Cubic size [m]	489	544	440	622	514
Circularity	1.17	1.18	1.12	1.14	1.17
Median axis slope [°]	45.5	27.5	31.4	27.5	22.1
Plan closure [°]	191.6	167.2	166.9	205.7	241.3
Profile closure [°]	66.3	66.3	64.1	66.4	68.0

between types 2 and 3. Consistent with L/H ratios, type 1 cirques have the highest average median axis slopes (45.5°) and differ significantly from all other types. The remaining types have slopes near or below 30°, with type 3 being somewhat steeper (31.4°) and type 5 being the gentlest (22.1°). Despite considerable variability, type 3 still differs significantly from type 5. In terms of plan closure, types 4 and 5 have higher means than types 2 and 3. Type 5 (241.3°) differs significantly from both types 2 and 3 whereas type 4 (205.7°) is only significantly different from type 3 and marginally different ($p = 0.096$) from type 2. Type 1 shows tight clustering around its mean (191.6°) but is not significantly different from the other types. All cirque types have roughly equal average profile closure values. Figure 8 shows a schematic illustration of the five cirque types. Figure 9 shows representative examples for each cirque type.

Figure 7: Box whisker diagrams for all variables, analysed with ANOVA. Circles denote outliers (1.5–3 interquartile ranges from box edge), asterisks denote extreme outliers (>3 interquartile ranges from box edge). ► p. 50


Minimum floor altitude (m a.s.l.)
2250
2000
1750
1500
1250
Type 1
Type 2
Type 3
Type 4
Type 5
Length to width (L/W) ratio
2.5
2.0
1.5
1.0
0.5
6
Length to height (L/H) ratio
3.5
3.0
2.5
2.0
1.5
1.0
0.5
87
88
79
1
Cubic size (m)
1500
1250
1000
750
500
250
64
26
57
66
79
Circularity
1.4
1.3
1.2
1.1
1.0
11
64
21
13
Median axis slope (°)
50
40
30
20
10
40
41
Plan closure (°)
350
300
250
200
150
100
50
83
Profile closure (°)
90
80
70
60
50

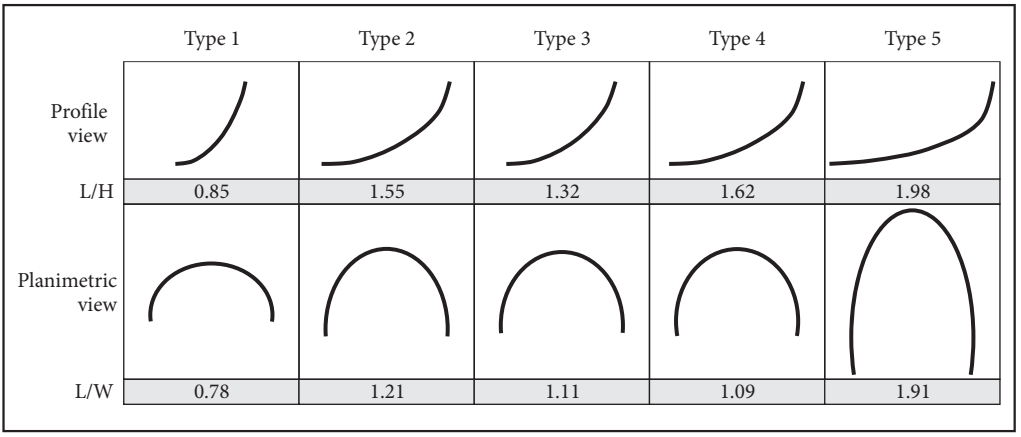


Figure 8: Schematic illustration of the five cirque types in planimetric and profile view.



Figure 9: Representative cirques for each cirque type. (A) Type 1: Cirque under Plaski Vogel on the upper Komna Plateau. (B) Type 2: Cirque under mount Mangrt in NW Julian Alps. (C) Type 3: Cirque under mount Triglav. (D) Type 4: Cirque under mount Raduha in NE Kamnik-Savinja Alps. (E) Type 5: Cirque under Mount Stol in the Karawanks. Types 1 and 3 shown as 3D DEM visualizations and types 2, 4 and 5 shown as field photographs.

3.4 Circular statistics

Each cirque type exhibits a very strong concentration around its mean direction, with $\bar{R}$ values of 0.79 or more (Table 6). A graphical display of median axis aspects in the form of percentage-based rose diagrams is shown in Figure 10. All cirque types showed a statistically significant preferred orientation (Rayleigh test: $p < 0.001$ for types 1–4 and $p = 0.005$ for type 5).

Table 6: Circular statistics for median axis aspect for all cirque types for the presented classification.

	Type 1	Type 2	Type 3	Type 4	Type 5
Mean direction [°]	344.7	268.9	136.7	25.8	87.0
Mean resultant length	0.94	0.84	0.82	0.79	0.81

The Mardia-Watson-Wheeler test confirmed the existence of statistically significant differences between the mean directions ($W = 96.61$, $df = 8$, $p < 0.001$) and pairwise comparisons using Watson's U^2 test showed that several of the differences between types are significant. Most notably, type 2 cirques differ significantly from types 3, 4 and 5, and marginally from type 1 as well ($p = 0.050$), facing mainly towards the west. Type 1 cirques are all northward-facing. Their median axis aspects overlap with type 4, but vary significantly (in the case of type 3) or marginally from the other types. Types 3, 4 and 5 all have easterly mean aspect directions, with types 3 and 4 being significantly different from one another.

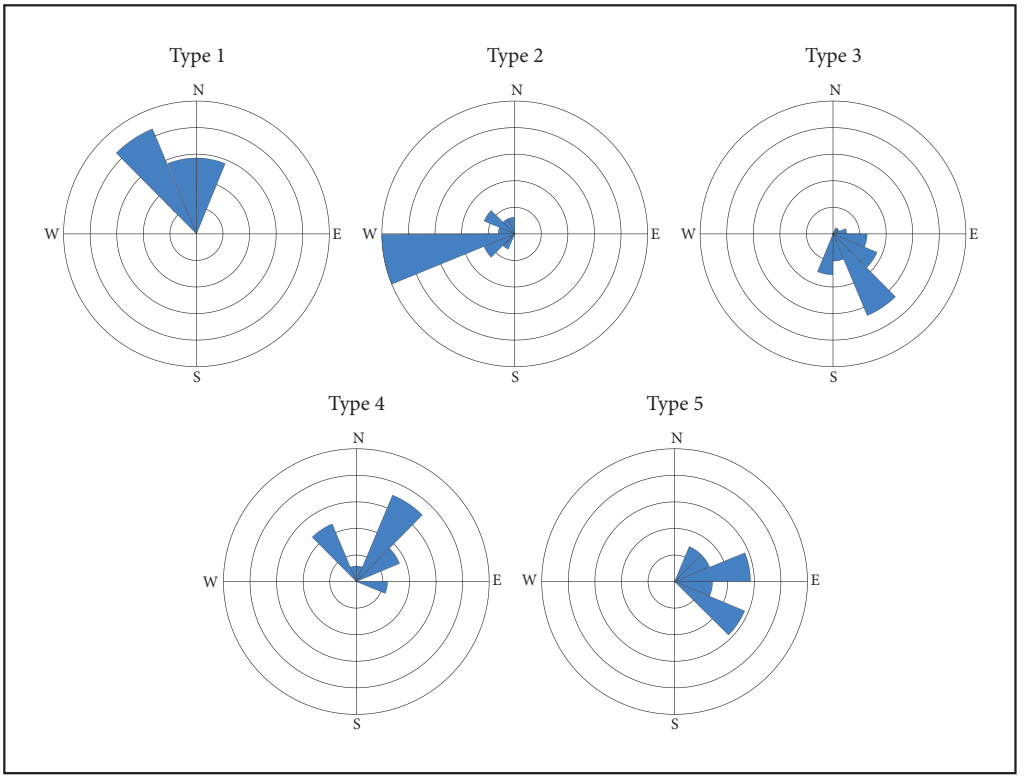


Figure 10: Percentage-based rose diagrams for median axis aspect by cirque type.

3.5 Chi-square tests

A total of 31 cirques contained a well-developed and preserved cirque threshold. While the results of Fisher's exact test ($p = 0.286$, Cramer's $V = 0.248$) show no statistically significant association between the presence of cirque thresholds and cirque type membership, some patterns are evident (Figure 11). Types 1 and 4 predominantly (85.7% and 76.5% respectively) contain no preserved cirque threshold while type 5 cirques contain a cirque threshold in 57.1% of cases.

In the case of lithology, Table 7 shows a moderate and statistically significant association between cirque type membership and type of bedrock. It should be noted that the category »Quaternary deposits« encompasses various surface sediments, including talus slope deposits, glacial and alluvial sediments. Similar steps were taken with the various limestone and dolomite bedrocks. Combining lithological categories was necessary to satisfy some of the assumptions of the analysis. As shown in Figure 12, limestones with and without Quaternary deposits appear in all 86 cirques and are the most represented bedrock type. Type 1 cirques occur exclusively in limestones, either with or without overlying Quaternary deposits, and types 2 and 3 show similarly high proportions (75% and 94.9% respectively) of solely limestone-based bedrock. Type 4 displays a much higher proportion (41.2%) of bedrock containing dolomites and clastic rocks. Type 5 cirques are the most predominantly (85%) covered by Quaternary deposits of some kind. Where these Quaternary deposits overlie bedrock, the latter remains the primary factor in cirque formation as the former mostly affect or indicate postglacial modification.

Table 7: Pearson Chi-square, Fisher's exact test, and Cramer's V results for bedrock type in relation to cirque type membership.

	Value	df	Asymptotic significance (2-sided)	Exact significance (2-sided)
Pearson Chi-Square	25.809[a]	16	0.057	
Fisher's Exact Test				**0.017**
Cramer's V	0.274			

[a] 19 cells (76.0%) have expected count less than 5. The minimum expected count is 0.24.

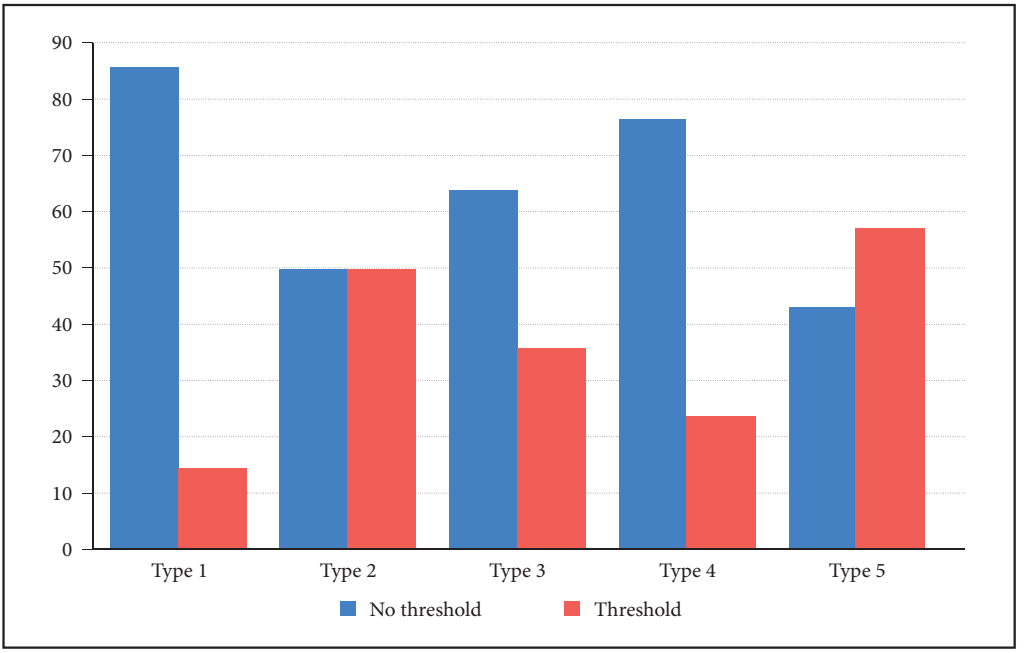


Figure 11: Percentage of cirques with threshold by cirque type.

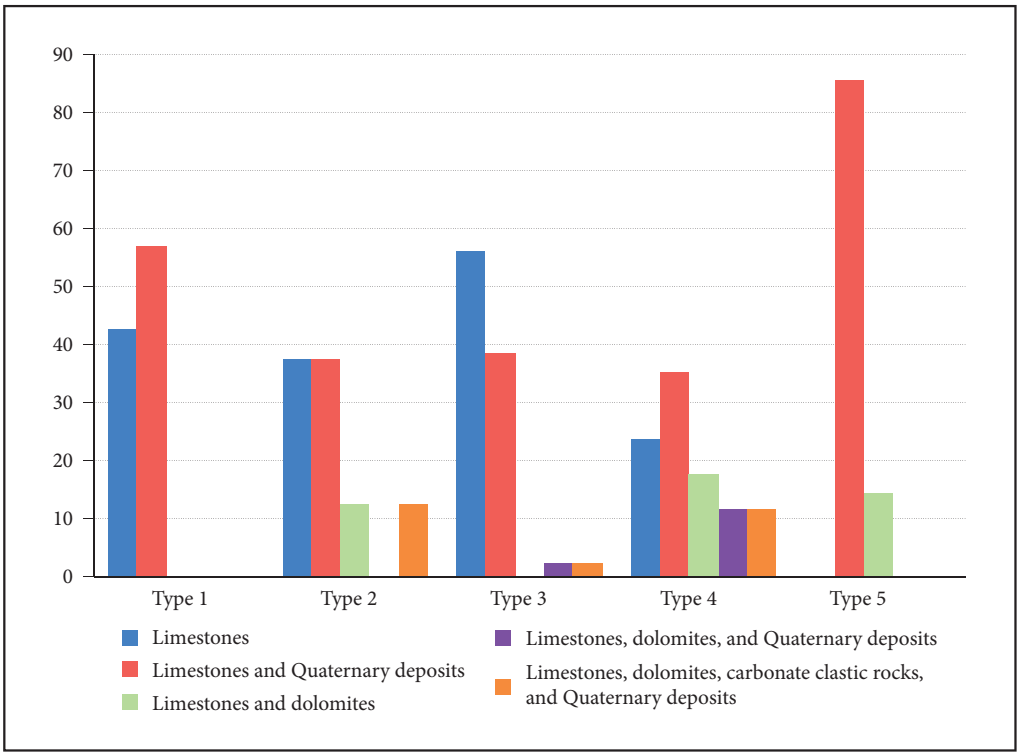


Figure 12: Percentage of bedrock types by cirque type.

4 Discussion

A systematic and objective classification of cirques in Slovenia revealed that among the 86 cirques included in the analysis only 31 exhibit a distinguishable cirque threshold, either due to the high intensity of post-glacial denudation and erosion processes (Bavec and Verbič 2004) or due to intense subglacial erosion in cirques where glaciers flowed beyond their cirques, forming no threshold to begin with. Paired with the lack of dating (Hughes et al. 2021) and research on Slovenian cirques in general this makes the interpretation and assignment of cirques to specific glaciations difficult (Barr and Spagnolo 2015). Based on the results of statistical analyses it is possible to interpret 5 distinct types of cirques in the Slovenian Alps.

Type 1 cirques are located at high altitudes around 1900 m a.s.l. and were formed exclusively in limestones which were later commonly covered by talus slope deposits. They are scattered across the peaks and ridges of the Kamnik-Savinja Alps, where they are most prevalent, along with the northern fringes of the Komna Plateau and the outskirts of the Križ Plateau. They are laterally enlarged and overdeepened, with the highest median axis slopes, which could be partially a result of karst vertical water drainage (Žebre and Stepišnik 2014). This is also likely a factor in their low rate of cirque threshold preservation. Their northward-facing aspects, paired with their relatively high plan closures, indicate reduced exposure to solar radiation (Evans 2006b). These cirques likely contained glaciers bound to their cirques that under favourable conditions effectively overdeepened their cirques rather than extending them (Evans 2006a). They were glaciated for extended periods of time owing to their sheltered high-altitude locations. Their identifying characteristics are their steep profiles and high median axis slopes, as well as their northward aspects, in which they are only similar to type 4.

Type 2 cirques are located at high altitudes around 1800 m a.s.l. and were formed predominantly in limestones. They are found almost exclusively in the Julian Alps on west-facing slopes, with notable con-

centrations around the Komna Plateau, the Križ Plateau and the ridge between the peaks of Mount Bavški Grintavec and Mount Jalovec. They are roughly circular in planimetric form, with lower plan closures. Coupled with higher L/H ratios, this indicates a greater exposure to solar radiation (Evans 2006a). Their predominantly west-facing aspects partially compensated for these unfavourable conditions, allowing these cirques to form on the lower reaches of the LGM glacial extent (Barr et al. 2017). Their westward aspects are their only identifying characteristic as they otherwise share many characteristics with type 3.

Type 3 cirques are located at the highest altitudes, with average floor altitudes around 2000 m a.s.l. They are formed predominantly in limestones with little occurrence of dolomites or clastic rocks. They are the most numerous cirque type, located around Mount Grintovec in the Kamnik-Savinja Alps, as well as in the Julian Alps on the Komna Plateau, the high-altitude plateaus, and the ridge between the peaks of Mount Bavški Grintavec and Mount Jalovec. They have a roughly circular form with lower plan closures and moderate median axis slopes. Their southeast-facing aspects exposed them to increased solar radiation, which is why they were likely formed by small glaciers at the highest altitudes, which enabled cirque growth despite higher ablation rates (Evans 2006b; Barr et al. 2017). Due to their large number and consequently higher variability, they lack a distinguishing characteristic and can only be differentiated from other types based on a combination of characteristics.

Type 4 cirques are located at the lowest altitudes around 1500 m a.s.l., which coincides with the highest occurrence of non-limestone bedrock. Like type 1 cirques, they were commonly covered by talus slope deposits. They are found in all mountain ranges with a notable concentration on the southeastern flanks of the Bohinj basin. These cirques are roughly circular with high plan closures and relatively shallow profiles. Their aspects are the most favourable, being mostly northeast and north-facing, which indicates that solar radiation was a key factor in their formation. These cirques received the least amount of insolation as their headwalls offered additional protection from the Sun during the afternoon, when the surface was somewhat warmer (Evans 1977; Evans 2006a; Barr and Spagnolo 2015). Given their location on the lower fringes of the LGM glacial extent and their morphology, these cirques were likely formed by small glaciers in areas where their favourably facing arcuate headwalls could shelter them from increased ablation brought on by lower altitudes (Evans 1977; Barr et al. 2017). The low degree of cirque threshold preservation was likely caused by a higher intensity of postglacial erosion. Their identifying characteristics are their low elevations along with high plan closures.

Similar to type 1, type 5 cirques are located at high altitudes around 1900 m a.s.l., but with a vastly different morphology. They are mainly found in the Karawanks with some in the Julian Alps. They have eastward aspects and formed in limestones and occasionally dolomites, but were later extensively covered by talus slope deposits along their lengths, indicating a higher rate of postglacial denudation and glaciogenic form and sediment erosion and redeposition (Bavec and Verbič 2004). They are the only cirque type with an elongated planimetric form, with lengths almost double their widths, and consequently they also have the highest plan closures. They are extremely shallow with the gentlest median axis slopes, indicating less glacial overdeepening (Evans 2006a), which is usually caused by glaciers that extended beyond their cirques due to very favourable conditions and lower ELAs. The increased ice accumulation during the LGM allowed these glaciers to extend down valleys despite increased karst drainage (Žebre and Stepišnik 2014; Dixon et al. 2016), with most of the cirque growth occurring during the beginning and ending stages of glaciations (Barr and Spagnolo 2015). In many cases, these cirques retained a cirque threshold, likely a result of gradual glacier retreat and hummocky moraine deposition. Their identifying characteristics are their high L/W and L/H ratios, along with high plan closures and eastward aspects.

It is also possible to infer some of the broader glaciation conditions based on the morphology of cirque types. Varied L/H ratios ranging from 0.85 to 1.98 suggests varied conditions across the three mountain ranges (Ferk et al. 2017). The Kamnik-Savinja Alps contain primarily higher altitude cirque types (75% being types 1, 2 and 3). Given their morphology, it is likely that the ELAs in this mountain range were higher (at 1900 m or above) and that the glaciation conditions were not favourable enough to allow glaciers to extend beyond their cirques, resulting in an absence of type 5 cirques. Instead, some ridges experienced substantial cirque development and overdeepening while others experienced shallower cirque growth. However, varied cirque aspects for these three types (NNW, W, SE) indicate that solar radiation was not a key factor, possibly due to increased cloud cover or wind accumulation (Barr and Spagnolo 2015). The presence of predominantly northeast-facing type 4 cirques on the fringes of the mountain range and the morphological differences between the higher altitude cirques indicate that other strong local topographic

or climatic factors were crucial for cirque formation. These factors caused local differences in subglacial erosion rates, resulting in varied cirque forms, and compensated for higher ablation rates at lower altitudes.

Half of the cirques in the Julian Alps are type 3 with southeast-facing aspects. There is also a considerable number of type 2 cirques, of which the majority are in this mountain range. The presence of cirques on contrasting aspects (west-facing type 2 and eastward-facing types 3 and 5) along many ridges and plateaus indicates favourable glaciation conditions, which is further confirmed by a significant number of type 4 cirques in the region. Judging by the shallow profiles and high plan closures of these low-altitude cirques, the ELAs in the Julian Alps were likely somewhat above 1600–1650 m as altitudes lower than that would be reflected in higher rates of subglacial erosion and a higher representation of overdeepened cirques at lower elevations (Mitchell and Montgomery 2006). The comparatively low frequency of elongated type 5 cirques despite lower ELAs may be a consequence of increased karst drainage (Žebre and Stepišnik 2014) or other topographic factors.

The Slovenian part of the Karawanks has comparatively few cirques, but the prevalence of type 5 cirques indicates very favourable glaciation conditions and ELAs significantly lower than 1900 m, which allowed the glaciers to create elongated cirques that transition into glacial valleys despite the increased karst drainage (Žebre and Stepišnik 2014). At the same time, the glacial ice in the cirques remained mostly frozen to the bed, resulting in reduced subglacial erosion and shallower cirques. Their aspects, however, are likely a consequence of the overall direction of the mountain range and the fact that the Austrian side of the mountain range with cirques potentially facing different directions was not included in the research. Therefore, the aspects of these cirques do not necessarily reflect any past climate conditions and are of limited interpretative use.

The obtained classification is objective, statistically supported, founded on quantitative data, and produced distinct classes. Emphasizing cirque morphometry, this approach provides a rapid and consistent method of partitioning cirques in Slovenia without excessively relying on a researcher's expertise and subjectivity or detailed analyses of each individual cirque. It allows for the subsequent classification of newly discovered cirques in Slovenia, but could be adapted to other cirque populations in the world using the same morphometric variables and accounting for different mountain altitude ranges. Furthermore, this classification offers a preliminary insight into the palaeoclimate properties of Slovenia's mountainous regions and is a foundation for more focused and efficient field studies into the morphometrically varied cirque types and helps determine which methods would likely be useful in their analysis.

5 Conclusion

Cirques, including their morphology and morphometry, are important to inferring palaeoclimate conditions, and an objective classification founded on quantitative data is crucial, especially for regions where cirque populations have yet to be systematically studied. The presented classification was performed using a hierarchical cluster analysis and verified using ANOVA, the Kruskal-Wallis, Watson's U^2 and Chi-square tests. 86 cirques were analysed and classified into five cirque types which can further be split into two subgroups based on altitude; low-altitude (type 4; 1500–1800 m) and high-altitude cirques (types 1, 2, 3 and 5; 1800–2000 m). Based on the prevailing cirque types it is possible to partially infer glaciation conditions in the Slovenian mountains. The Kamnik-Savinja Alps experienced higher altitude glaciation (75% of cirques at 1800–2000 m) with varied rates of subglacial erosion, resulting in both overdeepened and shallower cirques forming on varied aspects (NNW, W, SE) because of increased cloud cover or wind accumulation. The Julian Alps experienced more favourable glaciation conditions which led to more frequent cirque growth on favourable northeastern aspects in low-altitude fringe areas (1500–1650 m) while also enabling more extensive cirque formation on western and eastern aspects at higher altitudes (1800 m and above), with 50% of all cirques in this mountain range facing towards the southeast. The Karawanks experienced favourable glaciation conditions resulting in predominantly east-facing elongated cirques, where glaciers extended beyond the cirques and down valleys. This classification presents a fast and consistent method of classifying new cirque populations and offers an initial exploration into Slovenia's cirque population, establishing a foundation for more detailed future investigations into the factors affecting the formation and modification of the five cirque types.

ACKNOWLEDGEMENTS: The research was partially supported by the Slovenian Research and Innovation Agency Research Programme P6–0101 and the Slovenian Research and Innovation Agency Research Project J6–3141.

RESEARCH DATA: For information on the availability of research data related to the study, please visit the article webpage: https://doi.org/10.3986/AGS.14012.

6 References

Agostinelli, C., Lund, U. 2025: R package 'circular': Circular Statistics (version 0.5–2). *R package*. CRAN. https://doi.org/10.32614/CRAN.package.circular

Aniya, M., Welch, R. 1981: Morphometric analyses of antarctic cirques from photogrammetric measurements. *Geografiska Annaler. Series A, Physical Geography* 63–1,2. https://doi.org/10.2307/520563

Ardelean, F., Drăguț, L., Urdea, P., Török-Oance, M. 2013: Variations in landform definition: a quantitative assessment of differences between five maps of glacial cirques in the Țarcu Mountains (Southern Carpathians, Romania). *Area* 45–3.

Barr, I. D., Ely, J. C., Spagnolo, M., Clark, C. D., Evans, I. S., Pellicer, X. M., Pellitero, R. et al. 2017: Climate patterns during former periods of mountain glaciation in Britain and Ireland: Inferences from the cirque record. *Palaeogeography, Palaeoclimatology, Palaeoecology* 485. https://doi.org/10.1016/j.palaeo.2017.07.001

Barr, I. D., Spagnolo, M. 2013: Palaeoglacial and palaeoclimatic conditions in the NW Pacific, as revealed by a morphometric analysis of cirques upon the Kamchatka Peninsula. *Geomorphology* 192. https://doi.org/10.1016/j.geomorph.2013.03.011

Barr, I. D., Spagnolo, M. 2015: Glacial cirques as palaeoenvironmental indicators: Their potential and limitations. *Earth-Science Reviews* 151. https://doi.org/10.1016/j.earscirev.2015.10.004

Batschelet, E. 1981: Circular statistics in biology. Academic Press.

Bavec, M. 2001: Kvartarni sedimenti Zgornjega Posočja. *Ph.D. thesis*. Univerza v Ljubljani.

Bavec, M., Verbič, T. 2004: The extent of Quaternary glaciations in Slovenia. *Developments in Quaternary Science* 2–1. https://doi.org/10.1016/S1571–0866(04)80088–5

Carr, S. J., Coleman, C. G. 2007: An improved technique for the reconstruction of former glacier mass-balance and dynamics. *Geomorphology* 92–1,2. https://doi.org/10.1016/j.geomorph.2007.02.008

Coleman, C. G., Carr, S. J., Parker, A. G. 2009: Modelling topoclimatic controls on palaeoglaciers: implications for inferring palaeoclimate from geomorphic evidence. *Quaternary Science Reviews* 28–3,4. https://doi.org/10.1016/j.quascirev.2008.10.016

Dixon, J. L., von Blanckenburg, F., Stüwe, K., Christl, M. 2016: Glaciation's topographic control on Holocene erosion at the eastern edge of the Alps. *Earth Surface Dynamics* 4–4. https://doi.org/10.5194/esurf–4–895–2016

Ehlers, J., Gibbard, P. L., Hughes, P. D. (eds.) 2011: Quaternary glaciations – extent and chronology: A closer look. *Developments in Quaternary Sciences* 15. Elsevier.

Evans, I. S. 1977: World-wide variations in the direction and concentration of cirque and glacier aspects. *Geografiska Annaler. Series A, Physical Geography* 59–3,4. https://doi.org/10.2307/520797

Evans, I. S. 1997: Process and form in the erosion of glaciated mountains. In: Process and form in geomorphology. Routledge.

Evans, I. S. 2006a: Allometric development of glacial cirque form: Geological, relief and regional effects on the cirques of Wales. *Geomorphology* 80–3,4. https://doi.org/10.1016/j.geomorph.2006.02.013

Evans, I. S. 2006b: Local aspect asymmetry of mountain glaciation: A global survey of consistency of favoured directions for glacier numbers and altitudes. *Geomorphology* 73–1,2. https://doi.org/10.1016/j.geomorph.2005.07.009

Evans, I. S., Cox, N. J. 1974: Geomorphometry and the operational definition of cirques. *Area* 6–2.

Evans, I. S., Cox, N. J. 1995: The form of glacial cirques in the English Lake District, Cumbria. *Zeitschrift fur Geomorphologie* 39–2.

Evans, I. S., McClean, C. J. 1995: The land surface is not unifractal: variograms, cirque scale and allometry. *Zeitschrift fur Geomorphologie* 101.

Ferk, M., Gabrovec, M., Komac, B., Zorn, M., Stepišnik, U. 2017: Pleistocene glaciation in Mediterranean Slovenia. In: Quaternary glaciation in the Mediterranean mountains. *Special Publications* 433. Geological Society. https://doi.org/10.1144/SP433.2

Field, A. P. 2013: Discovering statistics using IBM SPSS statistics: and sex and drugs and rock 'n' roll. SAGE.

Fisher, N. I. 1993: Statistical analysis of circular data. Cambridge University Press. https://doi.org/10.1017/CBO9780511564345

Fisher, R. A. 1922: On the interpretation of χ^2 from contingency tables, and the calculation of p. *Journal of the Royal Statistical Society* 85–1. https://doi.org/10.2307/2340521

Gareth, J., Witten, D., Hastie, T., Tibshirani, R. 2013: An introduction to statistical learning : with applications in R. Springer.

Geological Survey of Slovenia 2007: Litostratigrafska karta Slovenije. *1:100,000 map*.

Gutiérrez, F., Gutiérrez, M. 2016: Periglacial landforms. In: Landforms of the Earth: An Illustrated Guide. Springer. https://doi.org/10.1007/978–3–319–26947–4_12

Holm, S. 1979: A simple sequentially rejective multiple test procedure. *Scandinavian Journal of Statistics* 6–2.

Hrvatin, M. 2016: Morfometrične značilnosti površja na različnih kamninah v Sloveniji. *Ph.D. thesis*. Univerza na Primorskem.

Hrvatin, M., Tičar, J., Zorn, M. 2020: Rocks and tectonic structure of Slovenia. In: The Geography of Slovenia: Small But Diverse. *World Regional Geography Book Series*. Springer. https://doi.org/10.1007/978–3–030–14066–3_2

Hughes, P. D., Allard, J. L., Woodward, J. C. 2021: The Balkans: glacial landforms from the Last Glacial Maximum. In: European Glacial Landscapes: Maximum Extent of Glaciations. Elsevier. https://doi.org/10.1016/B978–0–12–823498–3.00058–3

Hughes, P. D., Gibbard, P. L., Woodward, J. C. 2007: Geological controls on Pleistocene glaciation and cirque form in Greece. *Geomorphology* 88–3,4. https://doi.org/10.1016/j.geomorph.2006.11.008

IBM 2021: Hierarchical cluster analysis. *Software documentation*.

IBM 2022: IBM SPSS Statistics Base 29. *Software documentation*.

Knight, J., Harrison, S. 2014: Mountain glacial and paraglacial environments under global climate change: lessons from the past, future directions and policy implications. *Geografiska Annaler: Series A, Physical Geography* 96–3. https://doi.org/10.1111/geoa.12051

Kodelja, B., Žebre, M., Stepišnik, U. 2018: Poledenitev Trnovskega gozda. *E–GeograFF* 6. Založba Univerze v Ljubljani. https://doi.org/10.4312/9789612375614

Komac, B., Pavšek, M., Topole, M. 2020: Climate and weather of Slovenia. In: The Geography of Slovenia: Small But Diverse. *World Regional Geography Book Series*. Springer. https://doi.org/10.1007/978–3–030–14066–3_5

Mardia, K. V., Jupp, P. E. 1999: Directional statistics. Wiley. https://doi.org/10.1002/9780470316979

Mîndrescu, M., Evans, I. S. 2014: Cirque form and development in Romania: Allometry and the buzzsaw hypothesis. *Geomorphology* 208. https://doi.org/10.1016/j.geomorph.2013.11.019

Mitchell, S. G., Montgomery, D. R. 2006: Influence of a glacial buzzsaw on the height and morphology of the Cascade Range in central Washington State, USA. *Quaternary Research* 65–1. https://doi.org/10.1016/j.yqres.2005.08.018

Natek, K. 2007: Periglacial landforms in the Pohorje mountains. *Dela* 27. https://doi.org/10.4312/dela.27.247–263

Ogrin, D., Repe, B., Štaut, L., Svetlin, D., Ogrin, M. 2023: Climate classification of Slovenia based on data from the period 1991–2020. *Dela* 59. https://doi.org/10.4312/dela.59.5–89

Penck, A. 1905: Glacial features in the surface of the Alps. *The Journal of Geology* 13–1.

Perko, D., Ciglič, R., Hrvatin, M. 2021: Landscape macrotypologies and microtypologies of Slovenia. *Acta geographica Slovenica* 61–3. https://doi.org/10.3986/AGS.10384

R Foundation for Statistical Computing, R Core Team 2025: R: A language and environment for statistical computing. Computer software.

Rogerson, P. A. 2001: Statistical methods for geography. SAGE Publications. https://doi.org/10.4135/9781849209953

Singh, V. P., Singh, P., Haritashya, U. K. (eds.) 2011: Encyclopedia of snow, ice and glaciers. *Encyclopedia of Earth Sciences Series*. Springer. https://doi.org/10.1007/978–90–481–2642–2

Slovenian Environment Agency 2015: Lidar. *Dataset*.

Spagnolo, M., Pellitero, R., Barr, I. D., Ely, J. C., Pellicer, X. M., Rea, B. R. 2017: ACME, a GIS tool for automated cirque metric extraction. *Geomorphology* 278. https://doi.org/10.1016/j.geomorph.2016.11.018

Steinemann, O., Ivy–Ochs, S., Grazioli, S., Luetscher, M., Fischer, U., Vockenhuber, C., Synal, H. A. 2020: Quantifying glacial erosion on a limestone bed and the relevance for landscape development in the Alps. *Earth Surface Processes and Landforms* 45–6. https://doi.org/10.1002/esp.4812

Stephens, M. A. 1970: Use of the Kolmogorov–Smirnov, Cramér–Von Mises and related statistics without extensive tables. *Journal of the Royal Statistical Society. Series B (Methodological)* 32–1.

Stojilković, B., Stepišnik, U., Žebre, M. 2013: Pleistocenska poledenitev v Logarski dolini. *Dela* 40. https://doi.org/10.4312/dela.40.25–38

Surveying and Mapping Authority of the Republic of Slovenia 2016a: Digitalni model višin 5 × 5 m (DMV 0050). *Dataset*.

Surveying and Mapping Authority of the Republic of Slovenia 2016b: Digitalni model višin 12,5 × 12,5 m (DMV 0125). *Dataset*.

Vilborg, L. 1984: The cirque forms of Central Sweden. *Geografiska Annaler. Series A, Physical Geography* 66–1,2. https://doi.org/10.2307/520939

Watson, G. S. 1962: Goodness-of-fit tests on a circle. II. *Biometrika* 49–1,2. https://doi.org/10.1093/biomet/49.1–2.57

Zhenhua, C. 2011: Exploring new trends of university libraries by SPSS cluster analysis method – Take Wuhan University of Technology as an example. In: 2011 International Conference on Product Innovation Management (ICPIM 2011). Institute of Electrical and Electronics Engineers (IEEE). https://doi.org/10.1109/ICPIM.2011.5983578

Žebre, M., Stepišnik, U. 2014: Reconstruction of Late Pleistocene glaciers on Mount Lovćen, Montenegro. *Quaternary International* 353. https://doi.org/10.1016/j.quaint.2014.05.006

Žebre, M., Stepišnik, U. 2016: Glaciokarst geomorphology of the Northern Dinaric Alps: Snežnik (Slovenia) and Gorski Kotar (Croatia). *Journal of Maps* 12–5. https://doi.org/10.1080/17445647.2015.1095133

Žebre, M., Stepišnik, U., Kodelja, B. 2013: Sledovi pleistocenske poledenitve na Trnovskem gozdu. *Dela* 39. https://doi.org/10.4312/dela.39.157–170

Acta geographica Slovenica, 66-1, 2026, 61–80

LAND-USE DYNAMICS AND GRASSLAND SUCCESSION CHALLENGES IN THE NATURA 2000 SITE KRAS: THE SOCIOECONOMIC PERSPECTIVE

Danijel Davidović, Jure Čuš, Danijel Ivajnšič



NATAŠA PIPENBAHER

Example of secondary karst grassland undergoing shrub encroachment due to reduced management intensity. The mosaic of grasses, shrubs and trees illustrates an intermediate successional stage.

DOI: https://doi.org/10.3986/AGS.14021
UDC: 711.14:633.2.03(497.472)"2002/2024"
Creative Commons CC BY-SA 4.0

Danijel Davidović[1], Jure Čuš[2], Danijel Ivajnšič[1]

Land-use dynamics and grassland succession challenges in the Natura 2000 site Kras: The socioeconomic perspective

ABSTRACT: Grasslands in the Natura 2000 site Kras are biodiversity hotspots with ecological, cultural and socioeconomic importance. However, the region faces challenges due to grassland loss and encroachment of forests and shrubs. This study examines land-use changes from 2002 to 2024 and the socioeconomic factors influencing these dynamics. Spatial analysis revealed substantial declines in grasslands, predominantly replaced by overgrown areas and forests. Socioeconomic factors such as farm holder age, livestock density and proximity to forests and roads showed complex interactions affecting grassland persistence, loss and gain. These findings underscore the urgent need for targeted conservation measures integrating adaptive grazing, sustainable forestry and enhanced policy support to balance grassland conservation with economic viability.

KEYWORDS: geography, biodiversity, ecosystem services, ecological succession, semi-natural grasslands, Agri-Environment Climate Scheme (AECS), Slovenia

Dinamika rabe tal in izzivi sukcesije travišč na Natura 2000 območju Kras: družbeno-ekonomski vidik

POVZETEK: Travniki na območju Natura 2000 Kras so žarišča biodiverzitete z ekološkim, kulturnim in družbeno-gospodarskim pomenom. Kljub temu se regija sooča z izzivi zaradi krčenja travnikov in širjenja gozda in grmičevja. Raziskava proučuje spremembe rabe tal od leta 2002 do 2024 in socio-ekonomske dejavnike, ki vplivajo na njihovo dinamiko. Prostorska analiza je pokazala obsežno krčenje travnikov, na katerih se razširijo predvsem zaraščene površine in gozd. Socio-ekonomski dejavniki, kot so starost nosilca kmetije, število glav velike živine ter bližina gozdnega roba in cest so pokazali kompleksne interakcije, ki vplivajo na ohranjanje, krčenje in širjenje travnikov. Ugotovitve kažejo nujno potrebo po ciljno usmerjenih ohranitvenih ukrepih, ki vključujejo prilagodljivo pašo, trajnostno gozdarstvo ter okrepljeno politično podporo za usklajevanje ohranjanja travnikov in profitabilnosti kmetovanja.

KLJUČNE BESEDE: geografija, biodiverziteta, ekosistemske storitve, ekološka sukcesija, polnaravna travišča, Kmetijsko-okoljska podnebna plačila (KOPOP), Slovenija

The article was submitted for publication on January 27th, 2025.
Uredništvo je prejelo prispevek 27. januarja 2025.

[1] University of Maribor, Maribor, Slovenia
[2] Independent researcher, Voličina, Slovenia

danijel.davidovic@um.si (https://orcid.org/0000-0003-3515-6139), jure.cus@gmail.com, dani.ivajnsic@um.si (https://orcid.org/0000-0003-4419-5295)

1 Introduction

Semi-natural grasslands are among the world's most biodiverse ecosystems (Wilson et al. 2012; Chytrý et al. 2015). Formed through low-intensity human activities, these herbaceous ecosystems differ from natural grasslands, having developed from early agricultural practices in areas unsuitable for natural grassland growth (Hejcman et al. 2013; Gigante et al. 2024). In the European Union (EU), they cover over one-third of agricultural land, making them one of its most extensive habitats (Schils et al. 2022). Additionally, environmental factors such as precipitation and insolation, combined with practices like swidden agriculture and grazing, created globally remarkable plant diversity, with record species richness per 50 m² plots (Horvatić 1973; Tüxen et al. 1974; Poldini 1989; Kaligarič and Poldini 1996; Kaligarič and Škornik 2002; Škornik et al. 2010; Pipenbaher et al. 2011). Despite their recognized importance (Tindale et al. 2023), abandonment and reduction persist, as cessation of grazing or mowing triggers secondary succession toward climax vegetation (Hejcman et al. 2013; Gigante et al. 2024).

Grasslands are biodiversity hotspots supporting diversity of plants, insects, birds, and mammals (Söderström et al. 2001; Perko et al. 2017; Šumrada and Erjavec 2023). They contribute to nutrient cycling, water regulation, microclimate balance, wildfire control, and carbon sequestration, thus aiding climate change mitigation (Ribeiro and Šmid Hribar 2019; Zhao et al. 2020; Bai and Cotrufo 2022). Additionally, they enhance soil structure and organic matter while preventing erosion in open habitats and forest understories (Hrvatin et al. 2006; Liu et al. 2020; Zhao et al. 2020).

Beyond ecology, grasslands are integral to rural traditions and livelihoods. Low-intensity grazing and haymaking provide food, including meat, dairy, honey, and wild edible or medicinal plants (Dasselaar et al. 2013; Žuna Pfeiffer et al. 2018; Zhao et al. 2020; Kose et al. 2022). They sustain pollinators and natural pest control (Bartual et al. 2019) and contribute to recreation, tourism, education, landscape aesthetics, cultural heritage, and psychological well-being (Reed et al. 2005; Hopkins and Holz 2006; Milcu et al. 2013; Rogerson et al. 2016; Zhao et al. 2020).

In Slovenia's Kras region (eng. *Karst*, ita. *Carso*), semi-natural grasslands are of exceptional ecological value. Originating around 2500 years ago (Kaligarič et al. 2006), they reached maximum extent in the 18th century, covering 82% of the area (Kaligarič and Ivajnšič 2014). These grasslands are now part of the Natura 2000 network. Despite protection, they are rapidly declining: since Slovenia's EU accession, over 5% of protected grasslands have disappeared (Kaligarič and Ivajnšič 2014).

Overgrowth in Kras has been studied for more than four decades (Feoli and Chiapella 1979; Lausi et al. 1979; Feoli et al. 1980; Feoli and Scimone 1982; Favretto and Poldini 1986). Between 1763 and 2002, 75% of grasslands were replaced by other land uses, and machine learning models predict further losses – from 20% of the landscape in 2012 to 7% by 2050, 5% by 2075, and 3% by 2100 (Kaligarič and Ivajnšič 2014). This trajectory signals major ecological and socio-economic change.

Like elsewhere in Europe (Gigante et al. 2024), Kras grassland decline is driven by succession following depopulation, land abandonment, and aging farm holders (Kaligarič and Ivajnšič 2014; Iberl et al. 2023). Their naturally low fertility and productivity (Envall et al. 2021) lead farmers either to abandon or intensify them, both hastening degradation (Hülber et al. 2017). Planned afforestation has accelerated these trends. The region's potential vegetation – forests of downy oak (*Quercus pubescens*) and sessile oak (*Quercus petraea*) – was long modified by human activities such as logging, swidden agriculture, and grazing (Zwitter and Rasran 2023). By the 18th–19th centuries, these practices left much of Kras barren and eroded, prompting extensive reforestation from the 19th through the 20th centuries (Kladnik 2011; Zorn et al. 2015).

Grassland conservation depends on maintaining traditional farming, which is often less profitable than intensive methods (Dahlström et al. 2013). The Agri-Environment Climate Scheme (AECS) offers subsidies for practices that exceed basic standards, supporting biodiversity, landscape integrity, and climate mitigation (Ivajnšič et al. 2018). However, uptake in Slovenia remains low. During 2007–2013 and 2014–2020, nearly half the subsidized grasslands lacked high conservation value, and 41% of funds went to intensively managed areas (Kaligarič et al. 2019). Despite €0.5 billion invested, declines in grassland flora, birds, and butterflies persisted (Jugovic et al. 2013; Jančar 2014; Kmecl et al. 2014).

Subsidies can still yield positive outcomes. In 2002–2012, EU payments encouraged sheep farming, slowing secondary succession (Veldkamp and Lambin 2001; Kaligarič and Ivajnšič 2014). Similarly, dairy production expansion curbed forest spread, contradicting earlier forecasts that Trieste Kras would be fully forested by 2013 (Favretto and Poldini 1986; Ivajnšič et al. 2013).

This study examines land-use change over the past two decades within the Natura 2000 site Kras, focusing on semi-natural grasslands, to answer: (1) Which land-use transitions dominate and to what extent? (2) Are grasslands still declining, and what processes drive their dynamics? (3) What are the main environmental and socio-economic factors of these changes?

2 Methods

2.1 Region of interest

The Kras Plateau in southwestern Slovenia represents a typical mid-latitude karst landscape extending over 429 km². Geologically, it forms a northwest–southeast-oriented anticline of limestone and dolomite, bordered by the flysch synclines of the Vipava Valley and the Gulf of Trieste. Due to its highly permeable bedrock, surface water is almost absent (Stepišnik 2011), although annual precipitation exceeds 1500 mm, supporting predominantly deciduous forests.

According to the Ministry of Agriculture, Forestry and Food, 72% of the plateau has low arable production potential; nevertheless, it remains a strategically important agricultural area. The gently undulating relief supports livestock farming, viticulture, and olive and fruit cultivation. However, industrialization after World War II led to widespread agricultural abandonment, peaking during the 1980s, as documented by Habič (1979) and Kladnik (2011).

Approximately 93% of the plateau (401 km²) lies within the Natura 2000 network, spanning eight municipalities. The region has 20,130 inhabitants, a low population density of 50 inh./km², and an aging demographic (mean age 45.8 years; 24% aged 65+). Statistical Office of the Republic of Slovenia reports that 53% of residents have secondary education and 24% have higher education. Data from the Ministry of Agriculture, Forestry and Food indicate that the area includes 1,562 registered farms covering 5,857 ha (15% of the total area), dominated by grasslands (85%) (Figure 1). The average farm size is 3.8 ha, farm holders average 62 years of age, and livestock density is low, at 1.6 livestock units (LU) per holding.

2.2 Data collection and preprocessing

To assess land-use dynamics, we analyzed land-use data for 2002, 2012, and 2024 obtained in vector format from the Ministry of Agriculture, Forestry and Food. To ensure comparability, existing land-use categories were reclassified into ten standardized classes (Table 1) and rasterized at a 5 × 5 m resolution, balancing spatial detail and computational efficiency.

Socioeconomic data were derived from the Ministry of Agriculture, Forestry and Food subsidy application database in vector format, containing information on land-use ID, farm-holder age, and livestock units (LU). Personal data were anonymized by replacing real identifiers with generated codes. Within the study area, 16,374 GERK (Graphical units of agricultural land use) were identified, of which 12,754 (78%) are under agricultural subsidies.

Spatial data delineating the Natura 2000 site Kras were obtained in vector format from the Institute of the Republic of Slovenia for Nature Conservation. All datasets were transformed to the Slovenia 1996 / Slovene National Grid (EPSG: 3794). Calculations, reclassification, rasterization, and visualization were performed using QGIS, TerrSet, and Excel.

2.3 Spatio-temporal analysis of land-use dynamics

The area of each land-use category was calculated in hectares and as a percentage of the total Natura 2000 site Kras for 2002, 2012, and 2024. Net land-use change and annual change rates were determined for three periods: 2002–2012, 2012–2024, and 2002–2024 overall.

Dominant change processes were identified using the Landscape Change Processes Analysis module in TerrSet Habitat and Biodiversity Modeler. A decision-tree algorithm compared raster pairs for all time

Figure 1: Location of the research area. ► p. 65

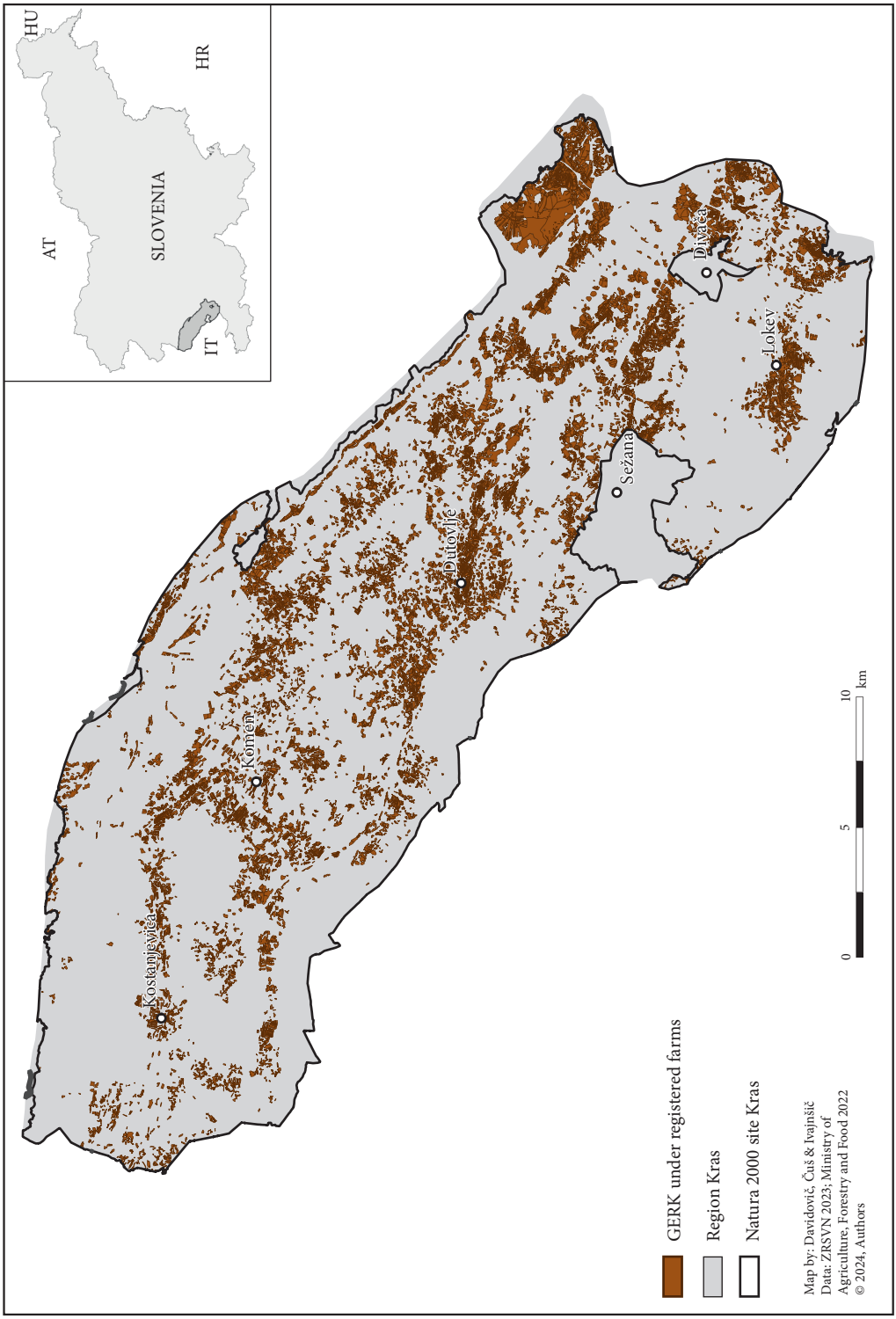

HU
HR
AT
SLOVENIA
IT
Kostanjevica
Komen
Dutovlje
Sežana
Divača
Lokev
GERK under registered farms
Region Kras
Natura 2000 site Kras
0
5
10
km
Map by: Davidovič, Čuš & Ivajnšič
Data: ZRSVN 2023; Ministry of Agriculture, Forestry and Food 2022
© 2024, Authors

Table 1: Land-use categories reclassification.

ID	Original categories*	Reclassified categories
1100	Arable	Arable
1180	Perennial plants on arable land	
1190	Greenhouse	
1211	Vineyard	Vineyard
1221	Intensive orchard	Orchard
1222	Extensive orchard	
1230	Olive grove	Olive grove
1240	Other crop	Other crop
1300	Perennial grassland	Grassland
1321	Bog grassland	
1410	Overgrown agricultural land	Overgrown
1420	Forest tree plantation	
1500	Trees and shrubs	
1600	Uncultivated agricultural land	
1800	Agricultural land overgrown with forest trees	
2000	Forest	Forest
3000	Built-up	Built-up
4220	Other wetlands	Other
5000	Dry open land with specific plant cover	
6000	Open land with no or insignificant plant cover	
7000	Water	

* Categories not present in the listed years: 2002 – Perennial plants on arable land, Greenhouse, Forest tree plantation, Uncultivated agricultural land, Agricultural land overgrown with forest trees, Other wetlands; 2012 – Other crop, Bog grassland; 2024 – Bog grassland, Other wetlands

intervals, evaluating changes in patch number, area, and perimeter. Each land-use category was assigned one of three process categories: (1) creation – increase in patch number and area, denoting new land uses; (2) attrition – decrease in both metrics, indicating land-use loss; and (3) dissection – increased patch number with decreased total area, signifying fragmentation (Eastman 2024).

Given their biodiversity importance and notable transformations, subsequent analyses focused on grasslands. The Change Analysis module within TerrSet Land Change Modeler was used to map grassland persistence, gains, and losses, as well as transitions to other land-use types. Broader spatial patterns were explored with the Spatial Trend of Change module using a ninth-order polynomial function, producing maps of grassland loss, overgrowth, and forest expansion.

2.4 Modelling socioeconomic factors

To examine the influence of socioeconomic factors on land-use change, we used data on average farmholder age and LU density from the Ministry of Agriculture, Forestry and Food. Additional spatial factors included distances from each farm holding to grassland persistence, gain, and loss zones, as well as to forest edges and roads, derived using the Proximity (raster distance) tool in QGIS. These factors reflect management intensity, spatial pressure, and accessibility affecting grassland dynamics.

Generalized Linear Models (GLMs) were fitted (family = gaussian; link = identity) in R (2024c), with the Rcmdr package (Fox et al. 2024), to test whether the predictors – (1) farm-holder age, (2) LU density, (3) forest proximity, and (4) road proximity – differentially explain grassland gain, loss, or persistence across the research area. This approach was selected since our response variables were not normally distributed.

The response variables were developed by calculating distance matrices from categories grassland gain, loss and persistence with the Proximity (raster distance) tool in QGIS. Moreover, explanatory variables were log- (farm-holder age, forest proximity and road proximity) or sqr- (LU density) transformed to secure normal distribution requirements. All models were evaluated at 0.05 α level. Model outputs were coefficients (β), standard errors (SE), t-values, and p-values for each predictor/explanatory variable.

3 Results

3.1 Land-use dynamics over two decades

Land-use analysis within the Natura 2000 site Kras for 2002 showed the dominance of forest cover, followed by grasslands and overgrown areas (Table 2). Forests were evenly distributed but fragmented in central zones, while grasslands prevailed in the central and southern parts. Overgrown patches were small and scattered. Built-up areas, vineyards, and arable land occurred mainly around larger settlements, occupying minimal total area (Figure 2, left).

By 2012, pronounced shifts were evident: forest area increased, grasslands declined sharply, and overgrown land moderately expanded. Arable land decreased, whereas built-up areas grew, with other categories showing minor variation (Figure 2, center).

In 2024, these trends largely continued. Forest cover slightly decreased, grasslands contracted further, and overgrown areas expanded substantially. Arable land recovered somewhat, vineyards declined, and built-up areas continued to grow at a slower pace. Other categories remained relatively stable (Figure 2, right).

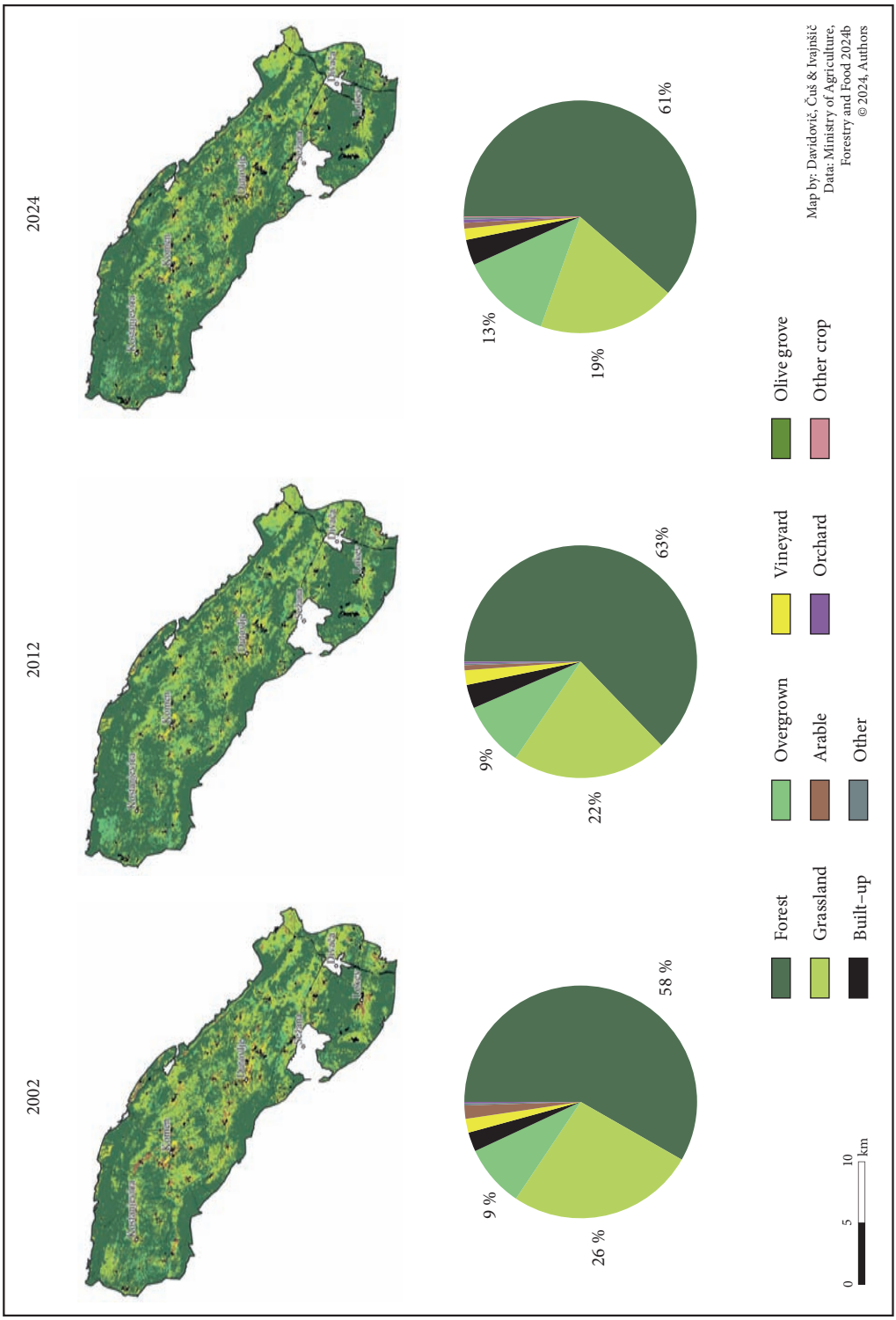
Across the entire 2002–2024 period, several dominant patterns emerged (Figure 3). Forests expanded by 1,247 ha (5%) to 24,618 ha (61% of the area), at an average rate of 56 ha/yr, mainly in central and northern sectors. Grasslands declined by 2,815 ha (27%) to 7,667 ha (19%), contracting by 128 ha/yr, especially near settlements and in the north. Overgrown areas rose by 1,646 ha (47%), reaching 5,125 ha (13%), with an average gain of 75 ha/yr, dispersed across the region. In absolute terms, the most pronounced changes were grassland loss and overgrowth expansion.

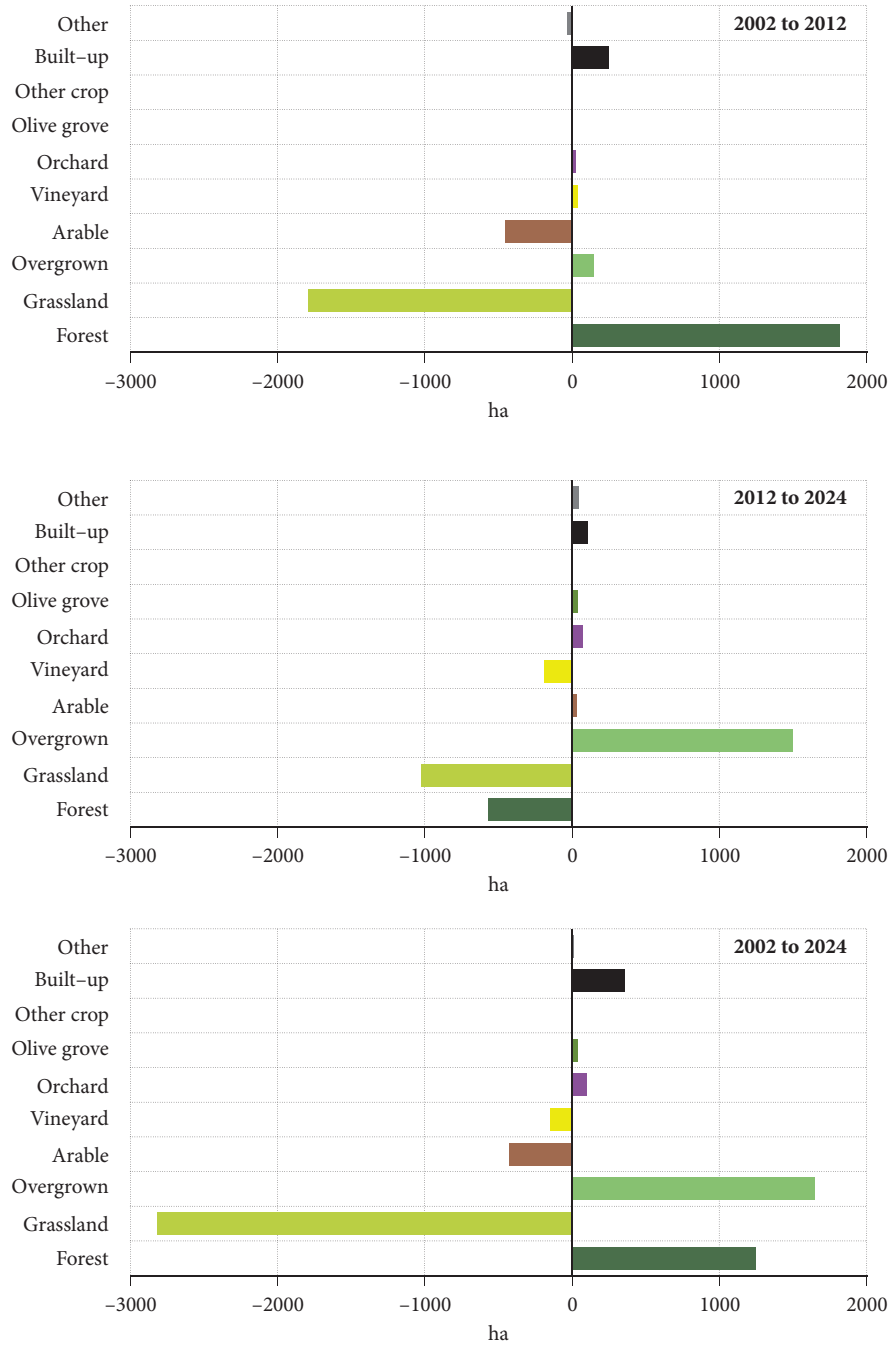
Other land-use classes also shifted: built-up areas increased by 33%, vineyards decreased 19%, and arable land shrank 57%. Orchards expanded 117%, while olive groves increased 23,430%. However, both together occupy only 215 ha (0.5%), and these extreme values may partly reflect methodological differences in data classification.

Table 2: Land-use changes in Natura 2000 site Kras (2002–2024).

Land use	Area 2002 (ha)	Area 2002 (%)	Area 2012 (ha)	Area 2012 (%)	Area 2024 (ha)	Area 2024 (%)	Δ 2002–2024 (ha)	Δ 2002–2024 (%)	Δ 2002–2024 (ha/year)
Forest	23375.57	58	25190.7	62.8	24618.2	61.4	1242.6	5.3	56
Grasslands	10481.85	26	8692.2	21.7	7666.9	19.1	−2814.9	−26.9	−128
Overgrown areas	3478.91	9	3629.4	9	5124.8	12.8	1645.9	47.3	75
Built-up areas	1075.89	3	1321.6	3.3	1430.9	3.6	355	33	16
Vineyards	770.64	2	809.8	2	621.8	1.6	−148.8	−19.3	−7
Arable land	742.01	2	286.7	0.7	319.6	0.8	−422.4	−56.9	−19
Other	113.27	0	80.5	0.2	121.3	0.3	8.1	7.1	0
Orchards	81.91	0	107.5	0.3	177.6	0.4	95.7	116.8	4
Other perennial crops	0.72	0	0	0	0.2	0	−0.6	−77.2	0
Olive groves	0.159	0	2.3	0	37.4	0.1	37.3	23429.6	2

Figure 2: Land use categories and structure. ► p. 68
Figure 3: Net land-use change by category. ► p. 69


2002
2012
2024
Koper
Izola
Piran
58 %
26 %
9 %
63%
22%
9%
61%
19%
13%
Forest
Grassland
Built–up
Overgrown
Arable
Other
Vineyard
Orchard
Olive grove
Other crop
0
5
10
km
Map by: Davidović, Čuš & Ivajnšič
Data: Ministry of Agriculture, Forestry and Food 2024b
© 2024, Authors


2002 to 2012
Other
Built–up
Other crop
Olive grove
Orchard
Vineyard
Arable
Overgrown
Grassland
Forest
−3000
−2000
−1000
0
1000
2000
ha
2012 to 2024
Other
Built–up
Other crop
Olive grove
Orchard
Vineyard
Arable
Overgrown
Grassland
Forest
−3000
−2000
−1000
0
1000
2000
ha
2002 to 2024
Other
Built–up
Other crop
Olive grove
Orchard
Vineyard
Arable
Overgrown
Grassland
Forest
−3000
−2000
−1000
0
1000
2000
ha

3.2 Spatial and temporal patterns of grassland change

During 2002–2012, creation was the dominant landscape process, affecting 77% of the region (Table 3). This reflected extensive expansion of forest and overgrown areas, particularly in the north, as well as the development of new vineyards, orchards, and olive groves. Dissection influenced 22% of the area, mainly within grasslands and agricultural zones, while attrition was limited and localized in the north, primarily reducing grasslands and cropland.

In the second period (2012–2024), dynamics shifted markedly: attrition became predominant, affecting 63% of the region, while dissection and creation impacted 19% and 18%, respectively. Although new land-use categories continued to emerge, the overall creation rate slowed, persisting mostly in forested areas near Komen and Dutovlje.

Across the full 2002–2024 period, two major processes prevailed – creation (79%) and dissection (21%). Creation reflected long-term forest and overgrowth expansion in northern and central sectors, whereas dissection indicated moderate fragmentation around urban areas. The dominance of creation over two decades highlights ongoing reforestation, natural succession, and agricultural decline, while the rise of attrition in the later period underscores accelerating grassland and farmland loss. Dissection decreased through time, showing reduced fragmentation.

Despite 60% persistence within the grassland class, major transformations occurred in 2002–2012. Grasslands declined by 27%, primarily around Lokvica and along main roads, contracting at 180 ha/yr. The south retained the most stable grasslands, while 13% of new grasslands emerged near settlements due to arable land abandonment (Figure 4, left).

Between 2012 and 2024, grassland dynamics stabilized: losses persisted but slowed to 21%, with a contraction rate of 85 ha/yr. Persistence rose to 69%, and new grassland formation declined to 10%. Although reduction continued, its pace lessened (Figure 4, centre).

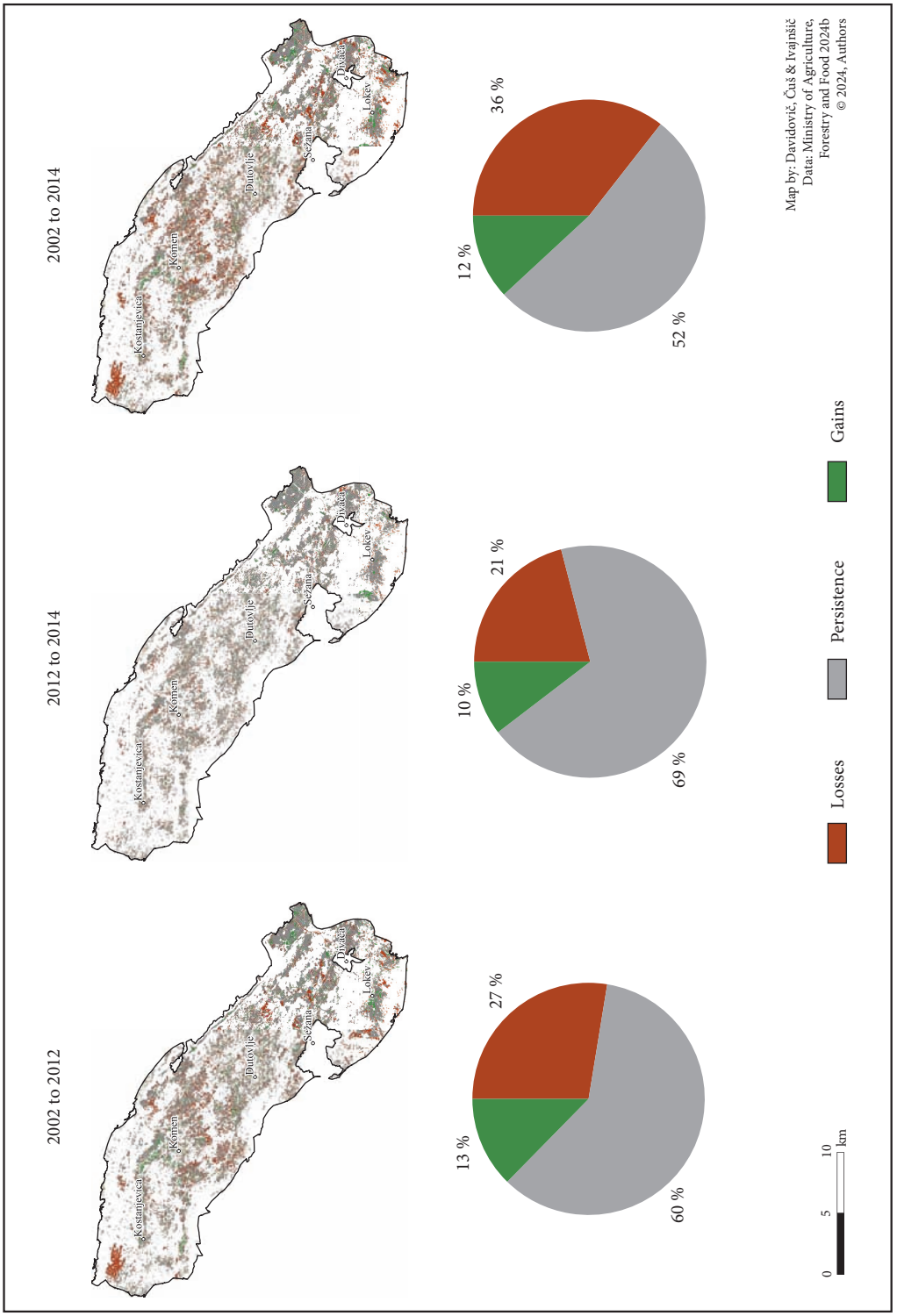
Over the full two decades, cumulative losses exceeded one-third (36%) of total grassland area, concentrated mainly in northern and central areas, where forests already border the plateau. The contraction rate averaged 128 ha/yr. Only 52% of grasslands remained stable, mainly in the south, while gains were minimal (12%), suggesting limited regeneration but indicating possible arable land abandonment (Figure 4, right).

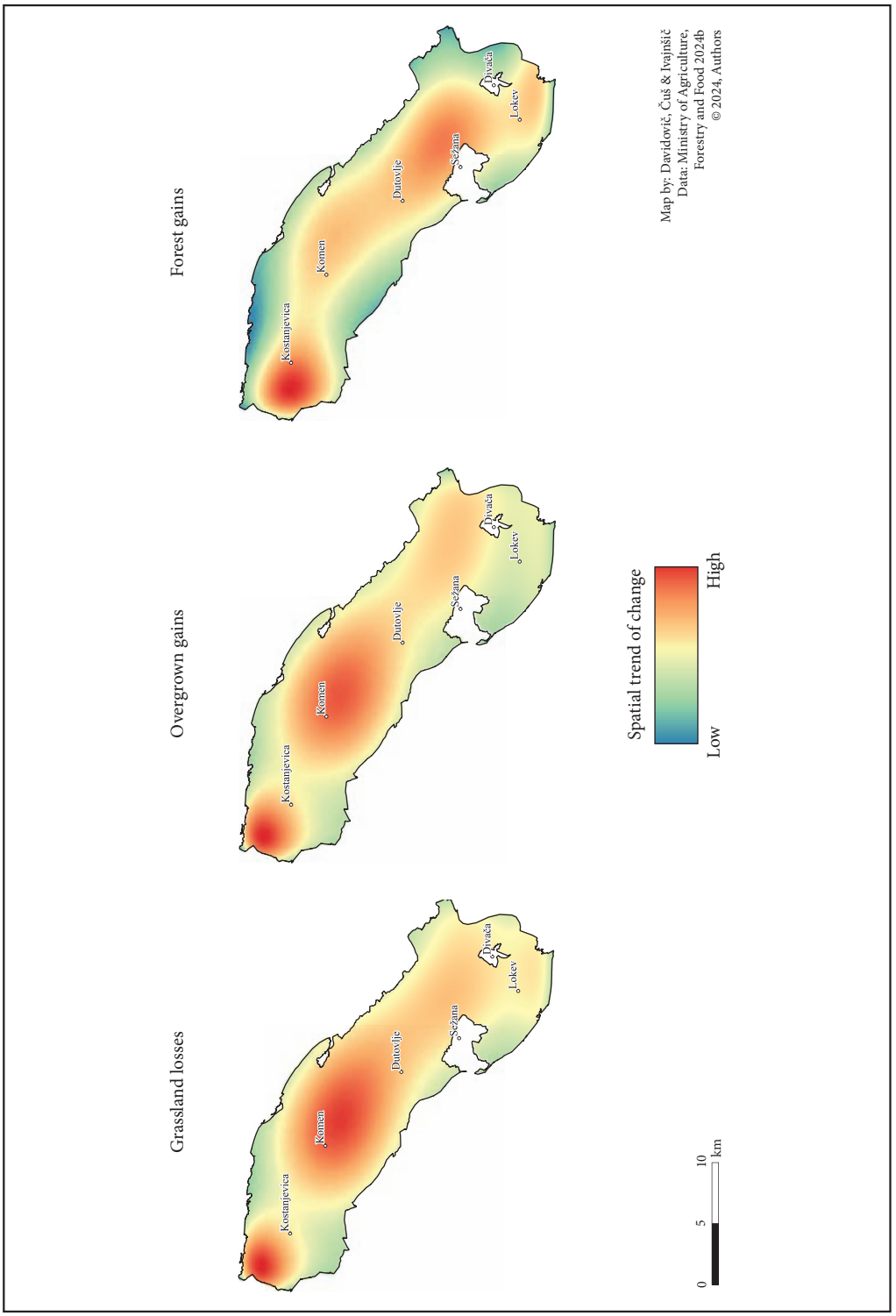
Spatial trend maps (Figure 5) reveal that landscape change was most dynamic in the central and northern parts of the region over the past two decades. The greatest grassland losses occurred around Kostanjevica na Krasu, Komen, Divača and Sežana. Overgrown areas expanded most intensively near Kostanjevica na Krasu and Komen, with additional hotspots around Sežana. Forest expansion was strongest near Kostanjevica na Krasu and Sežana and moderate in the Komen–Dutovlje area. The most stable zones are located along the regional margins, where higher elevations support climax forest communities. In contrast, southern areas show rapid grassland conversion directly into forest, with limited intermediate overgrowth.

Table 3: Dominant spatial process of grassland change in Natura 2000 site Kras (2002–2024).

Period	Process	Area (ha)	Area (%)
2002–2012	Attrition	80.54	0.20
	Creation	31060.44	77.42
	Dissection	8978.11	22.38
2012–2024	Attrition	25241.64	62.92
	Creation	7210.54	17.97
	Dissection	7666.92	19.11
2002–2024	Attrition	0.16	0.00
	Creation	31510.88	78.54
	Dissection	8608.06	21.46

Figure 4: Grassland transition dynamics. ► p. 71
Figure 5: Spatial trends of land-use changes. ► p. 72


2002 to 2012
2012 to 2014
2002 to 2014
Kostanjevica
Komen
Dutovlje
Sezana
Divaca
Lokev
13 %
27 %
60 %
10 %
21 %
69 %
12 %
36 %
52 %
Losses
Persistence
Gains
0
5
10
km
Map by: Davidovič, Čuš & Ivajnšič
Data: Ministry of Agriculture, Forestry and Food 2024b
© 2024, Authors


Grassland losses
Overgrown gains
Forest gains
Kostanjevica
Komen
Dutovlje
Sežana
Divača
Lokev
Spatial trend of change
Low
High
0
5
10
km
Map by: Davidovič, Čuš & Ivajnšič
Data: Ministry of Agriculture, Forestry and Food 2024b
© 2024, Authors

3.3 Socioeconomic factors of ecological succession

Results of the GLM analysis indicate that grassland dynamics are primarily shaped by spatial rather than demographic factors (Table 4). Grassland loss was primarily driven by landscape configuration. Forest proximity showed a moderate negative association ($\beta = -0.19$, $p = 0.02$), indicating that areas close to forests are more prone to conversion through shrub and tree encroachment. Road proximity had a moderate positive association ($\beta = 0.16$, $p = 0.04$), suggesting that accessibility facilitates gradual overgrowth. Neither farm-holder age ($\beta = -0.16$, $p = 0.77$) nor LU density ($\beta = 0.05$, $p = 0.38$) significantly affected this process.

Grassland persistence was most influenced by forest and road proximity. Forest proximity showed a strong negative association ($\beta = -0.56$, $p < 0.001$), confirming that encroaching forests substantially reduce grassland stability. Road proximity had a strong positive association ($\beta = 0.52$, $p < 0.001$), indicating that easier access enables continued management. LU density exhibited a moderate negative association ($\beta = -0.17$, $p = 0.02$), meaning that heavier grazing reduces long-term stability. Farm-holder age showed no significant effect ($\beta = 0.98$, $p = 0.23$).

Grassland gain was promoted by moderate grazing and limited by nearby forests. LU density had a moderate positive association ($\beta = 0.18$, $p = 0.02$), showing that balanced grazing supports regeneration. Forest proximity showed a moderate negative association ($\beta = -0.32$, $p = 0.01$), implying that forest adjacency constrains new grassland formation. Farm-holder age ($\beta = -0.39$, $p = 0.62$) and road proximity ($\beta = 0.09$, $p = 0.43$) were not significant.

Overall, the analysis shows that forest proximity, road proximity, and LU density are the principal factors of grassland change in the Natura 2000 site Kras. Forest edges accelerate succession and reduce persistence, road access enhances management but can also promote conversion, and moderate grazing intensity supports grassland renewal. Demographic factors such as farm-holder age exert only negligible influence.

Table 4: Descriptive statistics and regression analysis of grassland dynamics.

	Socioeconomic factors	$\bar{x}$	β	SE	t	p
Grassland losses	Age	61.6	–0.16	0.55	–0.3	0.77
	LU	1.8	0.05	0.05	0.88	0.38
	Forest proximity	**81.2**	**–0.19**	**0.08**	**–2.34**	**0.02**
	Road proximity	**169.5**	**0.16**	**0.08**	**2.03**	**0.04**
Grassland persistence	Age	63.2	0.98	0.82	1.19	0.23
	LU	**0.3**	**–0.17**	**0.08**	**–2.24**	**0.03**
	Forest proximity	**64.1**	**–0.56**	**0.12**	**–4.57**	**0.00**
	Road proximity	**117.8**	**0.52**	**0.11**	**4.63**	**0.00**
Grassland gains	Age	64.5	–0.39	0.79	–0.5	0.62
	LU	**0.7**	**0.18**	**0.08**	**2.36**	**0.02**
	Forest proximity	**93.8**	**–0.32**	**0.12**	**–2.72**	**0.01**
	Road proximity	161.4	0.09	0.11	0.78	0.43

$\bar{x}$ – mean; β – regression coefficient; SE – standard error; t – t-statistic; p – significance level.
Bold values indicate statistically significant results ($p < 0.05$; $\alpha = 0.05$).

4 Discussion

4.1 Processes driving grassland decline

Over the past two decades, the Natura 2000 site Kras experienced major land-use transitions, dominated by forest and overgrowth expansion and a pronounced grassland decline. These results confirm the long-term trend identified by Kaligarič and Ivajnšič (2014), who documented a drop in grassland cover from

82% in 1763 to 20% in 2012. Our findings (19% in 2024) align closely with these historical estimates, suggesting a continuing successional trajectory toward forest dominance, projected to reach 90% by 2100.

Forest and overgrown areas expanded by more than 50%, while grasslands contracted by over one-quarter, marking succession as the principal landscape process. These results mirror European trends of semi-natural grassland loss due to declining traditional land use and agricultural abandonment (Wilson et al. 2012; Dengler et al. 2014; Nita et al. 2019; Shipley et al. 2024). Land abandonment, depopulation, and farm-holder aging have reduced grazing and mowing, facilitating shrub and tree encroachment (Hülber et al. 2017; Loos et al. 2021). Minor increases in orchards and olive groves reflect localized intensification rather than broad agricultural recovery. Urban expansion, though spatially limited, has further replaced arable land and vineyards near settlements, emphasizing the need for integrated land-use planning to balance rural development and ecological integrity.

While natural succession remains the primary process behind grassland loss, anthropogenic and economic pressures accelerate it. Demographic effects were weak: farm-holder age showed no significant relationship to grassland dynamics ($p > 0.2$), likely due to uniformly older populations in the region. However, qualitative trends suggest that experienced farmers maintain traditional management beneficial for grassland stability (Ferreira-Rodríguez et al. 2021; Sucholas et al. 2022). Broader socioeconomic factors – particularly land-use profitability and market shifts – appear more decisive.

LU density is related to all processes, revealing a nonlinear relationship. High LU density correlated with grassland loss, supporting evidence that excessive grazing promotes degradation and succession (Eldridge et al. 2013; Pedley et al. 2023). Conversely, moderate LU values encouraged grassland gain, confirming that controlled grazing limits shrub encroachment and sustains open habitats (Rook and Tallowin 2003; Liang et al. 2021). These findings highlight the need for adaptive grazing management – reducing intensity on stable grasslands while promoting moderate grazing in overgrowing areas (Van Den Pol-van Dasselaar et al. 2020; Guo and Chen 2024).

Proximity to forests consistently emerged as the strongest spatial factor. Grasslands near forests were more prone to loss ($\beta = -0.19$, $p = 0.02$), confirming that adjacent forest edges accelerate succession via seed dispersal and altered microclimate (Lacasella et al. 2015; Rendeková et al. 2020). Yet, forest adjacency occasionally promoted persistence or gain by shielding grasslands from agricultural intensification (Wolański et al. 2021; Reeg et al. 2022). Hence, buffer-zone management and selective clearing along forest boundaries could balance protection and control of encroachment.

Road proximity exerted a dual effect. Grasslands closer to roads showed both higher persistence and higher loss rates – reflecting accessibility for management but also greater disturbance (Söderström et al. 2001; Deng et al. 2011). Remote sites were less disturbed yet more likely to undergo succession due to limited maintenance (Biró et al. 2013). Intermediate accessibility thus appears optimal, enabling periodic mowing and grazing without excessive pressure.

4.2 Ecological and socio-economic implications

Grassland transformation through abandonment and intensification has far-reaching ecological consequences. Fragmentation reduces landscape connectivity and biodiversity, disrupting pollination, dispersal, and trophic dynamics (Rösch et al. 2013; Staude et al. 2023). Shrub and forest encroachment lower habitat diversity and carbon storage potential (Rousset et al. 2024) and diminish erosion control (Liu et al. 2020). Biomass accumulation in overgrown areas increases wildfire risk, as demonstrated by large fires in 2022 and 2024.

Economically, grassland decline undermines local agriculture, tourism, and cultural identity (Premaratne and Somasiri 2015; Eriksson 2022). The disappearance of traditional landscapes weakens rural economies and erodes land-stewardship knowledge that once sustained ecological resilience.

Agri-environmental schemes have had limited success in halting grassland decline due to weak targeting, insufficient funding, and administrative barriers (Ivajnšič et al. 2018; Kaligarič et al. 2019). Many subsidized areas lacked high conservation value, and bureaucratic complexity discouraged participation. Effective policy should improve site selection, simplify procedures, ensure timely payments, and integrate local ecological knowledge (Žgavec et al. 2013; Dengler et al. 2014).

Climate change compounds these challenges. Rising temperatures, altered precipitation, and more frequent droughts intensify succession in sub-Mediterranean regions (Ivajnšič and Devetak 2020; Davidovič

et al. 2022). In Kras, overgrowth may raise evapotranspiration by 75% (Ivajnšič and Kaligarič 2015), altering species composition and threatening up to 63% of conservation-priority species by 2100 (Araújo et al. 2011; Damgaard 2022).

Conservation of semi-natural grasslands requires multi-scale, adaptive management integrating ecological, spatial, and socioeconomic dimensions:

- Adaptive grazing management: Reduce intensity in stable grasslands; apply moderate grazing to control shrub encroachment (Milazzo et al. 2023).
- Forest-edge management: Implement controlled clearing and maintain buffer zones to balance biodiversity and succession control (Iberl et al. 2023).
- Silvopastoral and mixed land-use systems: Integrate trees, shrubs, and pastures to diversify land cover, enhance carbon storage, and maintain open habitats while sustaining agricultural productivity (Mosquera-Losada et al. 2018).
- Targeted access planning: Maintain limited road access to enable management while minimizing disturbance (Sangha 2024).
- Policy reform: Strengthen incentives for extensive agriculture, promote market access for sustainable products, streamline bureaucracy, and improve communication with farmers (Žgavec et al. 2013; Hülber et al. 2017).
- Integration of traditional knowledge: Combine low-intensity practices with science-based management to enhance productivity and ecosystem services (Mekonen 2017; Bartual et al. 2019; Schils et al. 2022).

4.3 Study limitations

Several methodological constraints should be acknowledged. First, while national land-use datasets offer valuable regional coverage, integrating localized field observations would improve detection of management effects such as rotational grazing or periodic mowing. Second, the regression models include only selected socioeconomic predictors, excluding potentially influential environmental factors such as microclimate, biodiversity indicators, and climate-change effects. Future research should combine both socioeconomic and ecological factors to capture a fuller picture of grassland dynamics.

Finally, the use of proximity metrics (forest and road distances) effectively highlights spatial influences but may oversimplify landscape complexity. For example, distance to a road does not account for traffic intensity, seasonality, or disturbance frequency, all of which can differently affect grassland persistence or recovery. Incorporating traffic datasets or advanced landscape-connectivity models could therefore enhance understanding of spatial processes shaping grassland change.

5 Conclusion

The Natura 2000 site Kras is a vital ecological and cultural landscape where semi-natural grasslands sustain biodiversity and key ecosystem services. Over the past two decades, these grasslands have declined due to ecological succession, socio-economic change, and insufficiently effective conservation measures.

This study identified proximity to forests and roads as the strongest spatial factors of grassland dynamics, while livestock density and farm-holder age showed weaker, context-dependent effects. Forest encroachment – accelerated by natural succession and reduced traditional management – remains the principal threat. Grasslands near forest edges are most vulnerable to woody invasion, whereas limited road access constrains management practices such as mowing and grazing. Excessive livestock densities and the gradual loss of traditional ecological knowledge further intensify degradation risks.

Agri-environmental schemes, though conceptually sound, have proven only partly effective due to weak targeting, misallocated funding, and insufficient incentives for extensive management. A re-evaluation of policy frameworks is needed to improve the precision and local adaptation of support measures.

Conservation of Kras grasslands requires an integrated approach linking adaptive grazing, forest-edge management, and selective access planning with policy reform and community participation. Enhanced financial and technical assistance, combined with education and stakeholder cooperation, is essential to maintain ecological and cultural resilience.

In the context of climate change and socio-economic transition, decisive action is necessary to secure the biodiversity, ecosystem services, and heritage values of the Kras region. This study provides an empirical foundation for adaptive, multi-scale strategies that place grassland conservation at the core of sustainable landscape management.

ACKNOWLEDGMENT: The authors acknowledge the research project the project »Development of Research Infrastructure for the International Competitiveness of the Slovenian RRI Space-RI-SI-LifeWatch«, co-financed by the Republic of Slovenia, Ministry of Education, Science and Sport and the European Union from the European Regional Development Fund, the NOO project »ZELEN.KOM (3330-22-3514 (PP5))«, financed by Ministry of Higher Education, Science and Innovation Republic of Slovenia, as well as the Research Program »Slovene Identity and Cultural Awareness in Linguistic and Ethnic Contact Areas in Past and Present (P6-0372)«, financed by Slovenian Research and Innovation Agency.

RESEARCH DATA: For information on the availability of research data related to the study, please visit the article webpage: https://doi.org/10.3986/AGS.14021.

6 References

Araújo, M. B., Alagador, D., Cabeza, M., Nogués-Bravo, D., Thuiller, W. 2011: Climate change threatens European conservation areas: Climate change threatens conservation areas. *Ecology Letters* 14-5. https://doi.org/10.1111/j.1461-0248.2011.01610.x

Bai, Y., Cotrufo, M. F. 2022: Grassland soil carbon sequestration: Current understanding, challenges, and solutions. *Science* 377-6606. https://doi.org/10.1126/science.abo2380

Bartual, A. M., Sutter, L., Bocci, G., Moonen, A.-C., Cresswell, J., Entling, M., Giffard, B. et al. 2019: The potential of different semi-natural habitats to sustain pollinators and natural enemies in European agricultural landscapes. *Agriculture, Ecosystems & Environment* 279. https://doi.org/10.1016/j.agee.2019.04.009

Biró, M., Czúcz, B., Horváth, F., Révész, A., Csatári, B., Molnár, Z. 2013: Drivers of grassland loss in Hungary during the post-socialist transformation (1987–1999). *Landscape Ecology* 28-5. https://doi.org/10.1007/s10980-012-9818-0

Chytrý, M., Dražil, T., Hájek, M., Kalníková, V., Preislerová, Z., Šibík, J., Ujházy, K. et al. 2015: The most species-rich plant communities in the Czech Republic and Slovakia (with new world records). *Preslia* 87-3.

Dahlström, A., Iuga, A.-M., Lennartsson, T. 2013: Managing biodiversity rich hay meadows in the EU: a comparison of Swedish and Romanian grasslands. *Environmental Conservation* 40-2. https://doi.org/10.1017/s0376892912000458

Damgaard, C. 2022: Spatio-temporal modelling of the effect of selected environmental and land-use factors on species-rich calcareous grasslands: overgrazing and nitrogen deposition. *Basic and Applied Ecology* 72. https://doi.org/10.1016/j.baae.2023.07.001

Dasselaar, A. van den P., Golinski, P., Hennessy, D., Huyghe, C., Parente, G., Peyraud, J. L., Stienezen, M. W. J. 2013: Appreciation of current and future functions of grassland by international stakeholders in Europe. In: The Role of Grasslands in a Green Future: Threats and Perspectives in Less Favoured Areas. Proceedings of the 17th Symposium of the European Grassland Federation, Akureyri, Iceland, 23–26 June 2013. CABI.

Davidovič, D., Ivajnšič, D., Čuš, J. 2022: Interakcija naravnih in družbenih razmer kot pospeševalec zaraščanja Krasa. In: Primeri prostorskih analiz vplivov podnebnih sprememb: Monografija v okviru projekta Preprečevanje toplotnega stresa v urbanih sistemih v luči podnebnih sprememb (ARRS J7-1822). Univerza v Mariboru, Univerzitetna založba. https://doi.org/10.18690/um.fnm.8.2022.5

Deng, X., Huang, J., Huang, Q., Rozelle, S., Gibson, J. 2011: Do roads lead to grassland degradation or restoration? A case study in Inner Mongolia, China. *Environment and Development Economics* 16-6. https://doi.org/10.1017/S1355770X11000180

Dengler, J., Janišová, M., Török, P., Wellstein, C. 2014: Biodiversity of Palaearctic grasslands: A synthesis. *Agriculture, Ecosystems & Environment* 182. https://doi.org/10.1016/j.agee.2013.12.015

Eastman, R. J. 2024: TerrSet liberaGIS: Geospatial monitoring and modelling system. Clark University.

Eldridge, D. J., Soliveres, S., Bowker, M. A., Val, J. 2013: Grazing dampens the positive effects of shrub encroachment on ecosystem functions in a semi-arid woodland. *Journal of Applied Ecology* 50-4. https://doi.org/10.1111/1365-2664.12105

Envall, I., Bengtsson, J., Jakobsson, S., Rundlöf, M., Åberg, C., Lindborg, R. 2021: What is the effect of giving the grazers access to additional nutrient sources on biodiversity in semi-natural pastures? A systematic review protocol. *Environmental Evidence* 10-1. https://doi.org/10.1186/s13750-021-00230-2

Eriksson, O. 2022: Coproduction of food, cultural heritage and biodiversity by livestock grazing in Swedish semi-natural grasslands. *Frontiers in Sustainable Food Systems* 6. https://doi.org/10.3389/fsufs.2022.801327

Favretto, D., Poldini, L. 1986: Extinction time of a sample of Karst pastures due to bush encroachment. *Ecological Modelling* 33-2,4. https://doi.org/10.1016/0304-3800(86)90033-5

Feoli, E., Chiapella, L. F. 1979: Changements of vegetation pattern towards reforestation. *Colloquia Phytosociology* 8.

Feoli, E., Feoli-Chiapella, L., Ganis, P., Sorge, A. 1980: Spatial pattern analysis of abandoned grasslands of the Karst region by Trieste and Gorizia. *Studia Geobot* 1-1.

Feoli, E., Scimone, M. 1982: Gradient analysis in the spontaneous reforestation process of the Karst region. *Gortania* 3.

Ferreira-Rodríguez, N., Pavel, A. B., Cogălniceanu, D. 2021: Integrating expert opinion and traditional ecological knowledge in invasive alien species management: *Corbicula* in Eastern Europe as a model. *Biological Invasions* 23-4. https://doi.org/10.1007/s10530-020-02420-4

Fox, J., Marquez, M. M., Bouchet-Valat, M. 2024: Rcmdr: R Commander. R package version 2.9-5. *Software*.

Gigante, D., Angelucci, S., Bonini, F., Caruso, F., Di Cecco, V., Donnini, D., Morbidini, L. et al. 2024: Seminatural grasslands: An emblematic challenge for nature conservation in protected areas. *Land* 13-3. https://doi.org/10.3390/land13030386

Guo, Y., Chen, Y. 2024: A review of the impact of grazing on grassland ecosystems: Research progress and prospects. *Advances in Resources Research* 4-3. https://doi.org/10.50908/arr.4.3_455

Habič, P. 1979: Problematika geografskega vrednotenja krasa. *Geografski vestnik* 51.

Hejcman, M., Hejcmanová, P., Pavlů, V., Beneš, J. 2013: Origin and history of grasslands in Central Europe – a review. *Grass and Forage Science* 68-3. https://doi.org/10.1111/gfs.12066

Hopkins, A., Holz, B. 2006: Grassland for agriculture and nature conservation: Production, quality and multi-functionality. *Agronomy research* 4-1.

Horvatić, S. 1973: Syntaxonomic analysis of the vegetation of dry grassland and stony meadows in Eastern Adriatic coastal karst district based on the latest phytocoenological research. *Fragmenta Herbologica Jugoslavica* 32.

Hrvatin, M., Perko, D., Petek, F. 2006: Land use in selected erosion-risk areas of Tertiary low hills in Slovenia. *Acta geographica Slovenica* 46-1. https://doi.org/10.3986/AGS46103

Hülber, K., Moser, D., Sauberer, N., Maas, B., Staudinger, M., Grass, V., Wrbka, T., Willner, W. 2017: Plant species richness decreased in semi-natural grasslands in the Biosphere Reserve Wienerwald, Austria, over the past two decades, despite agri-environmental measures. *Agriculture, Ecosystems & Environment* 243. https://doi.org/10.1016/j.agee.2017.04.002

Iberl, K., Poschlod, P., Reisch, C. 2023: Restoration of calcareous grasslands by natural recolonization after forest clearing and its impact on the genetic variation of three common herb species. *Biodiversity and Conservation* 32-2. https://doi.org/10.1007/s10531-022-02518-2

Ivajnšič, D., Devetak, D. 2020: GIS-based modelling reveals the fate of antlion habitats in the Deliblato Sands. *Scientific Reports* 10-1. https://doi.org/10.1038/s41598-020-62305-3

Ivajnšič, D., Kaligarič, M. 2015: Can evapotranspiration be considered an additional indicator for understanding the changed landscape identity of the classic Karst? *Annales. Series historia naturalis* 25-2.

Ivajnšič, D., Pintarič, D., Škornik, S., Kaligarič, M., Pipenbaher, N. 2018: SOSKOPOP Haloze: podporni sistem potencialnim uveljaviteljem ukrepov KOPOP na nivoju travišč. *Revija za geografijo* 14-1.

Ivajnšič, D., Škornik, S., Kaligarič, M. 2013: Spremembe rabe tal med leti 1830 in 2008 na območju Movraškega Krasa in na bližnjih flišnih predelih. *Revija za geografijo* 8-1.

Jančar, T. 2014: Uničujoč vpliv kmetijske politike na travniške ptice. *Svet ptic* 20-2.

Jugovic, J., Črne, M., Pečnikar, Ž. F. 2013: The impact of grazing, overgrowth and mowing on spring butterfly (Lepidoptera: Rhopalocera) assemblages on dry karst meadows and pastures. *Natura Croatica* 22-1.

Kaligarič, M., Culiberg, M., Kramberger, B. 2006: Recent vegetation history of the North Adriatic grasslands: Expansion and decay of an anthropogenic habitat. *Folia Geobotanica* 41-3. https://doi.org/10.1007/BF02904940

Kaligarič, M., Čuš, J., Škornik, S., Ivajnšič, D. 2019: The failure of agri-environment measures to promote and conserve grassland biodiversity in Slovenia. *Land Use Policy* 80. https://doi.org/10.1016/j.landusepol.2018.10.013

Kaligarič, M., Ivajnšič, D. 2014: Vanishing landscape of the »classic« Karst: changed landscape identity and projections for the future. *Landscape and Urban Planning* 132. https://doi.org/10.1016/j.landurbplan.2014.09.004

Kaligarič, M., Poldini, L. 1996: New contributions on the typology of the vegetation of dry grasslands (Scorzoneretalia villosae H-IĆ 1975) in the North Adriatic karst. *Gortania* 19.

Kaligarič, M., Škornik, S. 2002: Contribution to the knowledge of the dry grassland vegetation on the highland areas of the Pohorje mountain (Slovenia). *Annales. Series historia naturalis* 12-1.

Kladnik, D. 2011: Širjenje gozda na krasu kot dejavnik prostorskega razvoja. *Geografski vestnik* 83-2.

Kmecl, P., Figelj, J., Jančar, T. 2014: Monitoring splošno razširjenih vrst ptic za določitev slovenskega indeksa ptic kmetijske krajine – poročilo za leto 2014. *Technical report*. DOPPS.

Kose, M., Melts, I., Heinsoo, K. 2022: Medicinal plants in semi-natural grasslands: Impact of management. *Plants* 11-3. https://doi.org/10.3390/plants11030353

Lacasella, F., Gratton, C., De Felici, S., Isaia, M., Zapparoli, M., Marta, S., Sbordoni, V. 2015: Asymmetrical responses of forest and »beyond edge« arthropod communities across a forest–grassland ecotone. *Biodiversity and Conservation* 24-3. https://doi.org/10.1007/s10531-014-0825-0

Lausi, D., Pignatti, S., Poldini, L. 1979: Statistische Untersuchungen über die Wiederbewaldung auf dem Triester Karst. In: Gesellschaftsentwicklung (Syndynamik). *Berichte der Internationalen Symposien der Internationalen Vereinigung für Vegetationskunde* 11. Springer Netherlands. https://doi.org/10.1007/978-94-011-7593-7_31

Liang, M., Liang, C., Hautier, Y., Wilcox, K. R., Wang, S. 2021: Grazing-induced biodiversity loss impairs grassland ecosystem stability at multiple scales. *Ecology Letters* 24-10. https://doi.org/10.1111/ele.13826

Liu, Y.-F., Liu, Y., Shi, Z.-H., López-Vicente, M., Wu, G.-L. 2020: Effectiveness of re-vegetated forest and grassland on soil erosion control in the semi-arid Loess Plateau. *CATENA* 195. https://doi.org/10.1016/j.catena.2020.104787

Loos, J., Krauss, J., Lyons, A., Föst, S., Ohlendorf, C., Racky, S., Röder, M. et al. 2021: Local and landscape responses of biodiversity in calcareous grasslands. *Biodiversity and Conservation* 30-8. https://doi.org/10.1007/s10531-021-02201-y

Mekonen, S. 2017: Roles of traditional ecological knowledge for biodiversity conservation. *Journal of Natural Sciences Research* 7-15.

Milazzo, F., Francksen, R. M., Abdalla, M., Ravetto Enri, S., Zavattaro, L., Pittarello, M., Hejduk, S. et al. 2023: An overview of permanent grassland grazing management practices and the impacts on principal soil quality indicators. *Agronomy* 13-5. https://doi.org/10.3390/agronomy13051366

Milcu, A., Hanspach, J., Abson, D., Fischer, J. 2013: Cultural ecosystem services: A literature review and prospects for future research. *Ecology and Society* 18-3. https://doi.org/10.5751/ES-05790-180344

Mosquera-Losada, M. R., Santiago-Freijanes, J. J., Rois-Díaz, M., Moreno, G., den Herder, M., Aldrey-Vázquez, J. A., Ferreiro-Domínguez, N. et al. 2018: Agroforestry in Europe: A land management policy tool to combat climate change. *Land Use Policy* 78. https://doi.org/10.1016/j.landusepol.2018.06.052

Nita, A., Hartel, T., Manolache, S., Ciocanea, C. M., Miu, I. V., Rozylowicz, L. 2019: Who is researching biodiversity hotspots in Eastern Europe? A case study on the grasslands in Romania. *PLoS ONE* 14-5. https://doi.org/10.1371/journal.pone.0217638

Pedley, D., McWilliam, W., Doscher, C. 2023: Forests from the grass: Natural regeneration of woody vegetation in temperate marginal hill farmland under minimum interference management. *Restoration Ecology* 31-3. https://doi.org/10.1111/rec.13852

Perko, D., Hrvatin, M., Ciglič, R. 2017: Determination of landscape hotspots of Slovenia. *Acta geographica Slovenica* 57-1. https://doi.org/10.3986/AGS.4618

Pipenbaher, N., Kaligarič, M., Škornik, S. 2011: Floristic and functional comparision of karst pastures and karst meadows from the North Adriatic Karst. *Acta Carsologica* 40-3. https://doi.org/10.3986/ac.v40i3.61

Poldini, L. 1989: La vegetazione del Carso isontino e triestino: studio del paesaggio vegetale fra Trieste, Gorizia e i Territori Adiacenti. Lint.

Premaratne, S., Somasiri, S. 2015: Strengthening livelihood of rural farmer populations through improved grasslands. In: Proceedings of the 23rd International Grassland Congress. Range Management Society of India.

Reed, H. E., Seastedt, T. R., Blair, J. M. 2005: Ecological consequences of C_4 grass invasion of a C_4 grassland: A dilemma for management. *Ecological Applications* 15-5. https://doi.org/10.1890/04-0407

Reeg, J., Strigl, L., Jeltsch, F. 2022: Agricultural buffer zone thresholds to safeguard functional bee diversity: Insights from a community modeling approach. *Ecology and Evolution* 12-3. https://doi.org/10.1002/ece3.8748

Rendeková, A., Miškovic, J., Mičieta, K., Michalová, M., Eliašová, M., Ballová, D. 2020: Changes in the diversity of dry calcareous grasslands after abandonment of traditional management in Devínska Kobyla national nature reserve (Southwestern Slovakia, Central Europe). *Ekológia (Bratislava)* 39-2. https://doi.org/10.2478/eko-2020-0008

Ribeiro, D., Šmid Hribar, M. 2019: Assessment of land-use changes and their impacts on ecosystem services in two Slovenian rural landscapes. *Acta geographica Slovenica* 59-2. https://doi.org/10.3986/AGS.6636

Rogerson, M., Brown, D. K., Sandercock, G., Wooller, J.-J., Barton, J. 2016: A comparison of four typical green exercise environments and prediction of psychological health outcomes. *Perspectives in Public Health* 136-3. https://doi.org/10.1177/1757913915589845

Rook, A. J., Tallowin, J. R. B. 2003: Grazing and pasture management for biodiversity benefit. *Animal Research* 52-2. https://doi.org/10.1051/animres:2003014

Rösch, V., Tscharntke, T., Scherber, C., Batáry, P. 2013: Landscape composition, connectivity and fragment size drive effects of grassland fragmentation on insect communities. *Journal of Applied Ecology* 50-2. https://doi.org/10.1111/1365-2664.12056

Rousset, C., Segura, C., Gilgen, A., Alfaro, M., Mendes, L. A., Dodd, M., Dashpurev, B. et al. 2024: What evidence exists relating the impact of different grassland management practices to soil carbon in livestock systems? A systematic map protocol. *Environmental Evidence* 13. https://doi.org/10.1186/s13750-024-00345-2

Sangha, S. 2024: Ecosystem Services and Urban Planning. *Journal of Applied Geographical Studies* 3-1. https://doi.org/10.47941/jags.1621

Schils, R. L. M., Bufe, C., Rhymer, C. M., Francksen, R. M., Klaus, V. H., Abdalla, M., Milazzo, F. et al. 2022: Permanent grasslands in Europe: Land use change and intensification decrease their multifunctionality. *Agriculture, Ecosystems & Environment* 330. https://doi.org/10.1016/j.agee.2022.107891

Shipley, J. R., Frei, E. R., Bergamini, A., Boch, S., Schulz, T., Ginzler, C., Barandun, M. et al. 2024: Agricultural practices and biodiversity: Conservation policies for semi-natural grasslands in Europe. *Current Biology* 34-16. https://doi.org/10.1016/j.cub.2024.06.062

Škornik, S., Vidrih, M., Kaligarič, M. 2010: The effect of grazing pressure on species richness, composition and productivity in North Adriatic Karst pastures. *Plant Biosystems – An International Journal Dealing with all Aspects of Plant Biology* 144-2. https://doi.org/10.1080/11263501003750250

Söderström, B., Svensson, B., Vessby, K., Glimskär, A. 2001: Plants, insects and birds in semi-natural pastures in relation to local habitat and landscape factors. *Biodiversity & Conservation* 10-11. https://doi.org/10.1023/A:1013153427422

Staude, I. R., Segar, J., Temperton, V. M., Andrade, B. O., de Sá Dechoum, M., Weidlich, E. W. A., Overbeck, G. E. 2023: Prioritize grassland restoration to bend the curve of biodiversity loss. *Restoration Ecology* 31-5. https://doi.org/10.1111/rec.13931

Stepišnik, U. 2011: Sediments in collapse dolines on the Kras plateau, Slovenia. *Acta geographica Slovenica* 51-2. https://doi.org/10.3986/AGS51201

Sucholas, J., Molnár, Z., Łuczaj, Ł., Poschlod, P. 2022: Local traditional ecological knowledge about hay management practices in wetlands of the Biebrza Valley, Poland. *Journal of Ethnobiology and Ethnomedicine* 18. https://doi.org/10.1186/s13002-022-00509-9

Šumrada, T., Erjavec, E. 2023: Will farmers cooperate to conserve biodiversity? The use of collective bonus in the High Nature Value farmland in Slovenia. *Acta geographica Slovenica* 63-3. https://doi.org/10.3986/AGS.11015

Tindale, S., Vicario-Modroño, V., Gallardo-Cobos, R., Hunter, E., Miškolci, S., Price, P. N., Sánchez-Zamora, P. et al. 2023: Citizen perceptions and values associated with ecosystem services from European grassland landscapes. *Land Use Policy* 127. https://doi.org/10.1016/j.landusepol.2023.106574

Tüxen, R., Horvat, I., Tüxen, R. 1974: Vegetation Südosteuropas: Tab. = Vegetation of Southeast-Europe. *Geobotanica selecta / hrsg. von R. Tüxen*. G. Fischer.

Van Den Pol-van Dasselaar, A., Hennessy, D., Isselstein, J. 2020: Grazing of dairy cows in Europe – An in-depth analysis based on the perception of grassland experts. *Sustainability* 12-3. https://doi.org/10.3390/su12031098

Veldkamp, A., Lambin, E. F. 2001: Predicting land-use change. *Agriculture, Ecosystems & Environment* 85-1. https://doi.org/10.1016/S0167-8809(01)00199-2

Wilson, J. B., Peet, R. K., Dengler, J., Pärtel, M. 2012: Plant species richness: The world records. *Journal of Vegetation Science* 23-4. https://doi.org/10.1111/j.1654-1103.2012.01400.x

Wolański, P., Bobiec, A., Ortyl, B., Makuch-Pietraś, I., Czarnota, P., Ziobro, J., Korol, M. et al. 2021: The importance of livestock grazing at woodland-grassland interface in the conservation of rich oakwood plant communities in temperate Europe. *Biodiversity and Conservation* 30-3. https://doi.org/10.1007/s10531-021-02115-9

Zhao, Y., Liu, Z., Wu, J. 2020: Grassland ecosystem services: A systematic review of research advances and future directions. *Landscape Ecology* 35-4. https://doi.org/10.1007/s10980-020-00980-3

Zorn, M., Kumer, P., Ferk, M. 2015: From forest to forest or where is the bare rocky Karst? *Kronika* 63-3.

Žuna Pfeiffer, T., Špoljarić Maronić, D., Petrošanec, S., Štolfa Čamagajevac, I., Stević, F. 2018: Steppe-like grassland as a refuge of the wild edible and medicinal plant species in anthropogenic landscape in north-eastern Croatia. *Plant Biosystems – An International Journal Dealing with all Aspects of Plant Biology* 152-5. https://doi.org/10.1080/11263504.2017.1415992

Zwitter, Ž., Rasran, L. 2023: Okoljska zgodovina med interdisciplinarnimi izzivi in rešitvami. In: Izzivi slovenskega zgodovinopisja v 21. stoletju: jubilejno 40. zborovanje slovenskih zgodovinark in zgodovinarjev. Zveza zgodovinskih društev Slovenije. Žgavec, D., Eler, K., Udovč, A., Batič, F. 2013: Contribution of agricultural policy measures to maintain grassland areas (the case of Radensko Polje Landscape Park). *Acta agriculturae Slovenica* 101-1. https://doi.org/10.14720/aas.2013.101.1.14949

Acta geographica Slovenica, 66-1, 2026, 81–98

KARSTIC MICROREFUGIA REFLECT DIVERSE BIOGEOGRAPHIC AFFINITIES OF VASCULAR PLANT SPECIES

Zoltán Bátori, Kata Frei, Gábor Li, Orsolya Valkó, András Vojtkó, Csaba Tölgyesi, Tünde Farkas, Alida Anna Hábenczyus, Ágnes Tóth, László Erdős, Zsófia Krivács, Balázs Deák



GÁBOR LI

Early-morning view of a doline field on the Bükk Plateau.

DOI: https://doi.org/10.3986/AGS.14564
UDC: 551.435.82:581.55(439)
574.1:551.435.82(439)
Creative Commons CC BY-SA 4.0

Zoltán Bátori[1], **Kata Frei**[1,2], **Gábor Li**[1,2], **Orsolya Valkó**[3], **András Vojtkó**[4], **Csaba Tölgyesi**[1,5], **Tünde Farkas**[6], **Alida Anna Hábenczyus**[5], **Ágnes Tóth**[1,2,3], **László Erdős**[3], **Zsófia Krivács**[1], **Balázs Deák**[3]

Karstic microrefugia reflect diverse biogeographic affinities of vascular plant species

ABSTRACT: Microrefugia are small areas that allow species to persist in changing environments. Dolines in karst landscapes may function as such safe havens. By analysing vegetation data from 270 plots collected within nine large dolines and on the surrounding plateau in Northern Hungary, we found that topographic complexity in dolines has the potential to support a wide array of plant species with diverse biogeographic affinities. To safeguard the large number of endangered plant species and the high biodiversity associated with dolines, conservation management should take into account the complex interactions among topographic complexity, environmental conditions, and species distributions in karstic microrefugia and their surrounding areas.

KEYWORDS: doline, environmental heterogeneity, grassland, mountain species, topography, Bükk Plateau, Hungary

Kraški mikrorefugiji odražajo biogeografsko raznolikost vaskularnih rastlinskih vrst

POVZETEK: Mikrorefugiji so majhna območja, ki omogočajo vrstam preživetje v spreminjajočih se okoljih. Vrtače v kraških pokrajinah lahko delujejo kot takšna varna zatočišča. Z analizo vegetacijskih podatkov iz severne Madžarske, zbranih na 270 popisnih ploskvah v devetih velikih vrtačah in na planoti izven njih, smo ugotovili, da topografska kompleksnost vrtač omogoča rast široke palete rastlinskih vrst z raznolikimi biogeografskimi značilnostmi. Da bi zaščitili veliko število ogroženih rastlinskih vrst in visoko biotsko raznovrstnost v vrtačah, bi morali v upravljanju in varstvu vrtač upoštevati kompleksne interakcije med topografsko kompleksnostjo, okoljskimi pogoji in razporeditvijo vrst v kraških mikrorefugijih in njihovi okolici.

KLJUČNE BESEDE: vrtače, okoljska heterogenost, travniki, gorske vrste, topografija, planota Bükk, Madžarska

The article was submitted for publication on July 8th, 2025.
Uredništvo je prejelo prispevek 8. julija 2025.

[1] University of Szeged, Department of Ecology, Szeged, Hungary
[2] University of Szeged, Doctoral School of Environmental Sciences, Szeged, Hungary
[3] HUN-REN Centre for Ecological Research, Institute of Ecology and Botany, 'Lendület' Seed Ecology Research Group, Vácrátót, Hungary
[4] Eszterházy Károly Catholic University, Department of Botany, Eger, Hungary
[5] University of Szeged, MTA-SZTE 'Momentum' Applied Ecology Research Group, Szeged, Hungary
[6] Aggtelek National Park Directorate, Jósvafő, Hungary

batori.zoltan@szte.hu (https://orcid.org/0000-0001-9915-5309), frei.kata@szte.hu (https://orcid.org/0000-0001-7585-7613), gaborli0622@gmail.com (https://orcid.org/0009-0000-2655-2194), festuca7@yahoo.com (https://orcid.org/0000-0002-0770-2107), toth.agnes.05@gmail.com (https://orcid.org/0009-0005-4681-4274), krivacs.zsofi@gmail.com (https://orcid.org/0009-0005-2422-6973), valko.orsolya@ecolres.hu (https://orcid.org/0000-0001-7919-6293), deak.balazs@ecolres.hu (https://orcid.org/0000-0001-6938-1997), erdos.laszlo@ecolres.hu (https://orcid.org/0000-0002-6750-0961), vojtkoa@gmail.com (https://orcid.org/0009-0006-9925-3981), alidaanna@gmail.com (https://orcid.org/0000-0003-0905-6724), farka.tunde74@gmail.com (https://orcid.org/0009-0001-4500-5011)

1 Introduction

Topographically complex landscapes often feature hotspots of biodiversity and promote ecosystem stability during large-scale environmental changes (Badgley et al. 2017). Microclimatic and edaphic gradients in such landscapes not only enable species to track regional climate changes, but also support the persistence of some populations by providing favourable local environmental conditions (Bátori et al. 2017; Ottaviani et al. 2019; Keppel et al. 2024). Therefore, range contraction is often not complete and, during episodes of changing climate, isolated (relict) populations can be left behind in enclaves with environmental conditions resembling the former ones (Hampe and Jump 2011). Such enclaves are known as microrefugia that may constitute the only chance of survival for a variety of species in many landscapes across the globe (Rull 2009; Dobrowski 2011; Keppel et al. 2012). For instance, Stewart and Lister (2001) highlighted that the European southern and eastern refugia for warm-adapted species were supplemented by microrefugia in Northern Europe during the Late Pleistocene. These microrefugia were likely associated with areas of sheltered topography that provided suitable climatic conditions for the long-term persistence of these species. On the other hand, specific topographic features (e.g., basins and valleys) promote cold-air pooling, supporting the survival of geographically restricted populations of cold-adapted plant and animal species during warmer climatic periods (Gentili et al. 2015). Some species may migrate towards areas at higher elevations (Walther et al. 2002), if there is no dispersal limitation (Willner et al. 2009).

Recent studies have demonstrated that specific microclimatic and soil conditions in topographically complex karst depressions (dolines) have the capacity to support an extremely high biodiversity with high turnover of species associated with different environmental conditions (Bátori et al. 2022a; Bátori et al. 2023; Marcin et al. 2024). As dolines are widespread topographic features in many karst landscapes worldwide, they play a key role in supporting global biodiversity, including many rare and endangered species (Su et al. 2017; Čarni et al. 2022; Bátori et al. 2023; Frei et al. 2023). For instance, the endangered rainforest-dwelling cycad species *Zamia decumbens* Calonje, Meerman, M.P. Griff. & Hoese frequently occurs in the dolines of the Maya Mountains (Belize) (Herrera-Blitman et al. 2022; Calonje et al. 2024). The pristine patches of moist evergreen broadleaf forests in the bottom of large dolines (i.e., tiankengs) in China provide safe havens for a high number of pteridophytes, such as *Diplazium maximum* (D.Don) C.Chr. (Shui et al. 2022). Dolines in Central and Southern Europe have provided safe havens for plant species associated with colder and/or moister conditions during warmer and drier periods of the Quaternary (Lazarević et al. 2009; Bátori et al. 2023). The continuous persistence of these populations is associated with unique microsites in dolines, maintained by cold-air pooling and/or water and nutrient retention (Bátori et al. 2022a; Pastore et al. 2022; Frei et al. 2023). For instance, the critically endangered endemic plant species *Horstrissea dolinicola* Greuter, Gerstb. & Egli (Apiaceae) in Crete (Greece) only occurs in the bottom of some dolines that are frequently flooded in springtime (Egli et al. 1990). The persistent cold and moist conditions on the north-facing slopes and bottoms of dolines in Hungary provide habitats for rare and endangered plant species associated with a colder and/or moister microclimate compared to the surrounding regional climate, such as *Aconitum vulparia* Rchb., *Arabidopsis halleri* (L.) O'Kane & Al-Shehbaz, *Daphne mezereum* L., *Dracocephalum ruyschiana* L., *Dryopteris borreri* Newman, *Ophioglossum vulgatum* L., *Ribes alpinum* L., and *Rosa pendulina* L. (Vojtkó 1999; Virók and Farkas 2008; Lazarević et al. 2009; Bátori et al. 2017). Although these examples clearly demonstrate the role of cool and moist north-facing slopes and bottoms of dolines as current and potential future microrefugia, few studies have proposed that slopes with other aspects may also serve as crucial habitats for the survival of certain plant species (cf. Bátori et al. 2023). Moreover, there is no evidence indicating whether dolines serve as important microsites for vascular plant species representing diverse biogeographic affinities.

The biogeographic affinities of plant species indicate the geographic regions or climatic zones to which these species are historically or ecologically linked. In other words, they reflect where a species originated, evolved, or where it typically thrives under natural conditions. Here we compare the distribution of vascular plant species within dolines (south-, east-, west-, and north-facing slopes, and bottoms) and on the surrounding plateau in Hungary in relation to their biogeographic affinities (Mediterranean, mountain, endemic, European, continental, and cosmopolitan groups). Specifically, we addressed the following question: How do the number and cover of plant species with different biogeographic affinities differ between dolines and the surrounding plateau, as well as among various microsites within dolines? By addressing this question, we aim to improve our understanding of the role of dolines as local biodiversity hotspots and potential future microrefugia.

2 Materials and Methods

2.1 Study region and sampling design

We studied dolines covered by grasslands on the Bükk Plateau (Bükk Mountains, Northern Hungary, 48°04'31" N, 20°29'57" E, between 750–800 m asl) (Figure 1). The region has a warm-summer humid continental climate (Dfb type according to the Köppen–Geiger classification) (Peel et al. 2007), with a mean annual temperature of 6.3°C and a mean annual precipitation of 800 mm (Dövényi 2010). The dominant grassland vegetation types in dolines and on the surrounding plateau are *Arrhenatherum elatius* hay meadows, *Festuca rubra* hay meadows, semi-dry rocky grasslands, and wet meadows. In addition, *Fagus sylvatica* L. stands and *Picea abies* (L.) H. Karst. plantations also occur in the surroundings of dolines (Bátori et al. 2023).

We selected five microsites (south-, east-, west-, and north-facing slopes, and bottoms) in nine large dolines (diameter: 80–100 m, depth: 10–15 m) for vegetation sampling (Figure 1). For each doline, we also sampled a microsite on the surrounding plateau. We established five randomly placed 1 m × 1 m vegetation plots at each microsite (nine dolines × six microsites × five vegetation plots: 270 plots in total). We visually estimated and recorded the percentage cover of each vascular plant species in the plots in August 2021, at the peak of the growing season (plot-level data are provided in Bátori et al. (2023)). Nomenclature follows 'The World Flora Online' (https://www.worldfloraonline.org).

2.2 Temperature and moisture indicator values

In order to compare the microclimatic differences among the microsites (plateau, south-, east-, west-, and north-facing slopes, and bottoms), we calculated the unweighted mean Ellenberg-type indicator values (EIVs) for temperature (T) and moisture (F) at the plot level, using the system of Borhidi (1995). Each species is assigned a value for T and F, representing its realised optimum on a nine-point (T) or twelve-point (F) ordinal scale, defined along environmental gradients. The primary distinction between the Borhidi and Ellenberg systems is that the Borhidi system is specifically adapted to the Hungarian flora and assigns an indicator value to every species, with no allowance for an indifferent category. We performed the calculation of plot-level EIV values by dividing the sum of the indicator values – corresponding to a specific EIV – of the plant species occurring in the given plot by the number of plant species in the plot. Previous studies have shown that, despite the ordinal nature of EIVs, mean EIVs provide reliable estimates of the environmental conditions of a habitat (Tölgyesi et al. 2014; Wildi 2016).

2.3 Biogeographic affinities of species

We classified all vascular plant species according to their biogeographic affinities (Table 1, examples are also shown in Figure 1) and assigned them to six biogeographic groups using the PADAPT 1.0 database (Sonkoly et al. 2023) as follows: 1) Mediterranean group, such as *Silene viridiflora* L., *Teucrium chamaedrys* L., and *Waldsteinia geoides* Willd.; 2) mountain group, such as *Aconitum variegatum* L., *Astrantia major* L., and *Bupleurum longifolium* L.); 3) endemic group: *Centaurea scabiosa* subsp. *sadleriana* (Janka) Asch. & Graebn, and *Dianthus giganteiformis* subsp. *pontederae* (A. Kern.) Soó (both species are Pannonian endemics); 4) European group, such as *Allium scorodoprasum* L., *Origanum vulgare* L., and *Vicia cracca* L.; 5) continental group, such as *Anemonoides sylvestris* (L.) Galasso, Banfi & Soldano, *Iris variegata* L., and *Pulsatilla grandis* Wend.; and 6) cosmopolitan group, such as *Achillea millefolium* L., *Convolvulus arvensis* L., and *Trifolium repens* L.

2.4 Statistical analyses

We determined the diagnostic species of the plateau and doline microsites by calculating the phi (Φ) coefficient of all individual species, using the JUICE software (Tichý 2002). Only species having a phi value higher than 0.15 were considered diagnostic species (Fisher's exact test, $p < 0.05$) (Tichý and Chytrý 2006). Diagnostic species of the microsites were compared according to their biogeographic affinities.

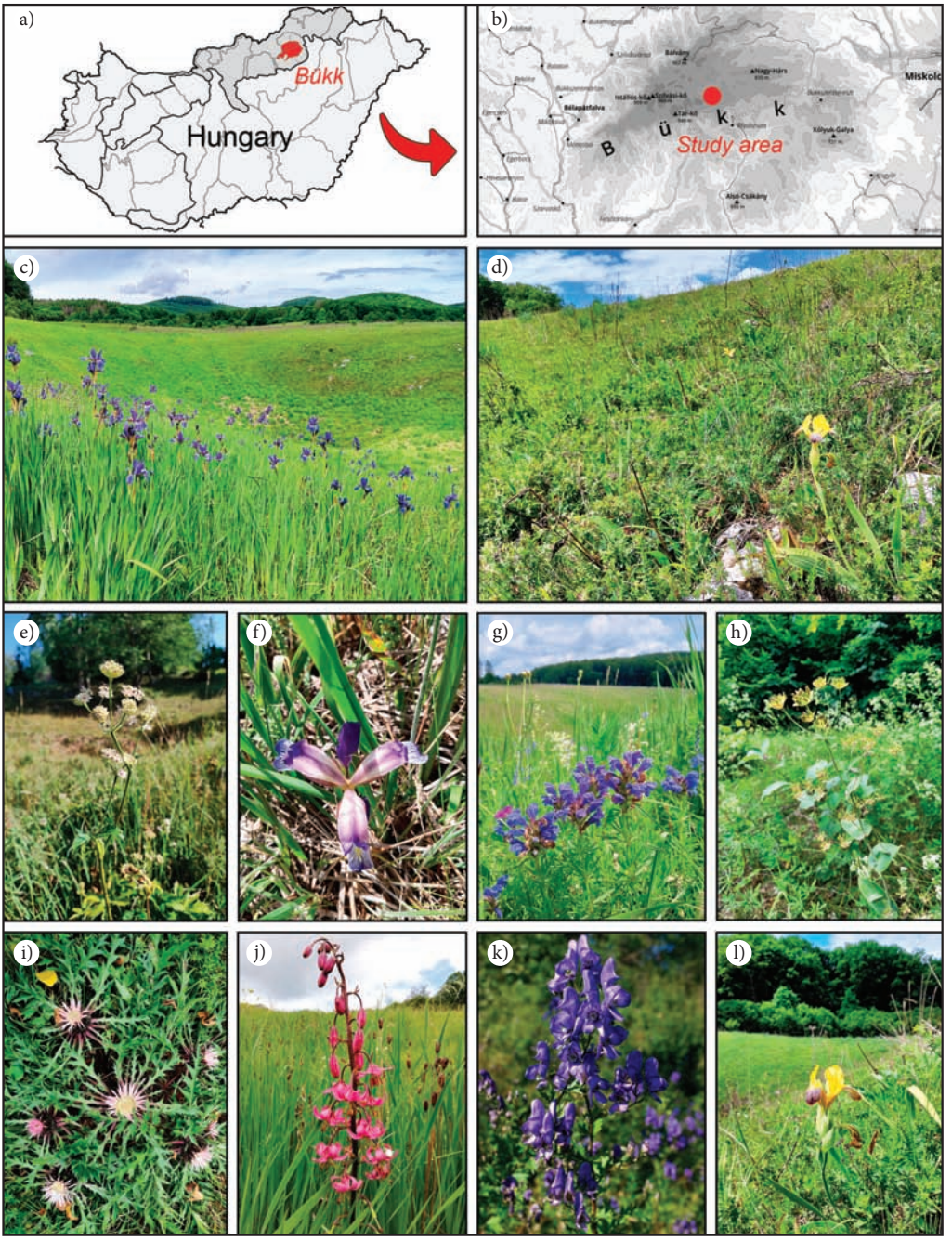


Figure 1: Map of the study region and study area, along with photos of microsites and characteristic rare and protected plant species. a) Study region in Hungary, b) study area in the Bükk Mountains, c) north-facing doline slope with a high cover of *Iris sibirica* L., d) south-facing doline slope with a high cover of *Iris variegata* L. and *Sempervivum globiferum* subsp. *hirtum* (L.) 't Hart & Bleij, e) *Astrantia major* L. in a doline bottom, f) *Iris graminea* L. on the plateau, g) *Dracocephalum ruyschiana* L. on an east-facing doline slope, h) *Bupleurum longifolium* L. on a north-facing doline slope, i) *Carlina acaulis* L. in a doline bottom, j) *Lilium martagon* L. in a doline bottom, k) *Aconitum variegatum* L. on a north-facing doline slope, and l) *Iris variegata* on a south-facing doline slope.

Table 1: A list of plant species assigned to the six biogeographic groups (Mediterranean, mountain, endemic, European, continental, and cosmopolitan groups).

Mediterranean group

Carex michelii
Colchicum autumnale
Cornus sanguinea
Cruciata glabra
Cruciata laevipes
Cruciata pedemontana
Geranium sanguineum
Muscari racemosum
Salvia verticillata
Sedum album
Silene viridiflora
Teucrium chamaedrys
Tragopogon dubius
Trifolium ochroleucon
Verbascum chaixii subsp. *austriacum*
Waldsteinia geoides

mountain group

Aconitum variegatum
Allium lusitanicum
Astrantia major
Bupleurum longifolium
Carlina acaulis
Centaurea phrygia subsp. *indurata*
Sempervivum globiferum subsp. *hirtum*

continental group

Ajuga genevensis
Anemonoides sylvestris
Asperula cynanchica
Carex montana
Cirsium pannonicum
Coronilla varia
Elymus hispidus
Euphorbia lucida
Geranium palustre
Gladiolus imbricatus
Glechoma hirsuta
Iris graminea
Iris variegata
Nonea pulla
Phleum phleoides
Potentilla recta
Pulsatilla grandis
Ranunculus polyanthemos
Scabiosa ochroleuca
Tanacetum corymbosum
Thalictrum lucidum
Trifolium montanum
Veronica austriaca subsp. *dentata*

cosmopolitan group

Achillea millefolium
Asplenium trichomanes
Botrychium lunaria
Briza media
Convolvulus arvensis
Dactylis glomerata
Deschampsia caespitosa
Koeleria cristata
Luzula campestris
Poa compressa
Poa pratensis s.l.
Potentilla reptans
Prunella vulgaris
Trifolium repens
Urtica dioica

endemic group

Centaurea scabiosa subsp. *sadleriana*
Dianthus giganteiformis subsp. *pontederae*

European group

Arrhenatherum elatius
Asplenium ruta-muraria
Astragalus glycyphyllos
Betonica officinalis
Betula pendula
Brachypodium pinnatum
Calamagrostis arundinacea
Calamagrostis epigejos
Campanula glomerata
Campanula patula
Campanula persicifolia
Cardamine pratensis
Carex caryophyllea
Carex hirta
Carex leporina
Carex pallescens
Carex pilosa
Carex praecox
Carex spicata
Carex tomentosa
Centaurea jacea agg.
Cerastium arvense subsp. *matrense*
Cirsium arvense
Cirsium eriophorum
Cirsium vulgare
Clinopodium acinos
Clinopodium vulgare
Genista tinctoria
Gentiana cruciata
Gentiana pneumonanthe
Gymnadenia conopsea
Helianthemum nummularium
Helictochloa praeusta
Helictotrichon pubescens
Hieracium umbellatum
Hylotelephium maximum
Hypericum hirsutum
Hypericum perforatum
Hypochaeris maculata
Iris sibirica
Jacobaea vulgaris
Knautia arvensis
Lathyrus pratensis
Leontodon hispidus
Leucanthemum vulgare
Lilium martagon
Linaria vulgaris
Linum catharticum
Lotus corniculatus
Luzula luzuloides
Lysimachia nummularia
Medicago falcata
Medicago lupulina
Mercurialis perennis
Pulmonaria mollis
Pulmonaria obscura
Ranunculus acris
Ranunculus auricomus
Ranunculus repens
Ribes uva-crispa
Rosa canina agg.
Rubus idaeus
Rumex acetosa
Salvia pratensis
Sanguisorba minor
Saponaria officinalis
Scorzoneroides autumnalis
Sedum acre
Selinum carvifolia
Seseli libanotis
Silene vulgaris
Solidago virgaurea
Stellaria graminea
Stellaria holostea
Succisa pratensis
Symphytum tuberosum
Taraxacum officinale
Thesium linophyllon
Thymus pulegioides subsp. *pannonicus*
Trifolium alpestre
Trifolium aureum

Dianthus deltoides
Digitalis grandiflora
Dracocephalum ruyschiana
Elymus repens
Euphorbia cyparissias
Fallopia convolvulus
Festuca heterophylla
Festuca pratensis
Festuca rubra
Festuca rupicola
Filipendula ulmaria
Filipendula vulgaris
Fragaria vesca
Galanthus nivalis
Galeopsis pubescens
Galium boreale
Galium mollugo
Galium schultesii
Galium verum
Molinia caerulea
Myosotis ramosissima
Nardus stricta
Ophioglossum vulgatum
Origanum vulgare
Parnassia palustris
Peucedanum palustre
Phleum pratense
Pimpinella saxifraga
Plantago media
Polygala comosa
Polygonatum odoratum
Potentilla argentea
Potentilla erecta
Potentilla heptaphylla
Primula elatior
Primula veris
Prunella grandiflora
Prunus spinosa
Trifolium medium
Trifolium pratense
Tussilago farfara
Valeriana officinalis subsp. *collina*
Verbascum thapsus
Veronica chamaedrys
Veronica officinalis
Veronica spicata
Vicia cracca
Vicia sepium
Vicia tetrasperma
Vincetoxicum hirundinaria
Viola canina
Viola hirta
Viola mirabilis
Viola reichenbachiana

We tested the effects of microsites (plateau, south-, east-, west-, and and bottoms) on the mean Ellenberg-type indicator values (temperature and moisture), and on the number and cover of species within each biogeographic group (Mediterranean, mountain, endemic, European, continental, and cosmopolitan groups). We used linear mixed-effects models (LMMs) with Gaussian error distribution for the mean indicator values and species cover data, and generalised linear mixed-effects models (GLMMs) with Poisson error distribution for the species number data – except for the species number data of the endemic group, for which we used a binomial error distribution because only two species with low frequency belonged to this group. In the models, the mean indicator values, as well as the number and cover of species in the vegetation plots were used as response variables, with microsite (plateau, south-, east-, west-, and north-facing slopes, and bottoms) included as a fixed factor, and doline ID as a random factor. We performed all analyses in R v. 4.2.2 (R Foundation … 2022) using the *lmer* and *glmer* functions of the 'lme4' package (Bates et al. 2015), the *Anova* function of the 'car' package to test model significances, and the *emmeans* function of the 'emmeans' package to calculate pairwise comparisons (Lenth 2023).

3 Results

A total of 211 vascular plant species were recorded in the plots. Vegetation on south-facing slopes indicated significantly warmer conditions than all other microsites, except for east-facing slopes, while vegetation on north-facing slopes and bottoms indicated the coldest conditions (Figure 2, Table 2). A similar pattern was observed for moisture conditions among the microsites, with vegetation on south-facing slopes indicating significantly drier, and on north-facing slopes and in bottoms significantly moister conditions compared to all other microsites.

We recorded 16 species (7.6%) belonging to the Mediterranean group, eight species belonging to the mountain group (3.8%), two species (0.9%) belonging to the endemic group, 147 species belonging to the European group (69.7%), 23 species (10.9%) belonging to the continental group, and 15 species belonging to the cosmopolitan group (7.1%) in the vegetation plots.

Considering the diagnostic species of the microsites, we found 13 diagnostic species for the plateau, 20 species for south-facing slopes, 18 species for east-facing slopes, 10 species for west-facing slopes, 23 species for north-facing slopes, and 20 species for bottoms. In terms of the distribution of biogeographic groups, south-facing slopes exhibited the highest diversity (six groups), while east-facing slopes and bottoms showed the lowest (three groups). The proportion of the Mediterranean group was highest on east-facing slopes (17%), while the proportion of the mountain group was highest on south- and north-facing slopes (5% and 4%, respectively) (Figure 3, Table 3). The proportions of the endemic and continental groups were highest on the plateau (8 and 31%, respectively), while the European group had the lowest proportion in this microsite (46%). Bottoms had the highest proportion of cosmopolitan species (15%).

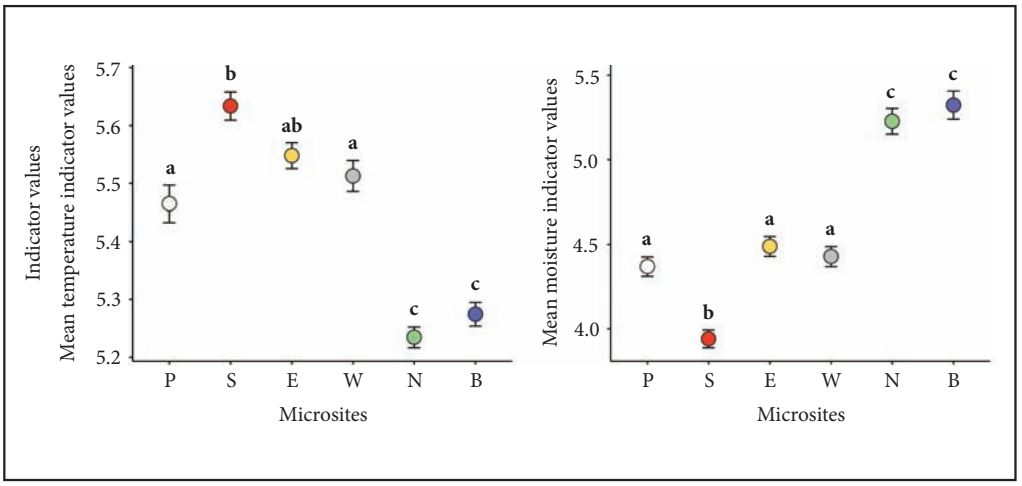


Figure 2: Mean Ellenberg-type indicator values for temperature and moisture (mean ± SE). Lowercase letters (a–c) indicate significant differences (LMMs, $p < 0.05$) among the microsites (P: plateau, S: south-facing slopes of dolines, E: east-facing slopes of dolines, W: west-facing slopes of dolines, N: north-facing slopes of dolines, and B: doline bottoms).

Table 2: Test results of linear mixed-effects models (LMMs) used for the mean Ellenberg-type indicator values (temperature and moisture) across the microsites (P: plateau, S: south-facing slopes of dolines, E: east-facing slopes of dolines, W: west-facing slopes of dolines, N: north-facing slopes of dolines, and B: doline bottoms). Pairwise differences ($p < 0.05$) are marked with boldface.

	Mean temperature indicator values		Mean moisture indicator values	
Microsite	F 47.56	*p* **<0.001**	F 73.47	*p* **<0.001**
	t	*p*	t	*p*
B – E	–8.45	**<0.001**	9.42	**<0.001**
B – N	1.23	0.820	1.08	0.888
B – P	–5.88	**<0.001**	10.77	**<0.001**
B – S	–11.10	**<0.001**	15.61	**<0.001**
B – W	–7.36	**<0.001**	10.10	**<0.001**
E – N	9.68	**<0.001**	–8.34	**<0.001**
E – P	2.57	0.110	1.35	0.755
E – S	–2.65	0.090	6.19	**<0.001**
E – W	1.09	0.887	0.68	0.984
N – P	–7.12	**<0.001**	9.69	**<0.001**
N – S	–12.33	**<0.001**	14.53	**<0.001**
N – W	–8.60	**<0.001**	9.02	**<0.001**
P – S	–5.21	**<0.001**	4.84	**<0.001**
P – W	–1.48	0.678	–0.68	0.984
S – W	3.73	**0.003**	–5.51	**<0.001**

Figure 3: Biogeographic affinities of the diagnostic species across the microsites (plateau, south-, east-, west-, and north-facing slopes of dolines, and doline bottoms). The numbers indicate the number and proportion of diagnostic species belonging to each group. ► p. 89

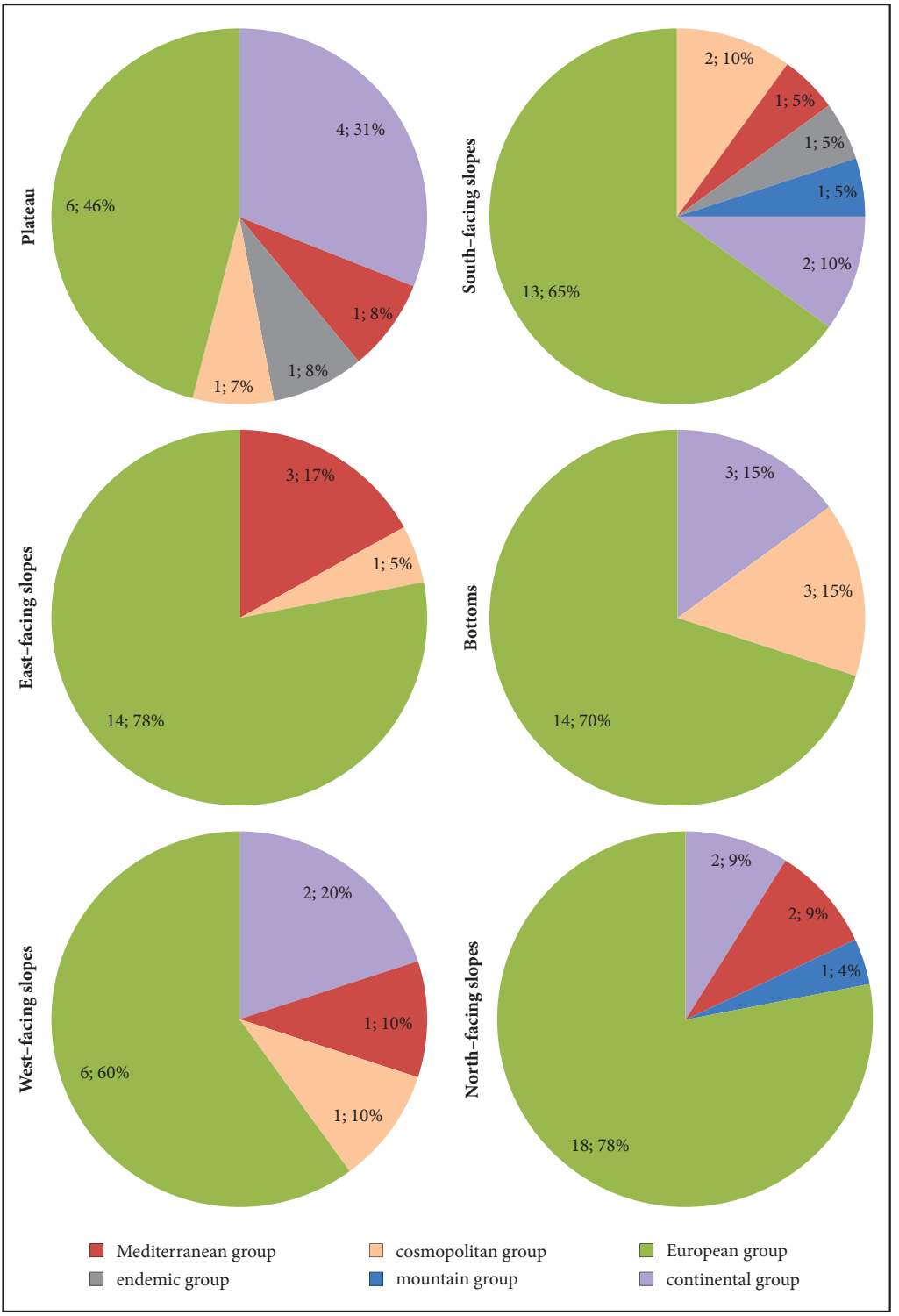

Plateau
4; 31%
6; 46%
1; 8%
1; 8%
1; 7%
South–facing slopes
2; 10%
1; 5%
1; 5%
1; 5%
2; 10%
13; 65%
East–facing slopes
3; 17%
1; 5%
14; 78%
Bottoms
3; 15%
3; 15%
14; 70%
West–facing slopes
2; 20%
1; 10%
6; 60%
1; 10%
North–facing slopes
2; 9%
2; 9%
1; 4%
18; 78%
Mediterranean group
cosmopolitan group
European group
endemic group
mountain group
continental group

Table 3: Diagnostic species of the plateau and doline microsites (south-, east-, west- and north-facing slopes, and bottoms) according to their biogeographic affinities (phi (Φ) coefficients of association between species and microsites are provided in Bátori et al. (2023)).

Plateaus

Mediterranean group: *Carex michelii*; **endemic group:** *Centaurea scabiosa* subsp. *sadleriana*; **European group:** *Seseli libanotis*, *Allium oleraceum*, *Galium verum*, *Filipendula vulgaris*, *Carex pallescens, Helictotrichon pubescens*; **continental group:** *Trifolium montanum*, *Phleum phleoides*, *Veronica austriaca* subsp. *dentata, Thalictrum lucidum*; **cosmopolitan group:** *Briza media*

South-facing doline slopes

Mediterranean group: *Teucrium chamaedrys*; **mountain group:** *Sempervivum globiferum* subsp. *hirtum*; **endemic group:** *Dianthus giganteiformis* subsp. *pontederae*; **European group:** *Polygonatum odoratum*, *Medicago lupulina*, *Arabis hirsuta*, *Digitalis grandiflora*, *Clinopodium acinos*, *Carex praecox*, *Thymus pulegioides* subsp. *pannonicus*, *Carex caryophyllea*, *Potentilla heptaphylla*, *Hylotelephium maximum*, *Festuca rupicola*, *Euphorbia cyparissias*, *Sedum acre*; **continental group:** *Iris variegata, Coronilla varia*; **cosmopolitan group:** *Koeleria cristata*, *Poa compressa*

East-facing doline slopes

Mediterranean group: *Verbascum chaixii* subsp. *austriacum*, *Cruciata laevipes*, *Waldsteinia geoides*; **European group:** *Viola hirta*, *Rosa canina* agg., *Galium mollugo*, *Veronica chamaedrys*, *Clinopodium vulgare*, *Acer platanoides*, *Lilium martagon*, *Veronica spicata*, *Hypericum hirsutum*, *Digitalis grandiflora*, *Origanum vulgare*, *Agrimonia eupatoria*, *Fallopia convolvulus*, *Stellaria holostea*; **cosmopolitan group:** *Convolvulus arvensis*

West-facing doline slopes

Mediterranean group: *Salvia verticillata*; **continental group:** *Carex montana*, *Tanacetum corymbosum*; **European group:** *Cirsium arvense*, *Trifolium alpestre*, *Pimpinella saxifraga*, *Salvia pratensis*, *Prunella grandiflora*, *Carex tomentosa*; **cosmopolitan group:** *Luzula campestris*

North-facing doline slopes

Mediterranean group: *Cruciata glabra*, *Colchicum autumnale*; **mountain group:** *Bupleurum longifolium*; **European group:** *Helictochloa praeusta*; *Luzula luzuloides*, *Alchemilla monticola*, *Filipendula ulmaria*, *Veronica chamaedrys*, *Leontodon hispidus*, *Rubus idaeus*, *Hypochaeris maculata*, *Trifolium aureum*, *Cirsium eriophorum*, *Dianthus deltoides*, *Agrostis capillaris*, *Potentilla erecta*, *Festuca pratensis*, *Ranunculus auricomus*, *Stellaria graminea*, *Rumex acetosa*, *Aegopodium podagraria*; **continental group:** *Ranunculus polyanthemos*, *Glechoma hirsuta*

Doline bottoms

European group: *Gentiana pneumonanthe*, *Selinum carvifolia, Plantago media*, *Calamagrostis epigejos*, *Vicia cracca*, *Ophioglossum vulgatum*, *Alopecurus pratensis*, *Carex pilosa*, *Leucanthemum vulgare*, *Calamagrostis arundinacea*, *Molinia caerulea*, *Lathyrus pratensis*, *Vicia sepium*, *Carex hirta*; **continental group:** *Gladiolus imbricatus*, *Elymus repens*, *Geranium palustre*; **cosmopolitan group:** *Deschampsia caespitosa*, *Potentilla reptans*, *Urtica dioica*

At the plot level, the number of species belonging to the Mediterranean group tended to be highest on east- and west-facing slopes and lowest in bottoms (Figure 4, Table 4). Their cover was similarly high on the plateau, as well as on south-, east-, and west-facing slopes, and lowest on north-facing slopes and in bottoms. The number of species belonging to the mountain group tended to be highest on north-facing slopes, while their cover tended to be highest in bottoms. The number of species belonging to the endemic group tended to be highest on south-facing slopes, while no endemic species occurred on north-facing slopes or in bottoms. The number and cover of species belonging to the European group tended to be lowest on south-facing slopes, and their cover was highest on north-facing slopes (Figure 5, Table 4). The number and cover of species belonging to the continental group tended to be lowest on north-facing slopes or in bottoms. The cover of species belonging to the cosmopolitan group tended to be lowest on the plateau and south-facing slopes, and highest in the bottoms.

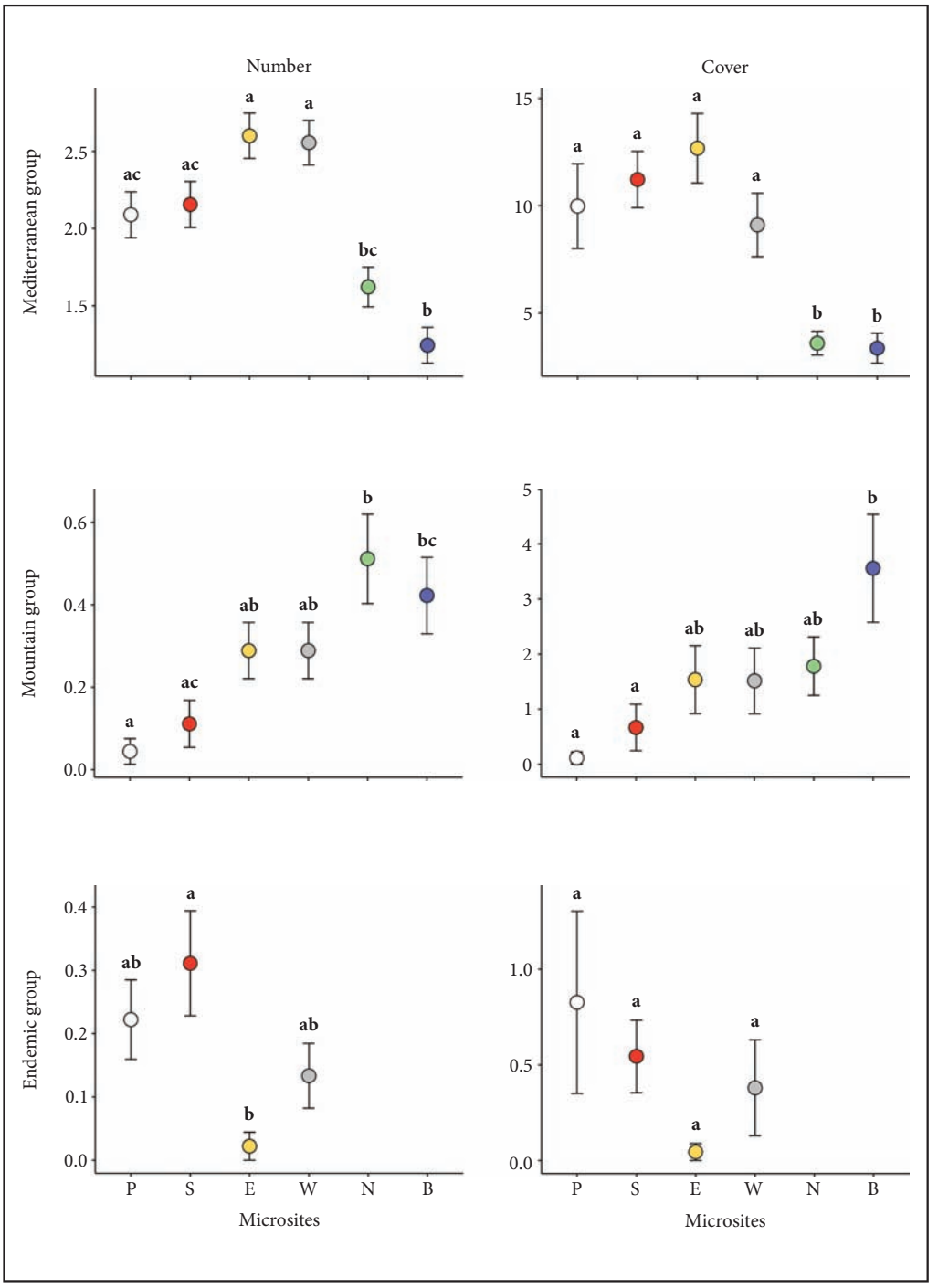


Figure 4: Number and cover of species belonging to the Mediterranean, mountain and endemic groups (mean ± SE) across the microsites. Lowercase letters (a–c) indicate significant differences (LMMs and GLMMs, $p < 0.05$) among the microsites (P: plateau, S: south-facing slopes of dolines, E: east-facing slopes of dolines, W: west-facing slopes of dolines, N: north-facing slopes of dolines, and B: bottoms).

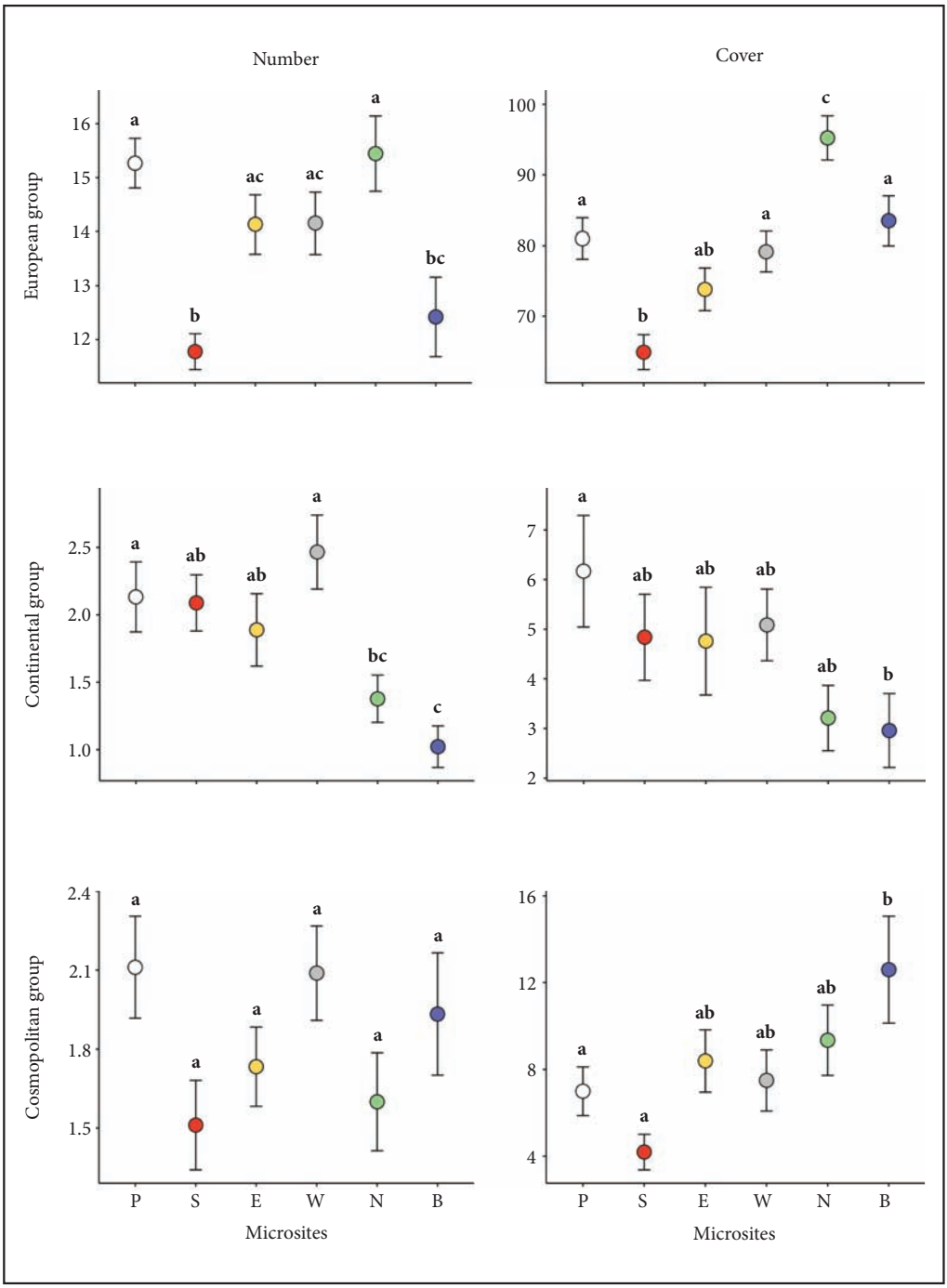


Figure 5: Number and cover of species belonging to the European, continental and cosmopolitan groups (mean ± SE) across the microsites. Lowercase letters (a–c) indicate significant differences (LMMs and GLMMs, $p < 0.05$) or marginally significant differences (LMMs and GLMMs, $0.05 < p < 0.08$) among the microsites (P: plateau, S: south-facing slopes of dolines, E: east-facing slopes of dolines, W: west-facing slopes of dolines, N: north-facing slopes of dolines, and B: bottoms of dolines).

THIS IS NOT A FINAL VERSION

Table 4: Test results of the linear mixed-effects models (LMMs) used for the cover of species groups and the generalized linear mixed-effects models (GLMMs) used for the number of species groups across the microsites (P: plateau, S: south-facing slopes of dolines, E: east-facing slopes of dolines, W: west-facing slopes of dolines, N: north-facing slopes of dolines, and B: doline bottoms). Significant pairwise differences ($p < 0.05$) are marked with boldface, while marginally significant differences ($0.05 < p < 0.08$) are marked with bold italics.

	Number of species belonging to the Mediterranean group		Cover of species belonging to the Mediterranean group		Number of species belonging to the mountain group		Cover of species belonging to the mountain group	
	F	*p*	F	*p*	F	*p*	F	*p*
Microsite	6.01	**<0.001**	9.44	**<0.001**	3.93	**0.001**	4.05	**0.001**
	t	*p*	t	*p*	t	*p*	t	*p*
B – E	–4.54	**<0.001**	–5.14	**<0.001**	1.06	0.897	2.44	0.145
B – N	–1.49	0.669	–0.13	1.000	–0.62	0.990	2.15	0.266
B – P	–3.07	**0.026**	–3.65	**0.004**	3.05	**0.028**	4.16	**0.001**
B – S	–3.27	**0.014**	-4.33	**<0.001**	2.68	0.080	3.49	**0.007**
B – W	–4.42	**<0.001**	–3.17	**0.021**	1.06	0.897	2.47	0.137
E – N	3.16	**0.020**	5.01	**<0.001**	–1.66	0.561	–0.30	1.000
E – P	1.58	0.612	1.49	0.674	2.48	0.129	1.72	0.521
E – S	1.37	0.748	0.80	0.967	1.83	0.447	1.05	0.900
E – W	0.13	1.000	1.97	0.364	0.00	1.000	0.03	1.000
N – P	–1.62	0.585	–3.52	**0.007**	3.34	**0.011**	2.01	0.337
N – S	–1.84	0.443	–4.20	**0.001**	3.12	**0.023**	1.35	0.759
N – W	–3.04	**0.029**	–3.04	**0.031**	1.66	0.561	0.32	1.000
P – S	–0.22	1.000	–0.68	0.984	–1.10	0.880	–0.67	0.985
P – W	–1.45	0.696	0.48	0.997	–2.48	0.129	–1.69	0.538
S – W	–1.24	0.820	1.17	0.853	–1.83	0.447	–1.02	0.910

	Number of species belonging to the endemic group		Cover of species belonging to the endemic group		Number of species belonging to the European group		Cover of species belonging to the European group	
	F	*p*	F	*p*	F	*p*	F	*p*
Microsite	1.96	0.076	2.42	**0.037**	7.15	**<0.001**	12.21	**<0.001**
	t	*p*	t	*p*	t	*p*	t	*p*
B – E	–0.12	1.000	–0.14	1.000	–2.23	0.225	2.36	0.173
B – N	0.00	1.000	0.00	1.000	–3.83	**0.002**	–2.87	**0.050**
B – P	–0.14	1.000	–2.65	0.090	–3.62	**0.004**	0.61	0.990
B – S	–0.14	1.000	–1.74	0.504	0.88	0.952	4.54	**<0.001**
B – W	–0.13	1.000	–1.22	0.828	–2.26	0.213	1.06	0.897
E – N	0.09	1.000	0.14	1.000	–1.62	0.587	–5.24	**<0.001**
E – P	–2.61	0.094	–2.51	0.127	–1.40	0.726	–1.75	0.498
E – S	–2.90	**0.043**	–1.60	0.599	3.10	**0.024**	2.18	0.252
E – W	–1.88	0.414	–1.08	0.891	–0.03	1.000	–1.30	0.783
N – P	–0.11	1.000	–2.65	0.090	0.22	1.000	3.48	**0.008**
N – S	–0.11	1.000	–1.74	0.504	4.70	**<0.001**	7.41	**<0.001**
N – W	–0.10	1.000	–1.22	0.828	1.59	0.606	3.93	**0.002**
P – S	–0.57	0.993	0.90	0.945	4.49	**<0.001**	3.93	**0.002**
P – W	1.24	0.818	1.43	0.709	1.37	0.743	0.45	0.998
S – W	1.77	0.489	0.53	0.995	–3.13	**0.022**	–3.48	**0.008**

➤ p. 94

	Number of species belonging to the continental group		Cover of species belonging to the continental group		Number of species belonging to the cosmopolitan group		Cover of species belonging to the cosmopolitan group	
	F	*p*	F	*p*	F	*p*	F	*p*
Microsite	6.75	**<0.001**	2.31	**0.045**	1.57	0.162	4.09	**0.001**
	t	*p*	t	*p*	t	*p*	t	*p*
B – E	–3.37	**0.010**	–1.60	0.602	0.70	0.982	2.16	0.259
B – N	–1.54	0.638	–0.22	1.000	1.19	0.841	1.67	0.551
B – P	–4.12	**0.001**	–2.85	***0.054***	–0.60	0.991	2.88	**0.049**
B – S	–3.99	**0.001**	–1.67	0.556	1.53	0.646	4.32	**<0.001**
B – W	–5.04	**<0.001**	–1.89	0.413	–0.52	0.995	2.63	0.095
E – N	1.90	0.404	1.37	0.743	0.49	0.997	–0.49	0.997
E – P	–0.82	0.964	–1.25	0.812	–1.30	0.788	0.72	0.979
E – S	–0.68	0.985	–0.07	1.000	0.83	0.962	2.16	0.260
E – W	–1.86	0.428	–0.29	1.000	–1.22	0.826	0.46	0.997
N – P	–2.69	***0.076***	–2.62	0.095	–1.78	0.478	1.21	0.832
N – S	–2.55	0.109	–1.44	0.701	0.34	0.999	2.65	0.089
N – W	–3.69	**0.003**	–1.66	0.557	–1.71	0.526	0.95	0.932
P – S	0.15	1.000	1.18	0.846	2.11	0.280	1.44	0.702
P – W	–1.05	0.902	0.96	0.930	0.07	1.000	–0.26	1.000
S – W	–1.19	0.842	–0.22	1.000	–2.04	0.319	–1.70	0.535

4 Discussion

To our knowledge, this study is among the first to assess the complex relationships between microsite diversity and the biogeographic affinities of plant species across a relatively large number of karstic microrefugia. We demonstrated that dolines have the potential to function as safe havens for plant species with various biogeographic affinities. We also demonstrated that the number and/or cover of species belonging to the Mediterranean group tended to be higher in warmer and drier microsites (i.e., the plateau and the south-, east-, and west-facing doline slopes), whereas those of the mountain group tended to be higher on cooler and moister north-facing slopes and/or in doline bottoms. Therefore, the current species pools and plant distributions in dolines indicate the presence of both 'warmer islands' and 'cooler islands' within short distances, providing habitats for a high diversity of species adapted to different climates.

We found that fine-scale topographic complexity in dolines facilitates the survival of plant species with diverse biogeographic affinities, likely due primarily to the unique microclimatic patterns within these landforms. Previous studies indicate that cold-air pooling and temperature inversions in dolines promote environmental stability and drive other key environmental factors, such as soil temperature, soil moisture, duration of snow cover, and frost frequency (Bárány-Kevei 1999; Bátori et al. 2019; Bátori et al. 2022a; Marcin et al. 2024). On the other hand, south-, east- and west-facing slopes in the Northern Hemisphere receive much more insolation than north-facing slopes, providing warmer and drier microsites than their surroundings (Bátori et al. 2023; Simpson et al. 2024). Due to increased insolation reaching the bottom of grassland dolines during the daytime, these areas experience higher temperatures than north-facing slopes for a certain period (Bátori et al. 2019). These microclimatic differences, resulting from the topographic complexity of dolines, may support the long-term persistence of species with specific climatic requirements during both warmer and cooler climatic periods. For instance, the occurrence of *Dracocephalum ruyschiana* in the dolines of the Bükk Mountains is presumed to date back millennia (Lazarević et al. 2009). During the warmer periods of the Pleistocene (i.e., the interglacials) and the Holocene, plant species migrated northwards in Europe (Stewart et al. 2010) or retreated to higher elevations in the mountains (cf. Walther et al. 2002). These migrations were presumably geographically structured across temperate Europe in relation to geomorphology and vegetation composition (Divíšek et al. 2020; Roleček et al. 2021). For instance, Bátori et al. (2022b) highlighted that both the western and eastern parts of the Carpathian Basin and their vicinity (i.e., eastern part and borderland of the Alps, and the Western Romanian Carpathians) have served as

migration routes for many karst-dwelling species now inhabiting the North Hungarian Mountains (Vojtkó 2001; Vojtkó 2016), including the Bükk Mountains. Warmer climatic periods during the Holocene (e.g., in the early Holocene, between 11,700 and 8,200 BP) might have facilitated both the migration of several sub-Mediterranean plant species from the south and the expansion of plant species with various ecological requirements from local and regional refugia (Willis et al. 2000; Magyari et al. 2010; see also the 'Flora Continuity Hypothesis' for the Carpathian Basin, Molnár et al. 2023). In the current climate, the north-facing slopes and bottoms of dolines serve as 'cool islands' for mountain species, such as *Aconitum variegatum* L., *Bupleurum longifolium* L., and *Carlina acaulis* L., while the other microsites support the persistence of many species belonging to the Mediterranean group, such as *Cruciata pedemontana* (Bellardi) Ehrend., *Teucrium chamaedrys* L., and *Waldsteinia geoides* Willd. The number of species belonging to the Mediterranean group did not differ significantly among the plateau, south-, east-, and west-facing slopes, which may be explained not only by microclimatic effects but also by other factors, such as soil depth and moisture (Bátori et al. 2023). Within the study area, the two Pannonian endemics – *Centaurea scabiosa* subsp. *sadleriana* (Janka) Asch. & Graebn. and *Dianthus giganteiformis* subsp. *pontederae* (A.Kern.) Soó – are xerophilous plants that predominantly inhabit the warmer and drier south-facing slopes and the plateau (Vojtkó 2001). We also found that the warm and dry south-facing doline slopes and the cool and moist doline bottoms did not favour the establishment of many species belonging to the European group, presumably due to the strong abiotic filters (e.g., extreme temperatures) in these microsites (Bátori et al. 2019; Bátori et al. 2023). The environmental stability on north-facing slopes and in bottoms did not favour the persistence of continental species adapted to climatic extremes (warm summers and cold winters) (cf. Spiecker 2003). Moreover, the relatively stable microclimatic conditions in doline bottoms may also result in lower diversity in the distribution of diagnostic species belonging to different biogeographic groups. The distribution of some cosmopolitan species in doline microsites and their surroundings (e.g., *Convolvulus arvensis* L. and *Trifolium repens* L.) may reflect past human disturbances, such as soil contamination, lime burning and overgrazing (cf. Bárány-Kevei et al. 2001; Bátori et al. 2020).

Climate models predict a substantial increase in temperature and summer drought for the Carpathian Basin in the coming decades (Bartholy et al. 2009). We suggest that dolines may play an important role in the long-term persistence of at least some plant species under anthropogenic climate change. Although species will respond individualistically to climate changes (Stewart et al. 2010), most species belonging to the Mediterranean group within our study area are expected to expand their distributions from the warmer and drier microsites to the cooler and moister microsites (i.e., north-facing slopes and doline bottoms). Even after biophysical thresholds are exceeded and the relatively buffered north-facing slopes and doline bottoms no longer function as safe havens for cool-adapted species, these microsites may still be valuable for other species that benefit from climate buffering (cf. Morelli et al. 2020).

5 Conclusion

We can conclude that dolines likely have the capacity to provide safe havens for plant species with different biogeographic affinities in the future. Therefore, management should take into account the complex relationships between microsite structure, environmental conditions, and species distributions in dolines and their surroundings, as well as the magnitude and rate of climate change, and the refugial capacity (cf. Keppel et al. 2024).

ACKNOWLEDGMENT: This research was funded by the National Research, Development and Innovation Office (NKFIH FK 142428 and ADVANCED 152502 grants). B.D., O.V., and C.T. were supported by the NKFIH ADVANCED 152232, NKFIH K 146137, and NKFIH KKP 144096 grants, respectively. K.F. and G.L. were supported by the Academic Excellence Scholarship Program of the Ministry for Culture and Innovation from the source of the National Research, Development and Innovation Fund (K.F.: EKÖP-24-3-SZTE-495, G.L.: EKÖP-24-3-SZTE-537). We especially thank Kata Frei for managing the correspondence with the journal's editorial office.

RESEARCH DATA: For information on the availability of research data related to the study, please visit the article webpage: https://doi.org/10.3986/AGS.14564.

6 References

Badgley, C., Smiley, T. M., Terry, R., Davis, E. B., DeSantis, L. R., Fox, D. L., Hopkins, S. S. B. et al. 2017: Biodiversity and topographic complexity: Modern and geohistorical perspectives. *Trends in Ecology and Evolution* 32-3. https://doi.org/10.1016/j.tree.2016.12.010

Bartholy, J., Pongracz, R., Torma, C., Pieczka, I., Kardos, P., Hunyady, A. 2009: Analysis of regional climate change modelling experiments for the Carpathian basin. *International Journal of Global Warming* 1-3. https://doi.org/10.1504/IJGW.2009.027092

Bates, D., Mächler, M., Bolker, B., Walker, S. 2015: Fitting linear mixed–effects models using lme4. *Journal of Statistical Software* 67. https://doi.org/10.18637/jss.v067.i01

Bárány-Kevei, I. 1999: Microclimate of karstic dolines. *Acta Climatologica* 32,33.

Bárány-Kevei, I., Goldie, H., Hoyk, E., Zseni, A. 2001: Heavy metal content of some Hungarian and English karst soils. *Acta Climatologica et Chorologica* 34,35.

Bátori, Z., Vojtkó, A., Farkas, T., Szabó, A., Havadtői, K., E-Vojtkó, A., Tölgyesi, C. et al. 2017: Large–and small–scale environmental factors drive distributions of cool–adapted plants in karstic microrefugia. *Annals of Botany* 119-2. https://doi.org/10.1093/aob/mcw233

Bátori, Z., Vojtkó, A., Maák, I. E., Lőrinczi, G., Farkas, T., Kántor, N., Tanács, E., Kiss, P. J., Juhász, O., Módra, G., et al. 2019: Karst dolines provide diverse microhabitats for different functional groups in multiple phyla. *Scientific Reports* 9-1. https://doi.org/10.1038/s41598-019-43603-x

Bátori, Z., Vojtkó, A., Keppel, G., Tölgyesi, C., Čarni, A., Zorn, M., Farkas, T. et al. 2020: Anthropogenic disturbances alter the conservation value of karst dolines. *Biodiversity and Conservation* 29. https://doi.org/10.1007/s10531-019-01896-4

Bátori, Z., Gallé, R., Gallé–Szpisjak, N., Császár, P., Nagy, D. D., Lőrinczi, G., Torma, A. et al. 2022a: Topographic depressions provide potential microrefugia for ground–dwelling arthropods. *Elementa: Science of the Anthropocene* 10-1. https://doi.org/10.1525/elementa.2021.00084

Bátori, Z., Bauer, N., Erdős, L., Vojtkó, A. 2022b: The vegetation of karsts in Hungary. In: Cave and Karst Systems of Hungary. C*ave and Karst Systems of the World*. Springer. https://doi.org/10.1007/978-3-030-92960-2_19

Bátori, Z., Valkó, O., Vojtkó, A., Tölgyesi, C., Farkas, T., Frei, K., Hábenczyus, A. A. et al. 2023: Environmental heterogeneity increases the conservation value of small natural features in karst landscapes. *Science of the Total Environment* 872. https://doi.org/10.1016/j.scitotenv.2023.162120

Borhidi, A. 1995: Social behaviour types, the naturalness and relative indicator values of the higher plants in the Hungarian Flora. *Acta Botanica Hungarica* 39.

Calonje, M., Meerow, A. W., Meerman, J., Francisco-Ortega, J., Griffith, M. P. 2024: Population genetics of *Zamia decumbens* (Zamiaceae, Cycadales), an endangered cycad from the Maya Mountains of Belize. *Plant Species Biology* 1–17. https://doi.org/10.1111/1442-1984.12473

Čarni, A., Čonč, Š., Breg Valjavec, M. 2022: Landform-vegetation units in karstic depressions (dolines) evaluated by indicator plant species and Ellenberg indicator values. *Ecological Indicators* 135. https://doi.org/10.1016/j.ecolind.2022.108572

Divíšek, J., Hájek, M., Jamrichová, E., Petr, L., Večeřa, M., Tichý, L., Willner, W., Horsák, M. 2020: Holocene matters: Landscape history accounts for current species richness of vascular plants in forests and grasslands of eastern Central Europe. *Journal of Biogeography* 47-3. https://doi.org/10.1111/jbi.13787

Dobrowski, S. Z. 2011: A climatic basis for microrefugia: The influence of terrain on climate. *Global Change Biology* 17-2. https://doi.org/10.1111/j.1365-2486.2010.02263.x

Dövényi, Z. (ed.) 2010: Magyarország kistájainak katasztere. MTA Földrajztudományi Kutatóintézet

Egli, B., Gerstberger, P., Greuter, W., Risse, H. 1990: *Horstrissea dolinicola*, a new genus and species of umbels (*Umbelliferae, Apiaceae*) from Kriti (Greece). *Willdenowia* 19.

Frei, K., Vojtkó, A., Farkas, T., Erdős, L., Barta, K., E–Vojtkó, A., Tölgyesi, C., Bátori, Z. 2023: Topographic depressions can provide climate and resource microrefugia for biodiversity. *iScience* 26. https://doi.org/10.1016/j.isci.2023.108202

Gentili, R., Baroni, C., Caccianiga, M., Armiraglio, S., Ghiani, A., Citterio, S. 2015: Potential warm-stage microrefugia for alpine plants: Feedback between geomorphological and biological processes. *Ecological Complexity* 21. https://doi.org/10.1016/j.ecocom.2014.11.006

Hampe, A., Jump, A. S. 2011: Climate relicts: Past, present, future. *Annual Review of Ecology, Evolution, and Systematics* 42-1. https://doi.org/10.1146/annurev-ecolsys-102710-145015

Herrera-Blitman, N., Calonje, M., Meerman, J., Aguilar, R., Meerow, A. W., Francisco-Ortega, J., Griffith, M. P. 2022: 1039 Zamia decumbens: Cycadales, Zamiaceae. *Curtis's Botanical Magazine* 39. https://doi.org/10.1111/curt.12459

Keppel, G., Van Niel, K. P., Wardell-Johnson, G. W., Yates, C. J., Byrne, M., Mucina, L., Schut, A. G. T. et al. 2012 Refugia: Identifying and understanding safe havens for biodiversity under climate change. *Global Ecology and Biogeography* 21-4. https://doi.org/10.1111/j.1466-8238.2011.00686.x

Keppel, G., Stralberg, D., Morelli, T. L., Bátori, Z. 2024 Managing climate-change refugia to prevent extinctions. *Trends in Ecology and Evolution* 39. https://doi.org/10.1016/j.tree.2024.05.002

Lazarević, P., Lazarević, M., Krivošej, Z., Stevanović, V. 2009: On the distribution of *Dracocephalum ruyschiana* (*Lamiaceae*) in the Balkan Peninsula. *Phytologia balcanica* 15-2.

Lenth, R. V. 2023: emmeans: Estimated marginal means, aka least–squares means. *R package version 1*.8.9. CRAN. https://doi.org/10.32614/CRAN.package.emmeans

Magyari, E. K., Chapman, J. C., Passmore, D. G., Allen, J. R., Huntley, J. P., Huntley, B. 2010: Holocene persistence of wooded steppe in the Great Hungarian Plain. *Journal of Biogeography* 37-5. https://doi.org/10.1111/j.1365-2699.2009.02261.x

Marcin, M., Raschmanová, N., Miklisová, D., Šupinský, J., Kaňuk, J., Kováč, L. 2024: Karst landforms as microrefugia for soil Collembola: Open versus forested dolines. *Elementa: Science of the Anthropocene* 12. https://doi.org/10.1525/elementa.2023.00107

Molnár, Á. P., Demeter, L., Biró, M., Chytrý, M., Bartha, S., Gantuya, B., Molnár, Z. 2023: Is there a massive glacial–Holocene flora continuity in Central Europe? *Biological Reviews* 98-6. https://doi.org/10.1111/brv.13007

Morelli, T. L., Barrows, C. W., Ramirez, A. R., Cartwright, J. M., Ackerly, D. D., Eaves, T. D., Ebersole, J. L. et al. 2020: Climate-change refugia: Biodiversity in the slow lane. *Frontiers in Ecology and the Environment* 18-5. https://doi.org/10.1002/fee.2189

Ottaviani, G., Keppel, G., Marcantonio, M., Mucina, L., Wardell-Johnson, G. 2019: Woody species in resource-rich microrefugia of granite outcrops display unique functional signatures. *Austral Ecology* 44-4. https://doi.org/10.1111/aec.12745

Pastore, M. A., Classen, A. T., D'Amato, A. W., Foster, J. R., Adair, E. C. 2022: Cold-air pools as microrefugia for ecosystem functions in the face of climate change. *Ecology* 103-8. https://doi.org/10.1002/ecy.3717

Peel, M. C., Finlayson, B. L., McMahon, T. A. 2007: Updated world map of the Köppen–Geiger climate classification. *Hydrology and Earth System Sciences*. 11-5. https://doi.org/10.5194/hess-11-1633-2007

R Foundation for Statistical Computing, R Core Team 2022: R: A language and environment for statistical computing (4.2.2). *Computer software*.

Roleček, J., Abraham, V., Vild, O., Svobodová Svitavská, H., Jamrichová, E., Plesková, Z., Pokorný, P., Kuneš, P. 2021: Holocene plant diversity dynamics show a distinct biogeographical pattern in temperate Europe. *Journal of Biogeography* 48-6. https://doi.org/10.1111/jbi.14082

Rull, V. 2009: Microrefugia. *Journal of Biogeography* 36. https://doi.org/10.1111/j.1365-2699.2008.02023.x

Shui, W., Chen, Y., Jian, X., Jiang, C., Wang, Q., Zeng, Y., Zhu, S. et al. 2022: Original karst tiankeng with underground virgin forest as an inaccessible refugia originated from a degraded surface flora in Yunnan, China. *Scientific Reports* 12. https://doi.org/10.1038/s41598-022-13678-0

Simpson, E. G., Fraser, I., Woolf, H., Pearse, W. D. 2024: Variation in near-surface soil temperature drives plant assemblage differentiation across aspect. *Ecology and Evolution* 14-7. https://doi.org/10.1002/ece3.11656

Sonkoly, J., Tóth, E., Balogh, N., Balogh, L., Bartha, D., Bata, K. C., Bátori, Z. et al. 2023: PADAPT 1.0 – the Pannonian Dataset of Plant Traits. *Scientific Data* 10. https://doi.org/10.1038/s41597-023-02619-9

Spiecker, H. 2003: Silvicultural management in maintaining biodiversity and resistance of forests in Europe – temperate zone. *Journal of Environmental Management* 67-1. https://doi.org/10.1016/S0301-4797(02)00188-3

Stewart, J. R., Lister, A. M. 2001: Cryptic northern refugia and the origins of the modern biota. *Trends in Ecology & Evolution* 16-11. https://doi.org/10.1016/S0169-5347(01)02338-2

Stewart, J. R., Lister, A. M., Barnes, I., Dalén, L. 2010: Refugia revisited: individualistic responses of species in space and time. *Proceedings of the Royal Society B: Biological Sciences* 277-1682. https://doi.org/10.1098/rspb.2009.1272

Su, Y., Tang, Q., Mo, F., Xue, Y. 2017: Karst tiankengs as refugia for indigenous tree flora amidst a degraded landscape in southwestern China. *Scientific Reports* 7. https://doi.org/10.1038/s41598-017-04592-x

Tichý, L. 2002: JUICE, software for vegetation classification. *Journal of Vegetation Science* 13-3. https://doi.org/10.1111/j.1654-1103.2002.tb02069.x

Tichý, L., Chytrý, M. 2006: Statistical determination of diagnostic species for site groups of unequal size. *Journal of Vegetation Science* 17-6. https://doi.org/10.1111/j.1654-1103.2006.tb02504.x

Tölgyesi, C., Bátori, Z., Erdős, L. 2014: Using statistical tests on relative ecological indicator values to compare vegetation units – Different approaches and weighting methods. *Ecological Indicators* 36. https://doi.org/10.1016/j.ecolind.2013.09.002

Virók, V., Farkas, R. 2008: Új növényfaj a hazai edényes flórában: a Haller-kövifoszlár (*Cardaminopsis halleri* (L.) Hayek). *Kitaibelia* 12.

Vojtkó, A. 1999: A *Valeriana simplicifolia* (Reichenb.) Kabath hazánkban és újabb adatok a Bükk hegység flórájához. *Kitaibelia* 4.

Vojtkó, A. (ed) 2001: A Bükk hegység flórája. Sorbus Kiadó.

Vojtkó, A. 2016: A Gömör–Tornai-karszt növényföldrajza. In: A Gömör–Tornai-karszt flórája. Enumeráció. *ANP Füzetek XIV*. Aggteleki Nemzeti Park Igazgatóság.

Walther, G. R., Post, E., Convey, P., Menzel, A., Parmesan, C., BeeBee, T. J. C., Fromentin, J. M. et al. 2002: Ecological responses to recent climate change. *Nature* 416. https://doi.org/10.1038/416389a

Wildi, O. 2016 Why mean indicator values are not biased. *Journal of Vegetation Science* 27-1. https://doi.org/10.1111/jvs.12336

Willis, K. J., Rudner, E., Sümegi, P. 2000: The full-glacial forests of Central and Southeastern Europe. *Quaternary Research* 53-2. https://doi.org/10.1006/qres.1999.2119

Willner, W., Di Pietro, R., Bergmeier, E. 2009: Phytogeographical evidence for post-glacial dispersal limitation of European beech forest species. *Ecography* 32-6. https://doi.org/10.1111/j.1600-0587.2009.05957.x

Acta geographica Slovenica, 66-1, 2026, 99–119

MAPPING AND ASSESSING FOREST FIRE SEVERITY USING REMOTE SENSING INDICES: A CASE STUDY OF TIZI OUZOU, ALGERIA

Boudjemline Fouzia



Forest fires in northern Algeria, including the Tizi Ouzou area, as seen in a Copernicus Sentinel-2 image captured on 12 August 2021. Image processed by ESA.

DOI: https://doi.org/10.3986/AGS.14459
UDC: 630*43:528.8(65-17)”2021”
Creative Commons CC BY-SA 4.0

Boudjemline Fouzia[1]

Mapping and assessing forest fire severity using remote sensing indices: A case study of Tizi Ouzou, Algeria

ABSTRACT: In Mediterranean regions, wildfires are exacerbated by rising temperatures and drought, stressing the need for rapid post-fire evaluation. This study employs Landsat-8 imagery to evaluate the effects of forest fires during summer 2021 in Tizi Ouzou region, Algeria. We calculated the Normalized Burn Ratio (NBR) and its difference (dNBR) from pre- and post-fire images, and analyzed the Normalized Difference Vegetation Index (NDVI) and Land Surface Temperature (LST) to evaluate vegetation loss and thermal response. Results indicate 24,700 hectares (~6.7%) with high severity, 55,200 ha (14.9%) with moderate–high and 94,500 ha (25.5%) with moderate–low. These findings highlight the value of combining spectral and thermal indices for wildfire assessment, offering guidance for restoration and management.

KEYWORDS: wildfire, remote sensing, land surface temperature, NDVI, dNBR, Tizi Ouzou, Algeria

Kartiranje in ocenjevanje resnosti gozdnih požarov z uporabo indeksov daljinskega zaznavanja: študija primera Tizi Ouzou, Alžirija

POVZETEK: V sredozemskih pokrajinah so gozdni požari vedno resnejši zaradi naraščajočih temperatur in suše, kar poudarja potrebo po hitri oceni stanja po požaru. Ta študija uporablja posnetke Landsat-8 za oceno učinkov gozdnih požarov poleti 2021 v regiji Tizi Ouzou v Alžiriji. Izračunali smo normalizirano razmerje požarne prizadetosti (NBR) in njegovo razliko (dNBR) iz posnetkov pred požarom in po njem ter analizirali normalizirani indeks razlike vegetacije (NDVI) in temperaturo površine tal (LST), da bi ocenili izgubo vegetacije in toplotni odziv. Rezultati kažejo, da je bilo zelo prizadetih 24.700 hektarjev (~6,7 %), 55.200 ha (14,9 %) zmerno do zelo prizadetih in 94.500 ha (25,5 %) zmerno do malo prizadetih. Rezultati poudarjajo pomen kombiniranja spektralnih in toplotnih indeksov za oceno posledic gozdnih požarov, saj ponujajo smernice za obnovo in upravljanje.

KLJUČNE BESEDE: gozdni požar, daljinsko zaznavanje, temperatura površine tal, NDVI, dNBR, Tizi Ouzou, Alžirija

The article was submitted for publication on May 16th, 2025.
Uredništvo je prejelo prispevek 16. maja 2025.

[1] Teacher Education College of Setif (ENS), Setif, Algeria
f.boudjemline@ens-setif.dz (https://orcid.org/0009-0002-7071-962X)

1 Introduction

Forest fires, increasingly recurrent across Mediterranean regions due to climatic shifts, land-use changes, and socio-economic transformations (Ganteaume and Barbero 2019; Dupuy et al. 2020), are among the primary contributors to environmental degradation in the Mediterranean Basin. They particularly effect on soil structure, hydrological processes, and vegetative cover (Lovreglio et al. 2010). The removal of protective vegetation layers exposes soils to erosion and alters infiltration dynamics, thereby accelerating land degradation (Stefanidis et al. 2022). In this context, rapid and accurate post-fire damage assessment is essential to guide effective forest management, ecological restoration, and risk mitigation (Brewer et al. 2005).

In this study, we distinguish between »wildfires«, defined as any uncontrolled fire in natural areas, and »forest fires«, which specifically affect forested ecosystems, following Keeley (2009). Burn severity, defined as the magnitude of ecological change and land cover alteration caused by fire, reflects the degree to which vegetation and soil are affected. It can be quantified through different indicators, such as the percentage of area burned, the proportion of vegetation destroyed, or the decrease in spectral indices like NDVI (Keeley 2009; Cansler and McKenzie 2012). However, measuring burn severity presents considerable challenges due to the complexity of fire effects and the heterogeneity of impacted landscapes (Cocke et al. 2005). Remote sensing technologies have emerged as effective tools in this domain, offering synoptic coverage and temporal consistency across vast and often inaccessible terrains. Their effectiveness in wildfire monitoring and burn severity assessment has been widely demonstrated in recent studies (Durlević et al. 2025; Sabljić et al. 2025). Spectral indices such as the Normalized Difference Vegetation Index (NDVI) and the Normalized Burn Ratio (NBR) are widely used to evaluate vegetation loss and fire impacts, both of which are directly related to burn severity (Harris et al. 2011). More recently, Land Surface Temperature (LST) has gained attention for its potential to reflect burn severity, as post-fire environments typically exhibit elevated temperatures due to reduced evapotranspiration and increased surface heat flux (Wendt et al. 2007; Veraverbeke et al. 2010; Vlassova et al. 2014).

Over the past two decades, catastrophic wildfires have repeatedly struck the Mediterranean – including France (2003), Greece (2007), Portugal (2017), Algeria, Turkey, and Greece (2021) – and across southern Europe in 2022, when nearly 900,000 ha burned (Mouillot et al. 2003; Turco et al. 2019; Koutsias et al. 2022; San-Miguel-Ayanz et al. 2022). These events underscore the region's vulnerability linked to climate variability, land-use change, and socio-economic pressures (Lukić et al. 2017; Vujović et al. 2024). These events reveal a critical research gap: while numerous studies have examined fire impacts in the Mediterranean, few have integrated thermal parameters such as LST with spectral indices (e.g., dNBR) to assess burn severity. This study is the first to systematically apply these indices to the Tizi Ouzou region using Landsat 8 imagery, providing new insights for regional wildfire management and contributing to improved post-fire assessment methodologies.

In Algeria, over 36,000 hectares of forest are destroyed by wildfires each year (Direction Générale des Forêts 2021). The economic losses in the forestry sector caused by these fires between 1985 and 2006 were estimated at over 113 billion Algerian dinars (approximately 1.11 billion euros) (Arfa et al. 2019). This financial assessment considers only the market value of the lost products – such as timber, cork, scrubland, esparto grass, and fruit trees – without accounting for the annual expenditures dedicated to firefighting efforts. In more recent years, Algeria has faced an escalating wildfire crisis, with the 2021 fire season alone recording 1,631 incidents that devastated approximately 100,101 hectares of vegetation (Direction Générale des Forêts 2021). These events were exacerbated by unprecedented heatwaves and prolonged droughts, trends that align with regional projections under current climate change scenarios.

Remote sensing analyses over the past four decades have revealed that approximately 81% of burnable land in Tizi Ouzou has experienced wildfires between 1984 and 2023, with over half of these zones subjected to repeated burns (Kouachi et al. 2024). This chronic recurrence illustrates the ecological pressure on Mediterranean landscapes. Researchers increasingly use GIS and statistical modeling to map fire-prone zones and inform prevention strategies (Oliveira et al. 2012; Rahmani and Benmassoud 2019; Lahmar and Akakba 2024; Castro-Melgar et al. 2025). These tools underscore the necessity of integrating local ecological conditions with community-based awareness and mitigation programs (Belgherbi et al. 2018).

The present study builds upon previous advances in wildfire assessment using remote sensing and GIS, particularly the integration of spectral indices and thermal metrics, to evaluate the potential of LST as a reliable indicator of burn severity in the forested areas of Tizi Ouzou Province. Utilizing a multi-sensor remote

sensing approach – particularly combining the dNBR, a spectral index derived from NIR and SWIR bands widely used to quantify burn severity, with LST, the radiative temperature of the land surface obtained from thermal infrared data – this research aims to generate a comprehensive spatial analysis of post-fire conditions in this Mediterranean hotspot. The study specifically explores how LST correlates with burn severity, and how pre-fire ecological factors, such as vegetation density and topographic variability, influence post-fire thermal responses.

Furthermore, geospatial tools will be applied to identify and prioritize high-severity zones for ecological restoration, evaluate site suitability for reforestation based on environmental criteria, and support the strategic allocation of fire management resources. The study also underscores the importance of community engagement in the design and implementation of rehabilitation efforts.

The present study addresses the following key research questions:

1. To what extent can Land Surface Temperature (LST) serve as a reliable indicator of burn severity in the forested areas of Tizi Ouzou Province?
2. How does LST correlate with the differenced Normalized Burn Ratio (dNBR) in assessing post-fire ecological transformations?
3. How can geospatial tools be applied to identify high-severity zones and support reforestation and fire management strategies?

By addressing these questions, this research aims to advance remote sensing methodologies for fire assessment and contribute to evidence-based ecological rehabilitation and policy development in Mediterranean Algeria.

2 Materials and methods

2.1 Study Area

The Tizi Ouzou study area is located in northern Algeria (Figure 1) and extends over approximately 2,958 km² between latitudes 36°30'–37°00' N, and longitudes 3°30'–4°30' E. Elevation ranges from 10 m in the coastal plains to 2,308 m at the Djurdjura Mountains, giving rise to a predominantly hilly and mountainous relief. Geologically, the region is composed of Cretaceous and Tertiary formations interspersed with recent alluvial

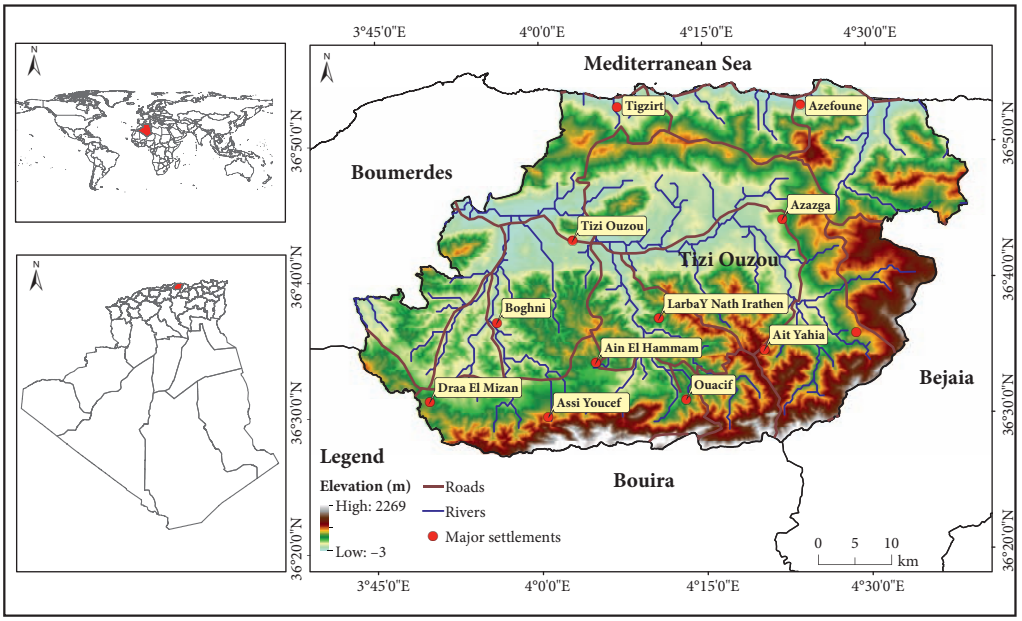


Figure 1: Study area map showing the location of the district of Tizi Ouzou.

deposits, while geomorphologically it is defined by rugged slopes, erosion-prone terrain, and valleys incised by rivers originating from the Djurdjura massif. Climatically, the area experiences a typical Mediterranean climate, characterized by hot, dry summers and mild, wet winters, with average annual precipitation ranging between 500 and 800 mm (Meddour and Derridj 2010). Forested land accounts for nearly 38% of the territory and is dominated by maquis shrublands) e.g., *Quercus coccifera, Pistacia lentiscus*) and coniferous stands of cedar (*Cedrus atlantica*) and Aleppo pine (*Pinus halepensis*) (Ammiche and Oumezzaouche 2018). The Tizi Ouzou province, encompassing ~112,180 ha of vegetated land, is highly vulnerable to wildfires due to dense forests, complex topography, and human pressures. Maquis vegetation occupies nearly half of the forest area, followed by state-owned forests, with smaller shares of reforested and communal lands (Conservation des forêts Tizi Ouzou 2021; Sahar et al. 2020). This ecological richness, however, is increasingly threatened by recurrent fires, many of which are linked to anthropogenic activities.

2.2 Data sources and methodology

The methodology adopted in this study is illustrated in Figure 2. Landsat-8 Operational Land Imager (OLI) and Thermal Infrared Sensor (TIRS) imagery were obtained from the United States Geological Survey Earth Explorer platform to assess wildfire impacts in the Tizi Ouzou region. Landsat-8, launched in 2013, is equipped with OLI and TIRS sensors that provide multispectral and thermal observations at spatial resolutions ranging from 15 to 100 m. These data enable detailed monitoring of vegetation dynamics, fire severity, and land surface temperature (Roy et al. 2014). The key characteristics of the Landsat-8 bands used in this study are summarized in Table 1.

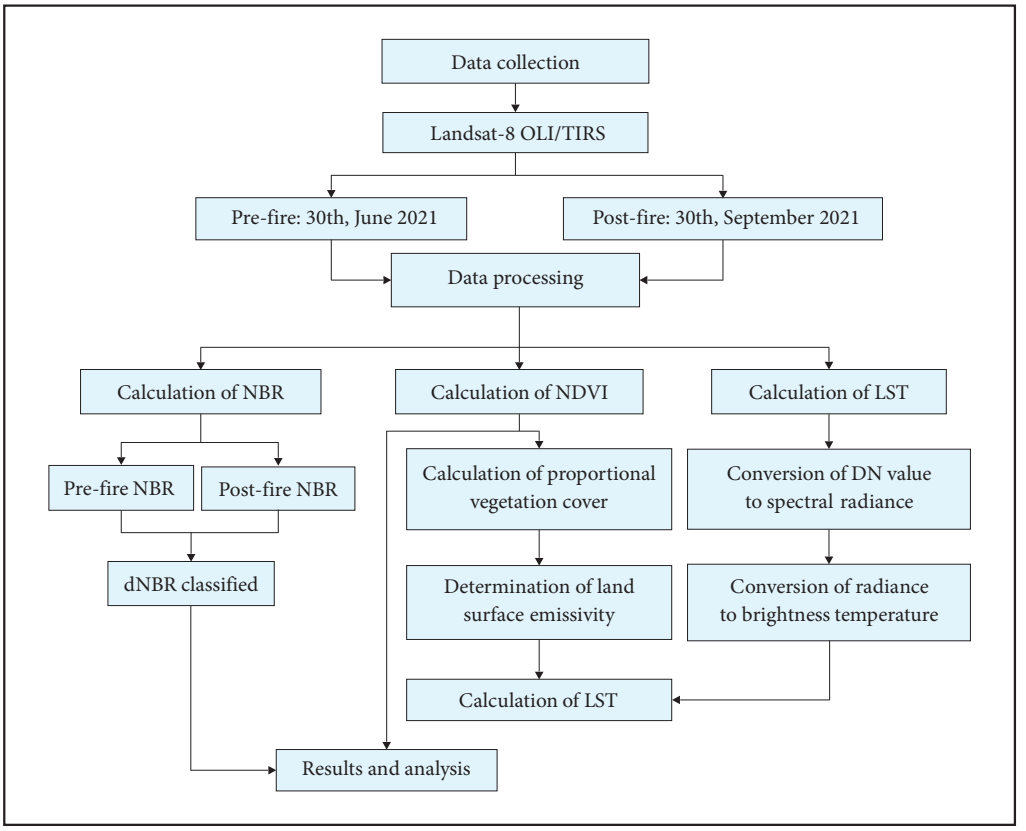


Figure 2: Flowchart illustrating the research methodology.

Table 1: Key characteristics of Landsat-8 OLI/TIRS data used in this study.

Band	Spectral region	Wavelengths (μm)	Resolution (m)	Sensor	Main applications
B4	Red	0.630–0.680	30	OLI	NDVI, NBR
B5	Near Infrared (NIR)	0.845–0.885	30	OLI	NDVI, NBR
B7	Shortwave Infrared-2	2.100–2.300	30	OLI	NBR
B10	Thermal Infrared	10.60–11.19	100 (resampled to 30)	TIRS	LST

Two cloud-free scenes were selected, dated 30 June 2021 (pre-fire) and 30 September 2021 (post-fire), corresponding to Path 193 / Row 35. These dates were chosen to bracket the major wildfire event that occurred on 9th August, 2021 and to best represent vegetation conditions immediately before and after the disturbance. Furthermore, according to Algerian National Office of Meteorology data portal, this period coincided with extreme summer meteorological conditions in northern Algeria, characterized by precipitation deficits and unusually high temperatures, which created favorable preconditions for wildfire ignition and spread. All Landsat-8 data were processed using ArcGIS 10.5, including atmospheric correction to reduce the influence of scattering and absorption, Scenes were atmospherically corrected and projection to UTM Zone 31N (WGS84) to ensure spatial consistency across the study area.

2.3 Remote sensing indices

2.3.1 Normalized Difference Vegetation Index (NDVI)

NDVI is a key metric in remote sensing for assessing vegetation cover, density, and health. It was first introduced by Rouse et al. (1973) and is calculated by taking the difference between the near-infrared (NIR) and red (R) reflectance values, divided by their sum, as shown in Equation 1:

$$\mathrm{NDVI} = \frac{(\mathrm{Band\ 5} - \mathrm{Band\ 4})}{(\mathrm{Band\ 5} + \mathrm{Band\ 4})} \tag{1}$$

NDVI values range from –1 to +1. Higher positive values (greater than 0.5) indicate dense and healthy vegetation, while values between 0.2 and 0.5 represent moderate or mixed vegetation. Values between 0 and 0.2 are often associated with barren land, urban areas, or exposed soil, and negative values (below zero) correspond to non-vegetated surfaces such as water, snow, or clouds (Carlson and Ripley 1997; Avdan and Jovanovska 2016; Ekumah et al. 2020).

NDVI is particularly useful for tracking vegetation changes in response to environmental conditions such as droughts, deforestation, or wildfires (Rouse et al. 1973). In post-fire studies, NDVI helps to assess vegetation loss and recovery by comparing pre- and post-fire conditions, as demonstrated in studies across Europe and the Mediterranean (Nolè et al. 2022; Zahabnazouri et al. 2025).

2.3.2 Estimation of Land Surface Temperature (LST)

The estimation of LST from Landsat 8 imagery was carried out in three main steps. First, the raw Digital Numbers (DN) of the thermal bands were converted into spectral radiance using the radiometric rescaling fac
tors provided in the metadata, as shown in Equation 2 (Avdan and Jovanovska 2016):

$$L_\lambda = M_L \times Q_{cal} + A_L \tag{2}$$

where Lλ represents the spectral radiance, ML is the band-specific multiplicative rescaling factor, Qcal is the quantized pixel value, and AL is the additive rescaling factor provided by the satellite metadata.

Once the spectral radiance is obtained, it is converted into Brightness Temperature (BT) by applying the thermal constants provided in the satellite image metadata. The temperature in degrees Celsius is derived by subtracting the absolute zero (273.15 K) from the brightness temperature, as illustrated in Equation (3) (Cook et al. 2014):

$$BT = \frac{K_2}{\ln\left(\frac{K_1}{L_\lambda}+1\right)} - 273.15 \tag{3}$$

In this equation, K_1 and K_2 are the band-specific thermal conversion constants (with values $K_1 = 774.8853$ and $K_2 = 1321.0789$) (Ru et al. 2021).

Second, the Normalized Difference Vegetation Index (NDVI) is computed to assess the Earth's surface emissivity and the proportion of vegetation. For Landsat 8, NDVI is derived from the reflectance values of Band 5 (Near-Infrared) and Band 4 (Red), as shown in Equation 1. The vegetation proportion (P_v) is calculated using Equation 4 (Rouse et al. 1973):

$$P_v = \left(\frac{NDVI - NDVI_{min}}{NDVI_{max} - NDVI_{min}}\right)^2 \tag{4}$$

This is followed by the calculation of Land Surface Emissivity (LSE,), which accounts for the emissive properties of the Earth's surface. According to the formula proposed by Sobrino et al. (2004), LSE is estimated based on the vegetation proportion (P_v) as shown in Equation (5):

$$\epsilon = 0.004P_v + 0.986 \tag{5}$$

Once the emissivity is determined, the final step involves computing the LST using the following Equation 6, suggested by Stathopoulou and Cartalis (2007):

$$LST = \frac{BT}{1+\left(\frac{\lambda BT}{\rho}\ln(\epsilon\lambda)\right)} \tag{6}$$

Here, $\lambda = 10.895$ μm is the wavelength for Landsat 8's thermal bands, and BT represents the brightness temperature in degrees Celsius (Avdan and Jovanovska 2016). The value ρ is a constant, calculated by the following Equation 7:

$$\rho = \frac{h \times c}{s} = 1.438 \times 10^{-2} Mk \tag{7}$$

where h is Planck's constant ($6.626 \times {}^{-34}$ Js), s is the Boltzmann constant (1.38×10^{-23} J/K), c is the speed of light (2.998×10^8 m/s) (Sobrino et al. 2004).

It is important to note that LST is not directly provided by the Landsat sensor but retrieved through these multi-step calculations. The derived LST values are closely related to air temperature and vegetation conditions, where elevated LST indicates reduced evapotranspiration, higher vegetation stress, and increased flammability, thus serving as a useful proxy for wildfire risk (Wasserman and Mueller 2023; Liu et al. 2024).

2.3.3 Normalized Burn Ratio (NBR) and differenced Normalized Burn Ratio (dNBR)

In this research, the NBR was used to identify areas impacted by wildfires (Fernández-Guisuraga et al. 2023), while the dNBR was employed to assess the intensity of burn severity (Maillard et al. 2022; Zhao et al. 2023) (Table 2). Several spectral indices, such as dNBR, have been used in previous studies to assess the effects of fires (Chu et al. 2016). NBR is a widely adopted technique for mapping burned areas before and after fire events (García and Caselles 1991; Key and Benson 2006; Escuin et al. 2008). Similarly, dNBR is frequently used for estimating burn severity based on satellite imagery (Key and Benson 2006; Miller and Thode 2007; Parks et al. 2014).

In this study, both NBR and dNBR indices were calculated to evaluate burn severity. The dNBR was particularly effective for delineating burned areas and classifying the extent of damage (Kurbanov et al. 2022). The NBR was computed for pre- and post-fire images of the Landsat satellite system, specifically using the near-infrared (NIR, Band 5) and mid-infrared (MIR, Band 7) bands, as these bands exhibit significant changes following a fire event (Epting et al. 2005; Roy et al. 2008). NBR is calculated using Equation (8):

$$\mathrm{NBR} = \frac{(\mathrm{Band\ 5} - \mathrm{Band\ 7})}{(\mathrm{Band\ 5} + \mathrm{Band\ 7})} \tag{8}$$

Subsequently, the dNBR was calculated by subtracting the post-fire NBR from the pre-fire NBR, as shown in Equation (9):

$$dNBR = \mathrm{NBR}_{\mathrm{pre-fire}} - \mathrm{NBR}_{\mathrm{post-fire}} \tag{9}$$

where dNBR = Difference in NBR before and after fires, $\mathrm{NBR}_{\mathrm{pre\text{-}fire}}$ = NBR image before fires and $\mathrm{NBR}_{\mathrm{post\text{-}fire}}$ = NBR image after fires.

This method allowed for the detection of vegetation changes caused by the fire. The theoretical values for NBR range from −1.0 to +1.0, with lower values typically indicating higher burn severity. The analysis was performed using the Raster Calculator function in ArcGIS 10.5.

Burn severity was classified according to the thresholds proposed by the United States Geological Survey (2016), with dNBR values typically ranging from −2 to +2 and unburned areas having values between −0.10 and +0.10. Specific thresholds were used to classify burn severity levels (Table 2), although these values may vary depending on the geographical context and site characteristics (Key and Benson 2006; Nasery and Kalkan 2020).

Table 2: Differenced Normalized Burn Ratio (dNBR) (Key and Benson 2006; United States Geological Survey 2016).

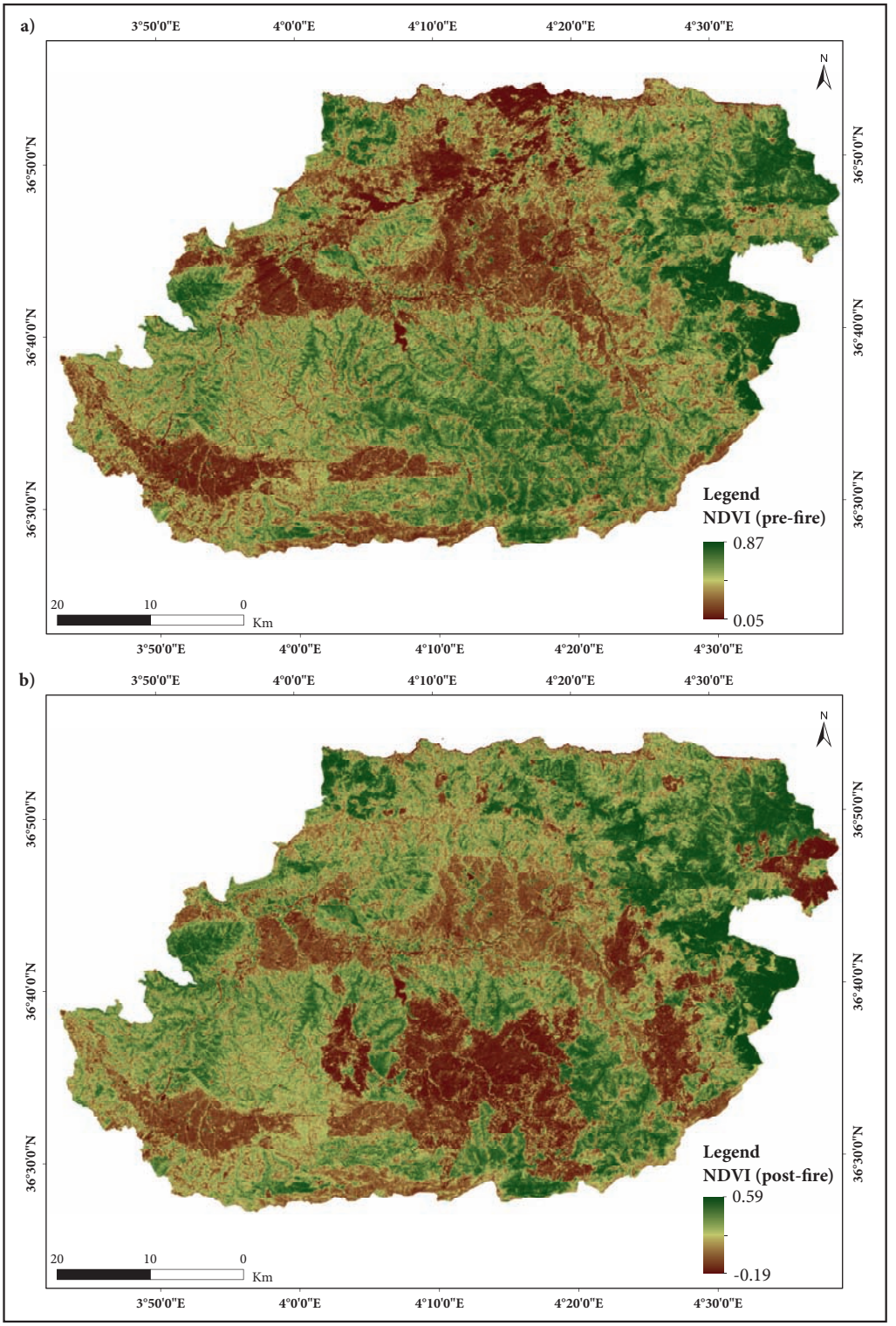
dNBR range	Burn severity
−0.50 < dNBR < −0.25	High, enhanced regrowth
−0.25 < dNBR < −0.10	Low, enhanced regrowth
−0.10 < dNBR < 0.10	Unburned
0.10 < dNBR < 0.27	Low severity
0.27 < dNBR < 0.44	Moderate-low severity
0.44 < dNBR < 0.66	Moderate-high severity
dNBR > 0.66	High severity

3 Results

3.1 Normalized Difference Vegetation Index (NDVI)

The pre-fire NDVI map (Figure 3a) scene shows strong spatial variation in vegetation density across the study area. High NDVI values (up to 0.87), represented by dark green tones in the eastern and southeastern zones, indicate dense and healthy vegetation, whereas moderate values (0.05 to 0.40) in the central and northern zones suggest sparser vegetation or croplands. Very low values (0.05) in the central-west reflect bare soils or urban areas, providing a baseline for post-fire comparison. In contrast, the post-fire NDVI map (Figure 3b)

Figure 3: NDVI Map for (a) pre-fire and (b) post-fire scenes of the study area. ➤ p. 107


a)
3°50'0"E
4°0'0"E
4°10'0"E
4°20'0"E
4°30'0"E
36°50'0"N
36°40'0"N
36°30'0"N
N
Legend
NDVI (pre-fire)
0.87
0.05
20
10
0
Km
b)
Legend
NDVI (post-fire)
0.59
-0.19

reveals a marked reduction clearly in vegetation cover large portion of the southern and central zones, display low to negative NDVI values (−0.19 to +0.10), highlighting burned or degraded surfaces. Surviving vegetation patches remain mainly in the east and northeast, with NDVI values up to 0.59, indicating areas of lower burn severity.

The widespread decline in NDVI across most of the area suggests significant vegetation loss and ecological disturbance, consistent with wildfire impacts observed in Mediterranean.

3.2 Land Surface Temperature (LST)

The LST analysis reveals notable spatial variations across the Tizi Ouzou region before and after the wildfire event (Figure 4). Pre-fire LST values ranged between 25.92°C to 50.16°C, with higher temperature concentrated in the central and southern parts of the study area, corresponded to the zones that later experienced severe burning as observed in Figure 4a. This correlation implies that elevated pre-fire surface temperatures may have contributed to increasing vegetation dryness and flammability, thereby facilitating the ignition and rapid spread of fire.

Conversely, the northern and northeastern parts of the region displayed relatively lower LST values, represented by blue to turquoise tones. These cooler areas are likely influenced by local environmental factors such as dense vegetation, shading from topographic variation, or higher elevation zones that reduce solar radiation absorption at the surface.

Overall, the spatial distribution of LST prior to the fire event highlights the utility of this parameter as a potential predictive indicator for wildfire risk assessment. Incorporating LST data into fire vulnerability models and early warning systems can significantly enhance preparedness and inform more effective fire management strategies.

Post-fire LST distribution across the Tizi Ouzou region exhibits a distinct thermal pattern when compared to the pre-fire scene. The average LST for the post-fire image is 29.35°C, indicating a general increase in surface temperature following the wildfire event, despite localized variations. Temperature ranges for the post-fire scene were 26.61°C to 46.83°C, as illustrated in Figure 4b.

Higher LST values are mainly concentrated in areas that experienced intense fire damage, particularly in the central and southern parts of the study area. These zones appear in red to orange hues and reflect residual surface heating associated with the loss of vegetation cover and changes in surface albedo. The increase in LST in burned regions is consistent with findings from previous studies, which report that burned surfaces can be significantly warmer – up to 7.6°C higher than unburned zones, and even more than 10°C in high burn severity areas (Vlassova et al. 2014).

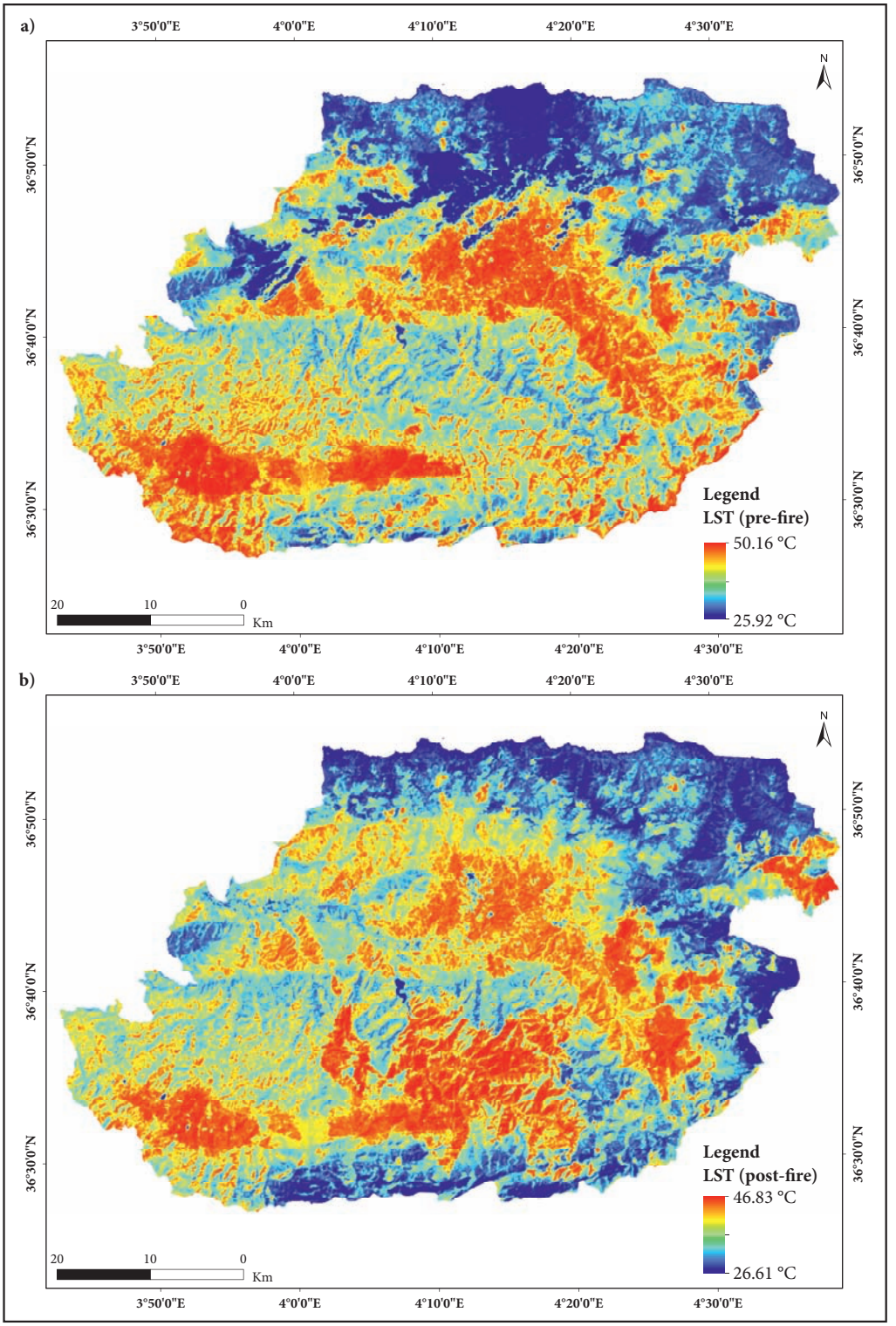
In contrast, areas in the northern and northeastern regions, which were either unaffected or less impacted by the fire, demonstrate relatively lower surface temperatures (shown in blue and green shades). This suggests that vegetation and soil conditions in unburned zones continued to moderate heat retention and reflectance, resulting in cooler post-fire LST values.

Overall, the observed LST increase in burned areas highlights the impact of wildfires on surface energy balance and emphasizes the role of LST as a valuable post-disturbance diagnostic tool in fire-affected landscapes.

3.3 Correlation between NDVI and LST

The scatterplots provided in Figure 5 illustrate the relationship between NDVI and LST both before and after the fire event. Before the fire, the data shows a relatively strong negative correlation between NDVI and LST, with an R^2 value of 0.5668, indicating that healthy vegetation significantly contributed to surface cooling. This pattern is consistent with several studies which confirmed that areas with dense vegetation exhibit lower surface temperatures due to shading effects and evapotranspiration (Vlassova et al. 2014). Such findings affirm the important role vegetation plays in regulating local microclimates. According to Yuan and Bauer (2007), higher NDVI values are typically associated with lower LST in forested ecosystems, emphasizing vegetation's critical cooling function.

Figure 4: LST Map for (a) pre-fire and (b) post-fire scenes of the study area. ► p. 109


a)
3°50'0"E
4°0'0"E
4°10'0"E
4°20'0"E
4°30'0"E
36°50'0"N
36°40'0"N
36°30'0"N
N
Legend
LST (pre-fire)
50.16 °C
25.92 °C
20
10
0
Km
b)
Legend
LST (post-fire)
46.83 °C
26.61 °C

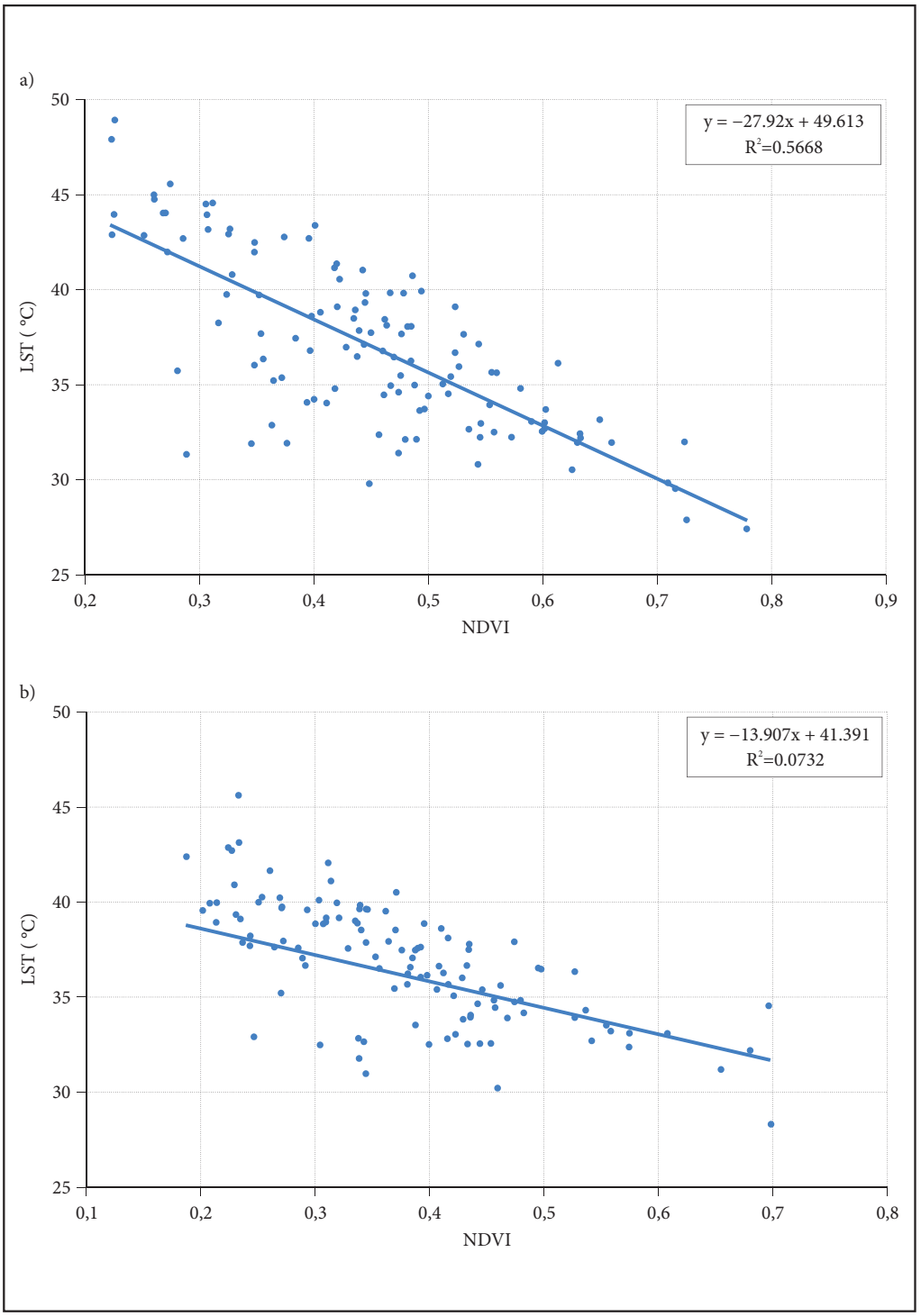


Figure 5: Correlation Matrix for NDVI-LST relationship (a) before and (b) after the wildfire event.

After the fire, the correlation between NDVI and LST weakens significantly, with an R^2 value dropping to 0.0752, this pattern highlights how fire disrupts the natural land-atmosphere interactions by removing vegetative cover, leading to hotter surface conditions. Similar results were observed by Chuvieco et al. (2019), who reported that post-fire landscapes maintain elevated LST due to the absence of vegetation, which increases soil heat absorption. The sharp reduction in the strength of the NDVI–LST relationship after the fire event indicates that vegetation loss severely alters land surface thermal properties. Over time, if vegetation regenerates, one would expect the correlation to gradually become stronger again, as shown by studies monitoring post-fire recovery (Digavinti and Manikiam 2021).

3.4 Normalized Burn Ratio (NBR)

The incorporation of both pre- and post-fire NBR indices into fire risk mapping plays a pivotal role in enhancing our understanding and anticipation of wildfire dynamics. NBR, derived from remote sensing techniques, serves as an essential metric for evaluating the intensity of vegetation damage resulting from fires, offering vital information on alterations within the landscape. Evaluating NBR values before and after fire incidents allows for a detailed examination of wildfire susceptibility patterns.

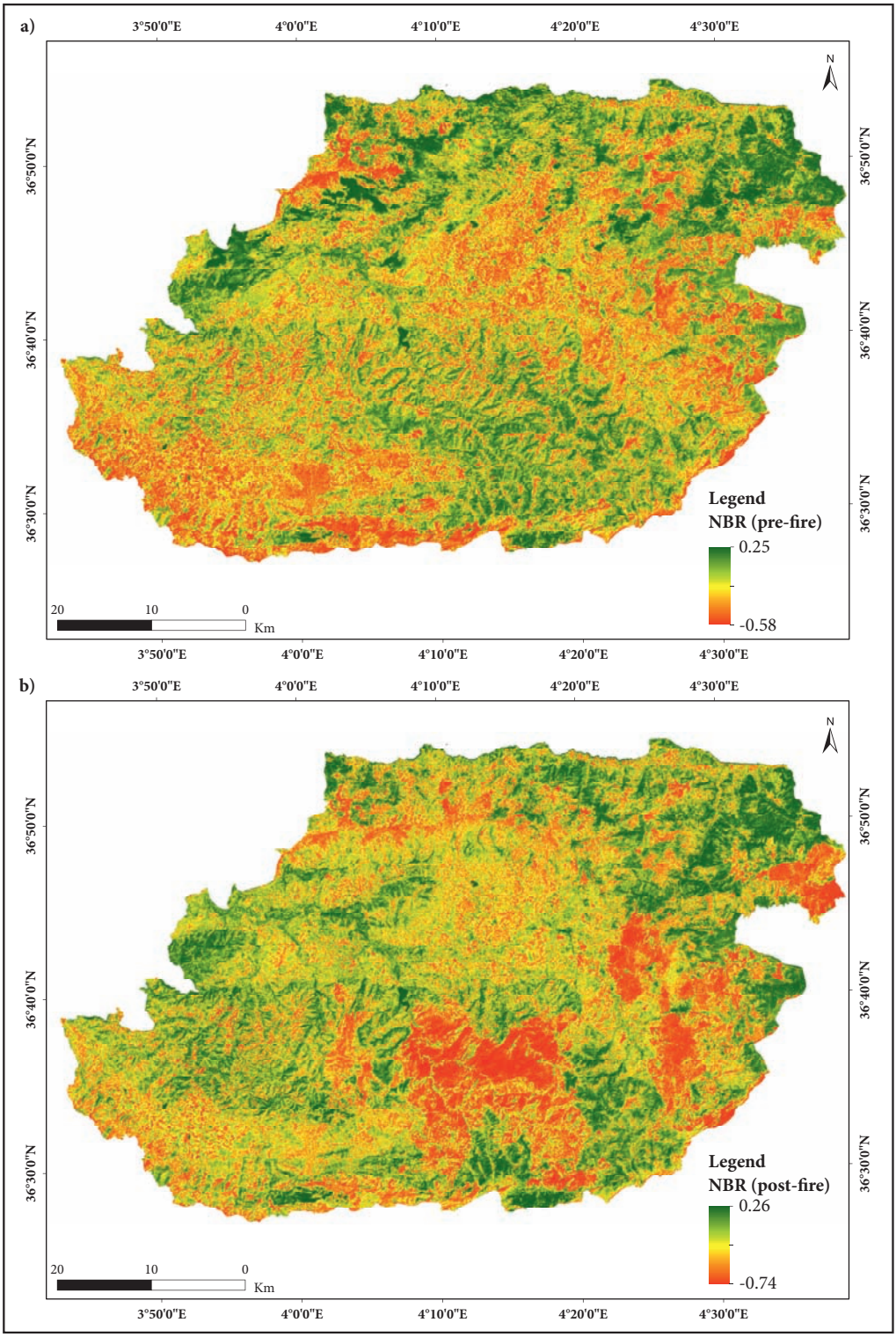
The pre-fire NBR on 30th June, 2021 (Figure 6a) provides a reference point for assessing vegetation health prior to fire occurrence. Lower pre-fire NBR readings may suggest existing vegetation stress or sparse coverage, potentially serving as indicators of higher ignition likelihood. Conversely, the post-fire NBR on 30th September, 2021 illustrates the degree of vegetation degradation caused by fire, highlighting zones with pronounced ecological transformations. When both sets of data are compared (Figure 6b), it becomes possible to pinpoint regions that underwent significant vegetation loss, thus identifying zones of critical impact. Elevated post-fire NBR values are often linked with severe burn damage, signifying regions at greater risk, while lower values may reflect milder impacts or areas where vegetation persisted post-fire. Furthermore, the analysis of NBR values showed that, during the pre-fire phase, readings ranged between −0.58, which corresponds to barren or non-vegetated surfaces, and +0.25, indicative of healthy, dense vegetation. In the post-fire phase, values ranged from −0.74 to +0.26 (Figure 6), illustrating the varying degrees of fire-induced changes across the study area.

The temporal comparison of NBR values, capturing both pre- and post-event conditions, supports a more dynamic and accurate interpretation of fire vulnerability. This method enhances mapping precision by accounting for landscape alterations driven by fire activity. Utilizing both pre- and post-NBR datasets in fire susceptibility assessments enables better identification of areas susceptible to intense vegetation loss and facilitates the evaluation of fire aftermath effects.This dual-index approach not only improves the reliability of fire risk assessments but also supports more informed decisions regarding mitigation planning, resource distribution, and sustainable land management.

3.5 Differenced Normalized Burn Ratio (dNBR)

Based on the dNBR values, five distinct burn severity classes were identified: unburned, low severity, moderate-low severity, moderate-high severity, and high severity. These classifications were used to generate the burn severity map (Figure 7). According to the dNBR classification (Table 3), 6.66% (24,684.66 ha) of the study area was categorized as high severity, 14.89% (55,200.69 ha) as moderate-high severity, 25.48% (94,491.81 ha) as moderate-low severity, and 34.26% (127,044.09 ha) as low severity. In addition, 14.97% (55,537.92 ha) of the land remained unburned, while vegetation regrowth was detected in 1.93% (7158.96 ha) as low regrowth and 1.81% (6700.05 ha) as high regrowth zones. Higher dNBR values were associated with severe fire damage, while lower values indicated better preserved vegetation. A related study by Guehaz and Sivakumar (2023) examined the forest fire that occurred on 5th July, 2021 in Khenchela province, Algeria, using space-borne remote sensing data. Their analysis, based on Landsat-8 and Sentinel-2 imagery, applied both dNBR and RdNBR indices to evaluate burn severity across affected municipalities such as Tamza, Chelia, Elhamma, and Bouhmama. According to their dNBR-based classification, 1.21% (1825.11 ha) of

Figure 6: NBR of (a) pre-fire and (b) post-fire scenes of the study area. ► p. 112


a)
3°50'0"E
4°0'0"E
4°10'0"E
4°20'0"E
4°30'0"E
36°50'0"N
36°40'0"N
36°30'0"N
N
Legend
NBR (pre-fire)
0.25
-0.58
20
10
0
Km
b)
Legend
NBR (post-fire)
0.26
-0.74

the area experienced high severity burns, 2.54% (3843.54 ha) suffered moderate-high severity, 2.59% (3927.97 ha) was classified under moderate-low severity, and 6.51% (9864.45 ha) experienced low severity. The most affected municipalities are Ouacifs, Ath Yenni, Larba y Nath Irathen, and Ain El Hammam. These findings were critical for mapping the spatial extent and intensity of fire impact (Guehaz and Sivakumar 2023).

Table 3: Differenced Normalized Burn Ratio (dNBR) thresholds proposed by the United States Geological Survey (2016).

Burn severity level	Burned area (ha)	Burned area (%)
High, enhanced regrowth	6700.05	1.81
Low, enhanced regrowth	7158.96	1.93
Unburned	55537.92	14.97
Low severity	127044.09	34.26
Moderate-low severity	94491.81	25.48
Moderate-high severity	55200.69	14.89
High severity	24684.66	6.66

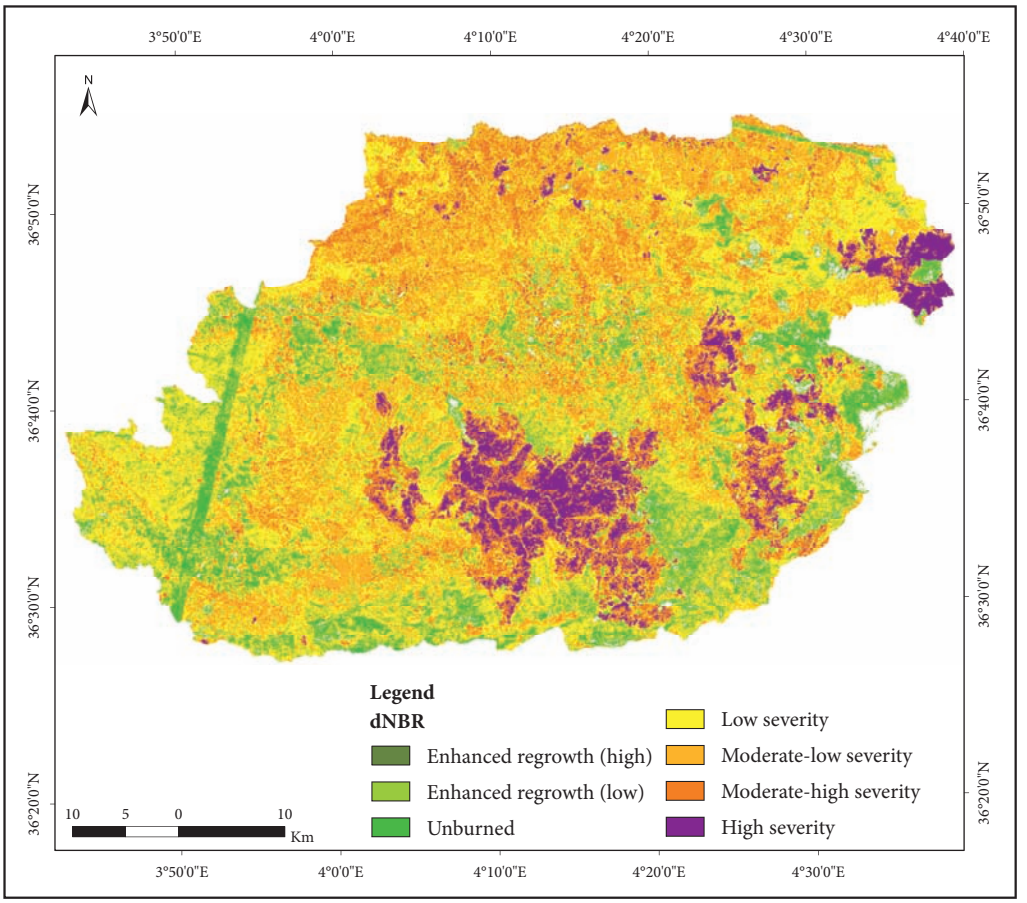


Figure 7: dNBR based burn severity map of the study area.

Furthermore, their study compared these results with those obtained using the relativized dNBR (RdNBR), which showed variations in severity levels: low (9.442 kha), moderate-low (3.077 kha), moderate-high (3.953 kha), and high severity (2.654 kha). The authors concluded that RdNBR provided a more accurate and reliable estimate of fire severity than dNBR alone, particularly due to its better sensitivity across heterogeneous landscapes. In comparison, the current study assessing the 2021 wildfire in Tizi Ouzou revealed a greater extent of burn severity.

This comparative analysis underscores the greater intensity and spatial extent of fire damage in Tizi Ouzou relative to Khenchela. While Khenchela showed only 1.21% under high severity, Tizi Ouzou high severity class was over five times larger. Such differences could stem from variations in vegetation cover, topography, and fire behavior, highlighting the importance of region-specific remote sensing assessments for effective post-fire recovery strategies.

4 Discussion

Our results underscore the critical role of multispectral remote sensing – particularly Landsat-derived indices – in accurately mapping forest fire severity and assessing post-fire ecological impacts. Consistent with global best practices, the dNBR remains a core metric for delineating burn severity across diverse forest types (Key and Benson 2006; Tran et al. 2018; Chuvieco et al. 2019). In the context of Mediterranean ecosystems, dNBR has repeatedly proven effective due to its sensitivity to changes in vegetation and soil reflectance in the shortwave infrared range. Our findings confirm this pattern, with dNBR outper forming NDVI in distinguishing high-severity burn zones in Tizi Ouzou.

Several studies affirm that no single index universally outperforms others; rather, the effectiveness of indices varies depending on forest type and fire regime. For instance, dNBR is often more responsive in resprouting forests, while dNDVI and dNDWI may yield better accuracy in seeder-dominated landscapes (Lentile et al. 2006; Miller and Thode 2007; Tran et al. 2018). This variability was also observed in our study: while dNBR captured the most intense burn zones, NDVI proved more useful in detecting early vegetation regrowth. This aligns with Zennir and Khallef (2023), who also adopted a multi-index approach in the Beni Salah Forest, suggesting that integrating indices offers a more robust characterization of fire effects.

In their analysis, Zennir and Khallef (2023) relied on Sentinel-2 data to detect severe burn zones, while our use of Landsat-8 demonstrated that comparable results can be achieved at a broader regional scale. This indicates that Landsat imagery, despite its coarser resolution, remains highly suitable for large-scale fire severity mapping in Algeria. Similarly, Chuvieco et al. (2018) highlighted the importance of combining multiple indices and leveraging both pre- and post-fire imagery. Our results support this approach, as the integration of NDVI and dNBR enabled us not only to delineate burned areas but also to quantify vegetation loss and partial recovery.

A more recent contribution by Sabljić et al. (2025) confirmed the value of spectral differencing in Mediterranean ecosystems. Their Sentinel-2 analysis captured both immediate fire impacts and recovery trends, findings that parallel our own NDVI-based monitoring of post-fire regrowth in Tizi Ouzou. Likewise, Zikiou et al. (2024) showed that areas with dense suffered more intense damage, a relationship we also observed: zones with higher pre-fire NDVI and elevated LST values in our study area corresponded to higher dNBR severity classes.

These findings reinforce the importance of integrating remote sensing and machine learning technologies in fire risk assessment and management, particularly in fire-prone regions like Algeria. Our findings further highlight the suitability of Landsat-8 OLI imagery, given its spatial and spectral resolution, for detecting burn severity and vegetation degradation (Veraverbeke et al. 2012; Roy et al. 2014). Temporal NDVI analysis in our study clearly demonstrated vegetation health loss post-fire, confirming remote sensing's role in ecological monitoring (De Santis and Chuvieco 2009). NDVI has shown particular utility in tracking regrowth trajectories over time, allowing researchers to monitor ecosystem resilience and degradation trends (Koutsias et al. 2004; Gitas et al. 2012).

Finally, GIS-based mapping of fire severity proved critical for guiding land management and restoration efforts. While earlier works (Keeley 2009; Fernandes 2013) highlighted the value of spatial data for fire policy, our study demonstrates its practical application in Tizi Ouzou, where severity maps can inform targeted reforestation and fire prevention strategies.

5 Conclusion

This study demonstrates the effectiveness of remote sensing and geospatial analysis in assessing forest fire severity and understanding post-fire ecological transformations in the Tizi Ouzou region during the 2021 wildfires. The integration of Landsat-8 imagery with atmospheric data and GIS-based mapping methods underscores the robustness of these tools in fire monitoring and management. The NDVI results highlighted a marked decline in vegetation cover, clearly capturing the loss of biomass, while the NBR and dNBR indices proved particularly effective in quantifying burn severity and delineating the spatial distribution of damage across different land cover types. In addition, the analysis of LST provided complementary insights into the thermal impacts of the fires, confirming areas of ecological stress and intensifying the interpretation of burn severity. Collectively, these findings underscore the capacity of geospatial technologies to generate rapid, reliable, and spatially explicit information to support wildfire monitoring and environmental management in Mediterranean regions. Nevertheless, some limitations were encountered. The use of medium-resolution Landsat 8 imagery constrained the level of detail in fire severity mapping, while the absence of extensive ground-truth data restricted the validation of the obtained results. Furthermore, vegetation indices may be influenced by seasonal agricultural practices, which can occasionally interfere with accurate fire-related classification. Future research should aim to integrate higher-resolution imagery (e.g., Sentinel-2 or PlanetScope), field-based validation campaigns, and advanced techniques such as multi-sensor fusion and machine learning approaches. Long-term monitoring of vegetation regrowth and resilience after wildfires would also enhance understanding of ecosystem recovery dynamics. Such improvements will contribute to the development of more effective strategies for fire risk assessment, ecosystem restoration, and sustainable land management in Algeria and similar Mediterranean environments.

RESEARCH DATA: For information on the availability of research data related to the study, please visit the article webpage: https://doi.org/10.3986/AGS.14459

6 References

Ammiche, S., Oumezzaouche, N. 2018: Valorisation des produits forestiers non ligneux dans la wilaya de Tizi-Ouzou: cas de la forêt des Béni Ghobri. *Ph.D. thesis*. Université Mouloud Mammeri.

Arfa, A. M. T., Benderradji, M. E. H., Saint-Gérand, T., Alatou, D. 2019: Cartographie du risque feu de forêt dans le Nord-est algérien: cas de la wilaya d'El Tarf. *Cybergeo: European Journal of Geography*. https://doi.org/10.4000/cybergeo.32304

Avdan, U., Jovanovska, G. 2016: Algorithm for automated mapping of land surface temperature using LANDSAT 8 satellite data. *Journal of Sensors* 2016-1. https://doi.org/10.1155/2016/1480307

Belgherbi, B., Benabdeli, K., Mostefai, K. 2018: Mapping the risk of forest fires in Algeria: application of the forest of Guetarnia in Western Algeria. *Ekológia* 37-3. https://doi.org/10.2478/eko-2018-0022

Brewer, C. K., Winne, J. C., Redmond, R. L., Opitz, D. W., Mangrich, M. V. 2005: Classifying and mapping wildfire severity. *Photogrammetric Engineering & Remote Sensing* 11. https://doi.org/10.14358/PERS.71.11.1311

Cansler, C. A., McKenzie, D. 2012: How robust are burn severity indices when applied in a new region? Evaluation of alternate field-based and remote-sensing methods. *Remote Sensing* 4-2. https://doi.org/10.3390/rs4020456

Carlson, T. N., Ripley, D. A. 1997: On the relation between NDVI, fractional vegetation cover, and leaf area index. *Remote Sensing of Environment* 62-3. https://doi.org/10.1016/S0034-4257(97)00104-1

Castro-Melgar, I., Tsagkou, A., Zacharopoulou, M., Basiou, E., Athinelis, I., Katris, E. A., Kalavrezou, I. E. et al. 2025: Wildfires during early summer in Greece (2024): Burn severity and land use dynamics through Sentinel-2 data. *Forests* 16-2. https://doi.org/10.3390/f16020268

Chu, T., Guo, X., Takeda, K. 2016: Remote sensing approach to detect post-fire vegetation regrowth in Siberian boreal larch forest. *Ecological Indicators* 62. https://doi.org/10.1016/j.ecolind.2015.11.026

Chuvieco, E., Lizundia-Loiola, J., Pettinari, M. L., Ramo, R., Padilla, M., Tansey, K., Mouillot, F. et al. 2018: Generation and analysis of a new global burned area product based on MODIS 250 m reflectance bands and thermal anomalies. *Earth System Science Data* 10-4. https://doi.org/10.5194/essd-10-2015-2018

Chuvieco, E., Mouillot, F., Van der Werf, G. R., San Miguel, J., Tanase, M., Koutsias, N., García, M. et al. 2019: Historical background and current developments for mapping burned area from satellite Earth observation. *Remote Sensing of Environment* 225. https://doi.org/10.1016/j.rse.2019.02.013

Cocke, A. E., Fulé, P. Z., Crouse, J. E. 2005: Comparison of burn severity assessments using Differenced Normalized Burn Ratio and ground data. *International Journal of Wildland Fire* 14-2. https://doi.org/10.1071/WF04010

Conservation des forêts Tizi Ouzou 2021: Bilan annuel des incendies de forêt, Campagne 2021. *Technical report*.

Cook, M., Schott, J. R., Mandel, J., Raqueno, N. 2014: Development of an operational calibration methodology for the Landsat thermal data archive and initial testing of the atmospheric compensation component of a Land Surface Temperature (LST) Product from the archive. *Remote Sensing* 6-11. https://doi.org/10.3390/rs61111244

De Santis, A., Chuvieco, E. 2009: GeoCBI: A modified version of the Composite Burn Index for the initial assessment of the short-term burn severity from remotely sensed data. *Remote Sensing of Environment* 113-3. https://doi.org/10.1016/j.rse.2008.10.011

Digavinti, J., Manikiam, B. 2021: Satellite monitoring of forest fire impact and regeneration using NDVI and LST. *Journal of Applied Remote Sensing* 15-4. https://doi.org/10.1117/1.JRS.15.042412

Direction Générale des Forêts 2021: Bilan des incendies de forêts en Algérie. Ministère de l'Agriculture et du Développement Rural. *Report*.

Dupuy, J. L., Fargeon, H., Martin-StPaul, N., Pimont, F., Ruffault, J., Guijarro, M., Fernandes, P. et al. 2020: Climate change impact on future wildfire danger and activity in southern Europe: A review. *Annals of Forest Science* 77-2. https://doi.org/10.1007/s13595-020-00933-5

Durlević, U., Srejić, T., Valjarević, A., Aleksova, B., Đeđanski, V., Vujović, F., Lukić, T. 2025: GIS-based spatial modeling of soil erosion and wildfire susceptibility ssing VIIRS and Sentinel-2 data: A case study of Šar Mountains National Park, Serbia. *Forests* 16-3. https://doi.org/10.3390/f16030484

Ekumah, B., Armah, F. A., Afrifa, E. K., Aheto, D. W., Odoi, J. O., Afitiri, A. R. 2020: Geospatial assessment of ecosystem health of coastal urban wetlands in Ghana. *Ocean & Coastal Management* 193. https://doi.org/10.1016/j.ocecoaman.2020.105226

Epting, J., Verbyla, D. Sorbel, B. 2005: Evaluation of remotely sensed indices for assessing burn severity in interior Alaska using Landsat TM and ETM+. *Remote Sensing of Environment* 96-3,4. https://doi.org/10.1016/j.rse.2005.03.002

Escuin, S., Navarro, R. Fernández, P. 2008: Fire severity assessment by using NBR (Normalized Burn Ratio) and NDVI (Normalized Difference Vegetation Index) derived from LANDSAT TM/ETM images. *International Journal of Remote Sensing* 29-4. https://doi.org/10.1080/01431160701281072

Fernandes, P. M. 2013: Fire-smart management of forest landscapes in the Mediterranean basin under global change. *Landscape and Urban Planning* 110. https://doi.org/10.1016/j.landurbplan.2012.10.014

Fernández-Guisuraga, J. M., Calvo, L., Quintano, C., Fernández-Manso, A., Fernandes, P. M. 2023: Fractional vegetation cover ratio estimated from radiative transfer modeling outperforms spectral indices to assess fire severity in several Mediterranean plant communities. *Remote Sensing of Environment* 290. https://doi.org/10.1016/j.rse.2023.113542

Ganteaume, A., Barbero, R. 2019: Contrasting large fire activity in the French Mediterranean. *Natural Hazards and Earth System Sciences* 19-5. https://doi.org/10.5194/nhess-19-1055-2019

García, M. L., Caselles, V. 1991: Mapping burns and natural reforestation using Thematic Mapper data. *Geocarto International* 6-1. https://doi.org/10.1080/10106049109354290

Gitas, I., Mitri, G., Veraverbeke, S., Polychronaki, A. 2012: Advances in remote sensing of post-fire vegetation recovery monitoring – A review. In: Remote Sensing of Biomass – Principles and Applications. IntechOpen. https://doi.org/10.5772/20571

Guehaz, R., Sivakumar, V. 2023: A case study about the forest fire occurred on 05 July 2021 over Khenchela province, Algeria, using space-borne remote sensing. *Frontiers in Remote Sensing* 4. https://doi.org/10.3389/frsen.2023.1289963

Harris, S., Veraverbeke, S., Hook, S. 2011: Evaluating spectral indices for assessing fire severity in chaparral ecosystems (Southern California) using MODIS/ASTER (MASTER) airborne simulator data. *Remote sensing* 3-11. https://doi.org/10.3390/rs3112403

Keeley, J. E. 2009: Fire intensity, fire severity and burn severity: A brief review and suggested usage. *International Journal of Wildland Fire* 18-1. https://doi.org/10.1071/WF07049

Key, C. H., Benson, N. C. 2006: Landscape assessment (LA). In: FIREMON: Fire effects monitoring and inventory system. *General technical report*. U.S. Department of Agriculture, Forest Service, Rocky Mountain Research Station.

Kouachi, M. E., Khairoun, A., Moghli, A., Rahmani, S., Mouillot, F., Baeza, M. J., Moutahir, H. 2024: Forty-year fire history reconstruction from Landsat data in Mediterranean ecosystems of Algeria following international standards. *Remote sensing* 16-13. https://doi.org/10.3390/rs16132500

Koutsias, N., Kalabokidis, K. D. Allgöwer, B. 2004: Fire occurrence patterns at landscape level: Beyond positional accuracy of ignition points with kernel density estimation methods. *Natural Resource Modeling* 17-4. https://doi.org/10.1111/j.1939-7445.2004.tb00141.x

Koutsias, N., Karamitsou, A., Nioti, F., Coutelieris, F. 2022: Assessment of fire regimes and post-fire evolution of burned areas with the dynamic time warping method on time series of satellite images – setting the methodological framework in the Peloponnese, Greece. *Remote Sensing* 14-20. https://doi.org/10.3390/rs14205237

Kurbanov, E., Vorobev, O., Lezhnin, S., Sha, J., Wang, J., Li, X., Cole, J. et al. 2022: Remote sensing of forest burnt area, burn severity, and post-fire recovery: A review. *Remote Sensing* 14-19. https://doi.org/10.3390/rs14194714

Lahmar, B., Akakba, A. 2024: Forest fire detection based on earlier pre-fire conditions using analysis hierarchic process (AHP) in a semi-arid climate. A case study: Belezma National Park, Algeria. *Acta Geographica Lodziensia* 114. https://doi.org/10.26485/AGL/2024/114/3

Lentile, L. B., Holden, Z. A., Smith, A. M., Falkowski, M. J., Hudak, A. T., Morgan, P., Lewis, S. A. et al. 2006: Remote sensing techniques to assess active fire characteristics and post-fire effects. *International Journal of Wildland Fire* 15-3. https://doi.org/10.1071/WF05097

Liu, J., Wang, Y., Guo, H., Lu, Y., Xu, Y., Sun, Y., Gan, W. et al. 2024: Spatial and temporal patterns and driving factors of forest fires based on an optimal parameter-based geographic detector in the Panxi region, Southwest China. *Fire Ecology* 20-1. https://doi.org/10.1186/s42408-024-00257-z

Lovreglio, R., Leone, V., Giaquinto, P., Notarnicola, A. 2010: Wildfire cause analysis: Four case-studies in southern Italy. *iForest-Biogeosciences and Forestry* 3-1. https://doi.org/10.3832/ifor0521-003

Lukić, T., Marić, P., Hrnjak, I., Gavrilov, M. B., Mladjan, D., Zorn, M., Komac, B. et al. 2017: Forest fire analysis and classification based on a Serbian case study. *Acta geographica Slovenica* 57-1. https://doi.org/10.3986/AGS.918

Maillard, O., Flores-Valencia, M., Michme, G., Coronado, R., Bachfischer, M., Azurduy, H., Vides-Almonacid, R. et al. 2022: Phenology patterns and postfire vegetation regeneration in the Chiquitania region of Bolivia using Sentinel-2. *Fire* 5-3. https://doi.org/10.3390/fire5030070

Meddour-Sahar, O., Derridj, A. 2010: Le risque d'incendie de forêt: évaluation et cartographie. *Science et changements planétaires/Sécheresse* 21-3.

Miller, J. D., Thode, A. E. 2007: Quantifying burn severity in a heterogeneous landscape with a relative version of the delta Normalized Burn Ratio (dNBR). *Remote Sensing of Environment* 109-1. https://doi.org/10.1016/j.rse.2006.12.006

Mouillot, F., Ratte, J. P., Joffre, R., Moreno, J. M., Rambal, S. 2003: Some determinants of the spatio-temporal fire cycle in a Mediterranean landscape (Corsica, France). *Landscape Ecology* 18. https://doi.org/10.1023/B:LAND.0000004182.22525.a9

Nasery, S., Kalkan, K. 2020: Burn area detection and burn severity assessment using Sentinel 2 MSI data: The case of Karabağlar district, İzmir/Turkey. *Turkish Journal of Geosciences* 1-2.

Nolè, A., Rita, A., Spatola, M. F., Borghetti, M. 2022: Biogeographic variability in wildfire severity and post-fire vegetation recovery across the European forests via remote sensing-derived spectral metrics. *Science of The Total Environment* 823. https://doi.org/10.1016/j.scitotenv.2022.153807

Oliveira, S., Oehler, F., San-Miguel-Ayanz, J., Camia, A., Pereira, J. M. 2012: Modeling spatial patterns of fire occurrence in Mediterranean Europe using Multiple Regression and Random Forest. *Forest Ecology and Management* 275. https://doi.org/10.1016/j.foreco.2012.03.003

Parks, S. A., Dillon, G. K., Miller, C. 2014: A new metric for quantifying burn severity: the relativized burn ratio. *Remote Sensing* 6-3. https://doi.org/10.3390/rs6031827

Rahmani, S., Benmassoud, H. 2019: Modelling of forest fire risk spatial distribution in the region of Aures, Algeria. *Geoadria* 24-2. https://doi.org/10.15291/geoadria.2846

Rouse, J. W., Haas, R. H., Schell, J. A., Deering, D. W. 1973: Monitoring the vernal advancement and retrogradation (green wave effect) of natural vegetation. Progress Report RSC 1978-2. *Technical Report.* NASA.

Roy, D. P., Boschetti, L., Justice, C. O., Ju, J. 2008: The collection 5 MODIS burned area product – Global evaluation by comparison with the MODIS active fire product. *Remote Sensing of Environment* 112-9. https://doi.org/10.1016/j.rse.2008.05.013

Roy, D. P., Wulder, M. A., Loveland, T. R., Woodcock, C. E., Allen, R. G., Anderson, M. C., Helder, D. et al. 2014: Landsat-8: Science and product vision for terrestrial global change research. *Remote Sensing of Environment* 145. https://doi.org/10.1016/j.rse.2014.02.001

Ru, C., Duan, S. B., Jiang, X. G., Li, Z. L., Jiang, Y., Ren, H., Leng, P. et al. 2021: Land surface temperature retrieval from Landsat 8 thermal infrared data over urban areas considering geometry effect: Method and application. *IEEE Transactions on geoscience and remote sensing* 60. https://doi.org/10.1109/TGRS.2021.3088482

Sabljić, L., Perić, Z. M., Bajić, D., Marković, S. B., Adžić, D., Lukić, T. 2025: Advancing wildfire monitoring: remote sensing techniques and applications in the Sana River Basin, Bosnia and Herzegovina. *Natural Hazards* 1-40. https://doi.org/10.1007/s11069-025-07518-3

Sahar, O., Hamel, H., Meddour, R. 2020: Etude des grands feux de forêts en Algérie: Cas de la wilaya de Tizi Ouzou. *Geo-Eco-Trop* 44-3.

San-Miguel-Ayanz, J., Durrant, T., Boca, R., Maianti, P., Libertá, G., Artés-Vivancos, T., Oom, D. et al. 2022: Advance report on wildfires in Europe, Middle East and North Africa 2021. *Technical report*. Publications Office of the European Union. https://doi.org/10.2760/039729

Sobrino, J. A., Jiménez-Muñoz, J. C., Paolini, L. 2004: Land surface temperature retrieval from LANDSAT TM 5. *Remote Sensing of Environment* 90-4. https://doi.org/10.1016/j.rse.2004.02.003

Stathopoulou, M., Cartalis, C. 2007: Daytime urban heat islands from Landsat ETM+ and Corine land cover data: An application to major cities in Greece. *Solar Energy* 81-3. https://doi.org/10.1016/j.solener.2006.06.014

Stefanidis, S., Alexandridis, V., Spalevic, V., Mincato, R. L. 2022: Wildfire effects on soil erosion dynamics: The case of 2021 megafires in Greece. *Agriculture & Forestry* 68-2. https://doi.org/10.17707/AgricultForest.68.2.04

Tran, B. N., Tanase, M. A., Bennett, L. T., Aponte, C. 2018: Evaluation of spectral indices for assessing fire severity in Australian temperate forests. *Remote Sensing* 10-11. https://doi.org/10.3390/rs10111680

Turco, M., Jerez, S., Augusto, S., Tarín-Carrasco, P., Ratola, N., Jiménez-Guerrero, P., Trigo, R. M. 2019: Climate drivers of the 2017 devastating fires in Portugal. *Scientific Reports* 9-1. https://doi.org/10.1038/s41598-019-50281-2

United States Geological Survey 2016: Landsat – Earth Observation Satellites. Fact sheet. https://doi.org/10.3133/fs20153081

Veraverbeke, S., Hook, S., Hulley, G. 2012: An alternative spectral index for rapid fire severity assessments. *Remote Sensing of Environment* 123. https://doi.org/10.1016/j.rse.2012.02.025

Veraverbeke, S., Lhermitte, S., Verstraeten, W. W., Goossens, R. 2010: The temporal dimension of differenced Normalized Burn Ratio (dNBR) fire/burn severity studies: The case of the large 2007 Peloponnese wildfires in Greece. *Remote Sensing of Environment* 114-11. https://doi.org/10.1016/j.rse.2010.05.029

Vlassova, L., Pérez-Cabello, F., Mimbrero, M. R., Llovería, R. M., García-Martín, A. 2014: Analysis of the relationship between land surface temperature and wildfire severity in a series of Landsat images. *Remote Sensing* 6-7. https://doi.org/10.3390/rs6076136

Vujović, F., Valjarević, A., Vila-Subirós, J., Šiljeg, A., Lukić, T. 2024: Geospatial modeling of wildfire susceptibility on a national scale in Montenegro: A comparative evaluation of F-AHP and FR methodologies. *Open Geosciences* 16-1. https://doi.org/10.1515/geo-2022-0694

Wasserman, T. N., Mueller, S. E. 2023: Climate influences on future fire severity: A synthesis of climate-fire interactions and impacts on fire regimes, high-severity fire, and forests in the western United States. *Fire Ecology* 19-1. https://doi.org/10.1186/s42408-023-00200-8

Wendt, C. K., Beringer, J., Tapper, N. J., Hutley, L. B. 2007: Local boundary-layer development over burnt and unburnt tropical savanna: An observational study. *Boundary-Layer Meteorology* 124. https://doi.org/10.1007/s10546-006-9148-3

Yuan, F., Bauer, M. E. 2007: Comparison of impervious surface area and normalized difference vegetation index as indicators of surface urban heat island effects in Landsat imagery. *Remote Sensing of Environment* 106-3. https://doi.org/10.1016/j.rse.2006.09.003

Zahabnazouri, S., Belmont, P., David, S., Wigand, P. E., Elia, M., Capolongo, D. 2025: Detecting burn severity and vegetation recovery after fire using dNBR and dNDVI indices: Insight from the Bosco Difesa Grande, Gravina in Southern Italy. *Sensors* 25-10. https://doi.org/10.3390/s25103097

Zennir, R., Khallef, B. 2023: Forest fire area detection using Sentinel-2 data: Case of the Beni Salah national forest-Algeria. *Journal of Forest Science* 69-1. https://doi.org/10.17221/50/2022-JFS

Zhao, Y., Huang, Y., Sun, X., Dong, G., Li, Y., Ma, M. 2023: Forest fire mapping using multi-source remote sensing data: A case study in Chongqing. *Remote Sensing* 15-9. https://doi.org/10.3390/rs15092323

Zikiou, N., Rushmeier, H., Capel, M. I., Kandakji, T., Rios, N., Lahdir, M. 2024: Remote sensing and machine learning for accurate fire severity mapping in northern Algeria. *Remote Sensing* 16-9. https://doi.org/10.3390/rs16091517

Acta geographica Slovenica, 66-1, 2026, 121–146

NATIONAL-SCALE WATER BALANCE IN SLOVENIA (1972–2024): LONG-TERM TRENDS AND VARIABILITY IN WATER BALANCE COMPONENTS

Peter Frantar, Frank Herrmann, Mišo Andjelov



FRANK HERRMANN

The Unica River at Planina Polje near Hošperk Castle (ger. Haasberg).

DOI: https://doi.org/10.3986/AGS.14632
UDC: 556.1(497.4) "1972/2024"
Creative Commons CC BY-SA 4.0

Peter Frantar[1], Frank Herrmann[2], Mišo Andjelov[3]

National-scale water balance in Slovenia (1972–2024): Long-term trends and variability in water balance components

ABSTRACT: Climate change is altering hydrological processes and water availability, requiring robust long-term analyses based on consistent data and models. In the article, the main components of the hydrological water balance – precipitation, evapotranspiration, and runoff – in Slovenia for the period 1972–2024 are analysed. The analysis is based on results from a verified national-scale mGROWA water balance model. The objective of study is to identify trends that could be relevant for water resources management in a changing climate. A key finding is that evapotranspiration has increased significantly in large parts of the country. However, above-average precipitation in recent years has so far compensated for this increase, preventing a country-wide decline in average runoff. Finally, a hydro-climatological trend indicator is proposed as a future element for monitoring the water balance components in Slovenia.

KEYWORDS: hydrology, water balance modelling, mGROWA, climate change, hydro-climatological trend indicator, water resources management, Slovenia

Vsedržavni vodno bilančni model Slovenije (1972–2024): dolgoročni trendi in spremenljivost komponent vodne bilance

POVZETEK: Podnebne spremembe spreminjajo hidrološke procese in razpoložljivost vode, kar zahteva robustne dolgoročne analize na podlagi konsistentnih podatkov in modelov. V članku so analizirane glavne komponente hidrološke vodne bilance – padavine, evapotranspiracija in odtok – v Sloveniji za obdobje 1972–2024. Analiza temelji na rezultatih verificiranega modela vodne bilance mGROWA za območje Slovenije. Cilj študije je prepoznati trende, ki bi lahko bili pomembni za upravljanje vodnih virov v spreminjajočem se podnebju. Ključna ugotovitev je, da se je evapotranspiracija v velikem delu države znatno povečala, vpliv tega povečanja pa je bil manjši zaradi nadpovprečnih padavin v zadnjih letih, zato se povečanje ni izrazilo v manjšem povprečnem odtoku. Avtorji predlagamo hidro-klimatološki kazalnik trendov kot element spremljanja vodnobilančnih komponent v Sloveniji.

KLJUČNE BESEDE: hidrologija, modeliranje vodne bilance, mGROWA, podnebne spremembe, hidro-klimatološki kazalnik trendov, upravljanje vodnih virov, Slovenija

The article was submitted for publication on August 29th, 2025.
Uredništvo je prejelo prispevek 29. avgusta 2025.

[1] Slovenian Environment Agency, Ljubljana, Slovenia; Faculty of Environmental Protection, Velenje, Slovenia
[2] Forschungszentrum Jülich, Agrosphere Institute (IBG-3), Jülich, Germany
[3] Slovenian Environment Agency, Ljubljana, Slovenia

peter.frantar@gov.si, peter.frantar@fvo.si (https://orcid.org/0000-0003-0501-4930), f.herrmann@fz-juelich.de (https://orcid.org/0000-0003-4939-0479), miso.andjelov@gov.si (https://orcid.org/0009-0009-4383-7939)

1 Introduction

The global hydrological cycle is undergoing significant changes due to current climate change affecting regional water balance components. Rising temperatures and altered precipitation regimes influence evapotranspiration, snow cover duration, runoff distribution, and groundwater recharge, leading to shifts in water availability and hydrological extremes (e.g., Huntington 2006; Milly et al. 2008; Intergovernmental Panel on Climate Change 2023; Xiong et al. 2023). These climatic developments necessitate continuous regional water balance assessments to support water resources management and water security planning (European Commission 2015; Bevacqua et al. 2024).

Slovenia is located in Europe in the transition zone between the Alps, the Mediterranean, the Dinaric Alps, and the Pannonian Basin (Figure 1, top). In Slovenia previous national-scale water balance studies analysed the mean conditions for the periods 1961–1990 and 1971–2000 (Kolbezen and Pristov 1998; Frantar 2007; Frantar 2008), providing an important basis for the water resources management. More recent assessments have employed grid-based GROWA model to analyse annual water balance components at high spatial resolution (Tetzlaff et al. 2015; Andjelov et al. 2016). The latest development of this modelling is the mGROWA model (Herrmann et al. 2015), which provides the water balance at daily resolution.

This study applies the national-scale mGROWA model to analyse precipitation (P), evapotranspiration (ET) and runoff (Q) in Slovenia for the period 1972–2024. The objectives are to (i) assess long- and mid-term changes in the main water balance components, (ii) identify regions with significant recent changes that may require adaptation in water resources management, and (iii) propose a hydro-climatological trend indicator for continuous monitoring of the national water balance. Results are analysed at national level and at the level of the five major Slovenian hydrological regions (Figure 1).

The study presents a novel national-scale, high-resolution assessment of long-term and seasonal changes in water balance components in Slovenia. It is integrating mGROWA simulations with an enhanced hydro-climatological trend framework that combines LOESS-based continuous trend indicators, raster hydrograph visualisation, and spatially explicit statistical testing of regime shifts and trends.

2 Hydrological regions of Slovenia

Slovenia is hydrologically divided into two major river basin districts (RBDs): the Danube RBD and the Adriatic RBD, separated by the main topographic watershed. Approximately 81% of the national territory belongs to the Danube RBD, which includes the Sava, Drava, and Mura river basins, while the remaining 19% drains into the Adriatic Sea, primarily via the Soča River and smaller coastal rivers (Figure 1, subareas 3 and 4).

The Danube RBD is characterised by a strong east–west gradient in climate, topography, and water availability. Mountainous alpine and pre-alpine areas in the west receive higher P, while lower elevations in the east, particularly in the Drava and Mura basins, experience more continental conditions and lower P. This gradient is reflected in runoff formation and regional water availability, with major urban centres such as Ljubljana and Maribor located within the Sava and Drava basins, respectively.

The Adriatic RBD extends from the Alps in the north to the Mediterranean coast. P and Q generally decrease from the mountainous regions towards the south, resulting in a pronounced north–south gradient in water availability.

Large parts of Slovenia are characterised by karst hydrogeology with scarce surface water flows. Major structural depressions in Slovenia are filled with unconsolidated alluvial sediments that form productive aquifers with complex surface–groundwater interactions and highly heterogeneous flow paths of national importance, while smaller hydrogeological units, such as flysch formations, play a key role at the local scale. Detailed descriptions of Slovenian hydrology are provided by Kolbezen and Pristov (1998) and Frantar (2008). These pronounced physiographic and hydrogeological contrasts are reflected in distinct water balance regimes and justify the spatially differentiated analyses applied in the following sections.

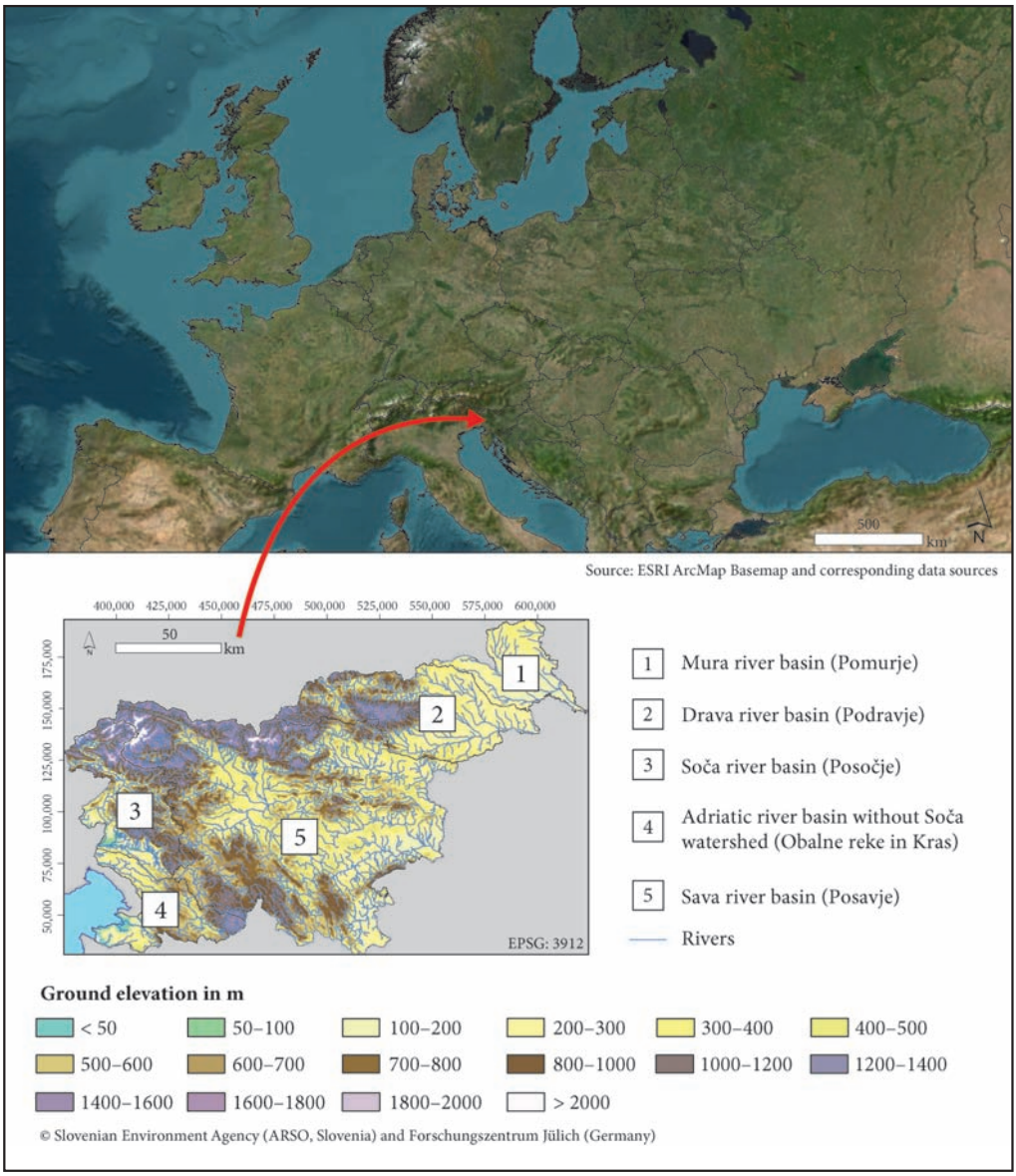


Figure 1: Location of Slovenia in Europe (top) and location of river basins and districts within Slovenia (bottom). In addition, the bottom map shows the nationwide ground elevation and the river network. The geographic coordinate system of the map of Slovenia is MGI 1901 / Slovene National Grid (EPSG: 3912), axis labels show metres.

3 Methodology

3.1 mGROWA modelling methodology and data basis in Slovenia

In previous national-scale water balance studies in Slovenia, the grid-based GROWA model was applied. This model solves the hydrological water balance equation $P = Q + ET \pm \Delta S$ for high-resolution spatial

grids, where P denotes precipitation, Q runoff, ET evapotranspiration, and ΔS changes in water storage. Earlier applications in the GROWA model focused on annual totals, but subsequent developments improved the representation of soil water storage dynamics and their varying contribution to evapotranspiration.

As a result of these developments, the deterministic, grid-based water balance model mGROWA (Herrmann et al. 2013; Herrmann et al. 2015) has been available for several years. It can be applied to assess the impact of climate variability and change on water resources at the scale of large river systems and entire countries (Herrmann et al. 2017; Herrmann et al. 2021). Figure 2 provides an overview of the main input data, simulated variables, and derived statistics, while detailed equations and algorithms are documented in the cited literature. In the following, the mGROWA model is described from a generic perspective, focusing on elements relevant for interpreting the results presented in this study.

Climatic input to the model includes air temperature, P, and reference evapotranspiration (ETo). These variables are typically provided by national meteorological services or derived from regional weather forecast and climate models. Adapted methods can be used to interpolate or downscale these variables and country-specific ETo methods can be used. The mGROWA model operates on daily time step; accordingly, meteorological inputs are prepared at daily resolution. Daily variability in P and ETo is derived from station-based observations, and these temporal patterns are internally transferred from spatially interpolated monthly grid data.

Geospatial input data (left column of Figure 2) describe land use, topography, soil properties, and surface imperviousness. They are used to parameterise the land surface and the rooting zone of vegetation and are essential for calculating soil water content and ET as a function of vegetation type, soil water storage capacity, slope, sealings and exposition. Additional geodata are used to characterise subsurface conditions relevant for Q generation. In particular, the depth to the groundwater table provides an important boundary condition and can serve as an interface to numerical groundwater models.

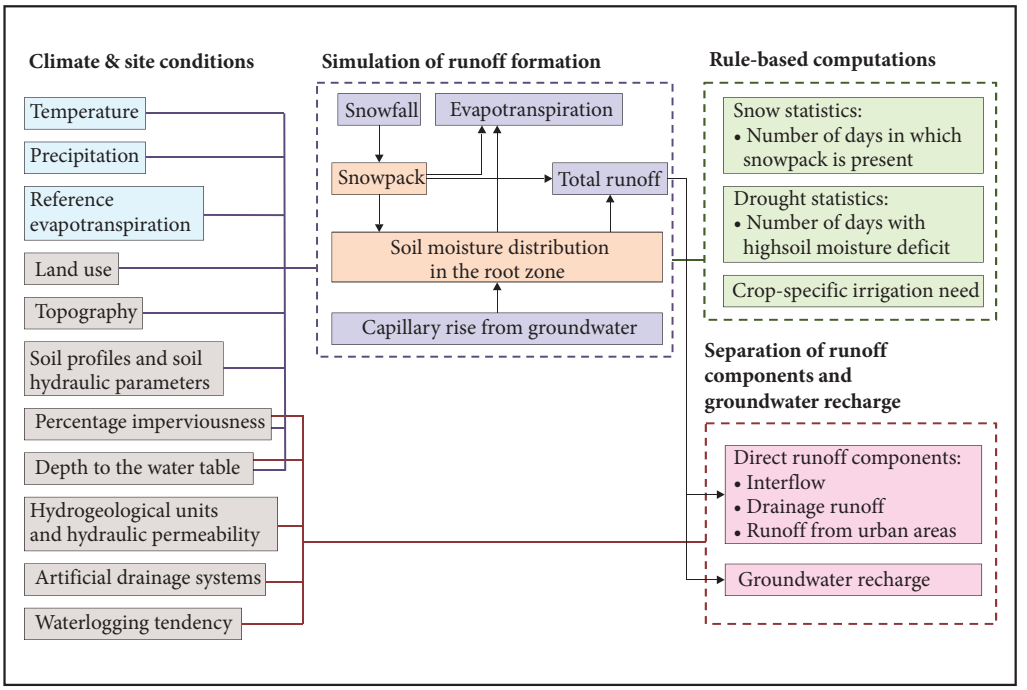


Figure 2: mGROWA modelling diagram. Cyan indicates the climatic input data, light brown indicates the geodata on site conditions, violet indicates the simulated hydrological variables, orange indicates the water storages considered, red-brown indicates simulated runoff components and groundwater recharge, light green indicates rule-based computations and statistics, lines indicate dependencies.

Runoff formation (central column in Figure 2) in mGROWA is simulated using physically based representations of snow processes, soil water dynamics, ET, and percolation. Snow accumulation and melt are primarily temperature-controlled and are simulated using methods originally implemented in the WaSiM-ETH model (Schulla 1997), including a temperature-index approach for snow melting, also considering the temperature – elevation dependency. Soil moisture dynamics are calculated using the multi-layer soil water balance model BOWAB (Engel et al. 2012), with the daily change in soil moisture representing the storage term of the water balance equation. Actual evapotranspiration is computed as a function of soil moisture using the Disse-function (Disse 1995) in combination with evapotranspiration coefficients analogous to the FAO crop coefficient concept (Allen et al. 1998). Capillary rise from groundwater into the root zone depends on groundwater depth and may occur under conditions of soil moisture deficit (conversion is performed by functional relationship of van Genuchten's equation (van Genuchten 1980) in combination with tabulated capillary rise rates). When soil water storage exceeds field capacity, excess water contributes to total runoff.

Total runoff simulated at daily time steps is aggregated to monthly values and subsequently separated into groundwater recharge and direct runoff components (right column bottom in Figure 2). Groundwater recharge is calculated in monthly time steps using the base flow index approach, which has been previously evaluated for Slovenia (Tetzlaff et al. 2015), while direct runoff components are obtained as residual terms. By simulating snow and soil water dynamics, the model can also provide spatiotemporal statistics such as snow cover duration or soil moisture deficit (right column top in Figure 2), which may be used as indicators of agricultural drought. The irrigation water requirements for specific crops can also be derived from this model (McNamara et al. 2024). These outputs are not analysed further in this study.

The data basis used for the mGROWA application in Slovenia is listed in Table 1. All datasets were transferred to a 100 m model grid using standard geographic information system methods, resulting in 2,027,330 active grid cells, each representing one hectare of the national territory. Monthly P and ETo fields

Table 1: Data basis used for the mGROWA water balance modelling in Slovenia.

Theme	Database / format / resolution	Source
Observed climate	Station-based, daily time steps (1972–2024): • Precipitation (P) • Reference evapotranspiration (ETo) • 2 m air temperature Grid-based 100 m, monthly time steps (1972–2024): • Precipitation (P) • Reference evapotranspiration (ETo)	Slovenian Environment Agency (ARSO)
Land use	• CORINE land cover layer (2006), grid-based 100 m • Imperviousness layer (2012), grid-based 20 m	European Environment Agency (EEA)
Soil	• Slovenian soil map (polygons) and over 10,000 soil profiles • European Soil Database derived data layers for gap filling	• Biotechnical Faculty, University of Ljubljana • Hiederer (2013)
Topography	Grid-based 100 m, Digital elevation model (DMV 100)	Surveying and Mapping Authority of the Republic of Slovenia (GURS)
Geology	• Geological map 1:100,000 • Hydrogeological map 1:500,000	Geological Survey of Slovenia (GeoZS)
Groundwater	Depth to groundwater table 1:25,000, grid-based	Slovenian Environment Agency (ARSO)
Artificial drainage	Artificially drained farmland 1:25,000, grid-based	• Slovenian Ministry of Agriculture, Forestry and Food (MKGP) • Tetzlaff et al. (2009)
Hydrology	• Catchment boundaries 1:25,000, polygons • Daily discharge (1981–2020), gauge-based	Slovenian Environment Agency (ARSO)
Base maps	River network, political boundaries, towns, digital elevation model	Surveying and Mapping Authority of the Republic of Slovenia (GURS)

were reconstructed at the Slovenian Environment Agency (ARSO) using ordinary kriging based on relative anomalies, which exhibit lower spatial variability than absolute values and are therefore better suited for interpolation. This geostatistical approach, originally proposed by Matheron (1963), has been established as standard practice for climatological data mapping at ARSO (Dolinar 2009).

3.2 Methods for assessing changes and trends

From a water resources management and planning perspective, long-term changes in the mean values of the water balance components P, ET, and Q are of primary importance. Therefore, the assessment begins with an analysis of interdecadal variability between the decades from 1972 to 2020 relative to the current World Meteorological Organization (WMO) reference period 1991–2020.

In addition to interdecadal changes, inter-annual and seasonal changes and shifts have gained increasing attention in regional water resources assessments (e.g., Ertl et al. 2018; Ertl et al. 2022). For the high-resolution mGROWA simulations, a standard visualisation was therefore used that combines area-specific time series of monthly and annual totals with a long-term trend line. In this study, this visualisation was extended by a hydro-climatological trend indicator enabling continuous monitoring of recent trends. Figure 6 shows this standard visualisation for P, ET, and Q for Slovenia. The upper panels display annual totals and a LOESS-42 trend line (Scherrer et al. 2024), representing a smooth nonlinear climate trend calculated using local linear regression (1st-order LOESS with a 42-year window; grey shading denotes 95% confidence limits). The main advantage of this filter is that extreme values are strongly smoothed while still influencing the trend direction. The 42-year window proved suitable for approximating a 30-year moving average. Unlike moving averages, LOESS-42 also provides unbiased values at the beginning and end of a time series, which is particularly important for monitoring. The difference between the latest LOESS-42 value and the 30-year average is used as a deficit or surplus indicator, describing whether recent trends deviate positively or negatively from the long-term reference.

As a second component of the visualisation, monthly totals are displayed as a raster hydrograph (following Strandhagen et al. 2006), allowing seasonal variability to be interpreted together with longer-term trends (Ehlers et al. 2016). Seasonal patterns and their shifts can thus be quickly compared and evaluated.

Visual interpretation of time series raises the question of whether statistically significant changes or trends have occurred in recent decades. This was addressed using statistical tests. Mauget (2003) applied the non-parametric Mann–Whitney–Wilcoxon test (MWW; Wilcoxon 1945; Mann and Whitney 1947) to detect multi-decadal regime shifts in water balance components, and this approach is recommended for evaluating changing climate signals (Pfeifer et al. 2015). The test examines two segments of annual time series for significant differences in mean values and distributions. In addition, the Mann–Kendall trend test (MK; Kendall 1938; Mann 1945) was used to detect monotonic trends (Helsel and Hirsch 1992).

Both tests were implemented in a grid-based manner, yielding spatial patterns of the probability of the alternative hypothesis, i.e., evidence of significant change or trend. For the MWW test, two time-span pairs were analysed: 1999–2024 versus 1973–1998 (26 years each, covering nearly the entire simulation period) and 2001–2020 versus 1981–2000 (20 years each), representing conditions before and after the year 2000, which often marks a more significant shift in climatological time series. For the MK test, the tail of the simulation from 1995–2024 was evaluated to assess the direction and significance of recent monotonic trends.

3.3 Methods for the evaluation of the runoff simulation

Before results of the mGROWA simulation are used for long-term water resources management, the quality of the calculated runoff balance must be evaluated. This evaluation is generally performed in suitable catchments based on measured discharge data. The long-term mean observed runoff for a 30-year hydrological period is calculated from stream-gauge hydrographs by averaging daily mean discharges. The simulated counterpart is obtained by zonal analysis of the total runoff grids produced by mGROWA for the areas contributing to each gauge.

Identifying suitable river catchments is a key step in this evaluation. Several criteria must be fulfilled: (i) long-term, gap-free discharge measurements must be available; (ii) catchment boundaries must be delineated

with sufficient certainty, which is often challenging in karst areas; (iii) human influence on runoff regimes and water use should be low; and (iv) gauges should be relatively evenly distributed across the country. Additional technical factors may also affect discharge measurements, but these are not discussed further here.

Agreement between observations and simulations for the selected catchments is assessed using objective performance measures. For the country-wide evaluation of long-term mean values, the area-weighted variants of the Nash–Sutcliffe efficiency (NSE; Nash and Sutcliffe 1970) and PBIAS (percent bias; Gupta et al. 1999) have proven useful (Herrmann et al. 2015). NSE describes how well observed and simulated values fit the 1:1 line, with a maximum value of 1.0. Values between 0.75 and 1.00 indicate very good performance, and values between 0.65 and 0.75 indicate good performance (Moriasi et al. 2007). PBIAS quantifies the overall tendency of a model to over- or underestimate observations. The optimal value is 0.0, with low-magnitude values indicating high simulation quality. Positive values indicate underestimation and negative values indicate overestimation. According to Moriasi et al. (2007), values within ±10% are considered very good, ±10% to ±15% good, and ±15% to ±25% satisfactory.

4 Results

4.1 Long-term water balance and interdecadal deviations

The water balance components P, ET, and Q are listed in Table 2 for the reference period 1991–2020, their deviations in the five decades from 1972 to 2020, and the five hydrological regions. During 1991–2020, Slovenia received an average annual P of 1455 mm/a. The dependence of P on topography and along a west–east gradient is visible in Figure 3A. The highest mean values, exceeding 3200 mm/a, occur in the Julian Alps (Soča River basin), while the lowest P, below 900 mm/a, is found in the northeastern plains of the Mura River basin. Almost nationwide, P was above the reference value (+33 mm/a) in 1972–1980, particularly in the northwest and southwest. In the following decades, 1981–1990 and 1991–2000, declines of −24 mm/a and −17 mm/a occurred, respectively. The decade 2001–2010 was also slightly below the reference level (−10 mm/a). In contrast, 2011–2020 was characterised by an average anomaly of +27 mm/a. During this period, the Drava River basin represented the driest region (Figure 3). Deviations in the hydrological regions vary in magnitude between decades, but the large-scale spatial gradients of P remain evident.

For 1991–2020, the average annual ET, simulated with mGROWA was approximately 710 mm/a (Table 2, Figure 4). ET exhibits pronounced spatial variability related to vegetation cover, soil physical properties, and topography (slope and exposition). Highest values (>850 mm/a) occur in lowland areas with dense vegetation and favourable climatic and soil-moisture conditions, especially in southwestern and central Slovenia. Lowest values (<500 mm/a) are found in alpine regions, where low temperatures, short growing seasons, and vegetation-free areas constrain ET. Because summer P regularly replenishes soil moisture across Slovenia, spatial P patterns are not directly reflected in ET patterns. The influence of rising temperatures is already visible in the persistent increase of ET anomalies over the five decades. In 2011–2020, a nationwide anomaly of +21 mm/a was reached relative to the reference period, indicating the need for the more detailed trend analyses presented in the following chapter.

Spatial and temporal patterns of runoff result from the combined effects of P and ET and are simulated accordingly in mGROWA. During 1991–2020, the average annual Q in Slovenia amounted to 741 mm/a (Table 2). The highest Q values (>2000 mm/a) occur in parts of the Julian Alps, whereas the lowest values (<100 mm/a) are found in the northeastern lowlands of the Mura River basin (Figure 5A). Q patterns are primarily controlled by P, consistent with previous studies (Kolbezen and Pristov 1998; Frantar 2008). Owing to above-average P, the first decade shows the highest Q almost nationwide. In the subsequent decades, interpretation becomes more complex. With increasing ET (Figure 4), deviations of Q (Figure 5) diverge more strongly from those of P (Figure 3). Thus, as climate change progresses, runoff correlates less directly with P. The strength of this decoupling varies regionally, reflecting the combined effects of changing P patterns and Slovenia's geodiversity, ranging from the Alps to the Dinaric karst, Mediterranean, and Pannonian regions. Consequently, country-level generalisations are more uncertain than basin-scale interpretations, which highlights the importance of regional trend analyses presented in the following section.

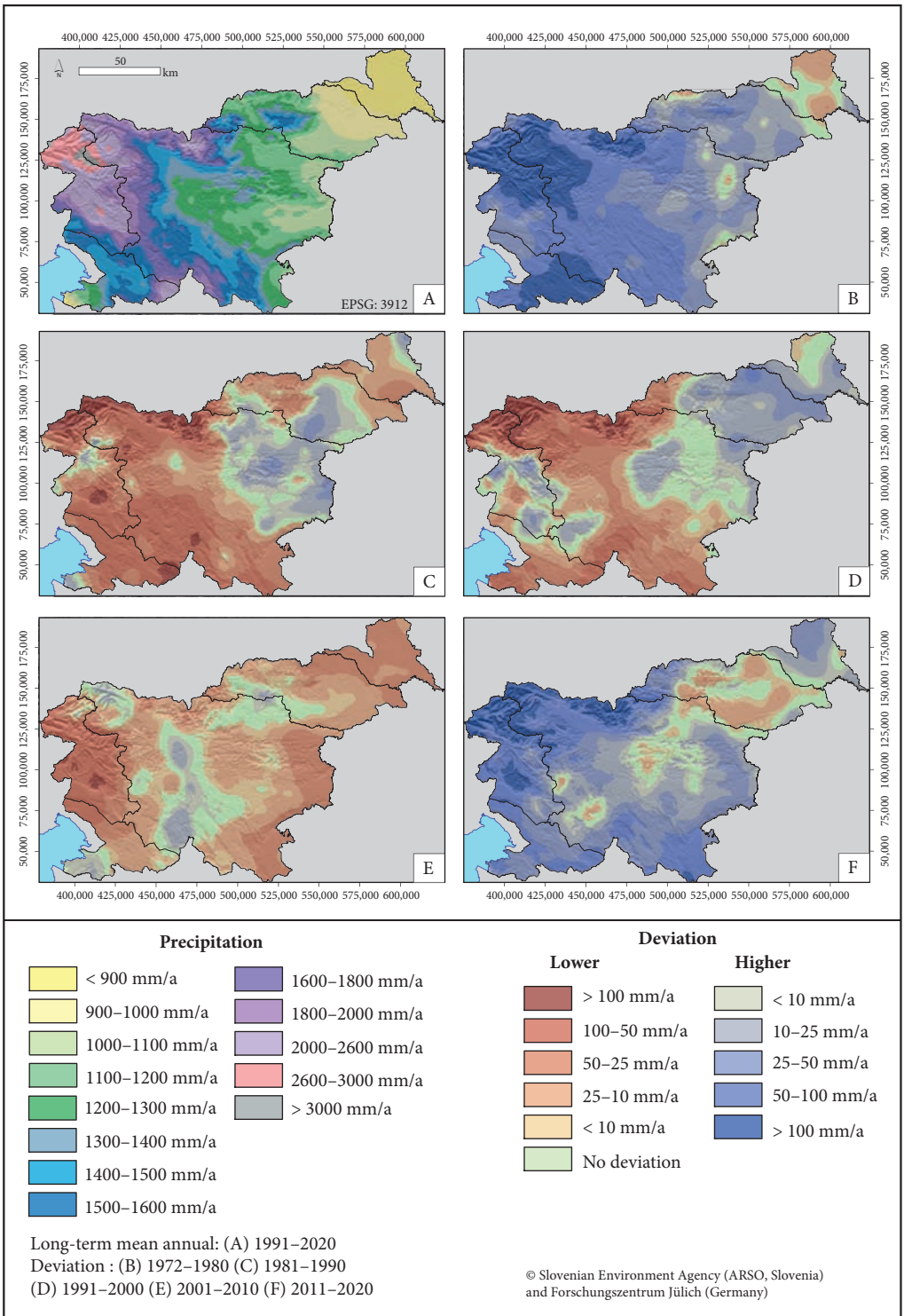
Table 2: mGROWA model results for the major water balance components precipitation (P), evapotranspiration (ET) and runoff (Q) in Slovenia and in the five major hydrological regions in the period 1991–2020 and corresponding interdecadal deviations. The interdecadal deviations have been calculated as decadal average minus long-term average. All values are in mm/a.

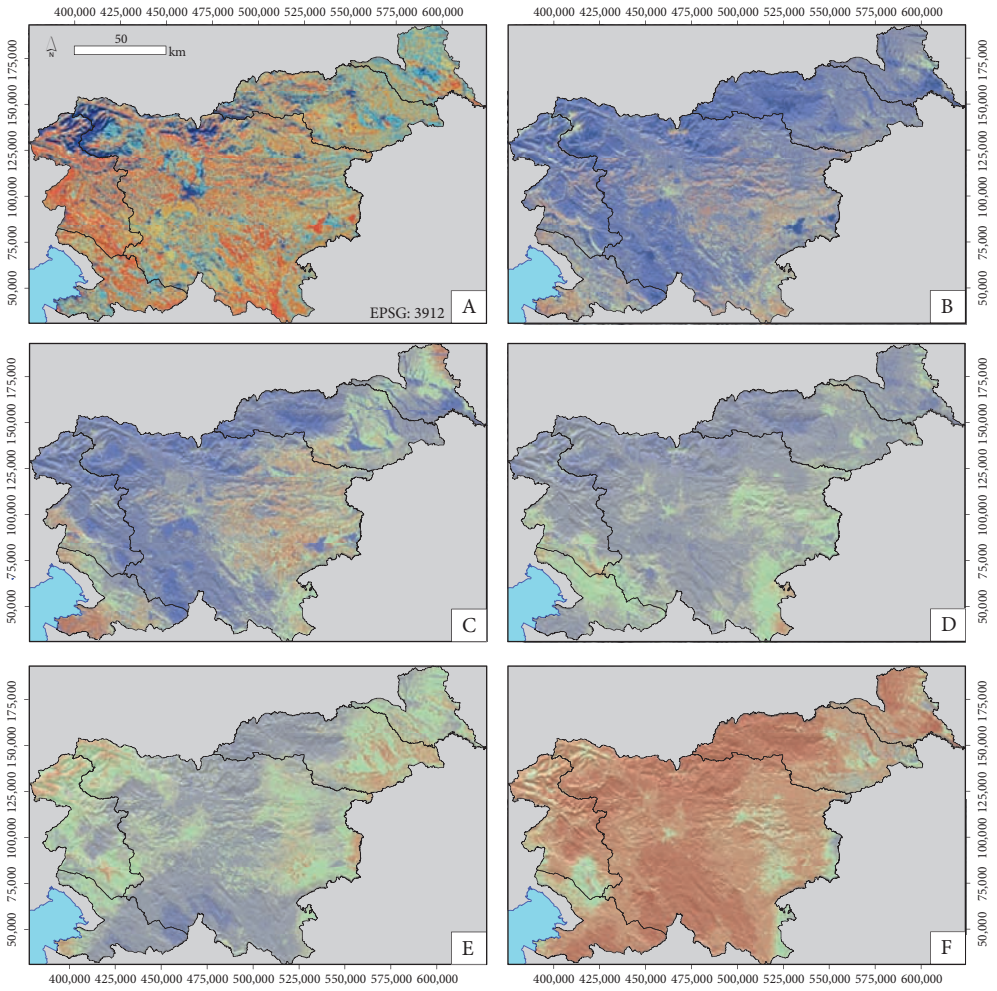
Region		Long-term average 1991–2020	Deviation 1972–1980	Deviation 1981–1990	Deviation 1991–2000	Deviation 2001–2010	Deviation 2011–2020
Slovenia	P	1455	+33	–24	–17	–10	+27
	ET	712	–38	–21	–14	–7	+21
	Q	741	+71	–2	+2	–10	+8
(1) Mura river basin (Pomurje)	P	827	–19	–7	+10	–21	+10
	ET	693	–42	–18	–18	–2	+20
	Q	132	+21	+14	+30	–25	–5
(2) Drava river basin (Podravje)	P	1130	+1	+3	+10	–5	–5
	ET	688	–50	–24	–17	–5	+21
	Q	441	+49	+31	+31	–8	–23
(3) Soča river basin (Posočje)	P	2222	+58	–47	–17	–53	+70
	ET	751	–45	–30	–14	–2	+16
	Q	1468	+104	–17	+2	–53	+51
(4) Adriatic river basin without Soča watershed (Obalne reke in Kras)	P	1491	+71	–57	–28	–12	+40
	ET	730	–19	–5	–7	–12	+20
	Q	759	+90	–55	–16	–6	+22
(5) Sava river basin (Posavje)	P	1463	+39	–24	–26	–2	+27
	ET	711	–36	–20	–13	–9	+22
	Q	750	+74	–3	–7	–1	+7

Figure 3: Observed long-term precipitation (P) patterns and interdecadal deviations in Slovenia from 1972 to 2020. The geographic coordinate system of the map of Slovenia is *MGI 1901 / Slovene National Grid (EPSG: 3912)*, axis labels show metres. ► p. 130

Figure 4: Modelled long-term evapotranspiration (ET) patterns and interdecadal deviations in Slovenia from 1972 to 2020. The geographic coordinate system of the map of Slovenia is *MGI 1901 / Slovene National Grid (EPSG: 3912)*, axis labels show metres. ► p. 131

Figure 5: Modelled long-term runoff (Q) patterns and interdecadal deviations in Slovenia from 1972 to 2020. The geographic coordinate system of the map of Slovenia is *MGI 1901 / Slovene National Grid (EPSG: 3912)*, axis labels show metres. ► p. 132


400,000 425,000 450,000 475,000 500,000 525,000 550,000 575,000 600,000
50,000 75,000 100,000 125,000 150,000 175,000
50
km
EPSG: 3912
A
B
C
D
E
F
Precipitation
< 900 mm/a
900–1000 mm/a
1000–1100 mm/a
1100–1200 mm/a
1200–1300 mm/a
1300–1400 mm/a
1400–1500 mm/a
1500–1600 mm/a
1600–1800 mm/a
1800–2000 mm/a
2000–2600 mm/a
2600–3000 mm/a
> 3000 mm/a
Deviation
Lower
> 100 mm/a
100–50 mm/a
50–25 mm/a
25–10 mm/a
< 10 mm/a
No deviation
Higher
< 10 mm/a
10–25 mm/a
25–50 mm/a
50–100 mm/a
> 100 mm/a
Long-term mean annual: (A) 1991–2020
Deviation : (B) 1972–1980 (C) 1981–1990
(D) 1991–2000 (E) 2001–2010 (F) 2011–2020
© Slovenian Environment Agency (ARSO, Slovenia)
and Forschungszentrum Jülich (Germany)



Evapotranspiration

- < 500 mm/a
- 500–550 mm/a
- 550–600 mm/a
- 600–650 mm/a
- 650–700 mm/a
- 700–750 mm/a
- 750–800 mm/a
- 800–850 mm/a
- > 850 mm/a

Deviation

Lower

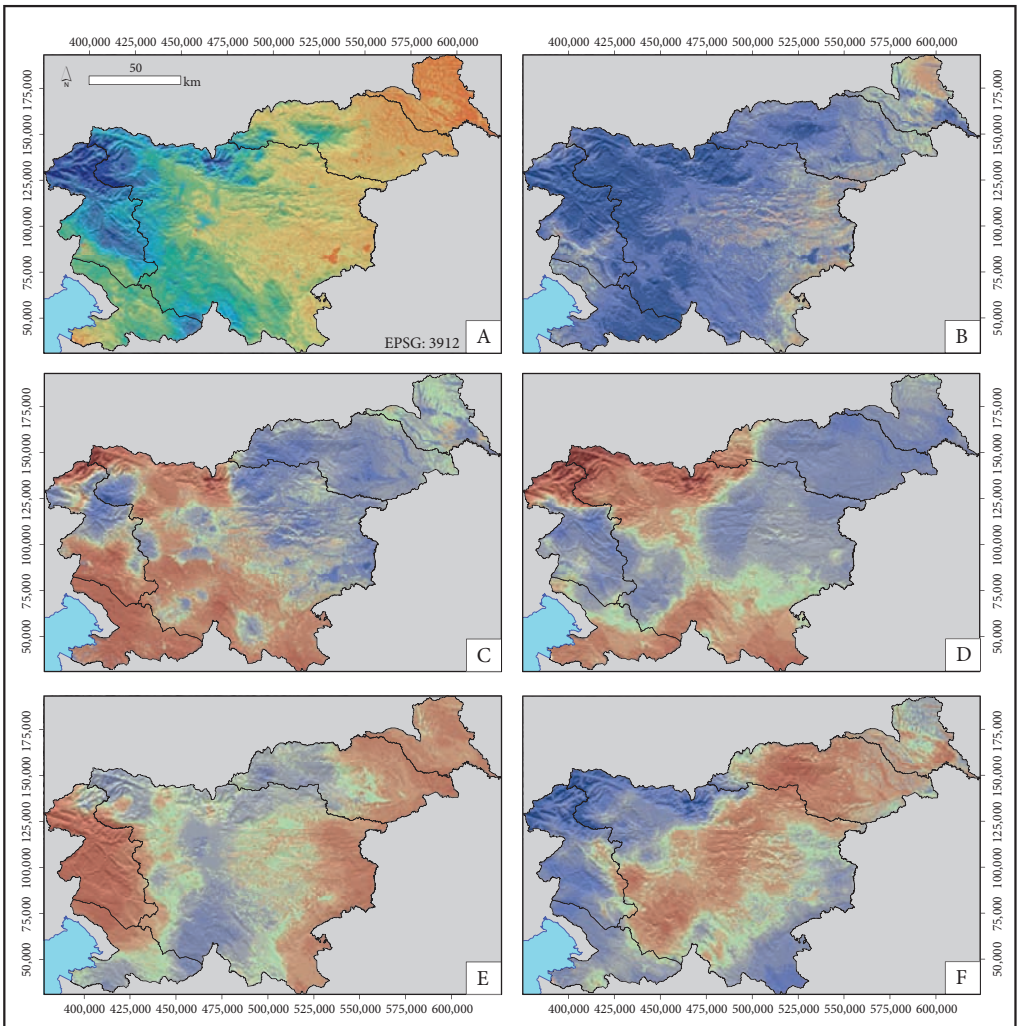
- > 100 mm/a
- 100–50 mm/a
- 50–25 mm/a
- 25–10 mm/a
- < 10 mm/a
- No deviation

Higher

- < 10 mm/a
- 10–25 mm/a
- 25–50 mm/a
- 50–100 mm/a
- > 100 mm/a

Long-term mean annual: (A) 1991–2020
Deviation : (B) 1972–1980 (C) 1981–1990
(D) 1991–2000 (E) 2001–2010 (F) 2011–2020

© Slovenian Environment Agency (ARSO, Slovenia)
and Forschungszentrum Jülich (Germany)



Long-term mean annual: (A) 1991–2020
Deviation : (B) 1972–1980 (C) 1981–1990
(D) 1991–2000 (E) 2001–2010 (F) 2011–2020

© Slovenian Environment Agency (ARSO, Slovenia)
and Forschungszentrum Jülich (Germany)

4.2 Temporal variability and trends in Slovenia's water balance

In Slovenia, months with unusually high P occur most frequently in September, October, and November (Figure 6), whereas months with below-average P are more common in winter. Annual P currently exhibits an upward trend (+87 mm). However, comparison of individual years with the trend line indicates that a small number of dry years could substantially weaken or even offset this trend. Monthly ET displays a pronounced seasonal cycle, with high values during summer when sufficient soil moisture is available and low values during winter. In response to global warming, annual ET totals show a relatively continuous upward trend that has intensified since year 2000 (+42 mm). The temporal behaviour of Q again reflects the superposition of P and ET. High winter P is transformed into high Q, in some cases delayed by temporary storage as snow, whereas low Q typically occurs during summer when ET is high. The current increase in annual P is largely compensated by rising ET, resulting in only a small net increase in Q (+42 mm).

Figures 7 to 11 show that general temporal patterns are similar across the five Slovenian hydrological regions, while trend magnitudes differ substantially. For example, Q in the alpine Soča River basin (area 3 in Figure 1) exhibits a clear increasing trend (Figure 9), whereas in strongly karstified areas near the Mediterranean coast (area 4 in Figure 1) virtually no substantial trend is detected (Figure 10). A more precise evaluation of the significance of identified changes and trends is provided by the two statistical tests.

Grid-based results of the MWW and MK tests (Figures 12 and 13) indicate that statistically significant changes and trends in water balance components occur with varying frequency across Slovenia's river basins and districts. The maps display probabilities of the alternative hypothesis for the MWW test (Figures 12A–12F) and for monotonic trends in the MK test (Figures 13B, 13D, 13F). High probabilities indicate changes or trends; probabilities above 0.85 denote high significance ($\alpha = 0.15$, commonly applied in geosciences). For the MK test, Kendall's Tau (Figures 13A, 13C, 13E) indicates trend direction, with positive values representing increases and negative values decreases.

Significant changes and trends in P are currently evident only in limited areas, mainly at higher altitudes in the Alps and Dinaric Alps. In contrast, significant changes and trends in ET are more widespread, although no high significance is reached in the southwest, the Adriatic region, and the southeast. Spatial patterns of ET further indicate that the influence of vegetation, groundwater depth, and topography varies regionally (e.g., Sava River basin in Figure 12D). Because variability in P and ET is superimposed in a complex manner at larger catchment scales, no significant change in the overall Q regime is detected at that level. However, at smaller spatial scales within river systems, significant local changes occur. Overall, ET has changed significantly across approximately half of Slovenia in recent decades. At the river-basin and district aggregation level shown in Figure 1, only changes in spatiotemporal ET patterns in the Drava and Sava basins reach significance at the $\alpha = 0.15$ level.

The simulation results (grid data) shown in Figures 3 to 11 can be downloaded for free (see Frantar and Herrmann 2026).

5 Evaluation of the runoff simulation

For Slovenia, the 76 catchments were identified as suitable for evaluating the simulated Q (Figure 14). The evaluation was conducted for two 30-year periods, 1981–2010 and 1991–2020. For almost all gauges, good to very good agreement between observed and simulated values is evident, as most points are located close to the 1:1 line or at least within a maximum deviation of 30%. Individual deviations are difficult to explain in detail. Overall, they reflect a combination of uncertainties related to the evaluation methodology and the inherent uncertainties of the mGROWA model setup.

For the period 1981–2010, the NSE and PBIAS values are 0.86 and +10.5%, respectively, indicating very good overall model performance, but also a slight underestimation of Q. In the period 1991–2020, the NSE and PBIAS values are 0.74 and +15.4%, respectively, which can still be considered a good overall model performance. The underestimation is somewhat more pronounced in this period.

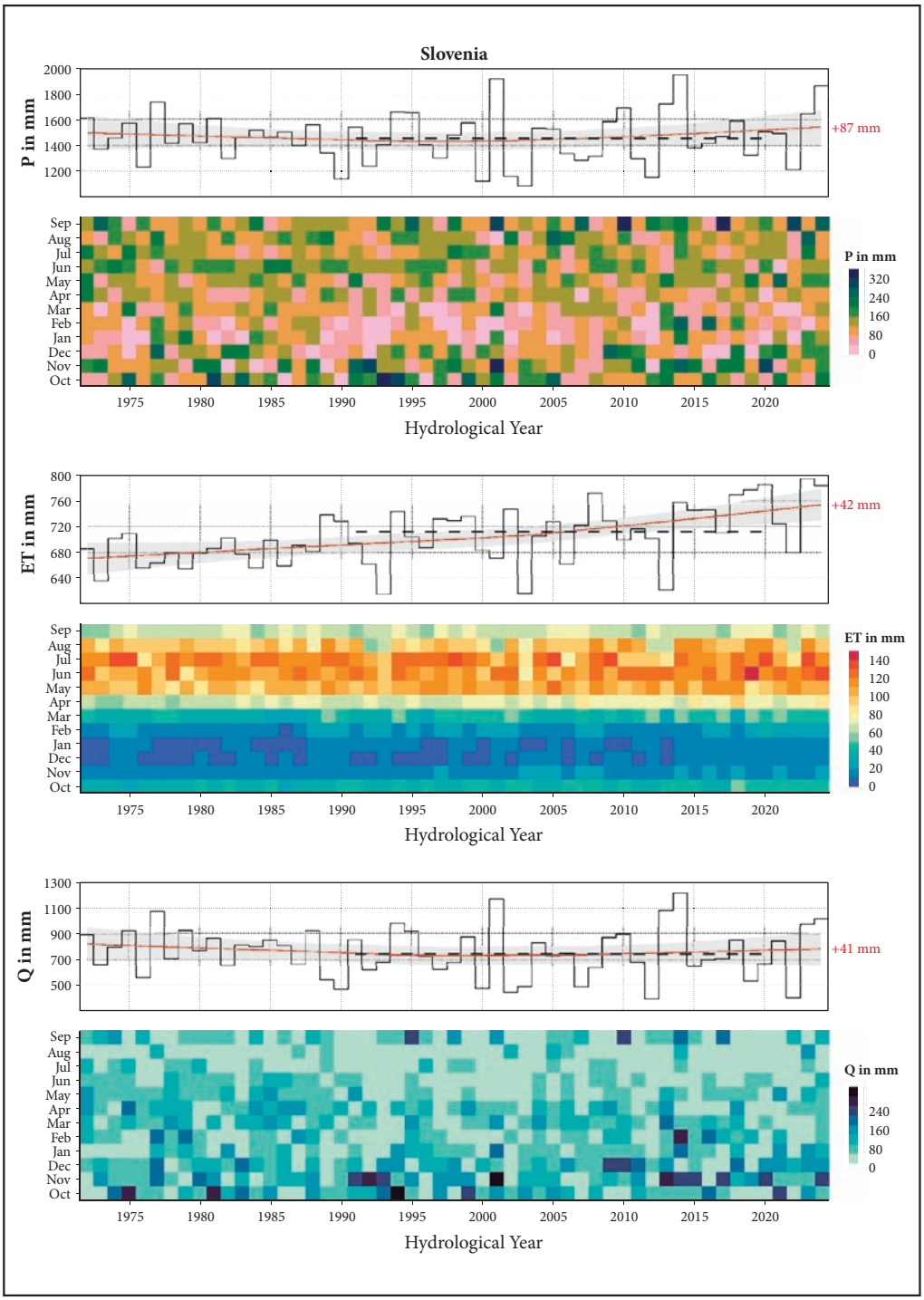


Figure 6: Time series of annual and monthly precipitation (P, top), evapotranspiration (ET, middle) and runoff (Q, bottom) in Slovenia from 1972 to 2024. LOESS-42 trend lines in red, 30-year average 1991–2020 dashed in black, 95%-confidence limits as grey band.

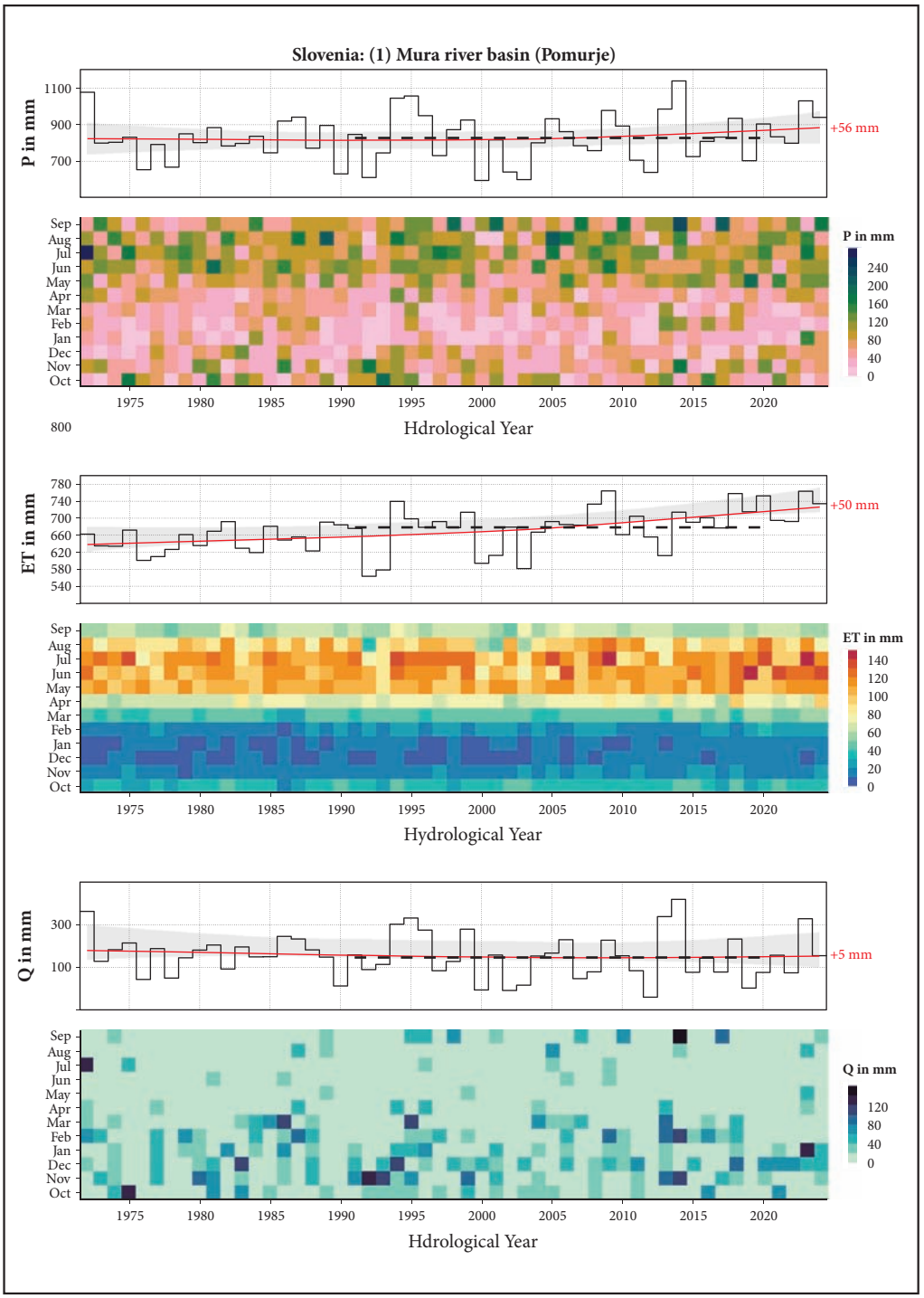


Figure 7: Time series of annual and monthly precipitation (P, top), evapotranspiration (ET, middle) and runoff (Q, bottom) in (1) Mura river basin (Pomurje) from 1972 to 2024. LOESS-42 trend lines in red, 30-year average 1991–2020 dashed in black, 95%-confidence limits as grey band.

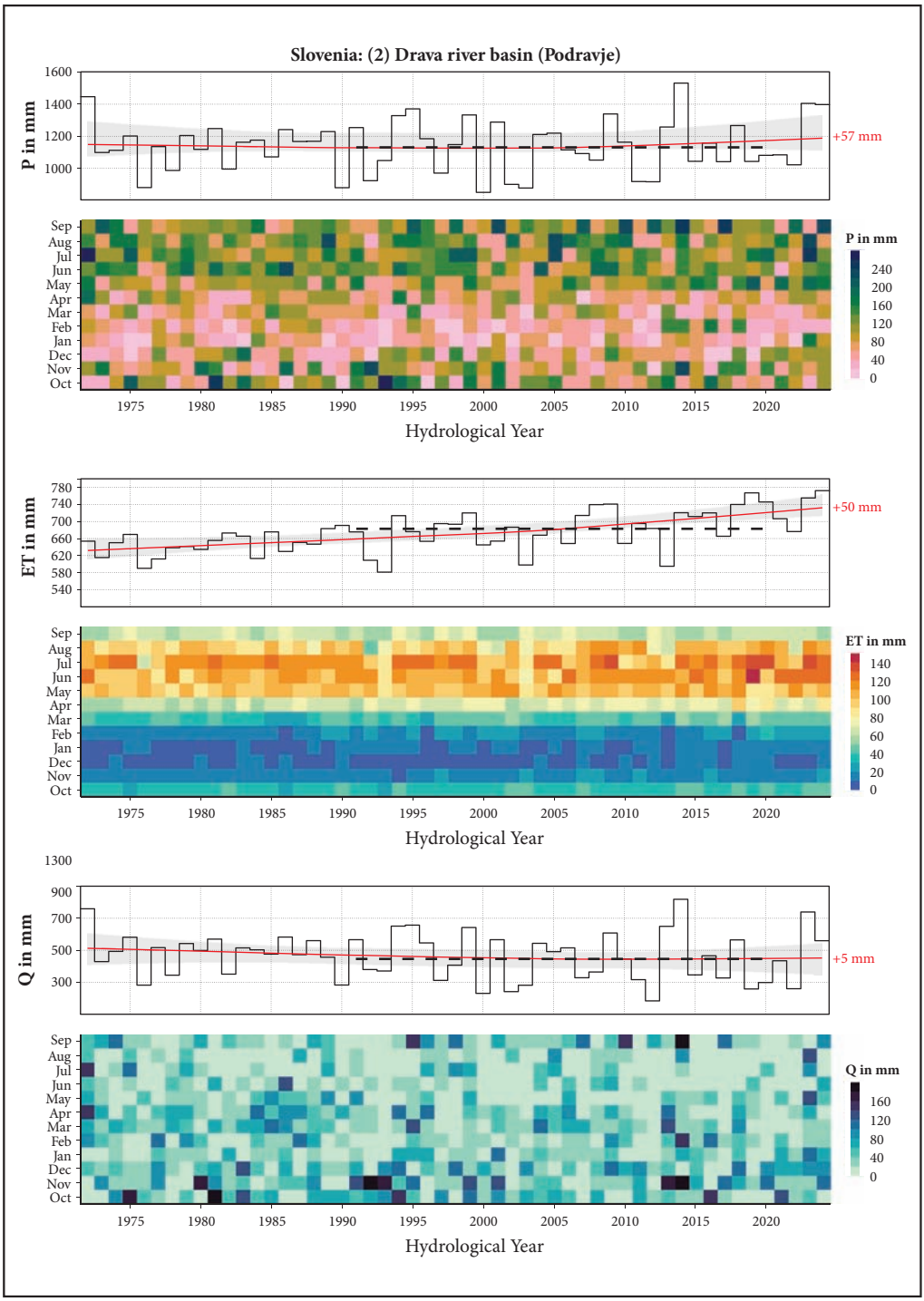


Figure 8: Time series of annual and monthly precipitation (P, top), evapotranspiration (ET, middle) and runoff (Q, bottom) in (2) Drava river basin (Podravje) from 1972 to 2024. LOESS-42 trend lines in red, 30-year average 1991–2020 dashed in black, 95%-confidence limits as grey band.

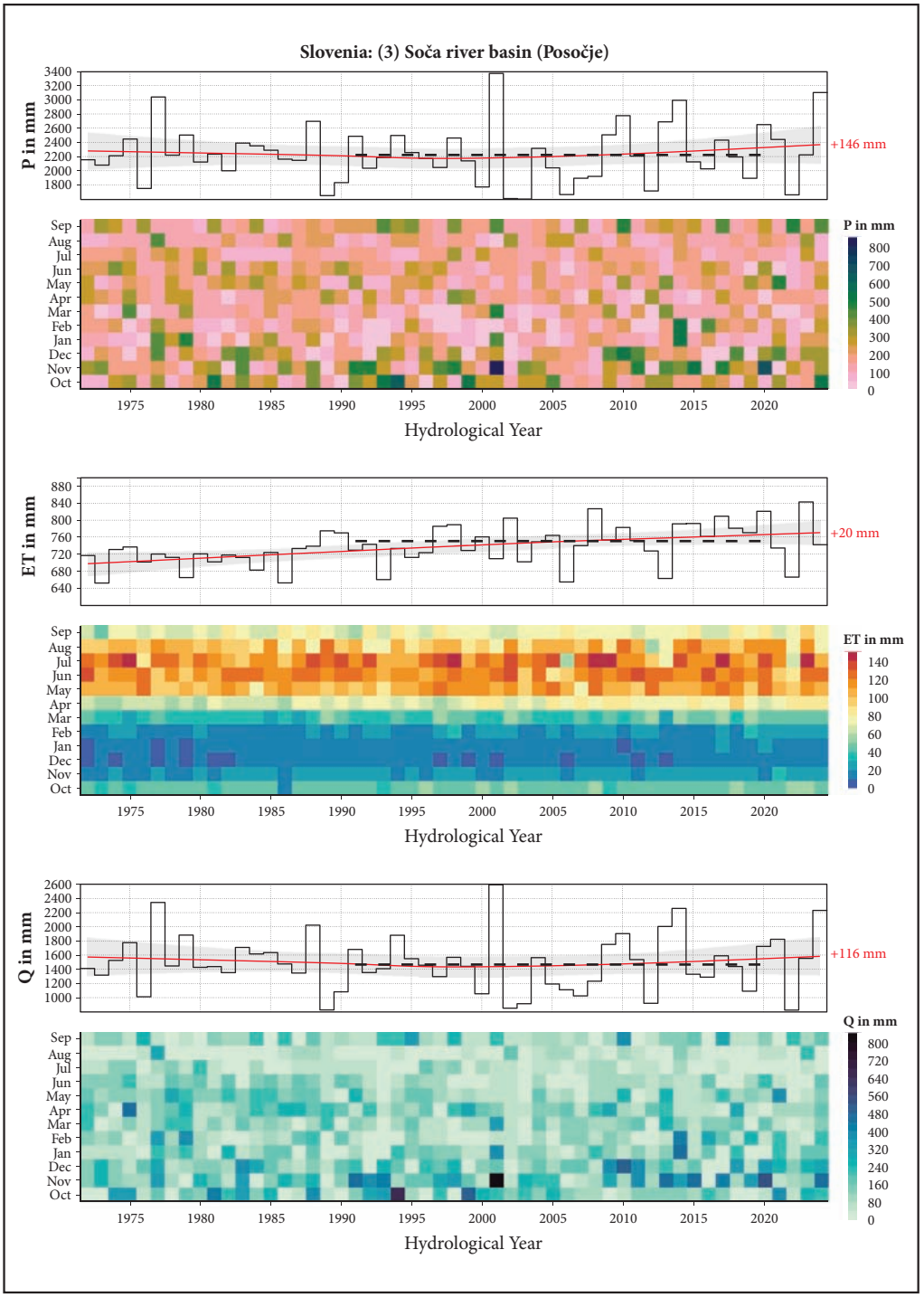


Figure 9: Time series of annual and monthly precipitation (P, top), evapotranspiration (ET, middle) and runoff (Q, bottom) in (3) Soča river basin (Posočje) from 1972 to 2024. LOESS-42 trend lines in red, 30-year average 1991–2020 dashed in black, 95%-confidence limits as grey band.

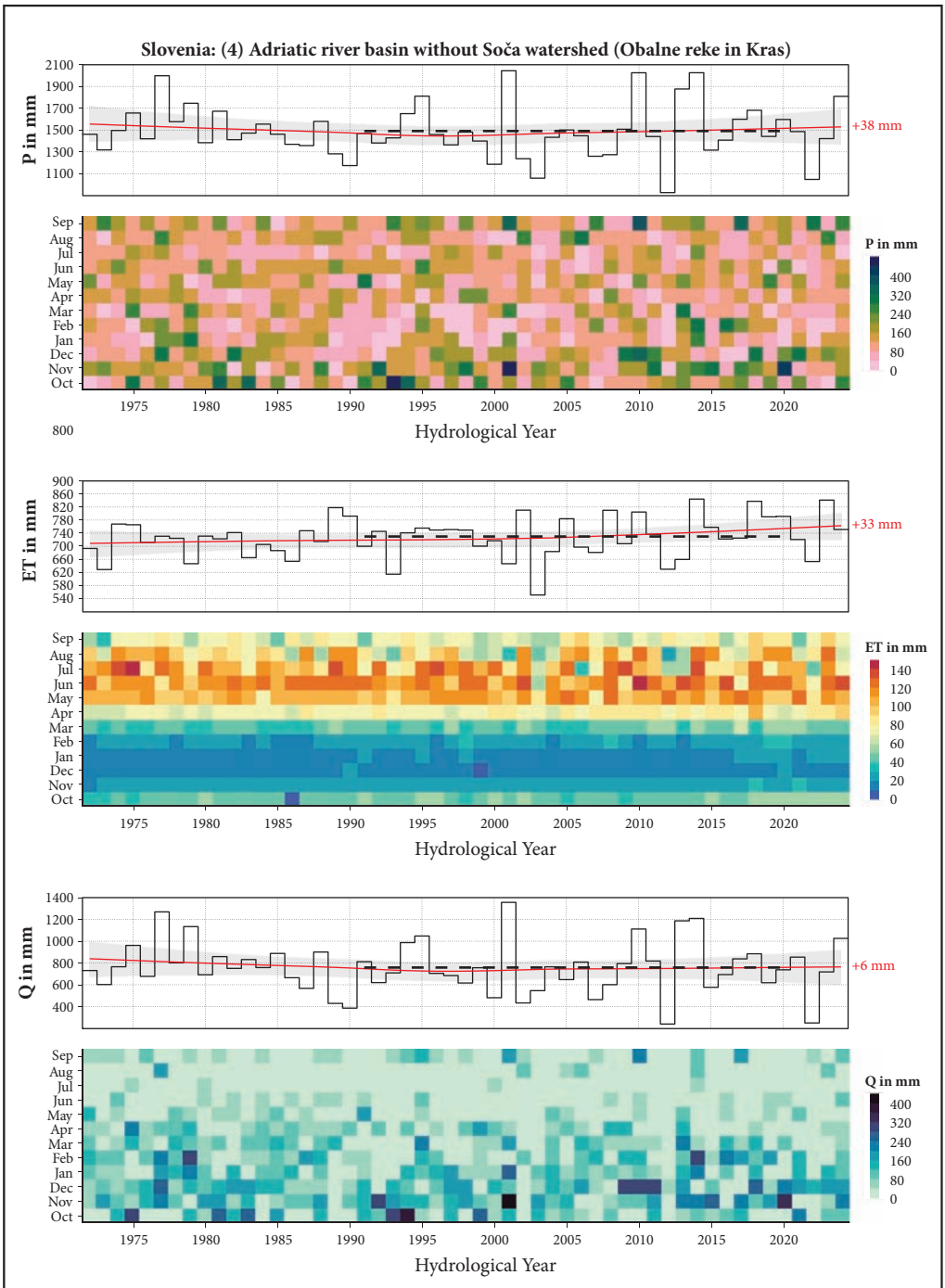


Figure 10: Time series of annual and monthly precipitation (P, top), evapotranspiration (ET, middle) and runoff (Q, bottom) in (4) Adriatic river basin without Soča watershed (Obalne reke in Kras) from 1972 to 2024. LOESS-42 trend lines in red, 30-year average 1991–2020 dashed in black, 95%-confidence limits as grey band.

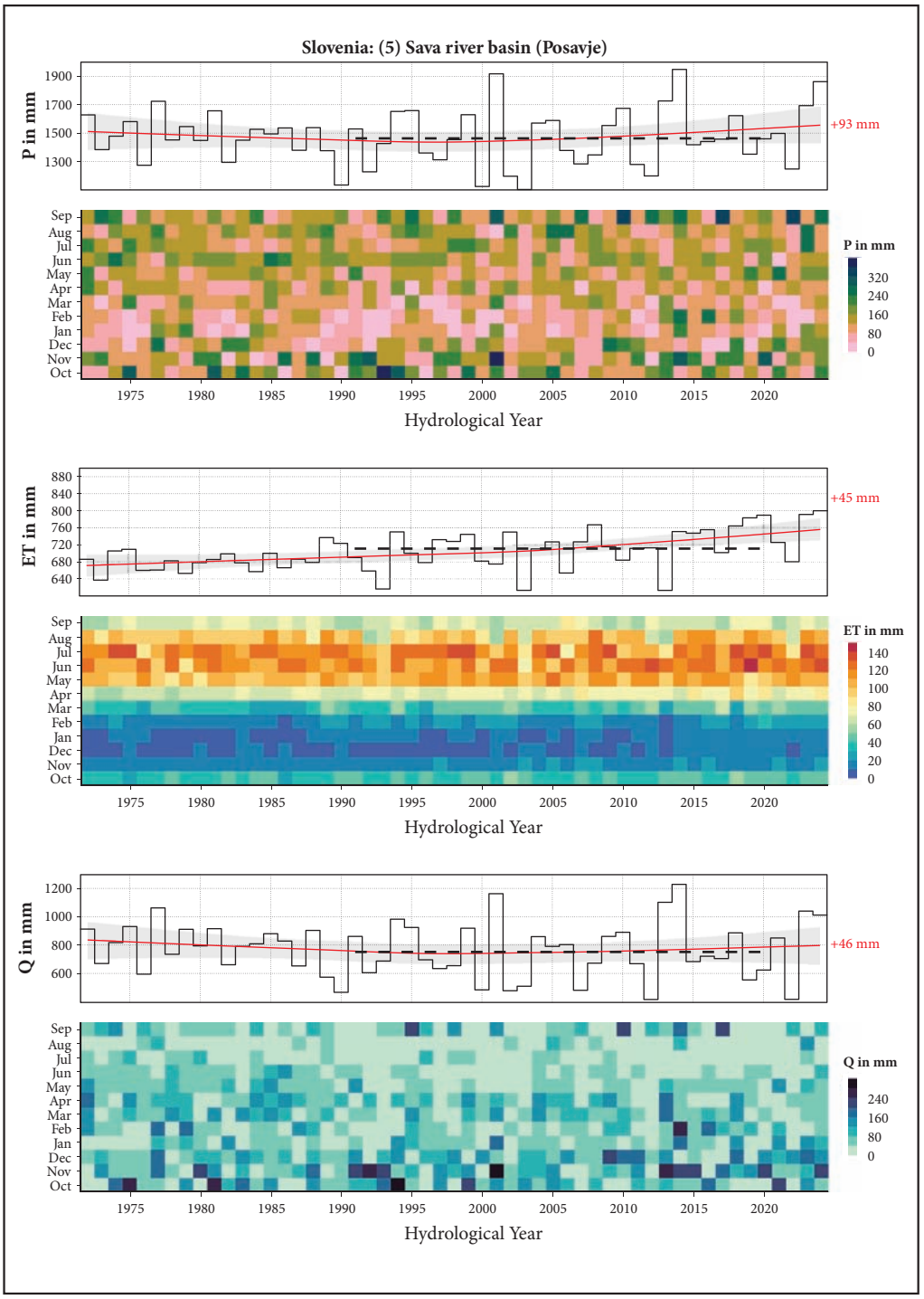


Figure 11: Time series of annual and monthly precipitation (P, top), evapotranspiration (ET, middle) and runoff (Q, bottom) in (5) Sava river basin (Posavje) from 1972 to 2024. LOESS-42 trend lines in red, 30-year average 1991–2020 dashed in black, 95%-confidence limits as grey band.

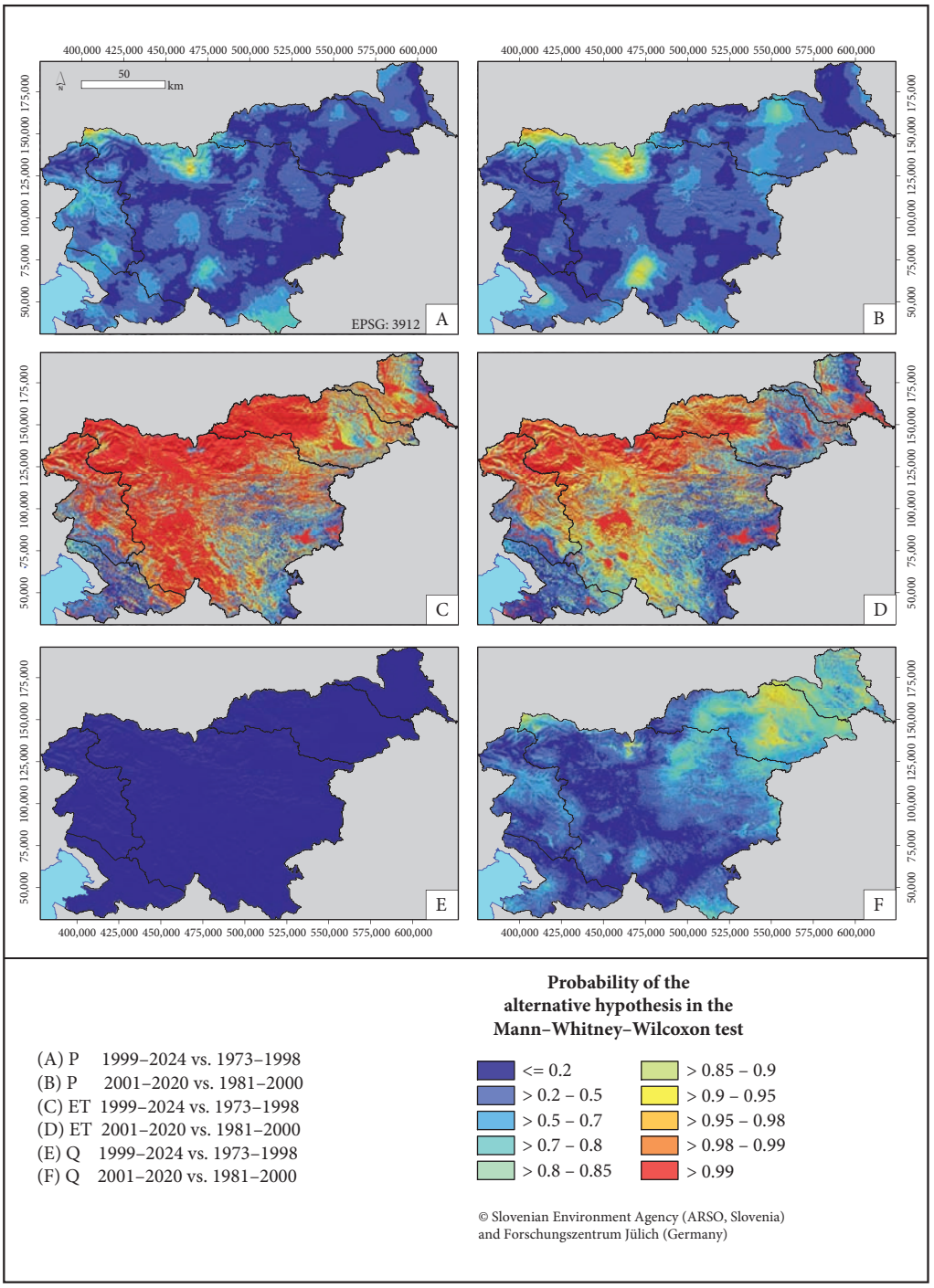


Figure 12: Grid-based probability of the alternative hypothesis in the Mann–Whitney–Wilcoxon test for the two sets of time spans and modelled long-term precipitation (P), evapotranspiration (ET) and runoff (Q). The geographic coordinate system of the map of Slovenia is *MGI 1901 / Slovene National Grid (EPSG: 3912)*, axis labels show metres.

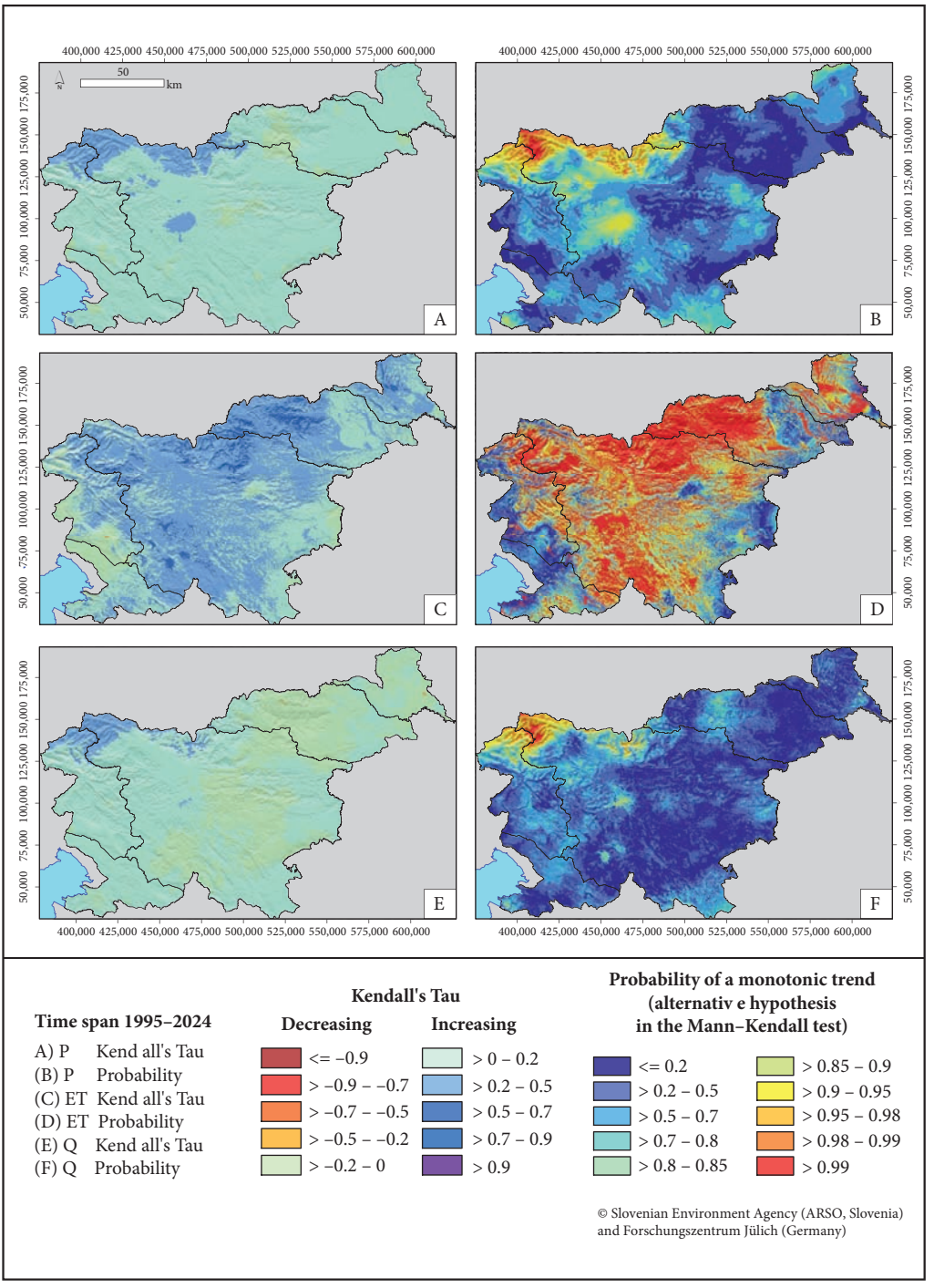


Figure 13: Grid-based probability of a monotonic trend (alternative hypothesis in the Mann–Kendall test) and Kendall's Tau for the time span 1995-2024 and modelled long-term precipitation (P), evapotranspiration (ET) and runoff (Q). The geographic coordinate system of the map of Slovenia is *MGI 1901 / Slovene National Grid (EPSG: 3912)*, axis labels show metres.

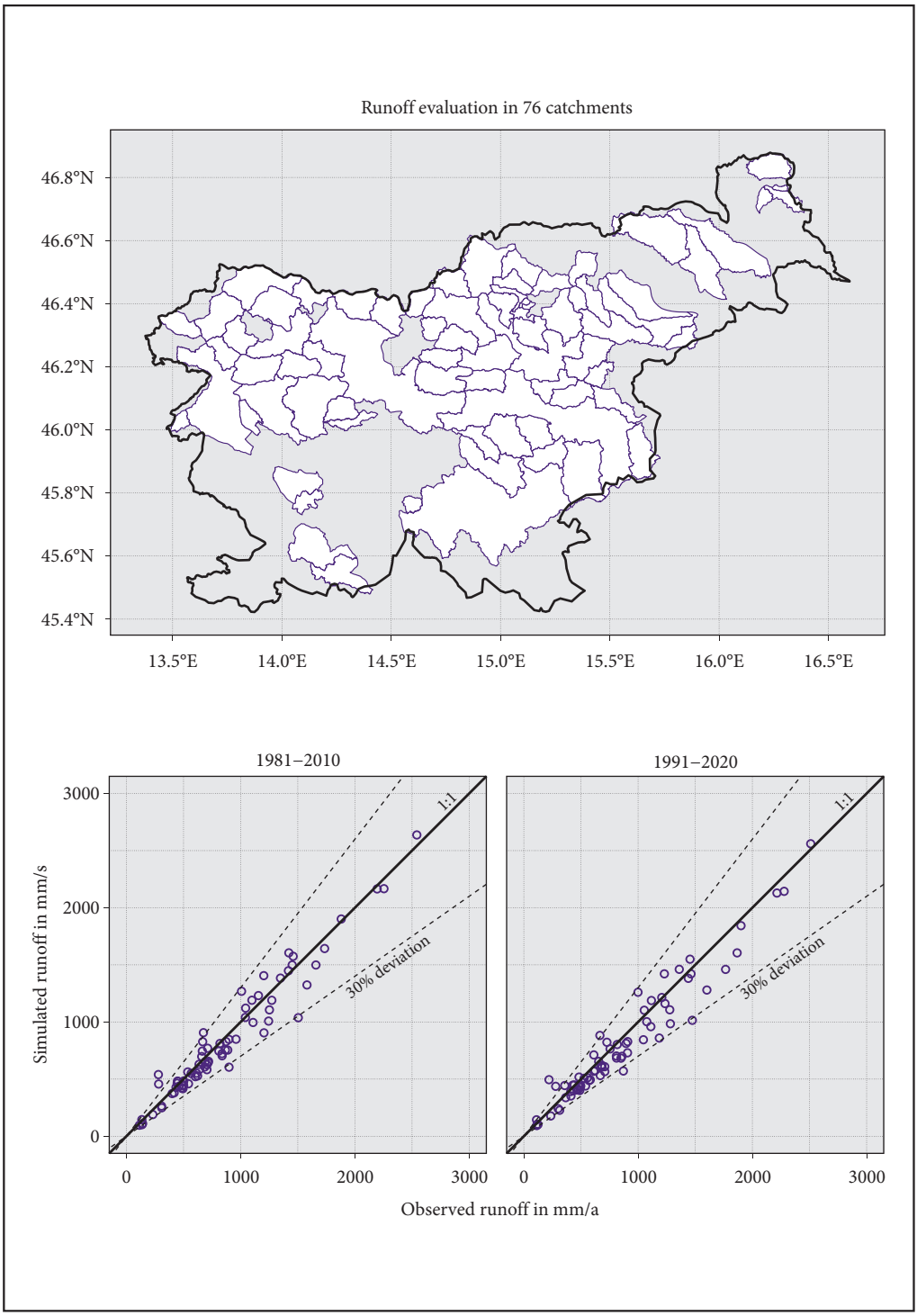


Figure 14: Simulated versus observed Q in Slovenia in 76 reference catchments and the two periods 1981–2010 and 1991–2020.

6 Discussion and implementation

The mGROWA simulation presented in this study is based on a temporally constant spatial distribution of parameters that represent the influence of land use, terrain, vegetation, and soil properties on evapotranspiration and runoff formation. Consequently, the effects of climate variability and change between 1972 and 2024 on the present land-surface state in Slovenia are examined. For example, land use changes and other human interventions were not reconstructed, and their potential impacts on the water balance were therefore not assessed. However, the mGROWA model would be technically capable of performing such analyses if suitable input data were available.

In the evaluation chapter, a slight underestimation of Q was identified. One important reason for this tendency is the use of uncorrected distributions of P. Point measurements of P and spatial interpolation are subject to bias. However, it is very difficult to determine the exact influence on the overall simulation bias. Moreover, correcting individual variables may obscure underlying uncertainties. This is illustrated by the fact that the magnitude of bias differs between the two evaluation periods, despite their 20-year overlap. A bias correction of P would not eliminate this discrepancy because it would have a consistent effect on the entire simulated period. Presumably, there is another relevant influence on the overall bias due to the methodology behind the calculation of ET. The parameters used in the simulation were set constant over time. The upward trend in ET levels (Figure 6), particularly since about 2005, supports this interpretation. From a modelling perspective we can conclude that this phenomenon must be further observed and further scientific efforts must be made to improve the parameterisation of the model.

The results chapter demonstrates pronounced spatial and temporal variability, as well as trends and changes in P, ET, and Q across Slovenia. The emerging picture is complex and reflects the superposition of regional climate variability with site-specific characteristics. Similar ranges of positive and negative, as well as significant and insignificant, changes in discharge have been reported for Slovenian rivers by Oblak et al. (2021). Based on observed changes, Stojilković and Brečko Grubar (2024) proposed a modern typology of discharge regimes in Slovenia. ETo represents a key driver of variability and change and forms the basis for ET calculation in mGROWA. Spatially variable ETo trends related to global warming were reported for Slovenia by Maček et al. (2018) and are also reflected in our reconstructed ET patterns. Comparable climate-related impacts on discharge regimes have been reported for Croatia (Čanjevac and Orešić 2018). In Austria, the COSERO model, which is conceptually similar to mGROWA, has recently been established (Zeitfogel et al. 2025), although detailed trend analyses based on this model are not yet available.

All of these studies highlight the need for continuous observation and evaluation of trends and changes. Importantly, the objective of this study was not to prove climate-change impacts on Slovenia's water balance, but to provide a data basis that supports water-resources management in identifying relevant long- and mid-term changes. Such changes do not necessarily require statistically significant trends in individual climate variables. Nevertheless, analysis of the LOESS-42 trend line and its 95% confidence limits provides a robust framework for assessing recent climatic variability and trends. The overlap of the 95%-confidence limits and the 30-year mean can be interpreted as an early indication of emerging change in one of the components under investigation.

With the implementation of mGROWA as a national water balance model, Slovenian water-resources management and other stakeholders will benefit from state-of-the-art, model-based assessments. The simulation will be continued at the Slovenian Environment Agency (ARSO), providing a long-term data basis for research and operational applications that extend beyond the scope of this study. The comprehensive data basis is already being used for various purposes, for example for reporting by the Slovenian government under the EU Water Framework Directive, for identifying regions with water stress, supporting policy decisions and allocation of water rights, for regional and local water-resources assessments, defining boundary conditions for groundwater models, assessing ecosystem services (Bogataj and Frantar 2025), and analysing drought severity. Finally, the mGROWA-based annual hydro-climatological trend indicator is intended to serve as essential contribution to a national Slovenian Water Resources and Drought Monitor.

7 Conclusion

The results of the mGROWA simulation for the period 1972–2024 provide a comprehensive data basis that contributes to an improved understanding of the spatio-temporal variability of water balance components in Slovenia under ongoing climate change. Statistical analyses demonstrate a significant increase in evapotranspiration over large parts of the country. However, due to above-average precipitation in recent years, this increase has not yet translated into a country-wide decline in mean runoff. The proposed hydroclimatological trend indicator has proven to be a useful tool and represents a promising future element for monitoring changes in water balance components in Slovenia.

From a scientific perspective, the existing simulation results also enable analyses of the influence of meteorological drought on the severity of hydrological drought. Shifts and changes in this relationship are expected in the future. Moreover, the current mGROWA setup can serve as a basis for comprehensive climate-impact studies, for example by linking outputs from Regional Climate Models (RCMs) or Shared Socioeconomic Pathways (SSPs) to mGROWA. This will allow the assessment of projected future water balance components and facilitate systematic comparisons with the current state of knowledge.

Finally, further improvements in the underlying data basis and in the mGROWA methodology itself are expected to reduce remaining uncertainties. Nevertheless, with regard to retrospective analyses, such improvements are not expected to lead to fundamentally different conclusions about the impact of climate change on the national-scale water balance in Slovenia.

ACKNOWLEDGEMENT: We would like to thank Jože Uhan, Mojca Dolinar, Joško Knez and Frank Wendland for organising the funding for the implementation of the mGROWA model in Slovenia as part of the established research collaboration between the Slovenian Environment Agency (ARSO) and Forschungszentrum Jülich (Germany).

RESEARCH DATA: For information on the availability of research data related to the study, please visit the article webpage: https://doi.org/10.3986/AGS.14632.

8 References

Allen, R. G., Pereira, L. S., Raes, D., Smith, M. 1998: Crop evapotranspiration – Guidelines for computing crop water requirements. FAO Irrigation and drainage paper 56. FAO – Food and Agriculture Organization of the United Nations.

Andjelov, M., Mikulič, Z., Tetzlaff, B., Uhan, J., Wendland, F. 2016: Groundwater recharge in Slovenia: Results of a bilateral German-Slovenian Research project. Forschungszentrum Jülich GmbH.

Bevacqua, E., Rakovec, O., Schumacher, D. L., Kumar, R., Thober, S., Samaniego, L., Seneviratne, S. I., Zscheischler, J. 2024: Direct and lagged climate change effects intensified the 2022 European drought. Nature *Geoscience* 17-11. https://doi.org/10.1038/s41561-024-01559-2

Bogataj, N., Frantar, P. 2025: Groundwater recharge as a basis for the assessment of ecosystem services on common land: The case of the Primorska region in Slovenia. *Acta geographica Slovenica* 65-3. https://doi.org/10.3986/AGS.14319

Čanjevac, I., Orešić, D. 2018: Changes in discharge regimes of rivers in Croatia. *Acta geographica Slovenica* 58-2. https://doi.org/10.3986/AGS.2004

Disse, M. 1995: Modellierung der Verdunstung und der Grundwasserneubildung in ebenen Einzugsgebieten. Fakultät für Bauingenieur- und Vermessungswesen der Universität Fridericiana zu Karlsruhe (TH).

Dolinar, M. 2009: Prostorska interpolacija mesečnih padavin (metodologija). *Internal report*. Ministrstvo za okolje in prostor, Agencija Republike Slovenije za okolje.

Ehlers, L., Herrmann, F., Blaschek, M., Duttmann, R., Wendland, F. 2016: Sensitivity of mGROWA-simulated groundwater recharge to changes in soil and land use parameters in a Mediterranean environment and conclusions in view of ensemble-based climate impact simulations. *Science of The Total Environment* 543, Part B. https://doi.org/10.1016/j.scitotenv.2015.04.122

Engel, N., Müller, U., Schäfer, W. 2012: BOWAB – Ein Mehrschicht-Bodenwasserhaushaltsmodell. In: Klimawandel und Bodenwasserhaushalt. *GeoBerichte* 20. Landesamt für Bergbau, Energie und Geologie. https://doi.org/10.48476/geober_20_2012

Ertl, G., Herrmann, F., Elbracht, J. 2022: Bestimmung der Grundwasserneubildungshöhen für Festgesteinsgebiete in Niedersachsen. Grundwasser 27. https://doi.org/10.1007/s00767-021-00503-0

Ertl, G., Herrmann, F., Schlinsog, T., Elbracht, J. 2018: Auswirkungen von Klimaänderungen auf die Grundwasserneubildung in Niedersachsen. *Wasser und Abfall* 20-9. https://doi.org/10.1007/s35152-018-0097-1

European Commission 2015: Guidance document on the application of water balances for supporting the implementation of the WFD – Final – Version 6.1 – 18/05/2015. *Technical report*. Publications Office. https://doi.org/10.2779/352735

Festgesteinsgebiete in Niedersachsen. *Grundwasser* 27. https://doi.org/10.1007/s00767-021-00503-0

Frantar, P. 2007: Geographical overview of water balance of Slovenia 1971–2000 by main river basins. *Acta geographica Slovenica* 47-1. https://doi.org/10.3986/AGS47102

Frantar, P. 2008 (ed.): Vodna bilanca Slovenije 1971–2000. Water balance of Slovenia 1971–2000. Ministrstvo za okolje in prostor, Agencija Republike Slovenije za okolje.

Frantar, P., Herrmann, F. 2026: National-scale water balance in Slovenia (1972–2024): Long-term trends and variability in water balance components. *Dataset*. Jülich DATA. https://doi.org/10.26165/JUELICH-DATA/UKYJHY

Gupta, H. V., Sorooshian, S., Yapo, O. P. 1999: Status of automatic calibration for hydrologic models: Comparison with multilevel expert calibration. *Journal of Hydraulic Engineering* 4-2. https://doi.org/10.1061/(ASCE)1084-0699(1999)4:2(135)

Helsel, D. R., Hirsch, R. M. 1992: Statistical methods in water resources. Elsevier.

Herrmann, F., Chen, S., Heidt, L., Elbracht, J., Engel, N., Kunkel, R., Müller, U. et al. 2013: Zeitlich und räumlich hochaufgelöste flächendifferenzierte Simulation des Landschaftswasserhaushalts in Niedersachsen mit dem Model mGROWA. *Hydrologie und Wasserbewirtschaftung* 57-5. https://doi.org/10.5675/HyWa_2013,5_2

Herrmann, F., Hübsch, L., Elbracht, J., Engel, N., Keller, L., Kunkel, R., Müller, U. et al. 2017: Mögliche Auswirkungen von Klimaänderungen auf die Grundwasserneubildung in Niedersachsen. *Hydrologie und Wasserbewirtschaftung* 61-4. https://doi.org/10.5675/HyWa_2017,4_3

Herrmann, F., Keller, L., Kunkel, R., Vereecken, H., Wendland, F. 2015: Determination of spatially differentiated water balance components including groundwater recharge on the Federal State level – A case study using the mGROWA model in North Rhine-Westphalia (Germany). *Journal of Hydrology: Regional Studies* 4, Part B. https://doi.org/10.1016/j.ejrh.2015.06.018

Herrmann, F., Keuler, K., Wolters, T., Bergmann, S., Eisele, M., Wendland, F. 2021: Mit der Modellkette RCP-GCM-RCM-mGROWA projizierte Grundwasserneubildung als Datenbasis für zukünftiges Grundwassermanagement in Nordrhein-Westfalen. *Grundwasser* 26. https://doi.org/10.1007/s00767-020-00471-x

Hiederer, R. 2013: Mapping soil properties for Europe – spatial representation of soil database attributes. *Technical report*. Publications Office of the European Union. https://doi.org/10.2788/94128

Huntington, T. G. 2006: Evidence for intensification of the global water cycle: Review and synthesis. *Journal of Hydrology* 319-1,4. https://doi.org/10.1016/j.jhydrol.2005.07.003

Intergovernmental Panel on Climate Change (IPCC) 2023: Summary for policymakers. Climate change 2021 – the physical science basis: Working Group I contribution to the sixth assessment report of the Intergovernmental Panel on Climate Change. Cambridge University Press. https://doi.org/10.1017/9781009157896.001

Kendall, M. G. 1938: A new measure of rank correlation. *Biometrika* 30-1,2. https://doi.org/10.1093/biomet/30.1-2.81

Kolbezen, M., Pristov, J. 1998: Površinski vodotoki in vodna bilanca Slovenije. Surface watercourses and water balance of Slovenia. Ministrstvo za okolje in prostor, Hidrometeorološki zavod Republike Slovenije. http://hmljn.arso.gov.si/vode/publikacije%20in%20poro%C4%8Dila/bilanca6190_2_BESEDILO.pdf

Maček, U., Bezak, N., Šraj, M. 2018: Reference evapotranspiration changes in Slovenia, Europe. *Agricultural and Forest Meteorology* 260–261. https://doi.org/10.1016/j.agrformet.2018.06.014

Mann, H. B. 1945: Nonparametric tests against trend. *Econometrica* 13-3. https://doi.org/10.2307/1907187

Mann, H. B., Whitney, D. R. 1947: On a test of whether one of two random variables is stochastically larger than the other. *The Annals of Mathematical Statistics* 18-1. https://doi.org/10.1214/aoms/1177730491

Matheron, G. 1963: Principles of geostatistics. *Economic Geology* 58-8. https://doi.org/10.2113/gsecongeo.58.8.1246

Mauget, S. A. 2003: Multidecadal regime shifts in U.S. streamflow, precipitation, and temperature at the end of the twentieth century. *Journal of Climate* 16-23. https://doi.org/10.1175/1520-0442(2003)016<3905:Mrsius>2.0.Co;2

McNamara, I., Flörke, M., Uschan, T., Baez-Villanueva, O. M., Herrmann, F. 2024: Estimates of irrigation requirements throughout Germany under varying climatic conditions. *Agricultural Water Management* 291. https://doi.org/10.1016/j.agwat.2023.108641

Milly, P. C., Betancourt, J., Falkenmark, M., Hirsch, R. M., Kundzewicz, Z. W., Lettenmaier, D. P., Stouffer, R. J. 2008: Stationarity is dead: Whither water management? *Science* 319-5863. https://doi.org/10.1126/science.1151915

Moriasi, D. N., Arnold, J. G., Liew, M. W. V., Bingner, R. L., Harmel, R. D., Veith, T. L. 2007: Model evaluation guidelines for systematic quantification of accuracy in watershed simulations. *Transactions of the ASABE* 50-3. https://doi.org/10.13031/2013.23153

Nash, J. E., Sutcliffe, J. V. 1970: River flow forecasting through conceptual models: Part I – A discussion of principles. *Journal of Hydrology* 10-3. https://doi.org/10.1016/0022-1694(70)90255-6

Oblak, J., Kobold, M., Šraj, M. 2021: The influence of climate change on discharge fluctuations in Slovenian rivers. *Acta geographica Slovenica* 61-2. https://doi.org/10.3986/AGS.9942

Pfeifer, S., Bülow, K., Gobiet, A., Hänsler, A., Mudelsee, M., Otto, J., Rechid, D. et al. 2015: Robustness of ensemble climate projections analyzed with climate signal maps: Seasonal and extreme precipitation for Germany. *Atmosphere* 6-5. https://doi.org/10.3390/atmos6050677

Scherrer, S. C., de Valk, C., Begert, M., Gubler, S., Kotlarski, S., Croci-Maspoli, M. 2024: Estimating trends and the current climate mean in a changing climate. *Climate Services* 33. https://doi.org/10.1016/j.cliser.2023.100428

Schulla, J. 1997: Hydrologische Modellierung von Flussgebieten zur Abschätzung der Folgen von Klimaänderungen. *Ph.D. thesis*. Züricher Geographische Schriften. Verlag Geographisches Institut ETH Zürich. https://doi.org/10.3929/ethz-a-001763261

Stojilković, B., Brečko Grubar, V. 2024: Discharge regimes of Slovenian rivers: 1991–2020. *Acta geographica Slovenica* 64-3. https://doi.org/10.3986/AGS.13654

Strandhagen, E., Marcus, W. A., Meacham, J. E. 2006: Views of the rivers: Representing streamflow of the Greater Yellowstone ecosystem. *Cartographic Perspectives* 55. https://doi.org/10.14714/CP55.328

Tetzlaff, B., Andjelov, M., Kuhr, P., Uhan, J., Wendland, F. 2015: Model-based assessment of groundwater recharge in Slovenia. *Environmental Earth Sciences* 74-7. https://doi.org/10.1007/s12665-015-4639-5

Tetzlaff, B., Kuhr, P., Vereecken, H., Wendland, F. 2009: Aerial photograph-based delineation of artificially drained areas as a basis for water balance and phosphorus modelling in large river basins. *Physics and Chemistry of the Earth, Parts A/B/C* 34-8,9. https://doi.org/10.1016/j.pce.2009.02.002

van Genuchten, M. T. 1980: A closed-form equation for predicting the hydraulic conductivity of unsaturated soils. *Soil Science Society of America Journal* 44-5. https://doi.org/10.2136/sssaj1980.03615995004400050002x

Wilcoxon, F. 1945: Individual comparisons by ranking methods. *Biometrics Bulletin* 1-6. https://doi.org/10.2307/3001968

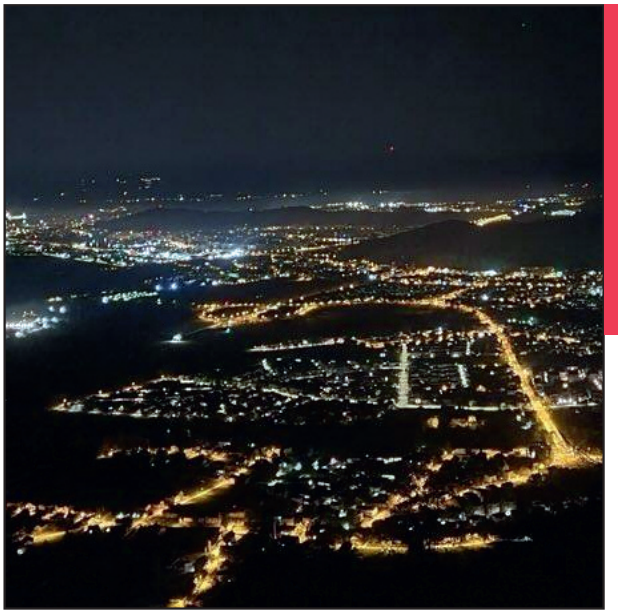
Xiong, J., Xu, L., Chandanpurkar, H. A., Famiglietti, J. S., Zhang, C., Ghiggi, G., Guo, S. et al. 2023: ET-WB: water-balance-based estimations of terrestrial evaporation over global land and major global basins. *Earth System Science Data* 15-10. https://doi.org/10.5194/essd-15-4571-2023

Zeitfogel, H., Herrnegger, M., Schulz, K. 2025: Regional-scale assessment of groundwater recharge and the water balance for Austria. *Journal of Hydrology: Regional Studies* 59. https://doi.org/10.1016/j.ejrh.2025.102297

Acta geographica Slovenica, 66-1, 2026, 147–177

SATELLITE-BASED ANALYSIS OF LIGHT POLLUTION IN SLOVENIA FOR THE PERIOD 2013–2022

Juš Gašparič, Ana Potočnik Buhvald, Dušan Petrovič



JUŠ GAŠPARIČ

Artificially illuminated night sky over Ljubljana.

DOI: https://doi.org/10.3986/AGS.14686
UDC: 504.6:628.9(497.4)"2013/2022"
Creative Commons CC BY-SA 4.0

Juš Gašparič[1], Ana Potočnik Buhvald[1], Dušan Petrovič[1]

Satellite-based analysis of light pollution in Slovenia for the period 2013–2022

ABSTRACT: Light pollution is a serious global issue that negatively affects human health, the environment, and wildlife, while also causing unnecessary energy consumption. Using satellite imagery from the S-NPP and NOAA-20 satellites, obtained via the Google Earth Engine platform, we analysed the situation in Slovenia from 2013 to 2022. Image processing involved inverse distance weighting interpolation and the kernel density estimation method. With time series we showed trends and ranges in the six major urban areas and with heat maps their spatial distribution. Special attention was given to the period of COVID-19 pandemic in 2020 by comparing the data with those from previous and subsequent years. The results revealed a slight overall increase in light pollution, consistent with global trends.

KEYWORDS: light pollution, spatial analysis, heat map, time series, VIIRS, Slovenian cities

Analiza svetlobnega onesnaženja v Sloveniji med letoma 2013 in 2022 na osnovi satelitskih posnetkov

POVZETEK: Svetlobno onesnaženje je resen globalni problem, ki negativno vpliva na zdravje ljudi, okolje in živali ter povzroča nepotrebno energetsko porabo. Z uporabo satelitskih posnetkov satelitov S-NPP in NOAA-20, pridobljenih prek platforme Google Earth Engine, smo analizirali stanje v Sloveniji med letoma 2013 in 2022. Posnetke smo obdelali z interpolacijo inverzne utežne razdalje in metodo ocene gostote jedra. S časovnimi vrstami smo prikazali trende in razpone na šestih večjih mestnih območjih, s kartami pojavnosti pa njihovo prostorsko razporeditev. Posebno pozornost smo namenili obdobju pandemije COVID-19 leta 2020 ter primerjali podatke z leti pred in po pandemiji. Rezultati kažejo rahlo splošno povečanje svetlobnega onesnaženja, kar je skladno z globalnimi trendi.

KLJUČNE BESEDE: svetlobno onesnaženje, prostorska analiza, karte pojavnosti, časovne vrste, VIIRS, slovenska mesta

The article was submitted for publication on August 4th, 2025.
Uredništvo je prejelo prispevek 4. avgusta 2025.

[1] University of Ljubljana, Faculty of Civil and Geodetic Engineering, Ljubljana, Slovenia

jus.gasparic97@gmail.com (https://orcid.org/0009-0009-3032-2530), ana.potocnik-buhvald@fgg.uni-lj.si (https://orcid.org/0000-0002-6662-1999), dusan.petrovic@fgg.uni-lj.si (https://orcid.org/0000-0001-5908-8180)

1 Introduction

According to the International Dark-Sky Association (IDA), light pollution encompasses the effects of artificial lighting and refers to the spread of artificial light into the environment, where it disrupts natural processes and functions. It originates mainly from improperly directed or overly intense sources such as streetlights, advertising billboards, illuminated buildings, and traffic lights (Chepesiuk 2009), and its increase is partly attributed to solid-state lighting (SSL), particularly light-emitting diodes (LEDs), which account for nearly 50% of global lighting sales (Barentine 2025). Light pollution is not only an environmental or astronomical issue but also a spatial and geographical phenomenon (Lamphar 2020), as it reflects the distribution of human activities, settlement structures, transport networks, and land-use patterns, and is closely linked to urbanisation and infrastructural development. Nighttime illumination therefore serves as an indirect indicator of social, economic, and spatial dynamics (Wu et al. 2023). Artificial light at night also disrupts circadian rhythms and contributes to energy waste and climate-related impacts (Brayley and Wakefield 2022; Garavito et al. 2023; Duan et al. 2024), although the present study focuses on its spatial and temporal dimensions.

Light pollution is analysed using ground-based and satellite measurements that differ in accuracy and spatial coverage. Common local instruments include Sky Quality Meters (SQM), digital cameras, and lux or luminance meters (Widmer et al. 2022). SQM values are expressed in magnitudes per square arcsecond (mag/arcsec^2), whereas other instruments measure illuminance (lux) or luminance (cd/m^2). Urban areas typically record 16–18 mag/arcsec^2, while darker sites reach around 22 mag/arcsec^2 or more (Žiberna and Gulič 2020). At the global scale, key datasets are provided by satellites operated by the National Oceanic and Atmospheric Administration (NOAA), particularly the Visible Infrared Imaging Radiometer Suite Day/Night Band (VIIRS DNB) sensor (Chen et al. 2021b), which enables long-term monitoring and visualisation of spatial and temporal changes. Analyses indicate that 83% of the global and 99% of the European population live under light-polluted skies (Falchi et al. 2016), and data from the Suomi National Polar-orbiting Partnership (S-NPP) satellite show a 2.2% annual global increase over the past decade (Kyba et al. 2023), while declines are rare and mainly associated with military conflicts (Li et al. 2018). In Central Europe, studies using VIIRS data report increasing radiance around major transport corridors, industrial zones, and expanding suburban areas in Austria, northern Italy, and Croatia (Widmer et al. 2022; Wallner et al. 2023).

In Slovenia, both approaches have been applied. Ground-based measurements include 48 locations near Maribor in 2012 (average 17.96 mag/arcsec^2), night skiing analyses at Rogla (20.20 mag/arcsec^2) and Mariborsko Pohorje (19.83 mag/arcsec^2) in 2018, and measurements in Gornja Radgona (17.25 mag/arcsec^2) and Senovo (17.87 mag/arcsec^2) in 2021 (Žiberna 2016; Žiberna and Gulič 2020; Kalšek et al. 2021). Several studies have also employed VIIRS data: Žiberna and Konečnik (2021) analysed distribution patterns by statistical regions, municipalities and Natura 2000 sites, while detailed analyses show that in 2017 the most illuminated municipalities were Ankaran (Luka Koper, 9.5 nW/cm^2/sr), Ljubljana (5.4 nW/cm^2/sr) and Maribor (4.8 nW/cm^2/sr) (Žiberna et al. 2018; Horvat et al. 2023). Radiance, expressed in nanowatts per square centimetre per steradian (nW/cm^2/sr), represents the luminous power emitted into the atmosphere and is a key indicator in remote sensing studies of nighttime illumination (LUC and Hoare 2024).

The aim of this study is to examine the extent of light pollution in Slovenia and its surroundings using satellite imagery from the NOAA VIIRS DNB sensor. Spatial patterns, differences, and trends are presented using heatmaps and multi-yeartime series. This approach provides a more detailed understanding of long-term illumination dynamics and allows us to assess the effects of extraordinary events such as the COVID-19 pandemic. The structure of the analysis is illustrated in Figure 1.

Based on these considerations, the study addresses the following research questions:

(1) How did light pollution levels change in six selected Slovenian urban areas between 2013 and 2022 (chapters 3.1 and 3.2)?
(2) What spatial patterns of nighttime illumination can be observed at the city (chapter 3.2) and national scale (chapter 3.4)?
(3) How did an exceptional event such as the COVID-19 pandemic influence radiance levels in the country's largest urban area (chapter 3.3)?

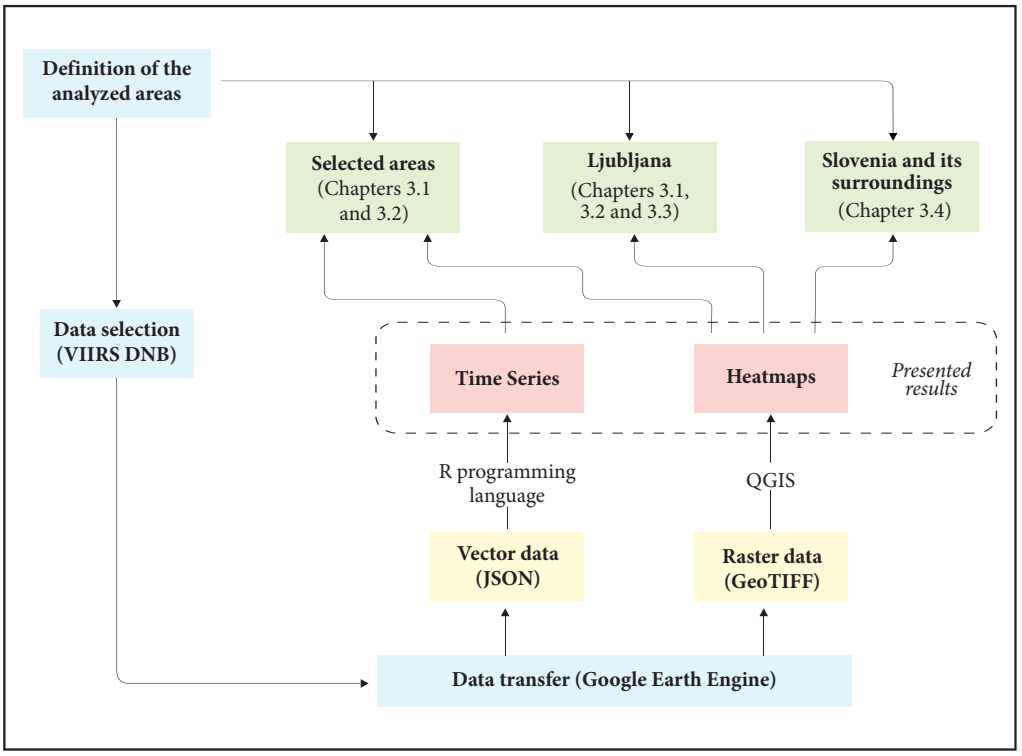


Figure 1: Analysis of Light Pollution in Slovenia flow chart.

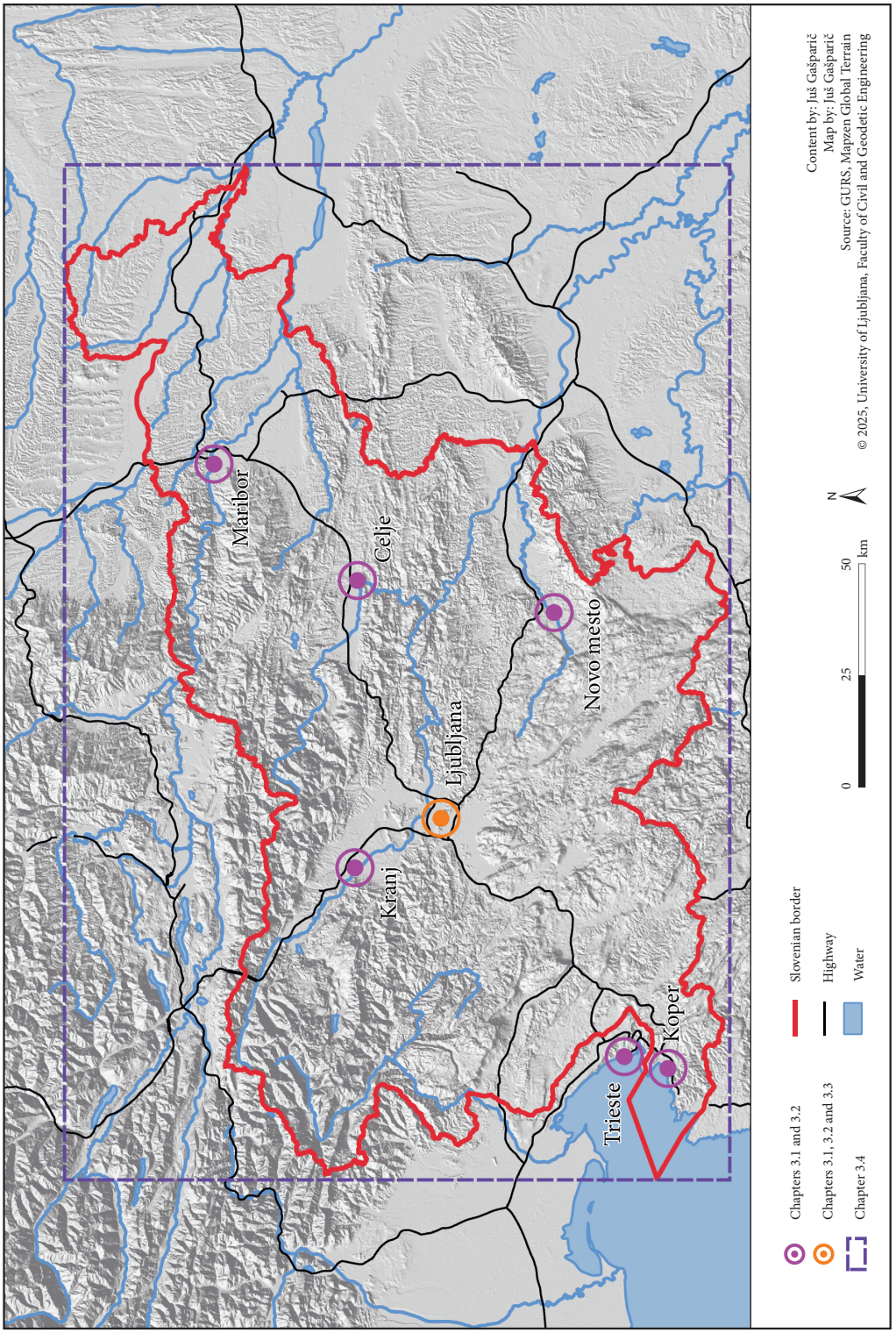
2 Methodology

2.1 Analysed area

Slovenia is a small but highly diverse country in terms of landscape and topography, commonly divided into Alpine, Pannonian, Dinaric and Mediterranean landscape types (Perko, Ciglič and Hrvatin 2021). As one of the most centralised countries in Europe, most political, economic and cultural activity is concentrated in Ljubljana (Vlaj 2012), while other major urban centres – Maribor, Celje, Kranj, Novo mesto and Koper – represent important regional, economic and employment centres, where investments, creative occupations, research activities and commuting flows are concentrated (Bole 2011; Ravbar 2011; Nared et al. 2017). The coastal cities of Koper and Trieste (Italy) form a cross-border port and logistics region of international relevance (Sessa 2021; Valinger Sluga and Ažman Momirski 2024). These spatial and economic characteristics shape patterns of nighttime illumination and provided the framework for analysing light pollution in three complementary components (Figure 2):

(1) Six major and economically important urban areas – Ljubljana, Maribor, Celje, Kranj, Novo mesto and the cross-border Koper–Trieste (Italy) region (with Novo mesto included instead of Velenje due to its strong industrial base and regional representation, and the Koper area extended to Trieste (Italy) because of their closely connected port and transport systems) (chapters 3.1 and 3.2).
(2) Focus on Ljubljana during COVID-19 pandemic (chapter 3.3).

Figure 2: Overview of the study areas and the three analytical components. ► p. 151


Maribor
Celje
Ljubljana
Novo mesto
Kranj
Trieste
Koper
Chapters 3.1 and 3.2
Chapters 3.1, 3.2 and 3.3
Chapter 3.4
Slovenian border
Highway
Water
0
25
50
km
N
Content by: Juš Gašparič
Map by: Juš Gašparič
Source: GURS, Mapzen Global Terrain
© 2025, University of Ljubljana, Faculty of Civil and Geodetic Engineering

(3) The entire Slovenian territory including adjoining parts of neighbouring countries (chapter 3.4), as light pollution extends beyond administrative borders.

To contextualise spatial differences in nighttime illumination, we compiled basic demographic, infrastructural and regional indicators for each analysed area (Table 1).

Table 1: Selected data of the analysed urban areas (data obtained by Infrastructure Agency of the Republic of Slovenia, Statistical Office of the Republic of Slovenia and Municipality of Trieste).

Indicator	Ljubljana	Trieste (Italy)	Koper	Maribor	Celje	Kranj	Novo mesto
Area [km^2]	257	84	303	148	95	151	236
Population (2013)	282,994	206,772	53,322	111,374	48,657	55,527	36,285
Population (2022)	293,218	200,603	53,462	113,004	48,679	56,639	37,615
Population (trend 2013–2022)	+3.5%	−3.0%	+0.3%	+1.5%	0.0%	+2.0%	+3.7%
Total road length (2022) [km]	1219.5	/	675.4	720.8	431.5	422.2	613.1
Composite electricity consumption intensity (2022) [kWh/resident and kWh/business entity]	28,999	/	32,030	28,271	45,507	42,177	68,051

2.2 Data used

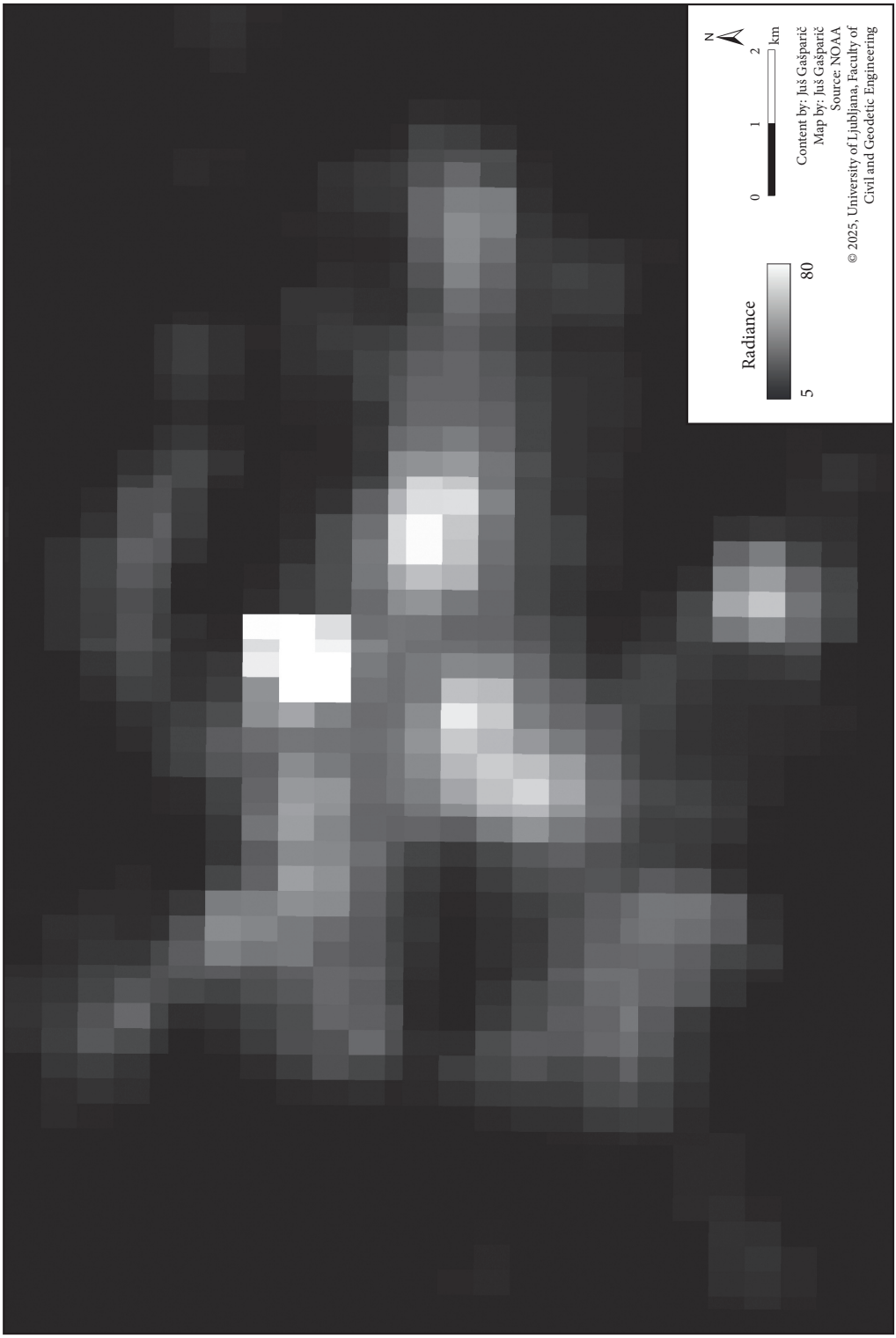
In this study, satellite data from the S-NPP and NOAA-20 satellites operated by NOAA and NASA were used. Both platforms carry five advanced instruments for high-resolution monitoring of the Earth's surface and climate (Keck 2011; Chen et al. 2020), including the VIIRS sensor, which acquires data in 22 spectral bands between 0.412 µm and 12.01 µm: 16 moderate-resolution bands, five high-resolution bands, and one panchromatic Day/Night Band (DNB). The DNB (0.5–0.9 µm) enables 24-hour observation with nearly constant 750 m spatial resolution across a 3,040 km swath and measures radiance over a wide dynamic range ($3.0 \times 10\text{-}9$ to $2.0 \times 10\text{-}2$ W/cm^2/sr) using calibrated detector arrays (Cao et al. 2013; Wolfe et al. 2013; Kolláth et al. 2018; Chen et al. 2021a; Wang et al. 2022). Nighttime light (NTL) data are recorded in radiance units (nW/cm^2/sr), suitable for detecting very weak light sources (Wang et al. 2022). Unlike the narrower spectral channels used for observing vegetation, ocean colour, clouds, and surface temperature, the DNB operates as a broad-band channel across the visible spectrum (Changyong et al. 2013) and supports monitoring of diverse nighttime light sources such as streetlights, building lighting, fishing vessels, gas flares, fires, auroras, and other human activities (Baynes 2024).

Monthly and annual NTL composites are generated from daily observations after removing atmospheric and lunar effects. Extreme values are excluded using a boxplot-based method based on the interquartile range (IQR = Q3 – Q1), omitting values outside Q1 – $1.5 \times$ IQR and Q3 + $1.5 \times$ IQR, this approach is robust and does not assume normal distribution. Final composites are calculated as the mean of the remaining observations, radiance values below 0.5 nW/cm^2/sr are set to zero to reduce background noise, and pixels affected by aurora are gap-filled with substitute values (Wang et al. 2022).

2.3 VIIRS Day/Night Band data and Google Earth Engine

We obtained the VIIRS Day/Night Band (DNB) data from the Google Earth Engine (GEE) Data Catalog. The analysis was based on annual composites from the datasets NOAA/VIIRS/DNB/ANNUAL_V21 (covering the period 2013–2021) and NOAA/VIIRS/DNB/ANNUAL V22 (for 2022). These datasets were developed and are maintained by the Earth Observation Group of the NOAA and National Centers for

Figure 3: NOAA VIIRS DNB ANNUAL 2022 maximum composite for the Ljubljana area, showing radiance values expressed in nanowatts per square centimetre per steradian (nW/cm^2/sr). ► p. 153


N
0
1
2
km
Radiance
5
80
Content by: Juš Gašparič
Map by: Juš Gašparič
Source: NOAA
© 2025, University of Ljubljana, Faculty of
Civil and Geodetic Engineering

Environmental Information (Elvidge et al. 2021). Although the 2022 data were obtained from the newer V22 product, both datasets represent annual VIIRS DNB night-time light composites produced within the same data framework and are therefore suitable for broad temporal comparison. Both datasets are publicly accessible via the GEE platform.These datasets contain yearly NTL composites expressed through various statistical indicators (median, average, maximum, and minimum), derived from cloud-free nighttime observations (Figure 3). In addition to these values, they include the total number of cloud-free observations for each pixel and the number of observations unaffected by sunlight or moonlight.

NTL data processing is based on monthly cloud-free averages. To remove extreme or irrelevant values caused by fires, auroras, and other sources of noise, the median radiance from the twelve-monthly composites is used. The background is filtered using a threshold determined by the data distribution across multiple years, enabling a consistent approach across the time series. The method also includes additional filters to reduce noise in polar regions, areas with high fire occurrence, and regions with low-intensity lighting such as rural settlements, diffuse glow from urban areas, and less illuminated surfaces (Elvidge et al. 2021). The processed VIIRS DNB data have a spatial resolution of 500 m (Widmer et al. 2022).

2.4 Data transfer

Raster and vector data were processed within the GEE environment using VIIRS DNB composites for the 2013–2022 period. Raster data in GeoTIFF format were extracted for predefined target areas defined by corner coordinates in the WGS84 coordinate system and subsequently exported from Google Earth Engine to Google Drive for further processing. These rasters contained annual radiance values and were subsequently imported into QGIS (version 3.36) for spatial visualisation and heatmap analysis. Vector data were derived from the same data catalogs after uploading manually delineated polygon layers representing the six urban areas selected for the first part of the study. The polygons encompassed zones with the highest radiance over built-up areas and were preferred to administrative municipal boundaries to ensure realistic inter-city comparisons, as municipal territories extend beyond urban cores and would otherwise lower average radiance values (Figure 4). GEE calculated annual minimum, mean, and maximum radiance statistics for each polygon, appending them as attributes to the geometries; each annual value represents the average of twelve-monthly composites (e.g., the maximum for Ljubljana in 2022 corresponds to the mean of that year's highest monthly values). The processed vector data were exported in JSON format and used to construct radiance time series for the six urban areas over 2013–2022.

2.5 Spatial analysis

Inverse Distance Weighted (IDW) interpolation is commonly used in spatial analyses to estimate unknown values based on known values from surrounding points. The method assumes that closer points have more influence than distant ones, which is achieved by assigning weights to the known data points according to their distance from the unknown location (Šumrada 2005). As distance increases, the weights decrease rapidly, with the rate of decrease controlled by the power value p (Barudžija et. al. 2024). When $p = 0$, all weights $_i$ are equal, resulting in a simple average of the neighbouring values. As p increases, the weights for distant points decrease more rapidly. At high p values, only the closest points significantly influence the interpolation (Equation 1).

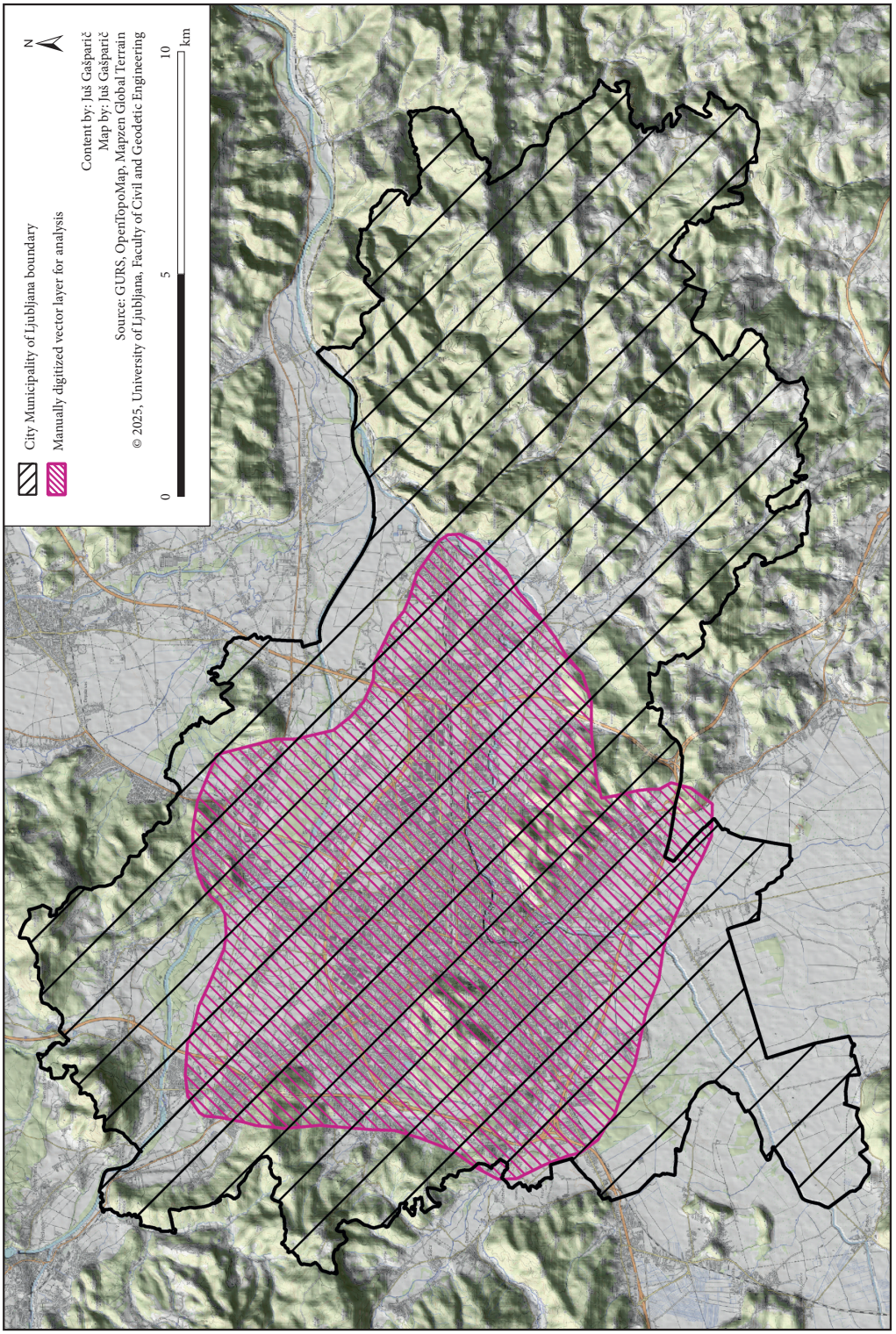
Mathematical expression IDW:

$$h_x(t_x) = \frac{\sum_{i=0}^{n} p_i(t_x,t_i) \cdot h_i}{\sum_{j=0}^{n} p_j(t_x,t_j)} \quad (1)$$

whereby

$$p_i(t_x, t_i) = \frac{1}{d_i(t_x, t_i)^k}$$

Figure 4: Comparison between the administrative area of the City Municipality of Ljubljana and the manually digitized area used for deriving radiance statistics. ► p. 155


City Municipality of Ljubljana boundary
Manually digitized vector layer for analysis
N
0
5
10
km
Content by: Juš Gašparič
Map by: Juš Gašparič
Source: GURS, OpenTopoMap, Mapzen Global Terrain
© 2025, University of Ljubljana, Faculty of Civil and Geodetic Engineering

and

$$d_i(t_x, t_i) = \sqrt{(x(t_x) - x(t_i))^2 + (y(t_x) - y(t_i))^2}$$

where:
- $h_x(t_x)$ is the interpolated value at point t_x,
- $h_i(t_i)$ is the given value at location t_i,
- p_i is a weight calculated based on distance,
- $d_i(t_x, t_i)$ is a distance between point and the known point t_i,
- k is a power that determines how quickly the influence of the point decreases with distance.

In practice, it is common to interpolate using the second power ($k = 2$), which means that the influence of the points decreases in inverse proportion to the square of the distance ($1/d^2$). The higher the potency, the faster the influence of distant points decreases (Benmoshe 2025). In our study, the points were the centroids of the pixels of the satellite images, which means that the points were uniformly distributed in space. In such a case, a reasonable choice is a weight value of k = 1, meaning that the influence of the points decreases inversely with distance ($1/d$). This moderate distance-decay function was selected to preserve broad spatial gradients in night-time light intensity while avoiding excessive local dominance of individual pixels. The interpolation distance was set to $d = 100$ m, which provides a fine output grid for visualisation while remaining consistent with the spatial resolution and positional uncertainty of the original VIIRS DNB observations. IDW interpolation was used to produce spatial NTL heatmaps of major urban centres in 2021 and of the City of Ljubljana during the COVID-19 pandemic (chapters 3.2 and 3.3).

Kernel Density Estimation (KDE) is a method for creating smooth density surfaces that show where data points are concentrated or sparse (Wang et al. 2020). It is especially useful for visualising spatial patterns, identifying so-called »hotspots«, and estimating distributions without assuming a specific shape (Milić et al. 2020). Instead of counting points within a defined area, KDE assigns each point a smooth kernel function, which spreads influence outward from the point. All kernels are then summed to generate a continuous density surface. The shape of the kernel determines how influence decays with distance, and the bandwidth (radius) defines the extent of this influence. A larger radius results in a smoother estimate (Equation 2).

Let $(x_1, x_2, \ldots, x_n)$ be independently and identically distributed samples drawn from some univariate distribution of unknown density f at any given point x. We are interested in estimating the shape of this function f. Its kernel density estimator is:

$$\hat{f}_h(x) = \frac{1}{n}\sum_{i=1}^{n} K_h(x - x_n) = \frac{1}{nh}\sum_{i=1}^{n} K\left(\frac{x - x_i}{h}\right) \quad (2)$$

where:
- $\hat{f}_h(x)$ is the estimated density at point x,
- n is the number of data points (sample size),
- $h > 0$ radius,
- x_i observed data point (sample value) from the dataset,
- $K(\cdot)$ is the kernel function.

For the shape of the kernel, we used the quartic (biweight) function $K(u)$, which is defined:

$$K(u) = \begin{cases} 15/16\ (1 - u^2)^2\,; & |u| \le 1 \\ 0\,; & |u| > 1 \end{cases}$$

In our analysis, KDE was applied to the centroids of pixels where radiance exceeded 20 nW/cm^2/sr to analyse their spatial distribution. Kyba et al. (2017) showed that most global artificial light emissions originate from regions with radiance values below this threshold, indicating that only the most intense sources exceed it, while Hügli (2021) used the same threshold to delineate highly illuminated urban areas. A radius of 5,000 m was chosen as a balance between spatial detail and interpretability. Using the default quartic kernel in QGIS (version 3.36), KDE produced a GeoTIFF raster in which pixel values represent estimated point density, with higher values indicating greater concentration. The result expresses density per unit area rather than absolute radiance, as in IDW; however, the term »radiance« was retained in the legend because the >20 nW/cm^2/sr threshold determined the output. KDE was used to visualise the spatial distribution of light pollution across Slovenia and its surroundings (chapter 3.4).

2.6 Heatmaps and time series

A heatmap is a cartographic technique used to display geospatial data using colour gradients. Different colour shades represent either the intensity of values (IDW interpolation) or the density of occurrences (KDE) within a specific area, a methodological approach similarly applied by Karpińska and Kunz (2019; 2023) to analyse spatial patterns and temporal variability of night-time sky brightness in urban environments. For visualising quantitative satellite data such as VIIRS, we used convergent and divergent colour scales. Areas with higher NTL values are represented using warm colours (e.g., red, orange), while cooler colours (e.g., green, blue) indicate lower intensities. The effectiveness of such cartographic choices in enhancing the readability and interpretability of light pollution maps has been demonstrated in previous studies (Kunz and Daab 2024). For the 2022 statistical visualisation, we used a monochromatic red palette, where more saturated tones reflect higher levels of light pollution. A key factor affecting the readability of heatmaps is the selection of an appropriate basemap, which provides spatial context and helps users better understand the locations being analysed. For visualisations, we used the Mapzen Global Terrain and OpenTopoMap as a basemap, while data from the Surveying and Mapping Authority of the Republic of Slovenia (GURS) were used to display the main roads, hydrological features, the national border, and the municipal boundary of Ljubljana. To overlay the raster analysis layer and the basemap effectively, transparency settings were adjusted to allow for simultaneous display with appropriate blending. However, care must be taken when combining colour-coded layers, as overlaying them can result in new colour tones. Users may misinterpret these as representing additional categories rather than a blend of two datasets. Such misinterpretations can lead to false conclusions, especially if mixed tones are perceived as separate classes.

Time series analysis allows for identifying trends and patterns over time. It enables us to track changes from year to year and relate them to environmental events. Additionally, time series can reveal cyclical patterns (if present) and allow for comparisons across multiple locations within the same timeframe which is crucial for understanding spatial disparities. In this study, time series graphs were essential for examining how light pollution levels evolved and what key factors influenced those changes (chapter 3.1). Data processing was conducted using R programming language (version 4.3.1). We created combined time series plots for all selected areas, standardising the y-axis radiance values (nW/cm^2/sr) across cities to enable easier comparison. Maximum, median, and minimum values of annual NTL composites were used as statistical indicators.

3 Results

3.1 Radiance analysis in major cities

Tables 2–7 show the raw annual radiance values obtained from manually delineated vector layers for each urban area. Alongside these values, the tables present the percentage change from the previous year, illustrating annual increases or decreases in radiance intensity. The time series graphs in Figure 5 show the evolution of minimum, maximum, and median radiance values between 2013 and 2022. Dark red points represent the median, while light red points represent the annual maximum and minimum radiance values. The lines connecting these points help visualise overall trends and variation in light pollution.

3.2 Spatial representation of NTL in major urban centres

The time series analysis reveals that the highest median levels of light pollution occurred in 2021. In that year, peak radiance values were recorded in Trieste (Italy) and Koper, Maribor, Celje (same level as in 2019), and Kranj (2018). In Novo mesto (2019) and Ljubljana (2017), the highest values were observed in earlier years, although the 2021 levels did not differ significantly. The heatmaps in Figures from 6 to 11 show the spatial distribution of light pollution in 2021, based on median VIIRS DNB composites.

Figure 5: Time series of radiance (nW/cm^2/sr) values in major urban centres between 2013 and 2022. ► p. 160
Figure 6: Spatial radiance (nW/cm^2/sr) distribution of light pollution in Ljubljana area. ► p. 161
Figure 7: Spatial radiance (nW/cm^2/sr) distribution of light pollution in Trieste (Italy) and Koper area. ► p. 162
Figure 8: Spatial radiance (nW/cm^2/sr) distribution of light pollution in Maribor area. ► p. 163
Figure 9: Spatial radiance (nW/cm^2/sr) distribution of light pollution in Celje area. ► p. 164
Figure 10: Spatial radiance (nW/cm^2/sr) distribution of light pollution in Novo mesto area. ► p. 165
Figure 11: Spatial radiance (nW/cm^2/sr) distribution of light pollution in Kranj area. ► p. 166

Table 2: Ljubljana: annual radiance statistics (nW/cm^2/sr) and change (%) compared to the previous year.

	minimum		mean		maximum	
	radiance	change	radiance	change	radiance	change
2013	6.83	/	10.79	/	28.11	/
2014	4.94	−27.7	13.13	21.7	21.34	−24.1
2015	8.54	72.9	12.96	−1.3	16.92	−20.7
2016	9.93	16.3	13.31	2.7	17.34	2.5
2017	9.03	−9.1	13.95	4.8	20.01	15.4
2018	9.55	5.8	13.57	−2.7	19.96	−0.2
2019	5.88	−38.4	13.55	−0.1	17.57	−12.0
2020	5.45	−7.3	12.71	−6.2	16.5	−6.1
2021	8.14	49.4	13.75	8.2	18.9	14.5
2022	8.08	−0.7	13.33	−3.1	19.9	5.3

Table 3: Trieste (Italy) and Koper: annual radiance statistics (nW/cm^2/sr) and change (%) compared to the previous year.

	minimum		mean		maximum	
	radiance	change	radiance	change	radiance	change
2013	10.23	/	15.8	/	23.93	/
2014	10.11	−1.2	16.32	3.3	22.81	−4.7
2015	10.91	7.9	15.44	−5.4	21.21	−7.0
2016	10.87	−0.4	15.64	1.3	21.07	−0.7
2017	11.14	2.5	16.29	4.2	20.78	−1.4
2018	11.79	5.8	15.7	−3.6	21.5	3.5
2019	12.05	2.2	15.9	1.3	20.97	−2.5
2020	11.25	−6.6	15.47	−2.7	20.28	−3.3
2021	12.19	8.4	16.34	5.6	21.49	6.0
2022	9.51	−22.0	15.6	−4.5	22.11	2.9

Table 4: Maribor: annual radiance statistics (nW/cm^2/sr) and change (%) compared to the previous year.

	minimum		mean		maximum	
	radiance	change	radiance	change	radiance	change
2013	7.74	/	14.05	/	19.83	/
2014	10.45	35.0	14.32	1.9	23.41	18.1
2015	9.91	−5.2	13.67	−4.5	17.4	−25.7
2016	10.83	9.3	15.01	9.8	22.69	30.4
2017	10.91	0.7	15.14	0.9	23.61	4.1
2018	11.68	7.1	14.83	−2.0	21.07	−10.8
2019	9.2	−21.2	15.02	1.3	19.35	−8.2
2020	7.36	−20.0	14.45	−3.8	18.14	−6.3
2021	12.54	70.4	16.27	12.6	25.15	38.6
2022	10.46	−16.6	15.51	−4.7	20.77	−17.4

Table 5: Celje: annual radiance statistics (nW/cm^2/sr) and change (%) compared to the previous year.

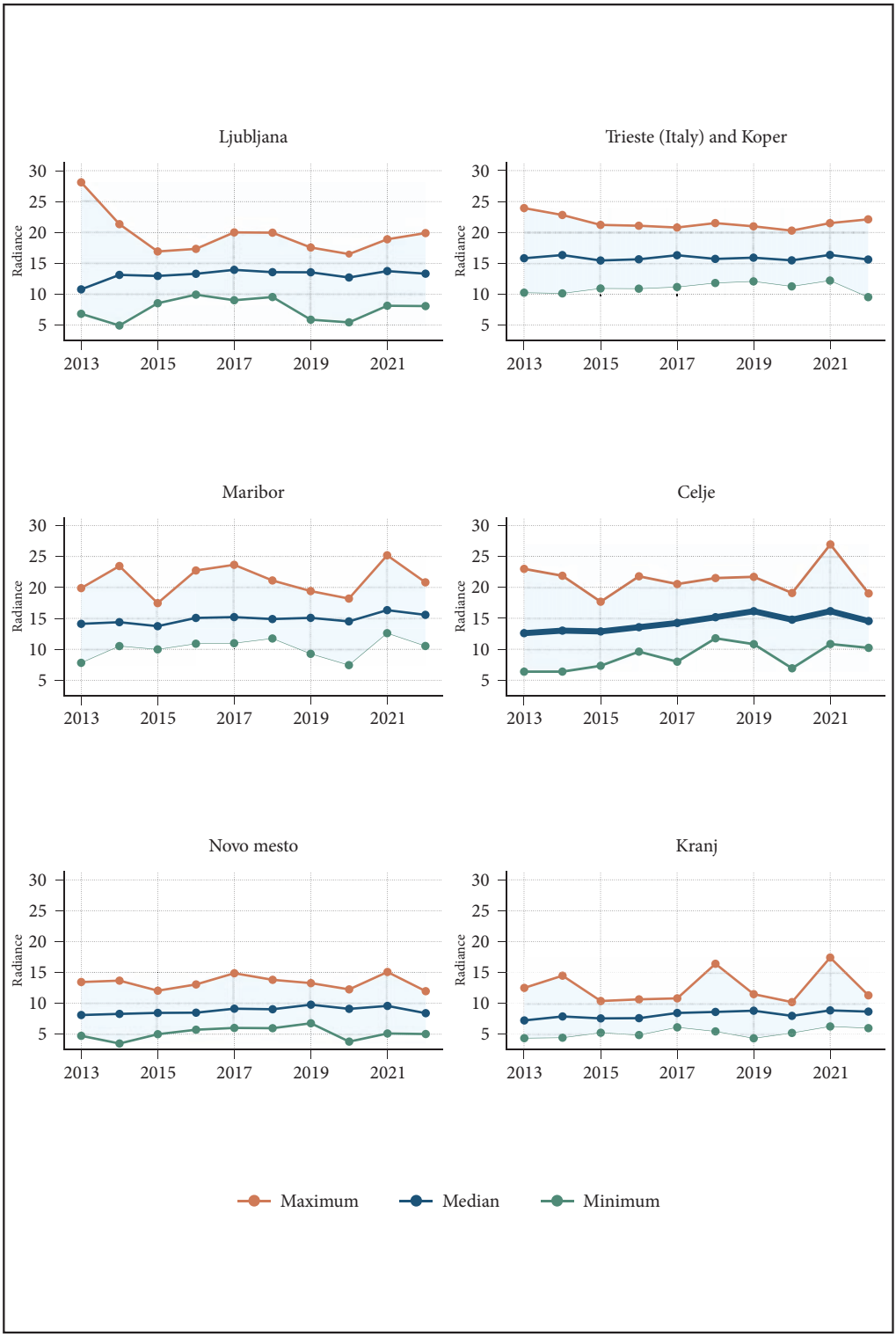
	minimum		mean		maximum	
	radiance	change	radiance	change	radiance	change
2013	6.39	/	12.61	/	23.02	/
2014	6.39	0.0	13.03	3.3	21.9	−4.9
2015	7.34	14.9	12.89	−1.1	17.7	−19.2
2016	9.63	31.2	13.58	5.4	21.81	23.2
2017	8.00	−16.9	14.26	5.0	20.56	−5.7
2018	11.79	47.4	15.19	6.5	21.53	4.7
2019	10.84	−8.1	16.17	6.5	21.72	0.9
2020	6.93	−36.1	14.8	−8.5	19.11	−12.0
2021	10.86	56.7	16.17	9.3	26.97	41.1
2022	10.24	−5.7	14.58	−9.8	19.04	−29.4

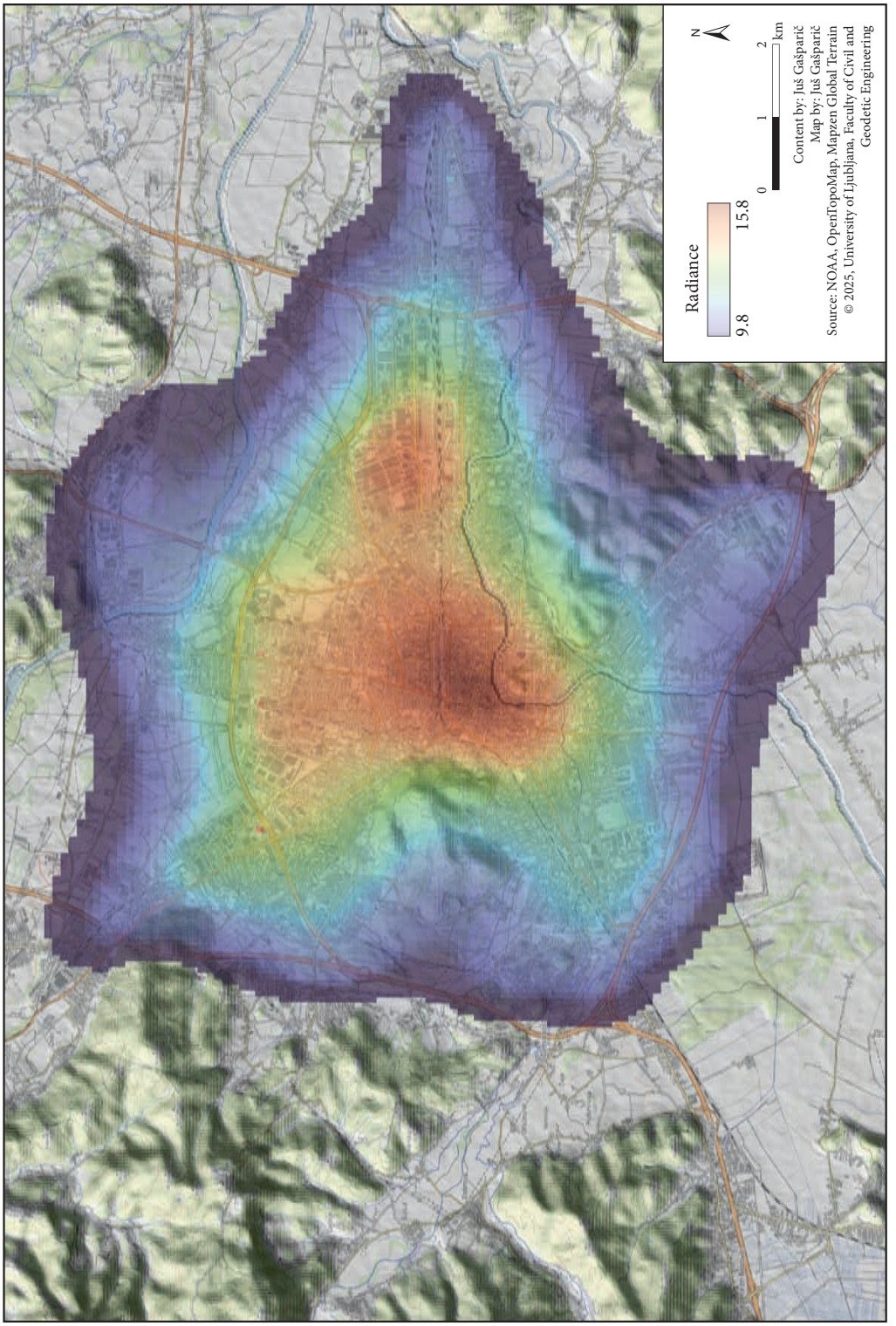
Table 6: Novo mesto: annual radiance statistics (nW/cm^2/sr) and change (%) compared to the previous year.

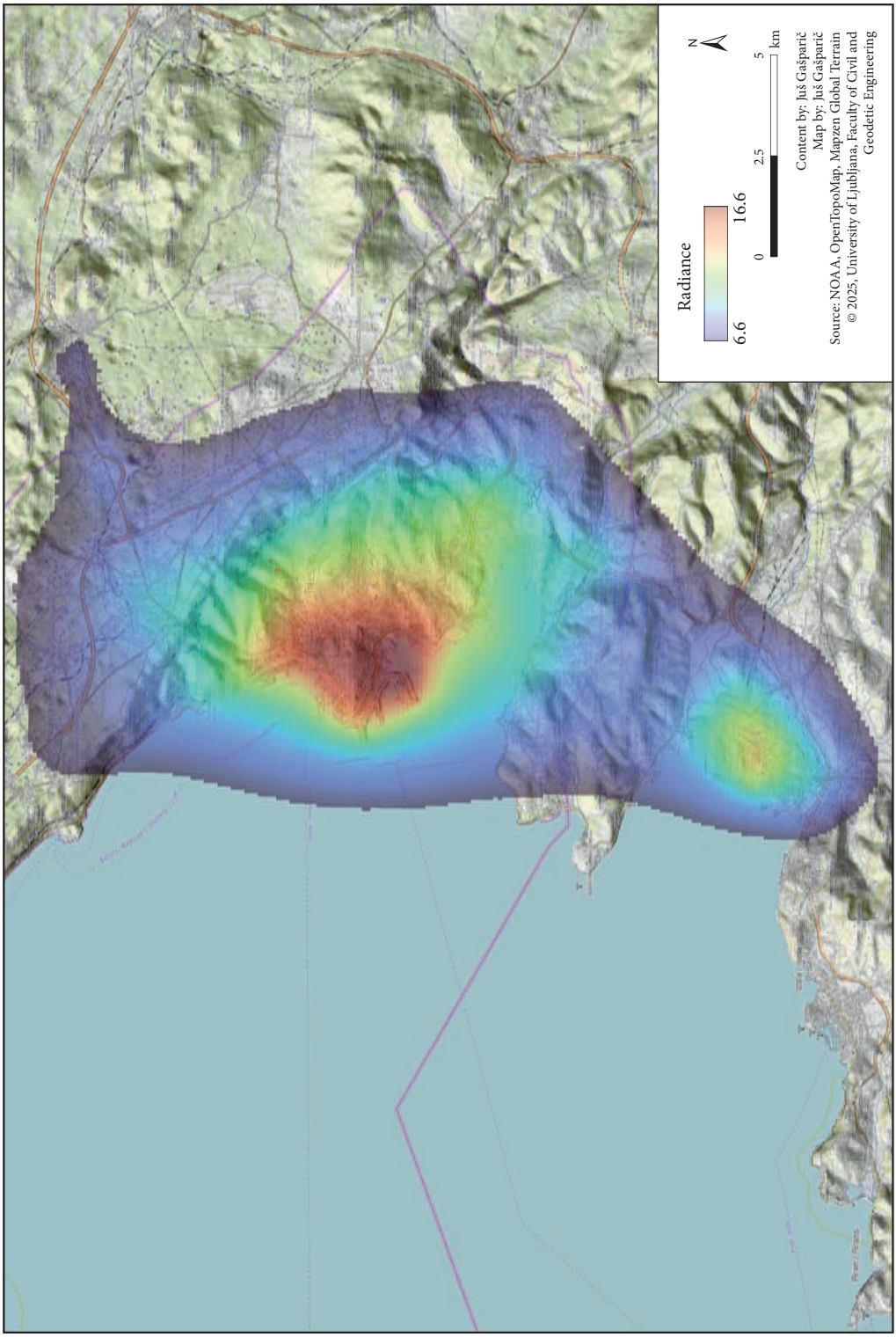
	minimum		mean		maximum	
	radiance	change	radiance	change	radiance	change
2013	4.78	/	8.14	/	13.48	/
2014	3.53	−26.2	8.32	2.2	13.70	1.6
2015	5.04	42.8	8.49	2.0	12.08	−11.8
2016	5.76	14.3	8.52	0.4	13.09	8.4
2017	6.05	5.0	9.16	7.5	14.90	13.8
2018	6.01	−0.7	9.07	−1.0	13.84	−7.1
2019	6.81	13.3	9.81	8.2	13.30	−3.9
2020	3.84	−43.6	9.14	−6.8	12.29	−7.6
2021	5.15	34.1	9.61	5.1	15.11	22.9
2022	5.07	−1.6	8.44	−12.2	12.00	−20.6

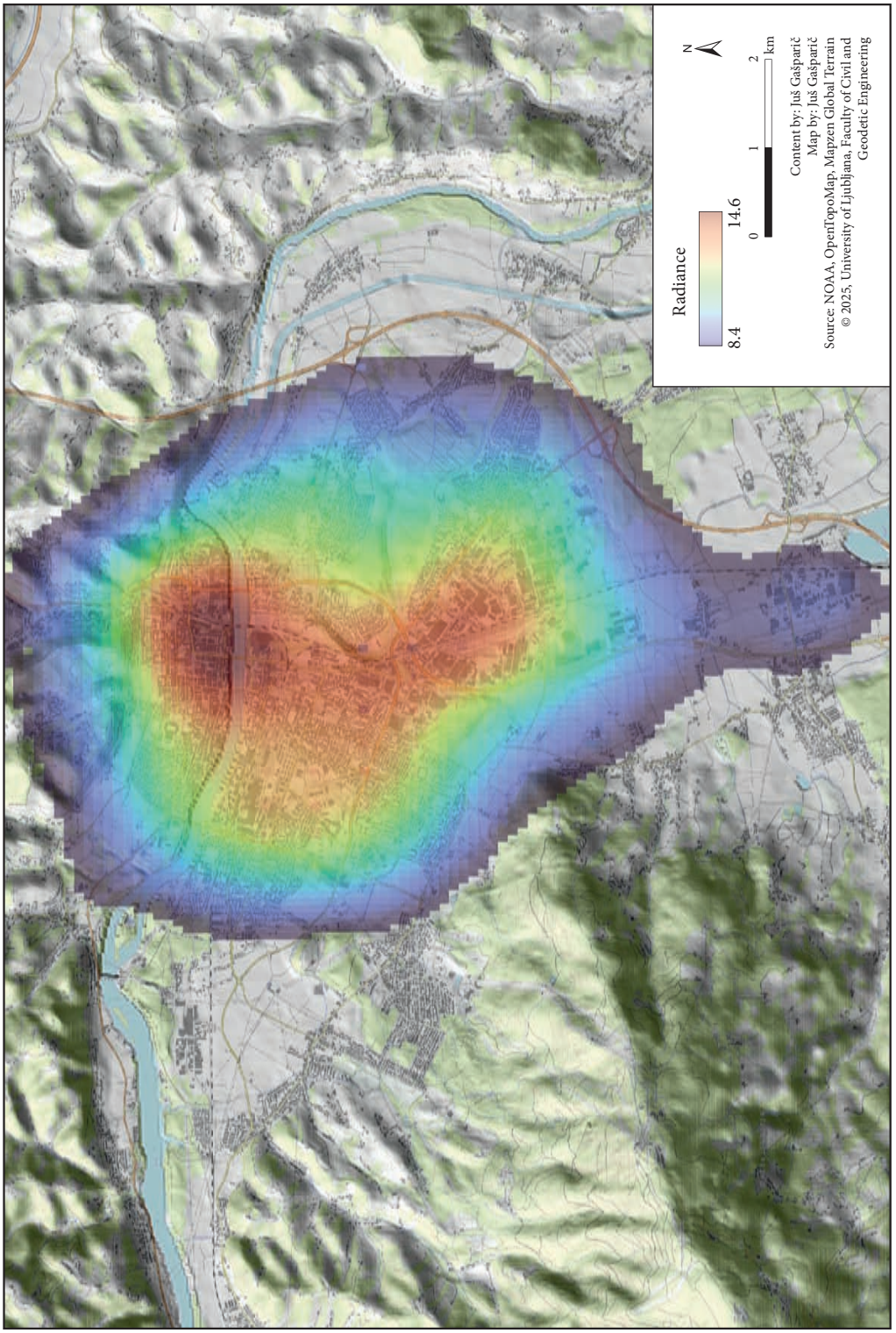
Table 7: Kranj: annual radiance statistics (nW/cm^2/sr) and change (%) compared to the previous year.

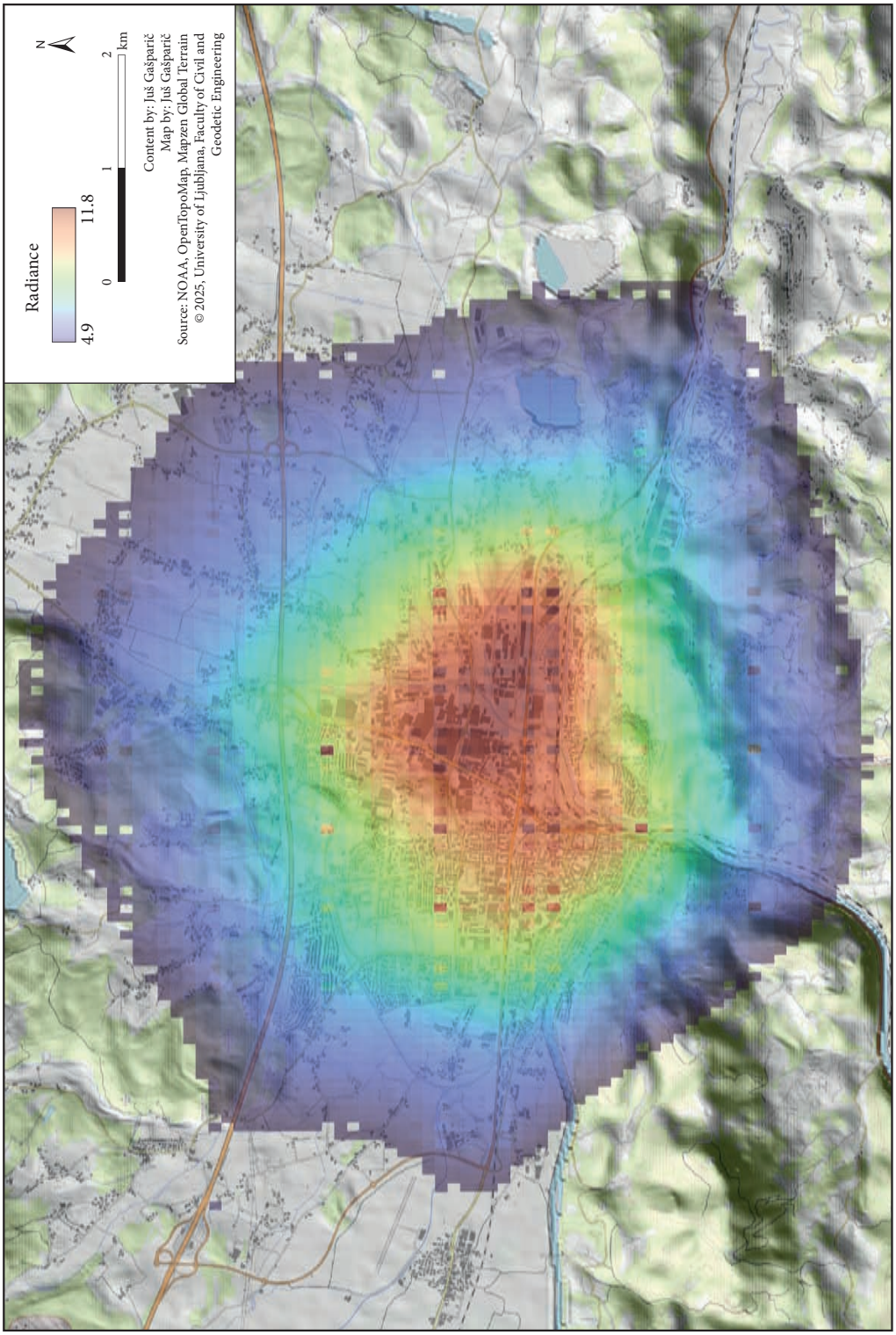
	minimum		mean		maximum	
	radiance	change	radiance	change	radiance	change
2013	4.35	/	7.23	/	12.49	/
2014	4.43	1.8	7.87	8.9	14.47	15.9
2015	5.23	18.1	7.55	−4.1	10.37	−28.3
2016	4.86	−7.1	7.59	0.5	10.64	2.6
2017	6.11	25.7	8.44	11.2	10.8	1.5
2018	5.45	−10.8	8.60	1.9	16.4	51.9
2019	4.33	−20.6	8.80	2.3	11.48	−30.0
2020	5.2	20.1	7.96	−9.5	10.19	−11.2
2021	6.25	20.2	8.85	11.2	17.41	70.9
2022	5.98	−4.3	8.65	−2.3	11.29	−35.2

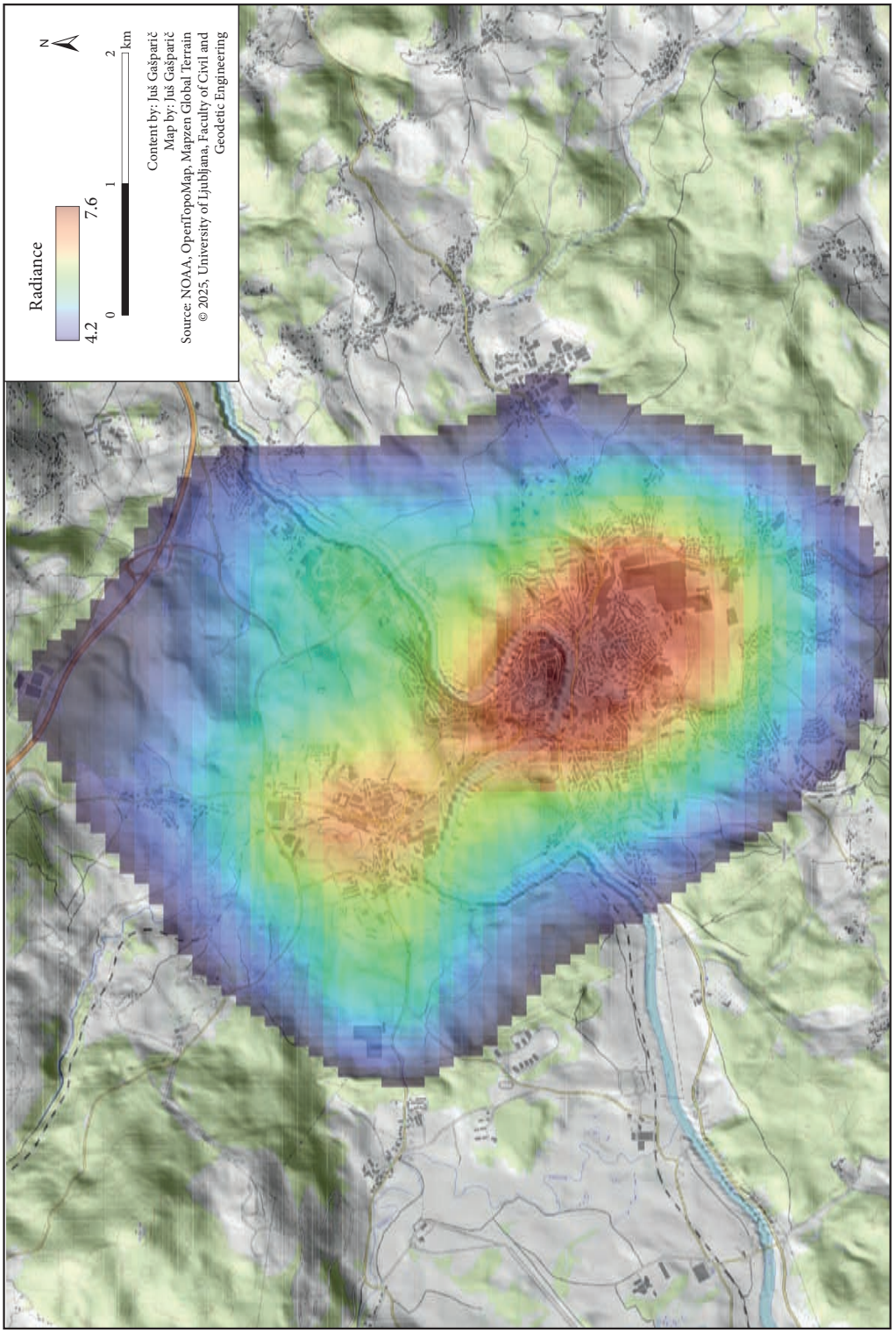

Ljubljana
Trieste (Italy) and Koper
Maribor
Celje
Novo mesto
Kranj
Radiance
30
25
20
15
10
5
2013
2015
2017
2019
2021
Maximum
Median
Minimum

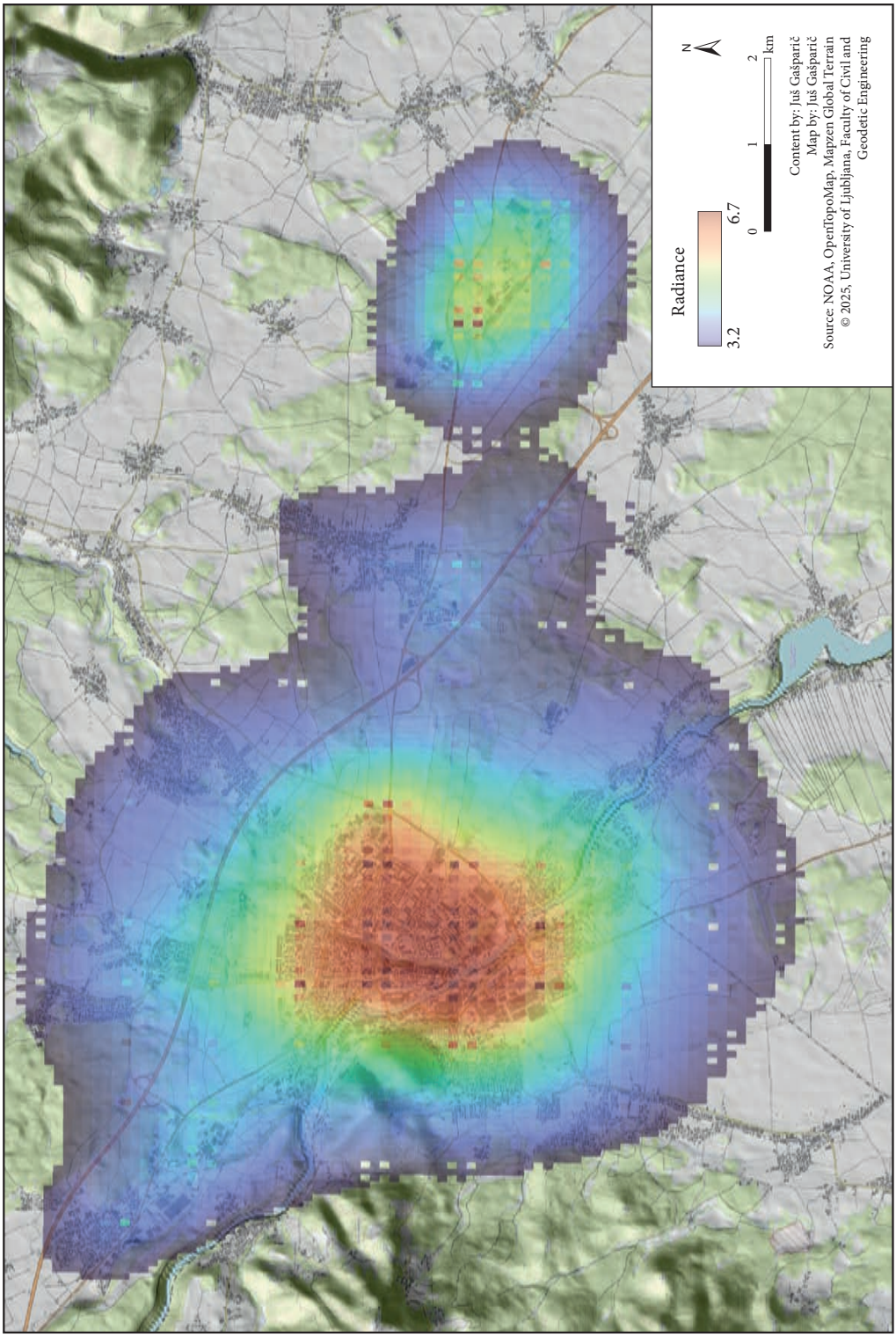

Radiance
9.8
15.8
N
0
1
2
km
Content by: Juš Gašparič
Map by: Juš Gašparič
Source: NOAA, OpenTopoMap, Mapzen Global Terrain
© 2025, University of Ljubljana, Faculty of Civil and Geodetic Engineering


N
Radiance
16.6
6.6
0
2.5
5
km
Content by: Juš Gašparič
Map by: Juš Gašparič
Source: NOAA, OpenTopoMap, Mapzen Global Terrain
© 2025, University of Ljubljana, Faculty of Civil and Geodetic Engineering


Radiance
14.6
8.4
N
0
1
2
km
Content by: Iuš Gašparič
Map by: Iuš Gašparič
Source: NOAA, OpenTopoMap, Mapzen Global Terrain
© 2025, University of Ljubljana, Faculty of Civil and Geodetic Engineering


Radiance
4.9
11.8
0
1
2
km
N
Content by: Juš Gašparič
Map by: Juš Gašparič
Source: NOAA, OpenTopoMap, Mapzen Global Terrain
© 2025, University of Ljubljana, Faculty of Civil and Geodetic Engineering


Radiance
4.2
7.6
0
1
2
km
N
Content by: Juš Gašparič
Map by: Juš Gašparič
Source: NOAA, OpenTopoMap, Mapzen Global Terrain
© 2025, University of Ljubljana, Faculty of Civil and Geodetic Engineering


Radiance
3.2
6.7
0
1
2
km
N
Content by: Juš Gašparič
Map by: Juš Gašparič
Source: NOAA, OpenTopoMap, Mapzen Global Terrain
© 2025, University of Ljubljana, Faculty of Civil and Geodetic Engineering

3.3 Difference in NTL before and after the COVID-19 pandemic in Ljubljana

This section presents absolute differences in NTL in Ljubljana between 2019 and 2020, and between 2020 and 2021 (Figures 12 and 13). The goal is to examine the effects of COVID-19 pandemic containment measures on light pollution levels, as visualised through comparative heatmaps. Analysis was conducted based on the maximum values of annual VIIRS DNB composites.The colour transitions on the maps are discrete, meaning attribute values are divided into classes, making boundaries between them more distinct. This visualisation enhances spatial interpretation and helps identify the main sources of light pollution. In the 2019–2020 comparison, the minimum visualised radiance difference is 1.0 nW/cm^2/sr, while in the 2020–2021 comparison, it is 2.0 nW/cm^2/sr. This difference (1.0–2.0) is necessary because there was a 6.1% decrease in 2020, followed by a 14.5% increase in 2021 (Table 2).

3.4 Minimum, average and maximum NTL values across Slovenia and its surroundings

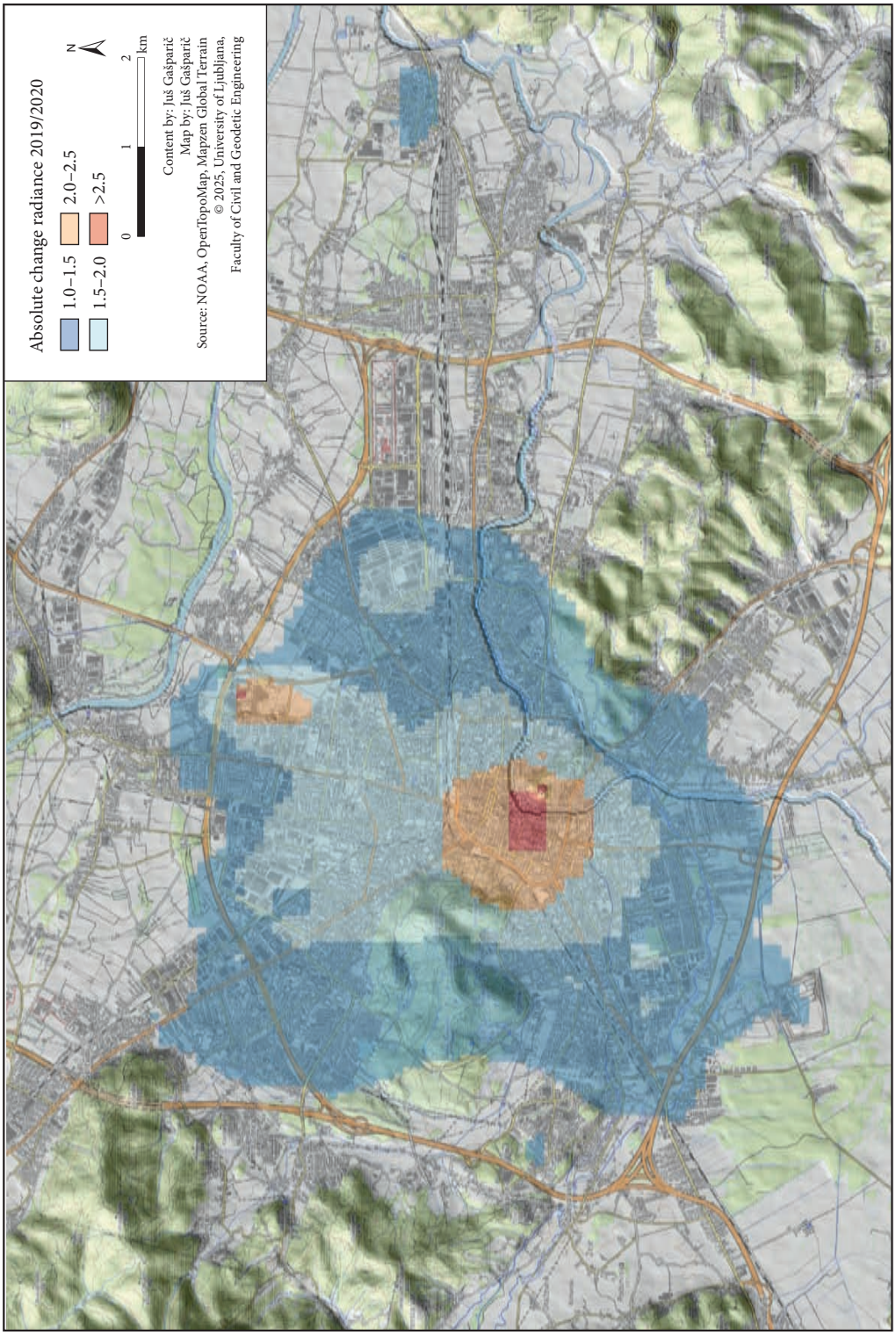
The time series graphs presented earlier revealed clear differences among the annual NTL composite statistics (minimum, median, and maximum radiance). To broaden the scope of the analysis, the spatial coverage was extended to encompass the entire territory of Slovenia and its wider surroundings, while the median statistic was replaced with the mean value. The resulting heatmaps visualize only those areas where radiance values exceeded 20 nW/cm^2/sr in 2022 as this threshold highlights the most intensely illuminated urban cores and allows for clearer differentiation from moderately or weakly lit surroundings (Figures from 14 to 16).

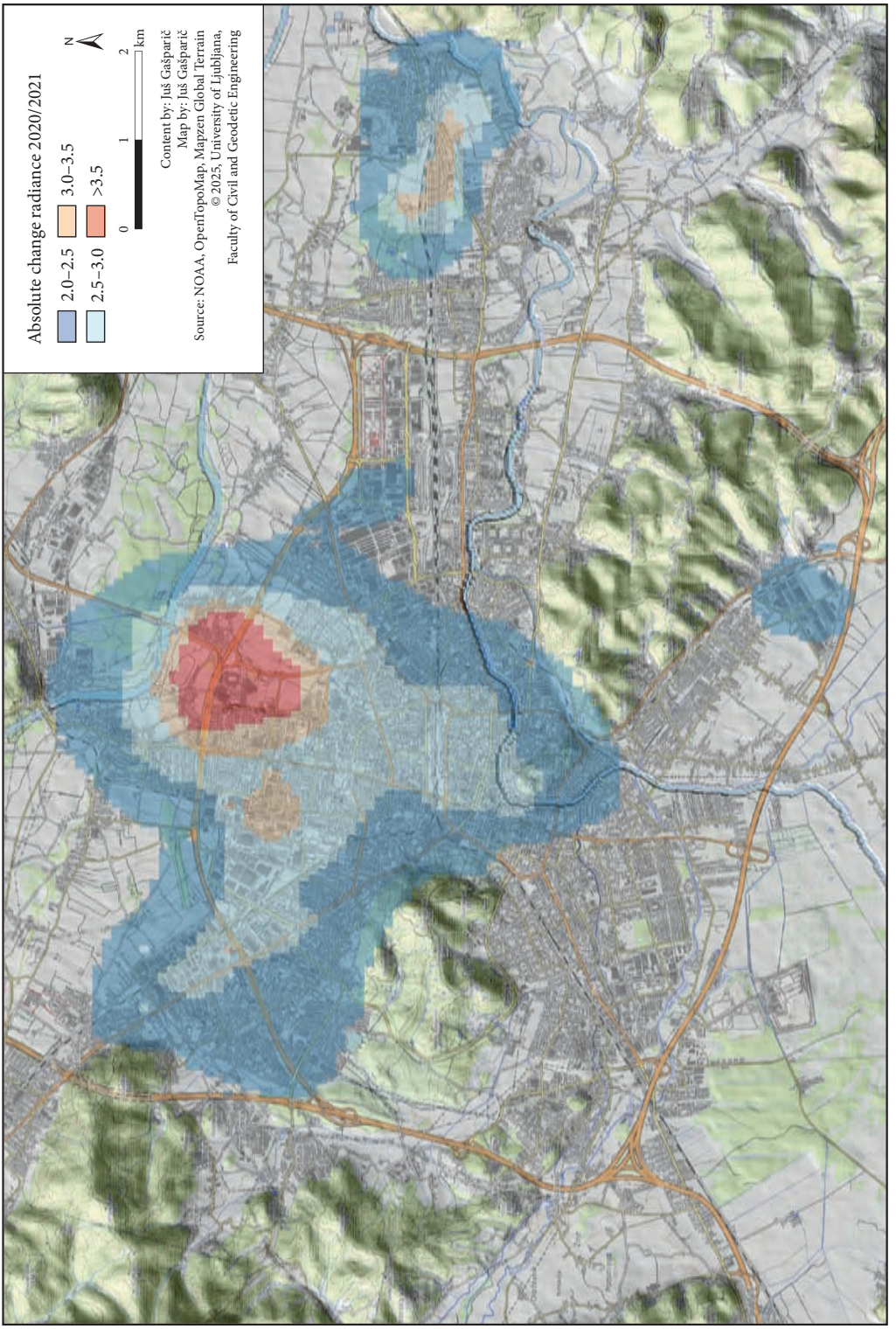
4 Discussion

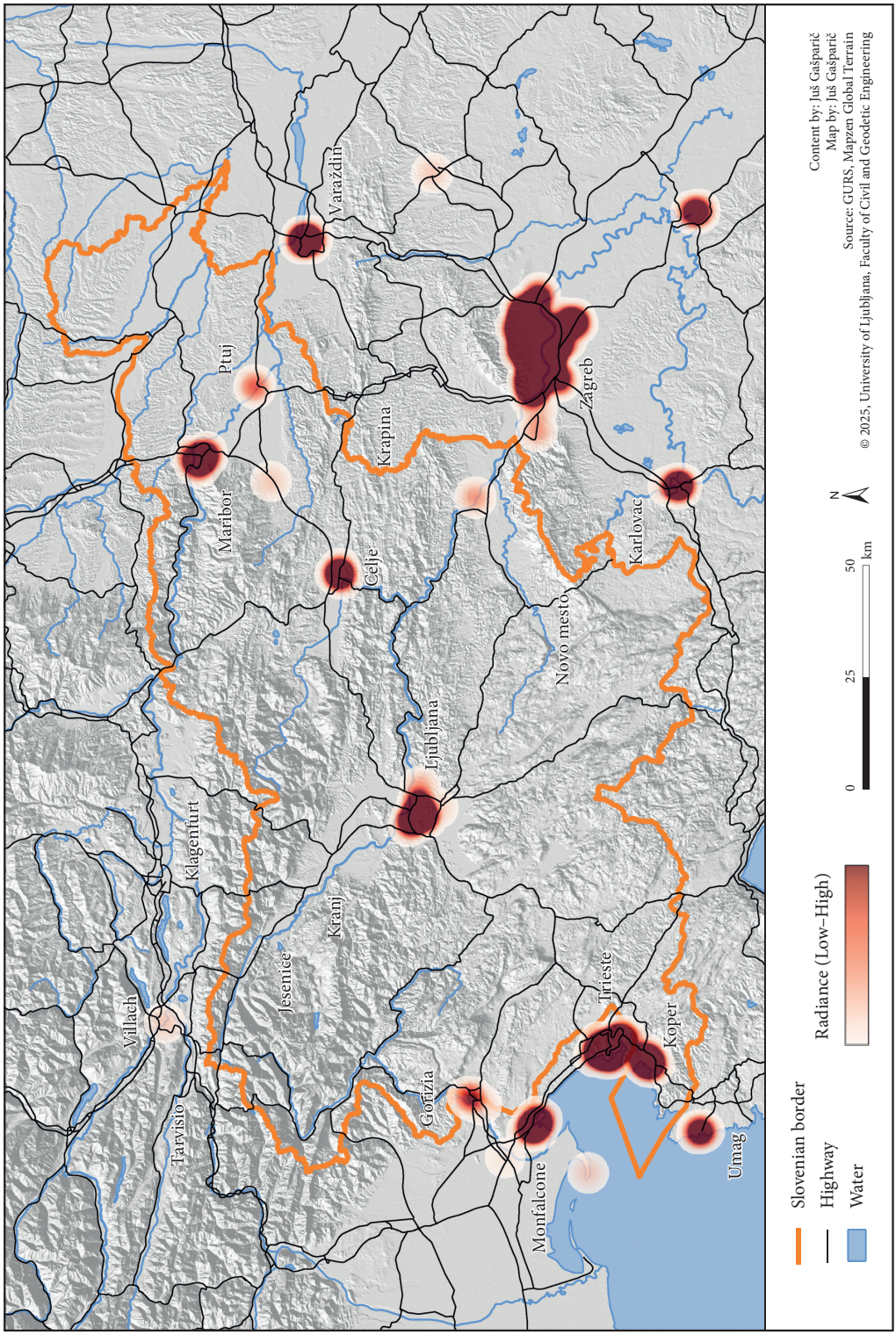
Tables 2–7 and time series (Figure 5) for six urban regions in Slovenia, including crossborder Trieste (Italy)–Koper area, from 2013 to 2022 present annual NTL radiance statistics. In Ljubljana, the mean radiance started at 10.8 nW/cm^2/sr in 2013, increased by +21.7% in 2014, and then fluctuated moderately between 12.7 and 13.9 nW/cm^2/sr through 2022 (−3.1% in the final year). The minimum values ranged between 6.8 and 9.9 nW/cm^2/sr, while the maximum decreased from 28.1 nW/cm^2/sr in 2013 to 19.9 nW/cm^2/sr in 2022 (−29% overall). Trieste (Italy)–Koper maintained mean values of about 15–16 nW/cm^2/sr, showing minor annual variability within ±4% and relatively stable maximum radiance around 21 nW/cm^2/sr. Maribor recorded moderate mean values (around 14–15 nW/cm^2/sr) with an increase in minimum values in 2021 by as much as 70%, while Celje showed increase in mean values by around 6% between 2015 and 2019. Novo mesto exhibited consistently lower radiance (around 8 nW/cm^2/sr) and limited interannual variation (−2% to +5%), whereas Kranj rose gradually from 7.2 nW/cm^2/sr in 2013 to approximately 8.0 nW/cm^2/sr (+11% in 2014, −4% in 2015). Interannual mean changes rarely exceeded ±10%, indicating relatively stable or slightly increasing NTL levels consistent with urbanization, infrastructure, and economic activity across the analysed cities. Novo mesto and Kranj show the lowest radiance, with Novo mesto typically about 2 nW/cm^2/sr higher, notable deviations include a 43% drop in Novo mesto's minimum radiance in 2020 and a >70% increase in Kranj's maximum in 2021. Overall, NTL shows a gradual increase with periodic fluctuations and local anomalies, particularly in 2020 and 2022. Similar regionally diverse trends across 38 EEA countries during 2014–2022 were reported by the European Topic Centre on Human Health and the Environment under the European Environment Agency (Widmer et al. 2022).

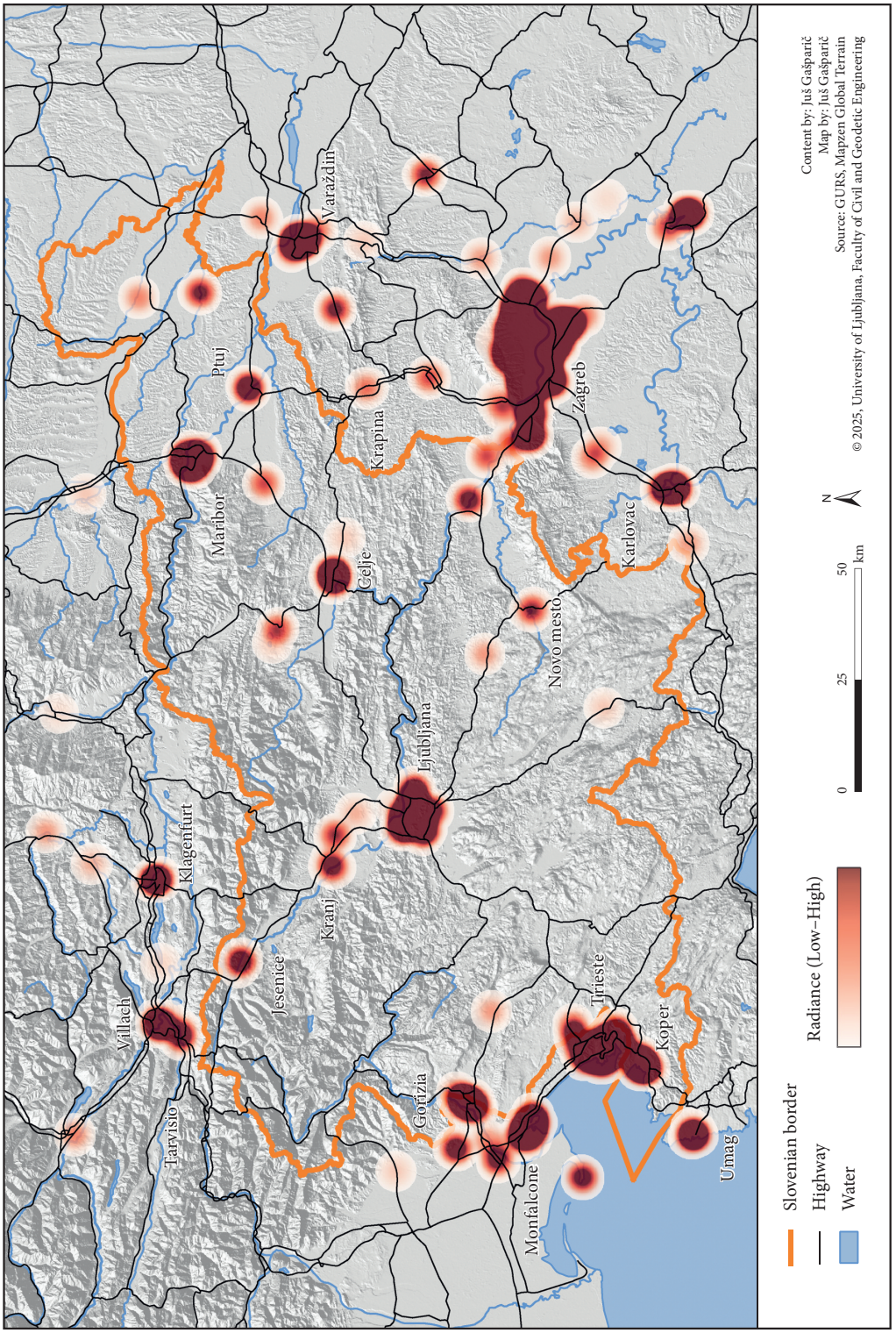
Figures 6–11 show the spatial distribution of radiance in selected Slovenian cities and Trieste (Italy), revealing a consistent pattern in which the highest NTL values concentrate in urban cores and decrease with distance. Given the coarse spatial resolution of VIIRS data, smaller individual sources of light are difficult to isolate unless they are very intense, whereas larger sources or clusters of emissions can still be

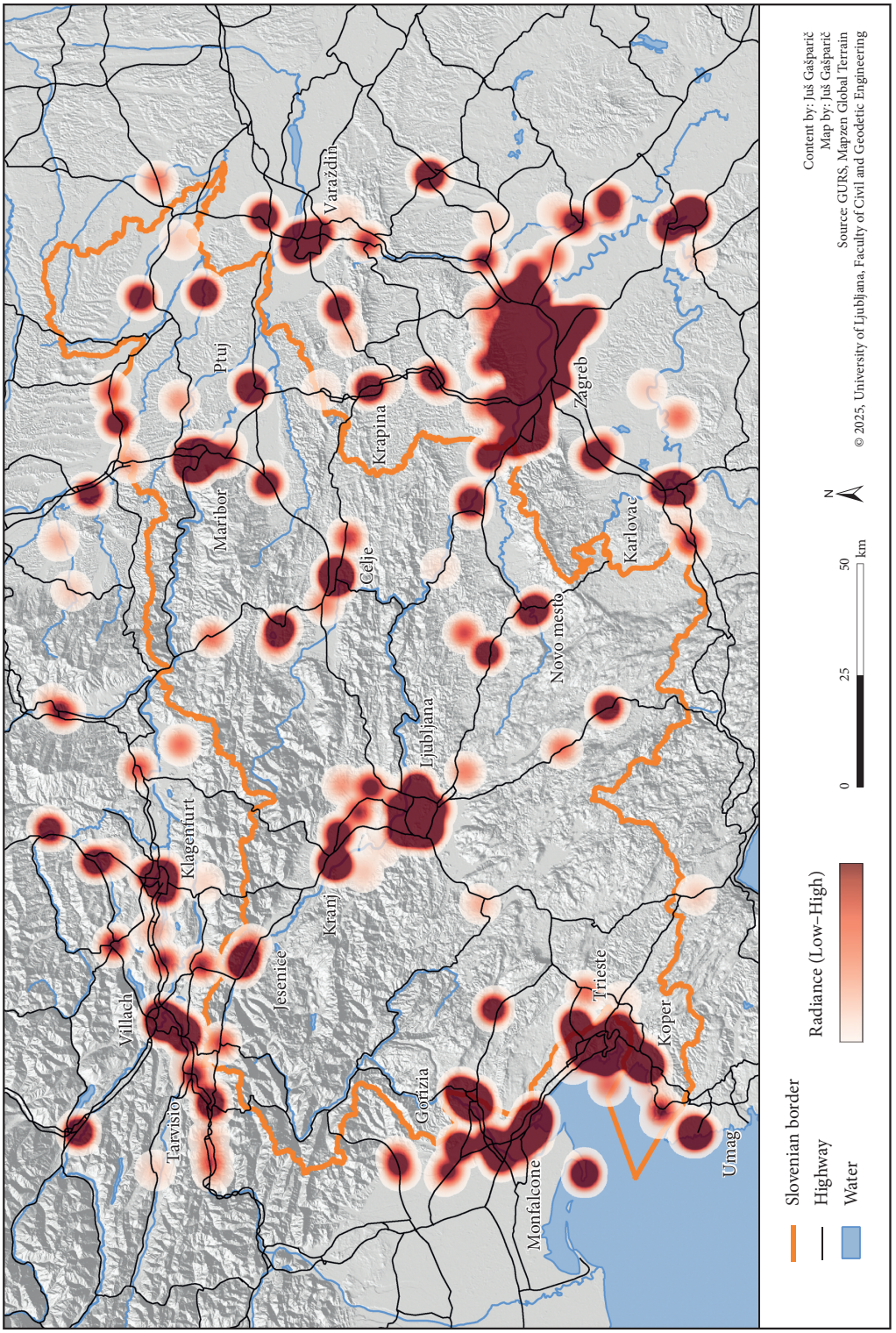
Figure 12: Change in NTL radiance (nW/cm^2/sr) in Ljubljana between 2019 and 2020. ► p. 168
Figure 13: Change in NTL radiance (nW/cm^2/sr) in Ljubljana between 2020 and 2021. ► p. 169
Figure 14: Minimum radiance values (above 20 nW/cm^2/sr) across the broader Slovenian region in 2022. ► p. 170
Figure 15: Average radiance values (above 20 nW/cm^2/sr) across the broader Slovenian region in 2022. ► p. 171
Figure 16: Maximum radiance values (above 20 nW/cm^2/sr) across the broader Slovenian region in 2022. ► p. 172


Absolute change radiance 2019/2020
1.0–1.5
1.5–2.0
2.0–2.5
>2.5
0
1
2
km
N
Content by: Juš Gašparič
Map by: Juš Gašparič
Source: NOAA, OpenTopoMap, Mapzen Global Terrain
© 2025, University of Ljubljana,
Faculty of Civil and Geodetic Engineering


Absolute change radiance 2020/2021
2.0–2.5
2.5–3.0
3.0–3.5
>3.5
0
1
2
km
N
Content by: Juš Gašparič
Map by: Juš Gašparič
Source: NOAA, OpenTopoMap, Mapzen Global Terrain
© 2025, University of Ljubljana,
Faculty of Civil and Geodetic Engineering


Slovenian border
Highway
Water
Radiance (Low–High)
0
25
50
km
N
Content by: Juš Gašparič
Map by: Juš Gašparič
Source: GURS, Mapzen Global Terrain
© 2025, University of Ljubljana, Faculty of Civil and Geodetic Engineering
Villach
Klagenfurt
Tarvisio
Jesenice
Kranj
Maribor
Ptuj
Gorizia
Ljubljana
Celje
Krapina
Varaždin
Zagreb
Novo mesto
Karlovac
Trieste
Koper
Monfalcone
Umag


Villach
Klagenfurt
Tarvisio
Jesenice
Kranj
Ljubljana
Gorizia
Monfalcone
Trieste
Koper
Umag
Maribor
Ptuj
Celje
Novo mesto
Varaždin
Krapina
Zagreb
Karlovac
Slovenian border
Highway
Water
Radiance (Low–High)
0
25
50
km
N
Content by: Iuš Gašparič
Map by: Iuš Gašparič
Source: GURS, Mapzen Global Terrain
© 2025, University of Ljubljana, Faculty of Civil and Geodetic Engineering


Villach
Tarvisio
Klagenfurt
Jesenice
Kranj
Ljubljana
Gorizia
Monfalcone
Trieste
Koper
Umag
Maribor
Ptuj
Celje
Varaždin
Krapina
Zagreb
Novo mesto
Karlovac
Slovenian border
Highway
Water
Radiance (Low–High)
0
25
50
km
N
Content by: Juš Gašparič
Map by: Juš Gašparič
Source: GURS, Mapzen Global Terrain
© 2025, University of Ljubljana, Faculty of Civil and Geodetic Engineering

recognized as broader illuminated areas. The highest radiance occurs in Ljubljana and Trieste (Italy), where urban density, transport infrastructure, and industrial areas (e.g., shopping centres in Ljubljana and ports in Trieste (Italy) and Koper) strongly influence brightness, in coastal areas emissions extend over the sea. Maribor displays high values spreading southward from the centre, shaped by major roads, the railway station, and surrounding hilly terrain where radiance declines. Celje exhibits a symmetrical and evenly distributed pattern without dominant sources, while Kranj shows comparatively low central values that decrease sharply outward, with the low minimum threshold highlighting features such as the motorway, the industrial zone near Šenčur, and Brnik Airport. Novo mesto maintains relatively low radiance despite its industrial development. Comparable spatial structures were identified in Toruń (Poland), where three zones of higher night-sky brightness contrasted with lower values farther from the city centre (Karpińska and Kunz 2019; Karpińska and Kunz 2023). Comparison with population size and road network length (Table 1) indicates a positive relationship: larger cities with more extensive road infrastructure, such as Ljubljana, exhibit higher radiance, whereas smaller centres like Novo mesto and Kranj show weaker emissions. Similar correlations between artificial light, economic activity, GDP growth, and road infrastructure development were reported by Kyba et al. (2017) and Das et al. (2021), confirming NTL as a reliable indicator of urban and infrastructural development.

During the COVID-19 pandemic (Figures 12 and 13), the largest radiance increases between 2019 and 2020 were observed within Ljubljana's ring road, intensifying toward the city centre and the Stožice Sports Centre, with notable changes also in the Šiška and Bežigrad districts, while areas such as Rudnik, Fužine, and Vrhovci showed little or no change. Compared with 2020, the strongest increases in 2021 occurred in northern Ljubljana around the Stožice Sports Centre, along the Kamnik railway line near building of the Zavarovalnica Triglav and VO-KA companies, and in the eastern industrial area near the Zalog rail yard. These patterns reflect COVID-19 pandemic containment measures, including temporary streetlight shutdowns in the city centre and rail yard, the ban on sports events in Stožice, and reduced illumination in major shopping centres. Across the entire 2013–2022 period, however, 2020 remains the only year in which NTL radiance declined consistently across all analysed cities, except Kranj, where minimum radiance increased by 20.1% (Table 6). This decrease represents a clear anomaly associated with the onset of pandemic restrictions, though within the broader decade-long variability of urban lighting dynamics in Slovenia the reductions appear temporary and did not alter the long-term trend. Comparable patterns were reported internationally using VIIRS DNB data: Xu et al. (2021) observed general NTL decreases in 20 major world cities during lockdowns, while Lan et al. (2021) showed that in China NTL changes reflected variations in human activity and policy measures rather than infection numbers. European studies reported similar declines, including about 14% in the Czech Republic (Pavlačka et al. 2023), around 50% in Polish cities (Ścieżor 2021), and up to 13% in Granada, Spain (Bustamante-Calabria et al. 2021).

According in our analyses in part 3, the minimum value map (Figure 14), radiance levels above 20 nW/cm^2/sr were detected in the largest urban centres, including Zagreb (Croatia), Trieste (Italy), Ljubljana, Maribor, and Celje, where high-intensity artificial lighting is concentrated. Other hotspots are also visible in cities such as Varaždin (Croatia), Monfalcone (Italy) and Umag (Croatia). In the average radiance map (Figure 15), the contrast between medium-sized cities and their rural surroundings becomes more pronounced. Clearly visible are smaller urban centres such as Krško and Nova Gorica (in combination with Gorizia, Italy), as well as Ptuj, Kranj, and industrial zones like Jesenice. Slightly less prominent are areas such as Velenje, Novo mesto, and Slovenska Bistrica. In the maximum radiance map (Figure 16), bright zones extend from major cities into their surrounding regions. This effect is most prominent around Zagreb (Croatia), Ljubljana and Trieste (Italy), likely reflecting patterns of urban expansion, intensive use of artificial lighting, and denser settlement structures. In addition to large cities, values exceeding the threshold are also visible in smaller centres such as Kočevje, Ajdovščina, Trebnje, Murska Sobota, Ljutomer, and Slovenj Gradec. Based on our observations, within the Ljubljana Basin, light pollution signatures are not clearly seen only in Kranj and Brnik Airport, but also in Domžale, Kamnik, and Mengeš. Similar trends are observed in neighbouring countries. In addition to major cities, light pollution can be attributed to both winter tourism (e.g., Kranjska Gora, Tarvisio in Italy, and Villach and Klagenfurt in Austria) and summer destinations (e.g., Portorož).

Weather conditions (cloud cover, snow) and natural phenomena (aurora, moonlight, wildfires) significantly influence satellite-based light pollution data. Cloud cover can increase perceived sky brightness

by reflecting light, with effects depending on urbanisation, while snow strongly amplifies brightness by reflecting all light sources, especially in already illuminated areas. Moonlight enhances surface and cloud visibility in imagery, whereas during new moon phases weather has less impact on detecting artificial light; in low-emission regions, aurora may also cause interference (Wang et al. 2022; Widmer et al. 2022). VIIRS DNB measurements are further affected by satellite viewing angle, particularly in dense urban areas where nadir observations yield higher radiance values than oblique views (Wang et al. 2022). In addition, the widespread adoption of LED lighting, which peaks in the blue spectral range (400–500 nm), lies near the lower limit of DNB spectral sensitivity (Kolláth et al. 2018). Because blue light scatters more than red or yellow light and VIIRS detectors do not respond equally across wavelengths, reduced sensitivity at shorter wavelengths means recorded values are less affected by artificial light, potentially producing overly optimistic estimates of light pollution reductions (Widmer et al. 2022; Balafoutis et al. 2025). Although satellite data indicate an annual radiance increase of about 1.8% between 2012 and 2016 (Kyba et al. 2017), these likely underestimates actual trends due to limited sensor response to modern LED spectra, and recent analyses confirm that the transition from sodium to LED lighting introduces systematic spectral bias into long-term satellite estimates (Barentine 2025). Although these limitations cannot be fully eliminated in satellite-based analyses, the use of annual composite VIIRS DNB data partly reduces the influence of short-term disturbances such as clouds, moonlight and temporary light sources. Spectral sensitivity and viewing-angle effects remain important sources of uncertainty when interpreting temporal trends.

In this study, light pollution was analysed using processed VIIRS DNB satellite data in the form of NTL composites, which provide a consistent basis for assessing the spatial and temporal extent of light pollution through heatmaps and time series. The method is less suitable for very dark areas because radiance values below 0.5 nW/cm^2/sr are set to zero in NASA's monthly and annual composites, while reflections from large glass surfaces, such as greenhouses, may locally overestimate radiance. Despite these limitations, VIIRS DNB remains the only long-term global source for light pollution monitoring and is therefore essential for informing mitigation strategies. Contrary to expectations, light pollution levels in Slovenia between 2013 and 2022 did not increase sharply, which may partly reflect the growing adoption of LED lighting and the related spectral limitations of VIIRS DNB sensors, a pattern also noted in other studies (Kyba et al. 2017; Žiberna and Ivajnšič 2018; Elvidge et al. 2022; Bhattarai and Lucieer 2024). Additional factors may include downward-facing luminaires that reduce scattering and intensity, as well as increasing public awareness of light pollution.

5 Conclusion

In this study, we conducted a detailed analysis of light pollution in Slovenia during the period 2013–2022. The findings show a slight overall increase in light pollution levels, accompanied by noticeable year-to-year fluctuations. The highest radiance values were recorded in major urban centres, particularly Ljubljana, Maribor, Celje, and the coastal area of Trieste (Italy)–Koper. In these cities, light pollution was most intense in industrial and high-traffic zones, where commercial, port, and transport infrastructures are concentrated. Time series analysis revealed that the year 2020 was a clear anomaly, showing a decrease in light pollution levels across all analysed cities, coinciding with reduced economic and traffic activity due to COVID-19 pandemic containment measures. In 2021, radiance values increased again, reaching or even exceeding pre-pandemic levels, while in 2022, a slight decline was observed in most cities. Spatial analysis with heatmaps showed that light pollution is not limited to city centres but is spreading toward suburban and peri-urban areas. The brightest zones follow major transport corridors and industrial belts, where radiance extends outward from urban cores. Mapping results for 2022 confirmed that the most illuminated areas were Ljubljana, Maribor, Celje, and the Trieste (Italy)–Koper coastal zone. Overall, the study indicates that light pollution in Slovenia did not decrease significantly between 2013 and 2022 but instead maintained a slightly increasing trend with local variations reflecting the influence of economic activity, infrastructure, and exceptional social conditions.

RESEARCH DATA: For information on the availability of research data related to the study, please visit the article webpage: https://doi.org/10.3986/AGS.14686.

6 References

Balafoutis, T., Skandali, C., Niavis, S., Doulos, L. T., Zerefos, S. C. 2025: Light pollution beyond the visible: Insights from people's perspectives. *Urban Science* 9-7. https://doi.org/10.3390/urbansci9070251

Barentine, J. 2025: Artificial light at night: State of the science 2025. *Briefing*. DarkSky International. https://doi.org/10.5281/zenodo.8071915

Barudžija, U., Ivšinović, J., Malvić, T. 2024: Selection of the value of the power distance exponent for mapping with the inverse distance weighting method: Application in subsurface porosity mapping, northern Croatia Neogene. *Geosciences* 14-6. https://doi.org/10.3390/geosciences14060155

Baynes, K. 2024: Nighttime lights. *Earthdata*. National Aeronautics and Space Administration.

Benmoshe, N. 2025: A simple solution for the inverse distance weighting interpolation (IDW) clustering problem. Sci 7-1. https://doi.org/10.3390/sci7010030

Bhattarai, D., Lucieer, A. 2024: Random forest regression: Exploring contributing factors to artificial night-time lights observed in VIIRS satellite imagery. *International Journal of Digital Earth* 17-1. https://doi.org/10.1080/17538947.2024.2324941

Bole, D. 2011: Changes in employee commuting: A comparative analysis of employee commuting to major Slovenian employment centers from 2000 to 2009. *Acta geographica Slovenica* 51-1. https://doi.org/10.3986/AGS51104

Brayley, O. D. M., Wakefield, A. 2022: The biological effects of light pollution on terrestrial and marine organisms. *International Journal of Sustainable Lighting* 24-1. https://doi.org/10.26607/ijsl.v24i1.121

Bustamante-Calabria, M., Sánchez de Miguel, A., Martín-Ruiz, S., Ortiz, J. L., Vílchez, J. M., Pelegrina, A., García, A. et al. 2021: Effects of the COVID-19 lockdown on urban light emissions: Ground and satellite comparison. *Remote Sensing* 13-2. https://doi.org/10.3390/rs13020258

Cao, C., Xiong, X., Wolfe, R., DeLuccia, F., Liu, Q., Blonski, S., Lin, G. et al. 2013: Visible/Infrared Imager Radiometer Suite (VIIRS) Sensor Data Record (SDR) User's Guide. NOAA Technical Report NESDIS 142, Version 1.1. *Technical report*. U.S. Department of Commerce, National Oceanic and Atmospheric Administration.

Chen, H., Sun, C., Xiong, X., Sarid, G., Sun, J. 2021a: SNPP VIIRS Day Night Band: Ten years of on-orbit calibration and performance. *Remote Sensing* 13-20. https://doi.org/10.3390/rs13204179

Chen, H., Xiong, X., Link, D. O., Sun, C., Chiang, K. 2020: NOAA-20 Visible Infrared Imaging Radiometer Suite day-night band on-orbit calibration and performance. *Journal of Applied Remote Sensing* 14-3. https://doi.org/10.1117/1.JRS.14.034516

Chen, Z., Yu, B., Yang, C., Zhau, Y., Yao, S., Qian, X., Wang, C. et al. 2021b: An extended time series (2000–2018) of global NPP-VIIRS-like nighttime light data from a cross-sensor calibration. *Earth System Science Data* 13-3. https://doi.org/10.5194/essd-13-889-2021

Chepesiuk, R. 2009: Missing the dark: Health effects of light pollution. *Environmental Health Perspectives* 117-1. https://doi.org/10.1289/ehp.117-a20

Das, S., Ahmed, S., Haque, S. 2021: Assessing correlation between night-time light and road infrastructure: An empirical study. In: GIScience 2021 Short Paper Proceedings. UC Santa Barbara: Center for Spatial Studies. https://doi.org/10.25436/E27P4D

Duan, J., Li, Q., Yin, Z., Zhen, S., Cao, W., Yan, S., Zhang, Y. et al. 2024: Outdoor artificial light at night and insomnia-related social media posts. *JAMA Network Open* 7-11. https://doi.org/10.1001/jamanetworkopen.2024.46156

Elvidge, C. D., Zhizhin, M., Ghosh, T., Hsu, F. C., Taneja, J. 2021: Annual time series of global VIIRS nighttime lights derived from monthly averages: 2012 to 2019. *Remote Sensing* 13-5. https://doi.org/10.3390/rs13050922

Elvidge, C. D., Zhizhin, M., Keith, D., Miller, S. D., Hsu, F. C., Ghosh, T., Anderson, S. et al. 2022: The VIIRS Day/Night Band: A flicker meter in space? *Remote Sensing* 14-6. https://doi.org/10.3390/rs14061316

Falchi, F., Cinzano, P., Duriscoe, D., Kyba, C., Elvidge, C. 2016: The new world atlas of artificial night sky brightness. *Science Advances* 2-6. https://doi.org/10.1126/sciadv.1600377

Garavito, G. A., Bennin, F., Barnett, P., Vindrola-Padros, C. 2023: What are the effects of artificial light on human health? An evidence brief. *Report*. Rapid Research Evaluation and Appraisal Lab (RREAL).

Horvat, U., Konečnik Kotnik, E., Ivajnšič, D. 2023: Svetlobna onesnaženost na Dravskem polju. In: Dravsko polje. Univerzitetna založba Univerze v Mariboru. https://doi.org/10.18690/um.ff.11.2023.8

Hügli, F. 2021: Light pollution in European protected areas: Spatial variation of light pollution in Natura 2000 sites of the Member States of the European Union. *Master's thesis*. ETH Zürich and WSL.

Kalšek, L., Budna, Ž., Hedl, A., Ravnik, J. 2021: Ocena svetlobnega onesnaženja v Mariboru, Gornji Radgoni in Senovem. *Revija za geografijo* 16-2. https://doi.org/10.18690/rg.16.2.3210

Karpińska, D., Kunz, M. 2019: Light pollution in the night sky of Toruń in the summer season. *Bulletin of Geography. Physical Geography Series* 17. https://doi.org/10.2478/bgeo-2019-0017

Karpińska, D., Kunz, M. 2023: Spatial and temporal analysis of artificial light pollution of the city night sky: A case study from Toruń. *Miscellanea Geographica* 27-3. https://doi.org/10.2478/mgrsd-2023-0015

Keck, A. 2011: NPP: Building a bridge to a new era of Earth observations. *Informational report*. National Aeronautics and Space Administration.

Kolláth, K., Tong, K. P., Kolláth, Z. 2018: Recent trends in light pollution measured from space in Hungary. In: 4th International Conference on Research, Technology and Education of Space (HSPACE2018). Hungarian Astronautical Society (MANT, Magyar Asztronautikai Társaság).

Kunz, M., Daab, D. 2024: Cartographic visualisation of light pollution measurements. *Urban Science* 8-4. https://doi.org/10.3390/urbansci8040254

Kyba, C. C. M., Kuester, T., de Miguel, A. S., Baugh, K., Jechow, A., Hölker, F., Bennie, J., Elvidge, C. D. 2017: Artificially lit surface of Earth at night increasing in radiance and extent. *Science Advances* 3-11. https://doi.org/10.1126/sciadv.1701528

Kyba, C., Altıntaş, Y. Ö., Walker, C. E., Newhouse, M. 2023: Citizen scientists report global rapid reductions in the visibility of stars from 2011 to 2022. *Science* 379-6629. https://doi.org/10.1126/science.abq7781

Lamphar, H. 2020: Spatio-temporal association of light pollution and urban sprawl using remote sensing imagery and GIS: A simple method based on Otsu's algorithm. *Journal of Quantitative Spectroscopy and Radiative Transfer* 251. https://doi.org/10.1016/j.jqsrt.2020.107060

Lan, T., Shao, G., Tang, L., Xu, Z., Zhu, W., Liu, L. et al. 2021: Quantifying spatiotemporal changes in human activities induced by the COVID-19 pandemic using daily nighttime light data. *IEEE Journal of Selected Topics in Applied Earth Observations and Remote Sensing* 14. https://doi.org/10.1109/JSTARS.2021.3060038

Li, X., Liu, S., Jendryke, M., Li, D., Wu, C. 2018: Night-time light dynamics during the Iraqi Civil War. *Remote Sensing* 10-6. https://doi.org/10.3390/rs10060858

LUC, Hoare, L. 2024: Dark skies/light impact assessment. *Methodology report*. South Oxfordshire and Vale of White Horse.

Milić, N., Đurđević, Z., Mijalković, S., Erkić, D. 2020: Identifying street hotspots using a network kernel density estimation. Revija za kriminalistiko in kriminologijo 71-4.

Nared, J., Bole, D., Breg Valjavec, M., Ciglič, R., Goluža, M., Kozina, J., Razpotnik Visković, N. et al. 2017: Central settlements in Slovenia in 2016. *Acta geographica Slovenica* 57-2. https://doi.org/10.3986/AGS.4606

Pavlačka, D., Vyvlečka, P., Barvíř, R., Rypl, O., Burian, J. 2023: Influence of COVID-19 on night-time lights in Czechia. *Journal of Maps* 19-1. https://doi.org/10.1080/17445647.2023.2235381

Perko, D., Ciglič, R., Hrvatin, M. 2021: Landscape macrotypologies and microtypologies of Slovenia. *Acta geographica Slovenica* 61-3. https://doi.org/10.3986/AGS.10384

Ravbar, M. 2011: Creative social groups in Slovenia: Contribution to geographic studying of human resources. *Acta geographica Slovenica* 51-2. https://doi.org/10.3986/AGS51204

Ścieżor, T. 2021: Effect of street lighting on the urban and rural night-time radiance and the brightness of the night sky. *Remote Sensing* 13-9. https://doi.org/10.3390/rs13091654

Sessa, C. 2021: Territorial quality of life: A case study in the cross-border area Trieste-Koper-Istria. *Futuribili – Rivista di studi sul futuro e di previsione sociale* 26-1,2. https://doi.org/10.13137/1971-0720/34414

Šumrada, R. 2005: Strukture podatkov prostorske analize. Fakulteta za gradbeništvo in geodezijo Univerze v Ljubljani.

Valinger Sluga, M., Ažman Momirski, L. 2024: Planning ports in proximity: Koper and Trieste after 1945. *Planning Perspectives* 39-2. https://doi.org/10.1080/02665433.2023.2301411

Vlaj, S. 2012: The system of local self-government in Slovenia with a special emphasis on the status of the capital city Ljubljana. *Hrvatska i komparativna javna uprava: časopis za teoriju i praksu javne uprave* 12-3.

Wallner, S., Puschnig, J., Stidl, S. 2023: The reliability of satellite-based light trends for dark sky areas in Austria. *Journal of Quantitative Spectroscopy and Radiative Transfer* 311. https://doi.org/10.1016/j.jqsrt.2023.108774

Wang, S., Li, A., Wen, K., Wu, X. 2020: Robust kernels for kernel density estimation. *Economics Letters* 191. https://doi.org/10.1016/j.econlet.2020.109138

Wang, Z., Miguel, O. R., Shrestha, R., Yao, T., Kalb, V. 2022: Black Marble User Guide (Version 1.3). *User guide*. National Aeronautics and Space Administration.

Widmer, K., Beloconi, A., Marnane, I., Vounatsou, P. 2022: Review and assessment of available information on light pollution in Europe. ETC HE Report 2022/8. *Report*. Zenodo. https://doi.org/10.5281/zenodo.7314224

Wolfe, R. E., Lin, G., Nishihama, M., Tewari, K. P., Tilton, J. C., Isaacman, A. R. 2013: Suomi NPP VIIRS prelaunch and on-orbit geometric calibration and characterization. *Journal of Geophysical Research: Atmospheres* 118-20. https://doi.org/10.1002/jgrd.50873

Wu, B., Huang, H., Wang, Y., Shi, S., Wu, J., Yu, B. 2023: Global spatial patterns between nighttime light intensity and urban building morphology. *International Journal of Applied Earth Observation and Geoinformation* 124. https://doi.org/10.1016/j.jag.2023.103495

Xu, G., Xiu, T., Li, X., Liang, X., Jiao, L. 2021: Lockdown induced night-time light dynamics during the COVID-19 epidemic in global megacities. *International Journal of Applied Earth Observation and Geoinformation* 102. https://doi.org/10.1016/j.jag.2021.102421

Žiberna, I. 2016: Svetlobna onesnaženost na območju Maribora. *Revija za geografijo* 11-2.

Žiberna, I., Gulič, J. 2020: Svetlobna onesnaženost na območju Pohorja. *Proteus* 83-2,3,4,5.

Žiberna, I., Ivajnšič, D. 2018: Daljinsko zaznavanje svetlobne onesnaženosti v Sloveniji. *Revija za geografijo* 13-1.

Žiberna, I., Konečnik Kotnik, E. 2021: Svetlobna onesnaženost v Evropi in Sloveniji. Geografija v šoli 29-3. https://doi.org/10.59132/geo/2021/3/28-38

Acta geographica Slovenica, 66-1, 2026, 179–196

MACHINE LEARNING-BASED LANDSLIDE SUSCEPTIBILITY ASSESSMENT FOR SHALLOW LANDSLIDE MITIGATION IN THE GUMITIR MOUNTAIN AREA, INDONESIA

Entin Hidayah, Mokhammad Farid Maruf, Siti Norafida Jusoh, Joko Widodo, Afif Amiluddin



JAGAT ADI SAMUDRA

Potential landslides on the prone path of Mount Gumitir, Jember.

DOI: https://doi.org/10.3986/AGS.14449
UDC: 551.435.62(594.59)
Creative Commons CC BY-SA 4.0

Entin Hidayah[1], Mokhammad Farid Maruf[1], Siti Norafida Jusoh[2], Joko Widodo[3], Afif Amiluddin[4]

Machine learning-based landslide susceptibility assessment for shallow landslide mitigation in the Gumitir Mountain Area, Indonesia

ABSTRACT: Recurrent rainfall-induced landslides in Gumitir, East Java, threaten the Jember–Banyuwangi route. This study aims to develop mitigation strategies by analyzing influencing factors and predicting landslide-prone areas using logistic regression and random forest models. A dataset consisting of 96 landslide and 180 non-landslide points was randomly divided into a set for model training (70%) and testing (30%). The random forest model outperformed logistic regression with slope, elevation, flow accumulation, topographic wetness index, normalized difference vegetation index, and aspect identified as the most influential factors. These results support targeted and effective landslide risk mitigation.

KEYWORDS: landslide susceptibility assessment, logistic regression, random forest modeling, geospatial analysis, slope stability, hydrological factors, mountainous area

Ocena plazovitosti na podlagi strojnega učenja za zmanjšanje tveganja nastanka plitvih plazov na območju gore Gumitir v Indoneziji

POVZETEK: Ponavljajoči se plazovi, ki se na območju gore Gumitir na Vzhodni Javi sprožajo zaradi dežja, ogrožajo prometno povezavo med mestoma Jember in Banyuwangi. Namen članka je razviti strategije za zmanjšanje tveganja nastanka plazov na podlagi analize vplivnih dejavnikov in napovedi plazovitih območij z modeli logistične regresije in naključnih gozdov. Podatkovni niz, sestavljen iz 96 lokacij plazov in 180 lokacij brez plazov, je bil naključno razdeljen v množico za učenje (70%) in testiranje (30%) modelov. Z modelom naključnih gozdov so bili doseženi boljši rezultati kot z modelom logistične regresije, pri čemer so bili kot najvplivnejši dejavniki opredeljeni naklon, nadmorska višina, akumulacija toka, indeks topografske vlažnosti, normaliziran diferencialni vegetacijski indeks in ekspozicija. Rezultati podpirajo ciljno usmerjeno in učinkovito zmanjševanje tveganja nastanka plazov.

KLJUČNE BESEDE: ocena plazovitosti, logistična regresija, modeliranje z metodo naključnega gozda, geoprostorska analiza, stabilnost pobočij, hidrološki dejavniki, gorsko območje

The article was submitted for publication on May 14th 2025.
Uredništvo je prejelo prispevek 14. maja 2025.

[1] University of Jember, Department of Civil Engineering, Jember, Indonesia
[2] Universiti Teknologi Malaysia, Faculty of Civil Engineering, Johor Bahru, Johor, Malaysia
[3] Research Center for Geoinformatics, National Research and Innovation Agency (BRIN), Bogor, Indonesia
[4] Universitas Mochammad Sroedji, Civil Engineering Department, Engineering Faculty, Jember, Indonesia

entin.teknik@unej.ac.id (https://orcid.org/0000-0002-1233-6850), farid.teknik@unej.ac.id (https://orcid.org/0000-0002-5715-935X), snorafida@utm.my (https://orcid.org/0000-0002-7132-0883), jecko.emji2@gmail.com (https://orcid.org/0000-0002-0552-5100), afif@umsj.ac.id (https://orcid.org/0009-0000-8600-0922)

1 Introduction

Landslide hazards in tropical mountainous regions have intensified due to extreme rainfall patterns linked to climate change, threatening critical infrastructure such as road networks (Alcántara-Ayala 2025). It is the most significant geological hazard that poses a major threat to life, infrastructure, and environmental stability. A range of factors, such as intense rainfall, slope geometry, geological conditions, weak or collapsible soil materials, groundwater table position, deforestation, and many more, can influence the landslide occurrence. In tropical regions, this is further aggravated by the high-intensity rainfall events that elevate pore water pressure, reduce the shear strength in soil, and hence increase the slope failure probability (Rosly et al. 2023; Sarah et al. 2024). In Gumitir, East Java, Indonesia, many slopes have been explored for farming purposes and modified without comprehensive geotechnical investigation or proper design, hence inducing recurrent landslides along the Jember-Banyuwangi highway that disrupt regional connectivity, endanger lives, and incur high economic costs. The current approach to landslide mitigation is still reactive and not preventive. It focuses on landslide-prone spots only after a landslide has occurred. Addressing landslides at these specific spots provides only temporary solutions without addressing the root causes, leaving problems for the future, as is the case today. Referring to previous mitigation efforts, there is an urgent need to handle landslide occurrences. Hence, it is important to develop future landslide mitigation strategies to reduce adverse impacts and address landslide occurrences based on scientific approaches for landslide susceptibility mapping (Getachew and Meten 2021). To develop a more comprehensive landslide mitigation strategy, a vulnerability assessment is necessary (Abdulwahid and Pradhan 2017). In landslide vulnerability assessments, understanding the spatial causes of landslides and predicting potential landslide locations is crucial. Both geomorphological and environmental factors contribute significantly to landslides, making their investigation essential (Kohno and Higuchi 2023). These factors will naturally have a strong impact on the landslide distribution.

Recent disadvantages and advances in machine learning (ML) and geospatial analysis have enabled data-driven landslide susceptibility assessments in identifying risk zones. While advanced techniques like support vector machines (SVM), k-means, hierarchical clustering, self-organizing maps (SOMs), artificial neural networks (ANNs), and Bayesian networks have been applied in landslide susceptibility studies, their high computational complexity, extensive data requirements, and limited interpretability hinder practical adoption (Le et al. 2024; Teng et al. 2024). Decision trees in landslide prediction struggle with overfitting and parameter sensitivity, leading to unreliable predictions and reduced interpretability as deep trees obscure dominant factors, limiting their practical utility for policymakers (Park et al. 2019; Teng et al. 2024). The multi-layer perceptron (MLP) model requires high computational resources and a large training dataset, and although it offers high accuracy, it is difficult to interpret due to its nature (Teng et al. 2024). Random forest (RF) and logistic regression (LR) methods minimize error and provide reasonable spatial resolutions (Huang, F. et al. 2023). The application of LR is highly beneficial for predicting landslide susceptibility, representing the outcomes based on the influential factors triggering landslides (Huang, F. et al. 2023). Meanwhile, RF has several advantages, including reducing the risk of overfitting (Munawar et al. 2022; Rong et al. 2023). This algorithm can be used for the problems of both regression and classification (Saha et al. 2022; Le et al. 2024) and is effective for determining variable importance by measuring the decrease in model accuracy (Achour and Pourghasemi 2020; Huang, F. et al. 2023; Rong et al. 2023). However, most studies focus on the accuracy of susceptibility mapping without translating results into actionable mitigation frameworks, especially in tropical road networks where slope stability, drainage, and vegetation dynamics interact uniquely. Furthermore, the role of aspect (slope orientation) in landslide initiation remains understudied, as its influence is often conflated with elevation and rainfall patterns. In shallow landslides, south-facing slopes exhibit distinct soil properties (higher silt, slower pore-pressure dissipation), necessitating aspect-specific models for accurate predictions (Guo and Ma 2023).

This study proposes an integrated ML-geospatial framework using the example of landslide risks in Gumitir, East Java, through three primary objectives: (1) identifying dominant geospatial triggers of landslides, including slope, elevation, aspect, and hydrological factors, (2) evaluating the comparative performance of RF and LR models in predicting landslide-prone zones under tropical mountainous conditions, and (3) translating susceptibility mapping results into spatially targeted mitigation strategies to enhance road resilience. The work seeks to determine the relative influence of geospatial variables on landslide susceptibility, assess the robustness of RF and LR in high-rainfall environments, and demonstrate

how predictive models can directly inform engineering interventions, such as reinforced drainage systems in high-flow accumulation areas or slope stabilization measures in steep terrain, to reduce risks proactively.

2 Study area

This study focuses on the Gumitir Mountain area, located along the road connecting Jember and Banyuwangi districts (Figure 1). The region lies on the border of both districts and is hereafter referred to as the »Gumitir Mountain Area.« It covers a micro-watershed of approximately 1,814.07 ha, with elevations ranging from 420 to 967 m above sea level.

The Gumitir Mountain Area is predominantly mountainous, with land cover consisting mainly of forest and plantations. This region has experienced multiple landslides in the past, particularly along the Jember–Banyuwangi road corridor, where slope failures have disrupted traffic and damaged infrastructure (Figure 2). As illustrated in Figure 2a), the observed failures are predominantly shallow translational soil slides developing within the weathered, clay-rich residual soil layer and occurring in proximity to the road embankment. Figure 2b) further shows damage to road infrastructure, including deformed guardrails and exposed utility cables, indicating the combined effects of slope instability, surface erosion, and localized drainage disturbance along the road corridor.

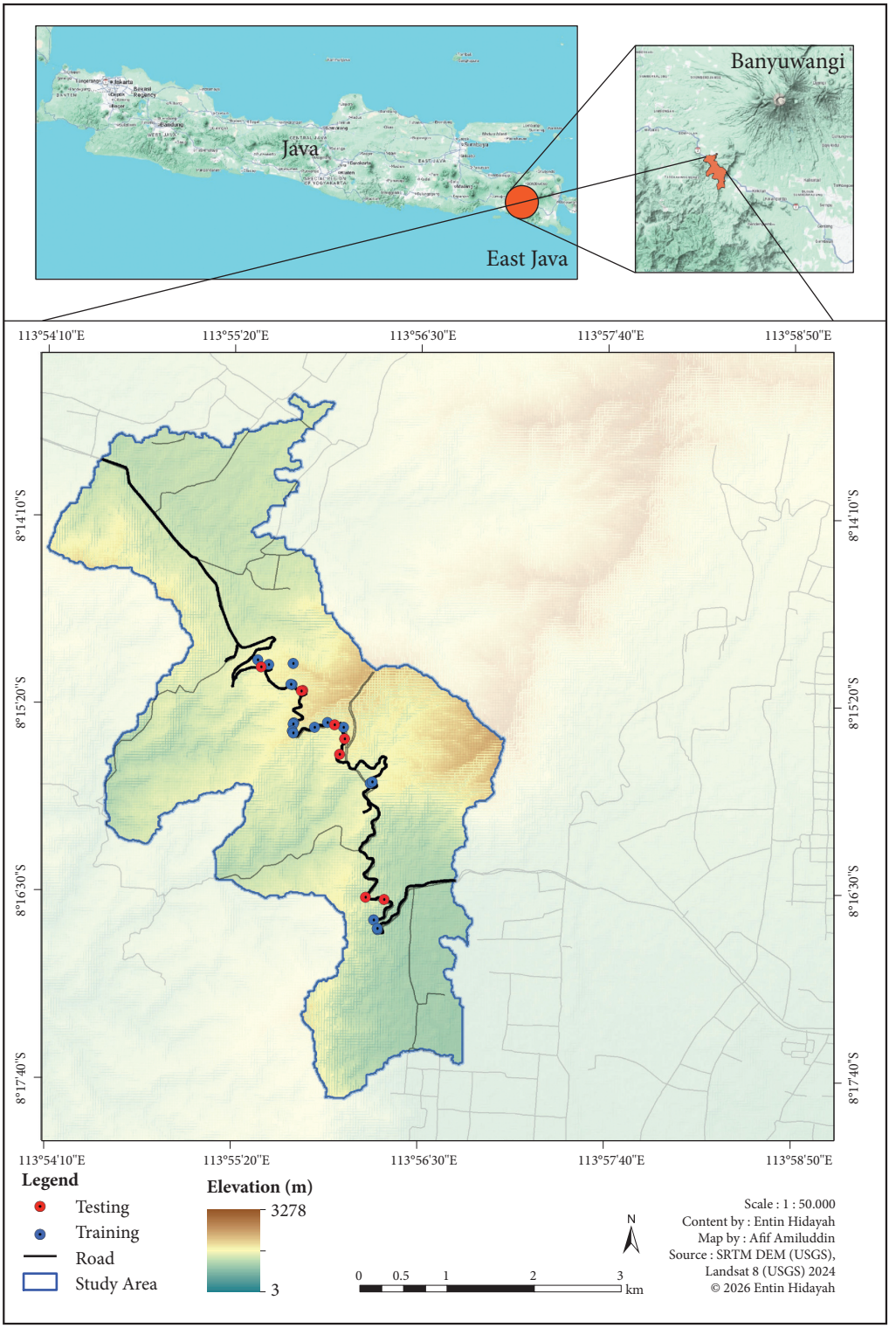
The concentration of mapped landslides along the road corridor may partly reflect an observational bias, as slope failures in remote and inaccessible valleys are more difficult to detect in the absence of road access. However, the morphological evidence observed adjacent to the road also indicates that road cuttings and localized drainage disturbances have directly contributed to slope instability in the Gumitir Mountain Area. Increasing population pressure has intensified land use in hilly terrain, making slope utilization and infrastructure development unavoidable. Consequently, mapping landslide-prone areas is essential for identifying potential hazards and supporting risk-informed and sustainable development planning.

Geologically, the Gumitir Mountain Area range is entirely underlain by the Batuampar Formation, consisting of medium-grained clastic sandstone deposited in a littoral environment. Prolonged tropical weathering has transformed this formation into thick, clay-rich residual soils with low permeability, resulting in a geologically fragile setting. Annual rainfall ranges from 1900 to 3000 mm, concentrated during the wet season (October–April). This setting is highly sensitive to intense tropical rainfall, as high seasonal precipitation promotes soil saturation, elevates pore-water pressure, and reduces effective shear strength. These processes collectively increase slope instability and predispose the area to rainfall-induced slope failures.

Figure 1: Study area. ➤ p. 183



Figure 2: a) Example of a shallow landslide causing road collapse along the Jember-Banyuwangi route in the Gumitir Mountain Area, and b) damage to road infrastructure, including guardrails and exposed utility cables, following a landslide event.


Java
East Java
Banyuwangi
113°54'10"E
113°55'20"E
113°56'30"E
113°57'40"E
113°58'50"E
8°14'10"S
8°15'20"S
8°16'30"S
8°17'40"S
Legend
Testing
Training
Road
Study Area
Elevation (m)
3278
3
0 0.5 1 2 3
km
N
Scale : 1 : 50.000
Content by : Entin Hidayah
Map by : Afif Amiluddin
Source : SRTM DEM (USGS),
Landsat 8 (USGS) 2024
© 2026 Entin Hidayah

3 Research methodologies

The research implementation is divided into three stages: (1) data preparation and processing, (2) identifying the factors that condition landslides based on landslide susceptibility mapping, and (3) determining landslide mitigation strategies.

The spatial dataset comprised 96 landslide occurrence points and 180 non-landslide points, derived from field surveys, remote sensing interpretation, and ancillary data. To evaluate the predictive performance of the models, the dataset was randomly divided into two subsets: 70% for model training and 30% for testing. This partitioning ensured that the model calibration and validation processes were conducted on mutually exclusive data, thereby minimizing the risk of over-fitting and enabling an unbiased assessment of predictive capability.

Two statistical and machine learning approaches, LR and RF, were applied to establish the relationship between landslide occurrences and conditioning factors.

3.1 Data preparation and processing of landslide conditioning factors

Geospatial data were obtained from the Shuttle Radar Topography Mission (SRTM) Digital Elevation Model (DEM) and Landsat 8 imagery. Six factors, which have been used in previous landslide susceptibility studies, were analyzed: elevation, aspect, slope, flow accumulation (FA), topographic wetness index (TWI), and normalized difference vegetation index (NDVI) (Liu, S. et al. 2021; Feng et al. 2022; Kohno and Higuchi 2023; Okoli et al. 2023). The data sources and processing methods are listed in Table 1.

Slope is a measure of the angle of the steepness of a land surface or slope. Aspect is the prevailing slope direction of a terrain surface, indicating how much an area is exposed to environmental factors like sunlight, wind, and rainfall, which subsequently influences the rate of weathering and the soil's moisture levels (Getachew and Meten 2021). Elevation often appears as a key predictor in landslide prediction models, although it may only serve as a proxy for other, more meaningful variables such as slope curvature or aspect (Hussain et al. 2022). TWI is one of the factors frequently used in landslide susceptibility studies (Dahim et al. 2023; Fan et al. 2023). TWI measures the potential for water accumulation in an area based on topography, which can affect slope stability and trigger landslides. TWI represents the spatial wetness level of a basin, expressed by equation (1) (Beven and Kirkby 1979):

$$TWI = ln\left(\frac{\partial}{tan\beta}\right) \quad \text{Equation (1),}$$

where ∂ represents the area drained per unit length of contour at a given point, and tan β is the slope angle at the point.

The FA represents the total area of land contributing surface runoff to a specific location, where water tends to accumulate. It is computed by summing the number of upstream cells that drain into a particular downslope cell from a given reference point. The FA is obtained for each cell in the DEM grid. The NDVI is a factor that describes the vegetation density in a certain area. Bare land without vegetation is more susceptible to landslides than forests or grasslands with higher NDVI (Acharya and Lee 2019). The NDVI value represents vegetation cover from low to high, with a value range from −1 to 1, respectively. The NDVI is formulated as in equation (2):

$$NDVI = \frac{(NIR-RED)}{(NIR+RED)} \quad \text{Equation (2),}$$

where NIR represents the near-infrared band, and RED represents the reflection values of the red band.

The values for each class of landslide conditioning factors, processed from various satellite image data sources, can be seen in Table 1 and Figure 3.

Figure 3: Influencing factors for landslide susceptibility mapping: a) elevation, b) aspect, c) TWI, d) FA, e) slope, f) NDVI. ► p. 185

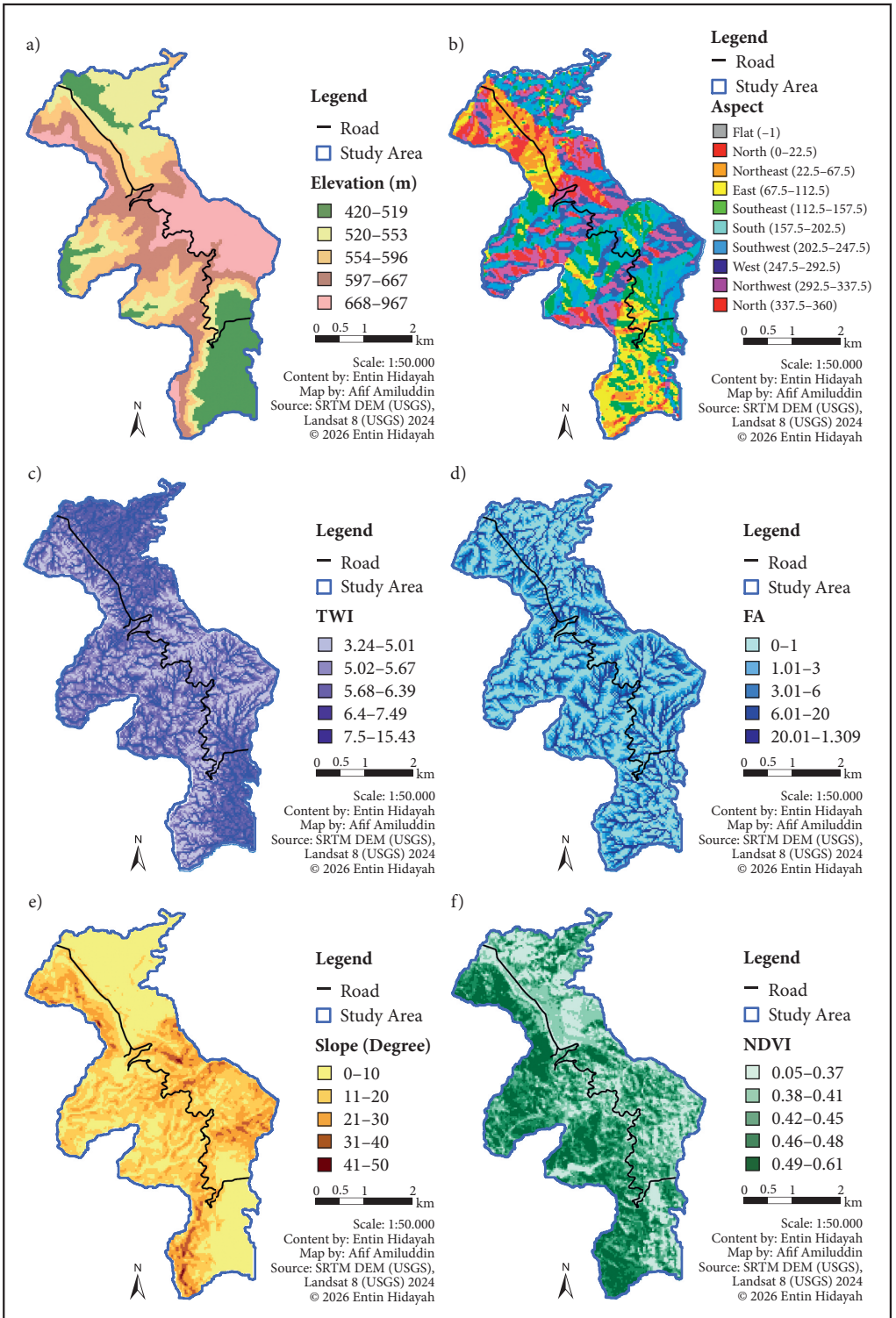

a)
Legend
Road
Study Area
Elevation (m)
420–519
520–553
554–596
597–667
668–967
0 0.5 1 2 km
Scale: 1:50.000
Content by: Entin Hidayah
Map by: Afif Amiluddin
Source: SRTM DEM (USGS), Landsat 8 (USGS) 2024
© 2026 Entin Hidayah
N
b)
Legend
Road
Study Area
Aspect
Flat (–1)
North (0–22.5)
Northeast (22.5–67.5)
East (67.5–112.5)
Southeast (112.5–157.5)
South (157.5–202.5)
Southwest (202.5–247.5)
West (247.5–292.5)
Northwest (292.5–337.5)
North (337.5–360)
0 0.5 1 2 km
Scale: 1:50.000
Content by: Entin Hidayah
Map by: Afif Amiluddin
Source: SRTM DEM (USGS), Landsat 8 (USGS) 2024
© 2026 Entin Hidayah
N
c)
Legend
Road
Study Area
TWI
3.24–5.01
5.02–5.67
5.68–6.39
6.4–7.49
7.5–15.43
0 0.5 1 2 km
Scale: 1:50.000
Content by: Entin Hidayah
Map by: Afif Amiluddin
Source: SRTM DEM (USGS), Landsat 8 (USGS) 2024
© 2026 Entin Hidayah
N
d)
Legend
Road
Study Area
FA
0–1
1.01–3
3.01–6
6.01–20
20.01–1.309
0 0.5 1 2 km
Scale: 1:50.000
Content by: Entin Hidayah
Map by: Afif Amiluddin
Source: SRTM DEM (USGS), Landsat 8 (USGS) 2024
© 2026 Entin Hidayah
N
e)
Legend
Road
Study Area
Slope (Degree)
0–10
11–20
21–30
31–40
41–50
0 0.5 1 2 km
Scale: 1:50.000
Content by: Entin Hidayah
Map by: Afif Amiluddin
Source: SRTM DEM (USGS), Landsat 8 (USGS) 2024
© 2026 Entin Hidayah
N
f)
Legend
Road
Study Area
NDVI
0.05–0.37
0.38–0.41
0.42–0.45
0.46–0.48
0.49–0.61
0 0.5 1 2 km
Scale: 1:50.000
Content by: Entin Hidayah
Map by: Afif Amiluddin
Source: SRTM DEM (USGS), Landsat 8 (USGS) 2024
© 2026 Entin Hidayah
N

Table 1: Classification, source, classification method, and references for the factors.

Factor	Classes	Source (provided by)
Elevation (m)	(i) 420.00–518.67, (ii) 518.68–553.00, (iii) 553.01–595.90, (iv) 595.91–666.69, (v) 666.70–967.00	SRTM DEM: 30m × 30m United States Geological Survey (USGS) via EarthExplorer (https://earthexplorer.usgs.gov/)
Aspect (°)	Flat: -1, North: 0.0–22.5, Northeast: 22.5–67.5, East: 67.5–112.5, Southeast: 112.5–157.5, South: 157.5–202.5, Southwest: 202.5–247.5, West: 247.5–292.5, Northwest: 292.5–337.5, North: 337.5–360	Derived from DEM: 30m × 30m
Topographic wetness index (TWI)	(i) 3.24–5.01, (ii) 5.02–5.67, (iii) 5.68–6.39, (iv) 6.40–7.49, (v) 7.5–15.43	Derived from DEM: 30m × 30m equation (2)
Flow accumulation (FA)	(i) 0.0–1.00, (ii) 1.01–3.00, (iii) 3.01–6.00, (iv) 6.01–20.00, (v) 20.01–1,309	Derived from DEM: 30m × 30m
Slope (°)	(i) 0–10, (ii) 11–20, (iii) 21–30, (iv) 31–40, (v) 41–50	Derived from DEM: 30m × 30m
Normalized difference vegetation index (NDVI)	(i) 0.05 - 0.37, (ii) 0.38 - 0.41, (iii) 0.42 - 0.45, (iv) 0.46 - 0.48, (v) 0.49 - 0.61	Landsat 8 (OLITIRS) United States Geological Survey (USGS) via EarthExplorer (https://earthexplorer.usgs.gov/)

3.2 Multicollinearity testing and feature selection in landslide susceptibility modeling

Analyzing the factors causing landslides is important in susceptibility studies, as each factor may have a different influence on prediction results (Bravo-López et al. 2023; Huang, F. et al. 2023; Saha et al. 2023). To ensure model accuracy, landslide-causing factors need to be tested for multicollinearity and Spearman's rank correlation to examine relationships between variables.

In regression models, independent variables should not have perfect linear relationships with each other. High correlation among variables can cause problems in modeling and result interpretation. Therefore, multicollinearity testing is necessary, typically by calculating the Variance Inflation Factor (VIF) (Liu, R. et al. 2022; Saha et al. 2023).

Multicollinearity diagnosis is essential before modeling to ensure that no susceptibility factors are influencing each other. Potential multicollinearity in the dataset can be identified if VIF values exceed 5 or tolerance values fall below 0.1 (Huang, F. et al. 2023). If two indicators in the dataset fall within the expected range, it suggests that there is no significant multicollinearity among the landslide susceptibility factors.

Spearman correlation analysis evaluates relationships among independent variables to identify the most relevant factors, reducing uncertainty and improving model performance. Factors with high correlation coefficients are considered redundant and should be removed (Bravo-López et al. 2023). A Spearman correlation coefficient of 0.70 or lower is typically used as a cut-off point for identifying suitable features (Gu et al. 2026).

3.3 Logistic regression model

The LR model is a form of linear regression normalized by the sigmoid function (logistic function). This approach is used to predict landslide occurrence by assuming a binary response variable, i.e., occurrence (landslide occurred) and non-occurrence (no landslide), based on categorical and continuous variables (Liu, Y. et al. 2022). A value of 1 indicates a location where a landslide has taken place, while a value of 0 represents an area where no landslide occurred. The landslide triggering parameters and their relationships are calculated using the logistic equation as in equation (3):

$$P = \frac{1}{1+e^{-z}} \quad \text{Equation (3),}$$

where P denotes the estimated likelihood of a landslide, ranging from 0 to 1 and forming an S-shaped curve, while z represents the combined effect of contributing factors like slope, as calculated using equation (4) below. Here, e is Euler's constant (approximately 2.71828), the base of the natural logarithm.

Equation (4),

where bi (i = 0, 1, 2, …, n) represents the LR coefficients, and xi (i = 0, 1, 2, …, n) represents the conditioning factors, with n being the number of input variables (Rong et al. 2023).

3.4 Random forest

RF has been utilized to solve complex problems in data science due to its high accuracy and interpretability. It operates effectively without the need for feature scaling or encoding categorical variables, and it typically involves minimal parameter adjustment (Sarkar et al. 2022). The RF algorithm determines its final prediction based on majority voting, aiming to minimize prediction error. It comprises numerous decision trees, each incorporating two layers of randomness. First, every tree is trained using a randomly drawn subset of the original dataset. Second, at each decision node, a random selection of features is evaluated to find the optimal split.

The overall workflow of RF involves: (1) randomly sampling subsets from the dataset; (2) constructing individual decision trees from each sample and generating predictions; and (3) aggregating the predictions, using the most common output for classification tasks and the average (mean) for regression tasks.

3.5 Model performance

The model's performance is evaluated by comparing the results of landslide susceptibility models using the area under the curve (AUC) value. AUC quantifies the area beneath the receiver operating characteristic (ROC) curve, which is a plot showing the model's performance by comparing the true positive rate (TPR) or sensitivity against the False Positive Rate (FPR) or 1-Specificity across different thresholds. The ROC curve helps assess the model's ability to differentiate between positive and negative classes, with a curve closer to the top-left corner indicating better performance. AUC values range from 0.5 to 1, where a higher AUC indicates superior model performance. An AUC of 0.5 suggests random guessing, while values closer to 1 reflect excellent predictive capability. In this study, the results of two models were validated using 48 landslides, and the accuracy of the model predictions was further assessed by calculating the proportion of landslide pixels in each vulnerability zone.

4 Results

4.1 Factors that most significantly influence landslide susceptibility in the Gumitir Mountain Area

The results of the multicollinearity test for all factors (Table 2) show that all VIF values are less than 5, and tolerance values exceed 0.1, indicating that all variables are independent and there is no potential multicollinearity among them. Therefore, the six factors, i.e., slope, aspect, elevation, TWI, FA, and NDVI, can be used for feature selection.

Otherwise, the conditioning factors need to be tested to meet the model analysis requirements for factor dependencies. Based on Table 3, Spearman's correlation test indicates that all factors have values below 0.7, suggesting that there is no interdependence among the factors. The six selected environmental factors, elevation, slope, aspect, FA, NDVI, and TWI, have different levels of influence on landslide contribution.

Table 2: Multicollinearity analysis.

Term	Elevation	Slope	Aspect	FA	NDVI	TWI
VIF	1.402	1.446	1.193	1.279	1.035	1.573
Tolerance	0.713	0.692	0.838	0.782	0.966	0.636

Table 3: Spearman correlation.

Factor	Elevation	Slope	Aspect	FA	NDVI	TWI
Elevation	1.000	0.521	0.177	–0.047	0.057	–0.376
Slope		1.000	–0.004	0.045	0.145	–0.488
Aspect			1.000	–0.018	–0.146	–0.047
FA				1.000	0.001	0.429
NDVI					1.000	–0.102
TWI						1.000

Therefore, these factors can be used in the classification process using RF, considering that the response variable is categorical.

4.2 Comparing the LR and RF applications for landslide susceptibility

Slope was identified as the primary factor affecting landslide susceptibility in the RF model, with an average merit value of 0.75, followed by FA, 0.7, and NDVI (0.64), elevation (0.6), and TWI (0.57). Aspect (0.54) exhibited comparatively lower contributions (Figure 4). These results underscore the critical role of slope steepness and hydrological conditions (FA) in driving landslide risks, while highlighting the secondary but non-negligible influence of vegetation cover and soil moisture dynamics.

The LR model identified specific thresholds for landslide triggers (Figure 5). The analysis was based on the odds ratios of several key factors influencing landslide susceptibility, including elevation, slope, aspect, FA, NDVI, and TWI. A larger odds ratio signifies a greater probability of a landslide occurring as the value of the factor increases. Areas with elevations between 662.04 m and 702.27 m show the highest odds ratio (8.1), indicating that these areas have the greatest chance of experiencing landslides compared to other elevation classes. Conversely, elevations below or above this range have lower odds ratios.

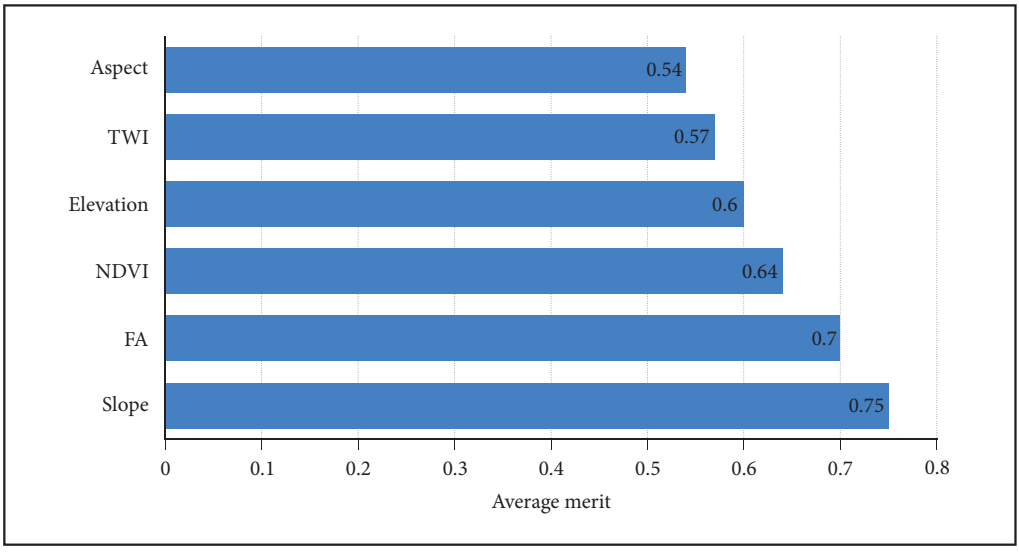
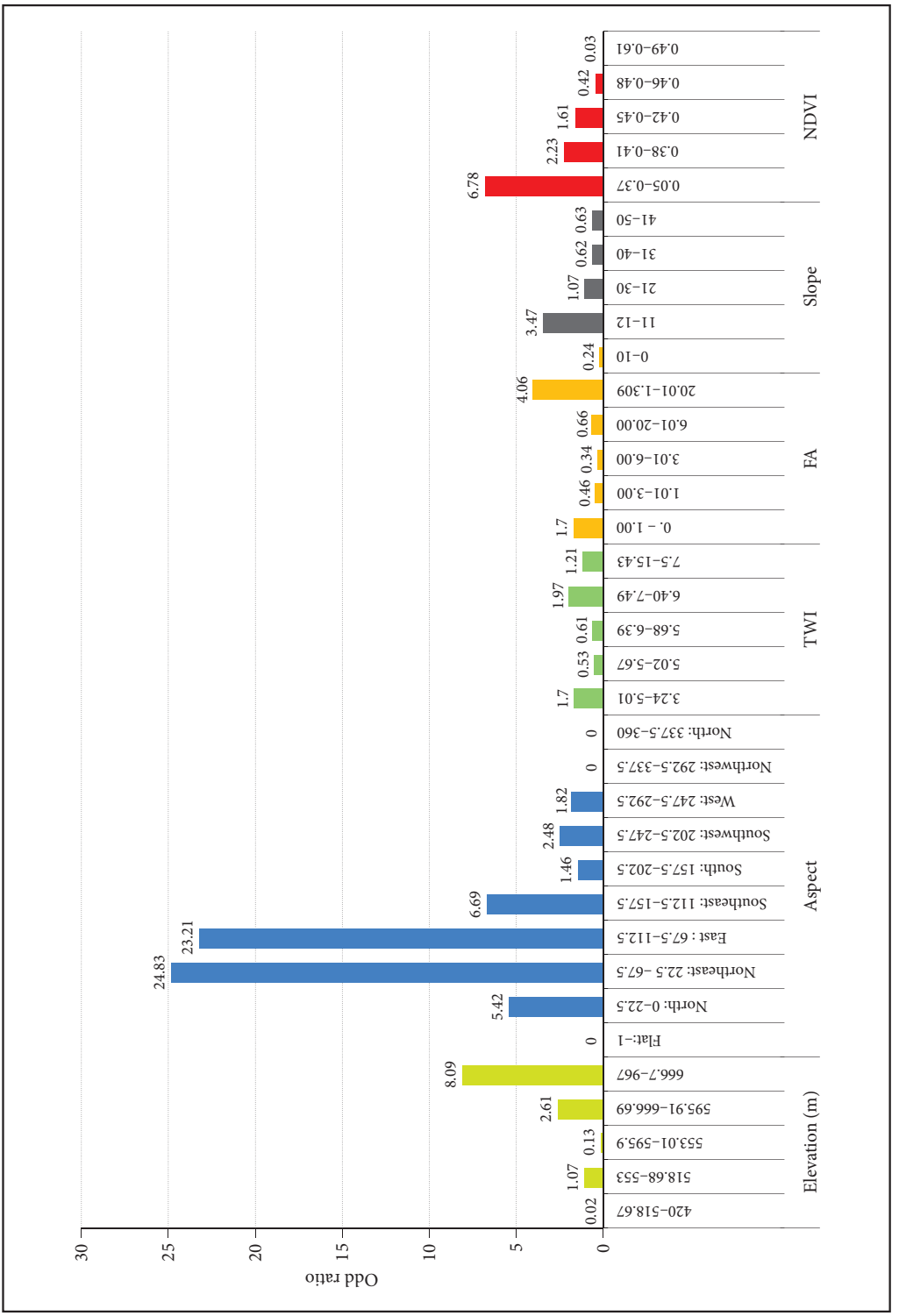


Figure 4: Average merit of the RF model.

Figure 5: Odds ratio of the logistic regression method. ➤ p. 189


Odd ratio
0
5
10
15
20
25
30
Elevation (m)
420–518.67
518.68–553
553.01–595.9
595.91–666.69
666.7–967
Flat:–1
Aspect
North: 0–22.5
Northeast: 22.5 –67.5
East : 67.5–112.5
Southeast: 112.5–157.5
South: 157.5–202.5
Southwest: 202.5–247.5
West: 247.5–292.5
Northwest: 292.5–337.5
North: 337.5–360
TWI
3.24–5.01
5.02–5.67
5.68–6.39
6.40–7.49
7.5–15.43
FA
0. – 1.00
1.01–3.00
3.01–6.00
6.01–20.00
20.01–1.309
Slope
0–10
11–12
21–30
31–40
41–50
NDVI
0.05–0.37
0.38–0.41
0.42–0.45
0.46–0.48
0.49–0.61
0.02
1.07
0.13
2.61
8.09
0
5.42
24.83
23.21
6.69
1.46
2.48
1.82
0
0
1.7
0.53
0.61
1.97
1.21
1.7
0.46
0.34
0.66
4.06
0.24
3.47
1.07
0.62
0.63
6.78
2.23
1.61
0.42
0.03

Slopes with a gradient of 10–20° show a high odds ratio of 3.5, followed by slopes with gradients of 0–10° (1.1) and 20–30° (1.0). This suggests that slopes with moderate gradients are more susceptible to landslides compared to very steep or very gentle slopes.

Aspects with orientations of 67.5–112.4° show a very high odds ratio of 24.8, and aspects of 112.5–157.4° have an odds ratio of 23.2. This indicates that slopes facing certain directions have a significantly higher landslide risk.

The highest FA values, between 2.92 and 11.3, correspond to an odds ratio of 4.1, suggesting that areas with elevated water FA are more susceptible to landslides. Areas with TWI values between 6.40 and 7.49 exhibit the highest odds ratio (1.97), indicating that locations with greater moisture accumulation and soil saturation tend to be more susceptible to landslides due to reduced soil shear strength and increased pore-water pressure.

While both models confirmed slope and hydrology as key drivers, RF provided granular insights into variable importance, whereas LR quantified risk thresholds for specific parameter ranges. RF prioritized slope stability (merit = 0.75), aligning with LR's identification of moderate slopes (10–20°) as high-risk zones. LR revealed extreme susceptibility of northeast-facing slopes (odds ratio > 20), a nuance not explicitly captured by RF's lower aspect merit (0.54). Both models emphasized the protective role of vegetation (RF: NDVI merit = 0.64; LR: low NDVI odds ratio = 6.8).

These findings highlight the complementary strengths of RF (variable ranking) and LR (threshold-specific risk quantification) in guiding targeted interventions. For example, stabilizing moderate slopes (10–20°) and restoring vegetation in low-NDVI areas could reduce risks by addressing both RF- and LR-identified vulnerabilities.

4.3 Landslide susceptibility map

The performance of the LR and RF models was evaluated using the ROC curve and AUC for the testing dataset (Figure 6). The LR model shows accuracy with an AUC value of 0.931, while the RF model has an AUC value of 0.865. This indicates that spatial landslide susceptibility analysis using both RF and LR models provides outstanding accuracy and can be relied upon for predicting landslides.

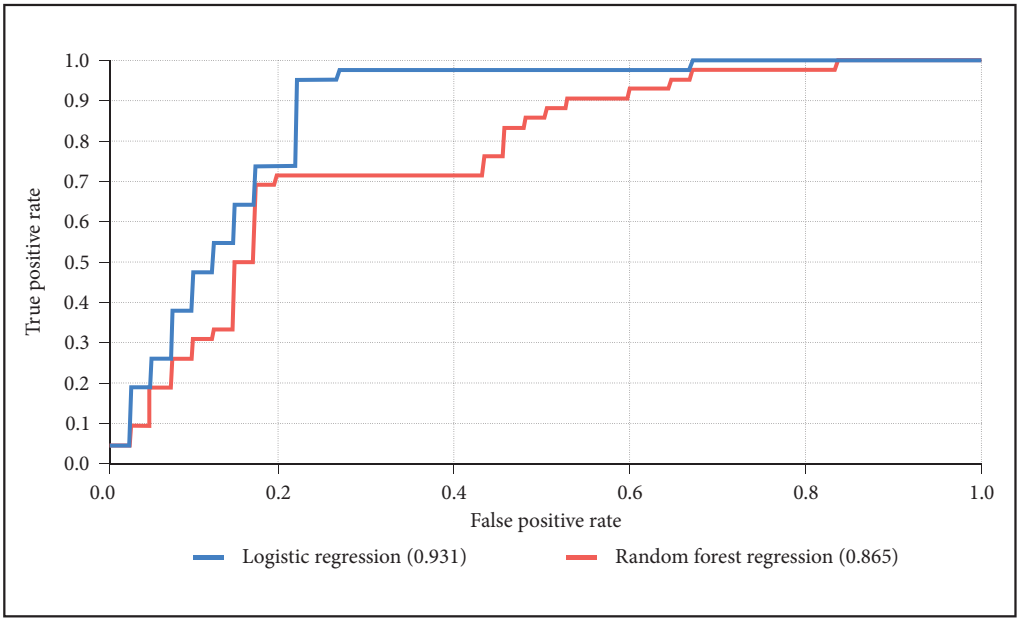


Figure 6: ROC curves illustrating the performance of the LR and RF models.

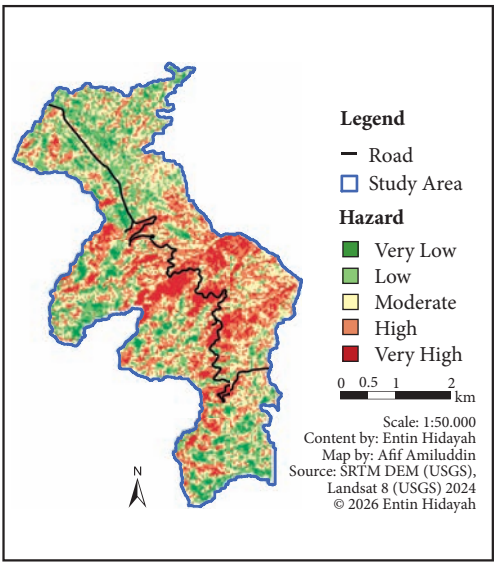


Figure 7: Landslide susceptibility mapping using RF.

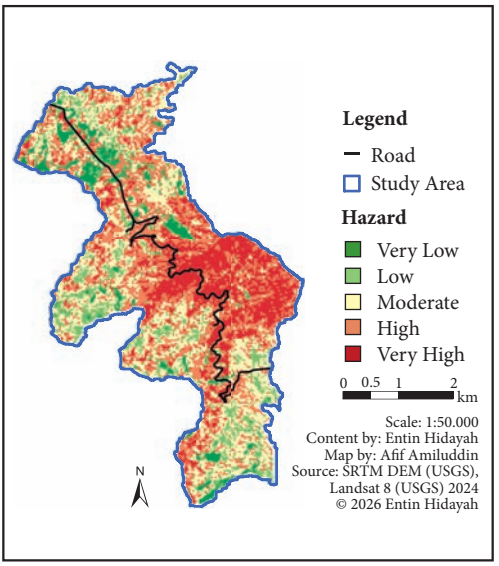


Figure 8: Landslide susceptibility mapping using LR.

Landslides with very high indices are primarily concentrated in the central area of the study region and along the road. The continuous landslide susceptibility index values generated by both models were then reclassified into five hazard classes (Very Low, Low, Moderate, High, and Very High) using the Natural Breaks (Jenks) classification method. This method identifies natural groupings inherent in the data to create an optimal classification. The final susceptibility maps for the RF and LR models are presented in Figure 7 and Figure 8, respectively. In the Gumitir mountain area, landslides are distributed on both sides of the road.

4.4 Proposed mitigation strategies

Based on the RF and LR models, which highlight slope, FA, NDVI, TWI, and aspect as the most critical factors, three integrated strategies are proposed to mitigate shallow landslides in the Gumitir Mountain Area.

The first strategy is slope stabilization and soil management. Terracing on moderate slopes (10–20°) reduces runoff and shear stress, while retaining structures in high FA areas (>2.9) counter hydrostatic pressure. These measures enhance slope resistance and mitigate landslide triggers.

The second strategy emphasizes hydrological control through drainage optimization by constructing swales or subsurface drains in zones with high TWI (>5.78) to divert excess water and balance soil moisture, combined with regular maintenance of natural waterways in high FA areas to avoid blockages during extreme rainfall events.

The third strategy involves vegetation and land use planning, prioritizing reforestation in low-NDVI zones (<0.2) using deep-rooted species such as vetiver grass and bamboo, as well as fast-growing shrubs like Calliandra to improve soil cohesion and ground cover. In addition, aspect-based zoning should restrict development on northeast–southeast-facing slopes (67.5–157.4°), which are highly susceptible due to solar radiation-induced weathering and moisture fluctuations, while maintaining these areas as buffer green belts.

Together, these slope management, hydrological interventions, and ecological restoration measures provide a comprehensive framework for reducing shallow landslide risks in the Gumitir Mountain Area while maintaining ecosystem stability and community resilience.

5 Discussion

The RF-LR synergy provides actionable insights, while RF prioritizes slope and FA, and LR identifies critical thresholds (e.g., elevation bands, aspect angles). In practice, landslide mitigation techniques are often applied partially, focusing on locations that are frequently impacted by landslides. This approach offers only a temporary fix and overlooks root causes, so landslide management needs a holistic understanding to avoid overlooked factors.

Slope angle has been proven to be a dominant predictor of shallow landslides in the RF model (merit value = 0.75) and in the LR model (odds ratio = 3.5 for slopes between 10–20°). Steeper slopes tend to have thinner soil, which increases the role of cohesion and boundary stress, thereby reducing the frequency of landslides despite the additional gravitational pull (Dehnavi et al. 2015; Prancevic et al. 2020). Steeper slopes increase landslide potential because the shear stress on steep slopes tends to rise, as also explained by Ghasemian et al. (2022). Generally, landslides often occur in areas with steep slopes greater than 25° (Ghasemian et al. 2022; Zárate et al. 2023). However, in this case, the slope angle in the range of 10–20° has proven to have a significant impact on shallow landslide occurrences during the rainy season. Landslide characteristics on lower slope gradients are generally triggered by high-intensity rainfall, which increases pore pressure in the soil and reduces soil particle cohesion, eventually triggering soil movement (Liu, Y. et al. 2021). Therefore, slopes that are not very steep are often considered relatively stable, and landslide risks on these slopes are frequently overlooked.

The FA also shows a significant influence on both methods. Water FA plays a crucial role in triggering landslides, especially in areas with high FA values. Rainfall increases soil moisture content and reduces matric suction, leading to a decline in slope stability and triggering landslides. Preferential and matrix flow in unsaturated conditions play important roles in this process (Petrella et al. 2023; Sun et al. 2023). Hydrogeological processes such as rainfall infiltration and groundwater circulation affect slope stability. Water flowing through large pores and cracks can accelerate the landslide process (Bishop et al. 2021; Petrella et al. 2023). In vulnerable areas, especially around water channels, rainwater tends to accumulate and increase hydrostatic pressure, reducing the shear strength, which in turn weakens the soil structure. This condition becomes even more critical during the rainy season when high rainfall causes a drastic increase in FA, magnifying the likelihood of landslides. Therefore, concentrated rainwater can quickly increase pore water pressure, which weakens the soil shear strength, especially in areas with poor drainage or irregular water channels.

The NDVI is an important indicator in determining landslide risk potential, with low NDVI indicating areas with minimal or no vegetation. The NDVI and rainfall are dynamic factors that influence landslides, with higher rainfall and lower NDVI increasing landslide threats (Huang, W. et al. 2023) because vegetation functions as a soil binder through root systems that strengthen slope stability, but only for shallow depth (< 1m) (Ni et al. 2018). Without adequate vegetation, steep slopes and areas with high FA become more vulnerable to soil failure. Therefore, monitoring NDVI in critical locations before the rainy season is crucial to mitigating landslide risks. Areas with low NDVI combined with high slope angles and large FA require special attention for preventive measures, such as planting stabilizing vegetation or soil conservation techniques to enhance slope stability and reduce disaster potential.

Based on TWI, variations in slope stability significantly influence landslide hazard and risk, as indicated by high and low odds ratios. High soil moisture can reduce soil cohesion and weaken slope shear strength, making it more vulnerable to failure, especially during heavy rains that increase soil moisture content. High TWI values are more prone to landslides (Dahim et al. 2023; Zárate et al. 2023). On the other hand, low TWI is generally associated with less moisture accumulation; in some contexts, very low TWI values can indicate very dry soil conditions and potentially have cracks or moisture deficiencies that can lead to soil failure when rain occurs. Low TWI has a strong influence on shallow landslides, especially in areas with high slope gradients and high drainage density (Gullà et al. 2021). Therefore, although high TWI consistently indicates increased landslide risk, low TWI should also be considered a risk factor, particularly in locations with steep slope gradients.

Aspect shows a lower influence compared to other factors, but remains important. Slope orientation can affect the distribution of sunlight and soil moisture, which in turn can influence slope stability. Aspect or slope orientation significantly influences landslide susceptibility, especially through slope hydrology mechanisms and rainfall patterns (Guo and Ma 2023). However, an aspect's influence cannot be evaluated in isolation

and must be considered alongside other factors such as elevation, slope gradient, and geological conditions (Cellek 2021).

The connections between these factors are simultaneous and interdependent in triggering landslides. For example, slope and FA may work together to increase risk, where steep slopes with accumulated water flow are more likely to experience landslides. Similarly, elevation and aspect can affect sunlight exposure and soil moisture levels, impacting vegetation conditions measured by NDVI.

The RF model can capture the complexity of these interactions by assigning different weights to each factor, while LR focuses more on the individual contribution of factors in specific classes. Using both methods simultaneously provide a more holistic understanding of landslide risk, allowing for more accurate and effective mitigation. These results highlight the model's superiority in providing deeper insights into the environmental dynamics underlying landslide risk, ultimately aiding in more effective risk mitigation decision-making. In this study, the RF model demonstrated better performance compared to LR. Similar findings were reported by Wang et al. (2020), where RF also outperformed other commonly used methods such as Frequency Ratio, Logistic Model Tree (LMT), and Classification and Regression Tree (CART) in landslide susceptibility mapping. This addition ensures consistency and provides a broader perspective on the applicability of RF in comparison with other methods.

6 Conclusion

This study demonstrates that the random forest (RF) model outperforms logistic regression (LR) in landslide susceptibility mapping by effectively capturing complex interactions among environmental factors. Slope gradient, flow accumulation (FA), vegetation density (normalized difference vegetation index, NDVI), and topographic wetness index (TWI) emerged as dominant drivers of landslide risk. Slope, with the highest merit value (RF) and elevated odds ratio (LR), underscores the vulnerability of moderate slopes (10–20°) to pore-pressure dynamics during heavy rainfall. The FA and NDVI further highlight the roles of concentrated water flow and vegetation deficits in slope destabilization, while TWI reveals that both extreme soil saturation and aridity threaten stability.

To address these risks, three integrated mitigation strategies are proposed for slope stabilization and soil management, including the implementation of terracing on moderate slopes, the planting of deep-rooted vegetation in low-NDVI areas, and the installation of geosynthetic-reinforced walls. Hydrological control measures are also recommended through the optimization of the drainage system by maintaining natural waterways to prevent blockages and overflows during rainfall events. In addition, vegetation restoration in low-NDVI areas and aspect-specific land-use zoning is proposed to restrict inappropriate development in landslide-prone areas.

Future research should focus on the application of advanced deep learning algorithms and high-resolution GIS-based modeling to better predict nonlinear interactions among environmental factors such as NDVI-aspect feedbacks and improve adaptation to climate-induced rainfall variability. Integrating socioeconomic factors including land-use practices, into predictive models could further enhance their applicability and decision-making value.

ACKNOWLEDGEMENTS: We would like to extend our sincere thanks to the Directorate General of Higher Education, Ministry of Education, Culture, Research, and Technology of the Republic of Indonesia, for providing financial support for this research through the DRTPM grant in 2024. We also express our gratitude to the Institute for Research and Community Service, University of Jember, and the Water Resource Management and Engineering Laboratory for their assistance and resources in facilitating this study.

RESEARCH DATA: For information on the availability of research data related to the study, please visit the article webpage: https://doi.org/10.3986/AGS.14449.

7 References

Abdulwahid, W. M., Pradhan, B. 2017: Landslide vulnerability and risk assessment for multi-hazard scenarios using airborne laser scanning data (LiDAR). *Landslides* 14-3. https://doi.org/10.1007/s10346-016-0744-0

Acharya, T. D., Lee, D. H. 2019: Landslide susceptibility mapping using relative frequency and predictor rate along Araniko highway. *KSCE Journal of Civil Engineering* 23-2. https://doi.org/10.1007/s12205-018-0156-x

Achour, Y., Pourghasemi, H. R. 2020: How do machine learning techniques help in increasing accuracy of landslide susceptibility maps?. *Geoscience Frontiers* 11-3. https://doi.org/10.1016/j.gsf.2019.10.001

Akturk, E., Guney, K., Aydin, M., Yildiz, F., Kaya, O. 2024: Land cover dynamics and environmental implications in Türkiye's riparian zones: A comprehensive seven-year study. *Forest* 15-7. https://doi.org/10.3390/f15071177

Alcántara-Ayala, I. 2025: Landslides in a changing world. *Landslides* 2022. https://doi.org/10.1007/s10346-024-02451-1

Beven, K. J., Kirkby, M. J. 1979: A physically based, variable contributing area model of basin hydrology / Un modèle à base physique de zone d'appel variable de l'hydrologie du bassin versant. *Hydrological Sciences Bulletin* 24-1. https://doi.org/10.1080/02626667909491834

Bishop, J. L., Yeşilbaş, M., Hinman, N. W., Burton, Z. F. M., Englert, P. A. J., Toner, J. D., McEwen, A. S. et al. 2021: Martian subsurface cryosalt expansion and collapse as trigger for landslides. *Science Advances* 7-6. https://doi.org/10.1126/sciadv.abe4459

Bravo-López, E., Del Castillo, T. F., Sellers, C., Delgado-García, J. 2023: Analysis of conditioning factors in Cuenca, Ecuador, for landslide susceptibility maps generation employing machine learning methods. *Land* 12-6. https://doi.org/10.3390/land12061135

Cellek, S. 2021: The effect of aspect on landslide and its relationship with other parameters. In: Landslides. IntechOpen. I. https://doi.org/10.5772/intechopen.99389

Dahim, M., Alqadhi, S., Mallick, J. 2023: Enhancing landslide management with hyper-tuned machine learning and deep learning models: Predicting susceptibility and analyzing sensitivity and uncertainty. *Frontiers in Ecology and Evolution* 11. https://doi.org/10.3389/fevo.2023.1108924

Dehnavi, A., Aghdam, I. N., Pradhan, B., Varzandeh, M., Morshed, H. 2015: A new hybrid model using step-wise weight assessment ratio analysis (SWARA) technique and adaptive neuro-fuzzy inference system (ANFIS) for regional landslide hazard assessment in Iran. *Catena* 135. https://doi.org/10.1016/j.catena.2015.07.020

Fan, H., Lu, Y., Shao, S., Li, L., Wang, Y., Lu, M., Li, J. et al. 2023: Evaluation and analysis of statistical and coupling models for highway landslide susceptibility. *Geomatics, Natural Hazards and Risk* 14-1. https://doi.org/10.1080/19475705.2023.2167612

Feng, L., Guo, M., Wang, W., Chen, Y., Shi, Q., Guo, W., Lou, Y. et al. 2022: Comparative analysis of machine learning methods and a physical model for shallow landslide risk modeling. *Sustainability* 15-6. https://doi.org/10.3390/su15010006

Getachew, N., Meten, M. 2021: Weights of evidence modeling for landslide susceptibility mapping of Kabi-Gebro locality, Gundomeskel area, Central Ethiopia. *Geoenvironmental Disasters* 8-1. https://doi.org/10.1186/s40677-021-00177-z

Ghasemian, B., Shahabi, H., Shirzadi, A., Al-Ansari, N., Jaafari, A., Kress, V., Renoud, S. et al. 2022: A robust deep-learning model for landslide susceptibility mapping: A case study of Kurdistan Province, Iran. *Sensors* 22. https://doi.org/10.3390/s22041573

Gullà, G., Conforti, M., Borrelli, L. 2021: A refinement analysis of the shallow landslides susceptibility at regional scale supported by GIS-aided geo-database. *Geomatics, Natural Hazards and Risk* 12-1. https://doi.org/10.1080/19475705.2021.1967204

Guo, Y., Ma, C. 2023: Elucidating the role of soil hydraulic properties on aspect-dependent landslide initiation. *Hydrology and Earth System Sciences* 27-8. https://doi.org/10.5194/hess-27-1667-2023

Gu, R., Ding, H., Yu, H., Wang, Q., Kong, L., Fan, J. 2026: Incorporating spatial heterogeneity into landslide susceptibility assessment: a GWRF–SHAP new method. *International Journal of Digital Earth* 19-1. https://doi.org/10.1080/17538947.2026.2639808

Huang, F., Teng, Z., Guo, Z., Catani, F., Huang, J. 2023: Uncertainties of landslide susceptibility prediction: Influences of different spatial resolutions, machine learning models, and proportions of training and testing dataset. *Rock Mechanics Bulletin* 2-1. https://doi.org/10.1016/j.rockmb.2023.100028

Huang, W., Ding, M., Li, Z., Yu, J., Ge, D., Liu, Q., Yang, J. 2023: Landslide susceptibility mapping and dynamic response along the Sichuan-Tibet transportation corridor using deep learning algorithms. *Catena* 222. https://doi.org/10.1016/j.catena.2022.106866

Hussain, M. A., Chen, Z., Shah, S. U., Shoaib, M., Ali, N., Ma, C. 2022: Landslide susceptibility mapping using machine learning. *Civil Engineering Journal* 8-2. https://doi.org/10.28991/CEJ-2022-08-02-02

Kohno, M., Higuchi, Y. 2023: Landslide susceptibility assessment in the Japanese Archipelago based on a landslide distribution map. *ISPRS International Journal of Geo-Information* 12-2. https://doi.org/10.3390/ijgi12020037

Le, X. H., Choi, C., Eu, S., Yeon, M., Lee, G. 2024: Quantitative evaluation of uncertainty and interpretability in machine learning-based landslide susceptibility mapping through feature selection and explainable AI. *Frontiers in Environmental Science* 12. https://doi.org/10.3389/fenvs.2024.1424988

Liu, R., Yang, X., Xu, C., Wei, L., Zeng, X. 2022: Comparative study of convolutional neural network and conventional machine learning methods for landslide susceptibility mapping. *Remote Sensing* 14-2. https://doi.org/10.3390/rs14020321

Liu, S., Yin, K., Zhou, C., Gui, L., Liang, X., Lin, W., Zhao, B. 2021: Susceptibility assessment for landslide initiated along power transmission lines. *Remote Sensing* 13-24. https://doi.org/10.3390/rs13245068

Liu, Y., Deng, Z., Wang, X. 2021: The effects of rainfall, soil type and slope on the processes and mechanisms of rainfall-induced shallow landslides. *Applied Sciences* 11-24. https://doi.org/10.3390/app112411652

Liu, Y., Zhao, L., Bao, A., Li, J., Yan, X. 2022: Chinese high resolution satellite data and GIS-based assessment of landslide susceptibility along highway G30 in Guozigou valley using logistic regression and MaxEnt model. *Remote Sensing* 14-15. https://doi.org/10.3390/rs14153620

Munawar, H. S., Hammad, A. W. A., Waller, S. T. 2022: Remote sensing methods for flood prediction: A review. *Sensors* 22-3. https://doi.org/10.3390/s22030960

Ni, J. J., Leung, A. K., Ng, C. W. W., Shao, W. 2018: Modelling hydro-mechanical reinforcements of plants to slope stability. *Computers and Geotechnics* 95. https://doi.org/10.1016/j.compgeo.2017.09.001

Okoli, J., Nahazanan, H., Nahas, F., Kalantar, B., Shafri, H. Z. M., Khuzaimah, Z. 2023: High-resolution Lidar-derived DEM for landslide susceptibility assessment using AHP and fuzzy logic in Serdang, Malaysia. *Geosciences* 13-2. https://doi.org/10.3390/geosciences13020034

Petrella, E., Raimondo, M., Chelli, A., Valentino, R., Severini, E., Diena, M., Celico, F. 2023: Processes and factors controlling the groundwater flow in a complex landslide: A case study in the northern Italy. *Hydrological Processes* 37-5. https://doi.org/10.1002/hyp.14891

Prancevic, J. P., Lamb, M. P., McArdell, B. W., Rickli, C., Kirchner, J. W. 2020: Decreasing landslide erosion on steeper slopes in soil-mantled landscapes. *Geophysical Research Letters* 47-10. https://doi.org/10.1029/2020GL087505

Rong, G., Li, K., Tong, Z., Liu, X., Zhang, J., Zhang, Y., Li, T. 2023: Population amount risk assessment of extreme precipitation-induced landslides based on integrated machine learning model and scenario simulation. *Geoscience Frontiers* 14-3. https://doi.org/10.1016/j.gsf.2023.101541

Rosly, M. H., Musa, H., Mohamad, B., Bolong, N. 2023: Relationship of rainfall intensity with slope stability. *Civil Engineering Journal* 9. https://doi.org/10.28991/CEJ-SP2023-09-06

Saha, S., Bera, B., Kumar, P., Sengupta, D., Bhattacharjee, S., Sengupta, N., Majumdar, P. et al. 2023: Geosystems and geoenvironment modelling and predicting of landslide in Western Arunachal Himalaya, India. *Geosystems and Geoenvironment* 2-2. https://doi.org/10.1016/j.geogeo.2022.100158

Park, S., Hamm, S. Y., Kim, J. 2019: Performance evaluation of the GIS-based data-mining techniques decision tree, random forest, and rotation forest for landslide susceptibility modeling. *Sustainability* 11-20. https://doi.org/10.3390/su11205659

Saha, S., Gayen, A., Bayen, B. 2022: Deep learning algorithms to develop flood susceptibility map in data-scarce and ungauged river basin in India. *Stochastic Environmental Research and Risk Assessment* 36. https://doi.org/10.1007/s00477-022-02195-1

Sarah, D., Zulfahmi, Z., Hilmi, M., Putra, Z., Madiutomo, N., Gunawan, G., Sumaryadi, S. et al. 2024: Back analysis of rainfall-induced landslide in Cimanggung District of Sumedang Regency in West Java using deterministic and probabilistic analyses. Geosciences 14-12. https://doi.org/10.3390/geosciences14120347

Sarkar, S. K., Ansar, S. Bin, Ekram, K. M. M., Khan, M. H., Talukdar, S., Naikoo, M. W., Islam, A. R. T. et al. 2022: Developing robust flood susceptibility model with small numbers of parameters in highly fertile regions of Northwest Bangladesh for sustainable flood and agriculture management. *Sustainability*14-7. https://doi.org/10.3390/su14073982

Sun, Q., Zhao, L., Qin, Y., Liu, B. 2023: Experimental study on the failure of loose accumulation landslides under rainfall conditions. *Frontiers in Earth Science* 11. https://doi.org/10.3389/feart.2023.1291592

Teng, F., Mao, Y., Li, Y., Qian, S., Nanehkaran, Y. A. 2024: Comparative models of support-vector machine, multilayer perceptron, and decision tree prediction approaches for landslide susceptibility analysis. *Open Geosciences* 16-1. https://doi.org/10.1515/geo-2022-0642

Wang, Y., Sun, D., Wen, H., Zhang, H., Zhang, F. 2020: Comparison of random forest model and frequency ratio model for landslide susceptibility mapping (LSM) in Yunyang county (Chongqing, China). *International Journal of Environmental Research and Public Health* 17-12. https://doi.org/10.3390/ijerph17124206

Guidelines for contributing authors in Acta geographica Slovenica

EDITORIAL POLICIES

1 Focus and scope

The *Acta geographica Slovenica* journal is issued by the ZRC SAZU Anton Melik Geographical Institute, published by the ZRC SAZU Založba ZRC, and co-published by the Slovenian Academy of Sciences and Arts.

Acta geographica Slovenica publishes original research articles from all fields of geography and related disciplines and provides a forum for discussing new aspects of theory, methods, issues, and research findings, especially in Central, Eastern, and Southeastern Europe.

Articles presenting new developments and innovative methods in geography are welcome. Submissions should address current research gaps and explore state-of-the-art issues. Research based on case studies should have the added value of transnational comparison and should be integrated into established or new theoretical and conceptual frameworks.

The target readership is researchers, policymakers, students, and others who are studying or applying geography.

The journal is indexed in the following bibliographic databases: Clarivate Web of Science (SCIE – Science Citation Index Expanded; JCR – Journal Citation Report/Science Edition), Scopus, ERIH PLUS, Directory of Open Access Journals (DOAJ), GEOBASE Journals, Current Geographical Publications, EBSCOhost, Georef, FRANCIS, SJR (SCImago Journal & Country Rank), OCLC WorldCat, Google Scholar, and CrossRef.

2 Types of articles

Unsolicited or invited original research articles and review articles are accepted. Articles and materials or sections of them should not have been previously published or be under consideration for publication elsewhere. The articles should cover subjects of current interest within the journal's scope.

3 Special issues

The journal also publishes special issues (thematic supplements). Special issues usually consist of invited articles and present a special topic, with an introduction by the (guest) editors. The introduction briefly presents the topic, summarizes the articles, and provides important implications.

4 Peer-review process

All articles are examined by the editor-in-chief. This includes fact-checking the content, spelling and grammar, writing style, appropriateness of AI use (eventual AI use must be clearly presented in methods), and figures. Articles that appear to be plagiarized, are badly or ghost-written, have been published elsewhere, are outside the scope of the journal, are written with ethical misuse of AI, or are of little interest to the readers of *Acta geographica Slovenica* may be rejected. If the article exceeds the maximum length, the author(s) must shorten it before the article is reviewed. The article is then sent to responsible editors, who check the relevance, significance, originality, clarity, and quality of the article. If accepted for consideration, the articles are sent to two or more peer reviewer(s) for double-blind review. Articles are rejected or accepted based on the peer reviews and the editorial board's decision.

5 Publication frequency

Acta geographica Slovenica is published three times a year.

6 Open-access policy

This journal provides immediate open access to the full-text of articles at no cost on the principle of open science, which makes research freely available to the public. There is no article processing fee (Article Processing Charge) charged to authors.

Digital copies of the journal are stored by the repository of ZRC SAZU and the digital department of the Slovenian national library NUK, dLib.

The journal's publication ethics and publication malpractice statement is available online, as well as information on subscriptions and prices for print copies.

AUTHOR GUIDELINES

Before submitting an article, please read the details on the journal's focus and scope, publication frequency, privacy statement, history, peer-review process, open-access policy, duties of participants, and publication ethics. See also the latest version of the author guidelines online. All the materials are available at https://ags.zrc-sazu.si.

1 Article structure

Research articles must be prepared using the journal's template (available at https://ags.zrc-sazu.si) and contain the following elements:

- **Title:** this should be clear, short, and simple.
- **Information about author(s):** submit names (without academic titles), affiliations, ORCiDs, and e-mail addresses through the online submission system (available at https://ags.zrc-sazu.si).
- **Highlights**: authors must provide 3–5 highlights in the form of bullets. This section must not exceed 400 characters, including spaces.
- **Abstract:** introduce the topic clearly so that readers can relate it to other work by presenting the background, why the topic was selected, how it was studied, and what was discovered. It should contain one or two sentences about each section (introduction, methods, results, discussion, and conclusions). The maximum length is 800 characters including spaces.
- **Keywords:** include up to seven informative keywords. Start with the research field and end with the place and country.
- **Main text:** the main text must not exceed 30,000 characters, including spaces (without the title, affiliation, abstract, keywords, highlights, reference list, and tables). Do not use footnotes or endnotes. Divide the article into sections with short, clear titles marked with numbers without final dots: **1 Section title**. Use only one level of subsections: **1.1 Subsection title**.

Research articles should have the following structure:

- **Introduction:** present the background of the research problem (trends and new perspectives), state of the art (current international discussion in the field), research gap, motivation, aim, and research questions.
- **Methods:** describe the study area, equipment, tools, models, programs, data collection, and analysis, define the variables, and justify the methods.
- **Results:** follow the research questions as presented in the introduction and briefly present the results.
- **Discussion:** interpret the results, generalize from them, and present related broader principles and relationships between the study and previous research. Critically assess the methods and their limitations, and discuss important implications of the results. Clarify unexpected results or lacking correlations.
- **Conclusion:** present the main implications of the findings, your interpretations, and unresolved questions, offering a short take-home message.

Review articles (narratives, best-practice examples, systematic approaches, etc.) should have the following structure:

- **Introduction:** include 1) the background; 2) the problem: trends, new perspectives, gaps, and conflicts; and 3) the motivation/justification.

- **Material and methods:** provide information, such as data sources (e.g., bibliographic databases), search terms and search strategies, selection criteria (inclusion/exclusion of studies), the number of studies screened and included, and the statistical methods of meta-analysis.
- **Literature review:** use subheadings to indicate the content of the various subsections. Possible structure: methodological approaches, models or theories, the extent of support for a given thesis, studies that agree with one another versus studies that disagree, chronological order, and geographical location.
- **Conclusions:** provide the implications of the findings and your interpretations (separate from facts), identify unresolved questions, summarize, and draw conclusions.

– **Acknowledgments:** use when relevant. In this section, authors can specify the contribution of each author.
– **Reference list:** see the guidelines below.

The journal also features in-depth articles known as ***Geoscapes***. These are a specialized type of research contribution that explore selected topics in greater detail. *Geoscapes* articles are published by invitation only and must be pre-approved by the editorial board.

2 Article submission

2.1 Open journal system

Author(s) must submit their contributions through the *Acta geographica Slovenica* Open Journal System (OJS; available at https://ags.zrc.sazu.si) using the Word document template (available at https://ags.zrc.sazu.si).

Enter all necessary information into the OJS. Any later addition, deletion, or rearrangement of names and affiliations of the author(s) in the authorship list should be made and confirmed by all co-authors before the manuscript has been accepted, and is only possible if approved by the journal editor.

To make anonymous peer review possible, the article text and figures should not include names of the author(s).

Do not use contractions or excessive abbreviations. Use plain text, with sparing use of **bold** and *italics* (e.g., for non-English words). Do not use auto-formatting, such as section or list numbering and bullets.

If a text is unsatisfactory, the editorial board may return it to the author(s) for proofreading or reject the article. See the section on the peer-review process (available at https//ags.zrc-sazu.si) for details. Author(s) may suggest reviewers when submitting an article.

2.2 Language

Articles are published in English. All articles have English and Slovenian abstracts.

Articles can be submitted in English or Slovenian.

Authors must take care to produce a high-quality English text. In the case of poor language, the article must be proofread/translated. In such a case, the translation or copyediting costs are borne by the author(s) and must be paid before layout editing. If authors are not Slovene native speakers, Slovenian abstracts are prepared by the editorial board.

2.3 Graphic file submission

Graphic files (figures) need to be submitted to the OJS packed in a single zip file not exceeding 50 MB. Multiple zip files can be uploaded if needed. See chapter 6 for details on how to prepare figures.

3 In-text citation

In-text citations should include the last name of the author(s) or the name of the publisher and the year of publication. Arrange citations by year of publication; for example: (Melik 1955; Melik et al. 1963; Gams 1982a; Gams 1982b; United Nations 1987; Royal Australian … 1988; Ford and Williams 2007). For references with more than two authors, cite only the first, followed by et al.: (Melik et al. 1956). Give page numbers only for direct quotations, for example: Perko (2016, p. 25) states: »Hotspots are …« For indirect citations, use this format: (Gunn 2002, cited in Matei et al. 2014).

When presenting publicly archived data, such as statistical and spatial data, describe the name of the dataset, the time frame, and the data provider in the main text, for example: »The 2000–2020 population data used in the analysis were provided by Eurostat« If the statistical data were published as a report, cite the document, for example: (European Commission … 2023).

When citing legal sources such as legislative acts, white papers, etc., provide the short formal title and the year, for example: »The European Commission's White paper on transport published in 2011 sets out ten strategic goals for a competitive and resource-efficient transport system.«

4 References

All references in the reference list must be cited in the text. Arrange references alphabetically and then chronologically if necessary. Identify more than one reference by the same author(s) in the same year with the letters a, b, c, etc., added to the year of publication: (1999a, 1999b). In case there are more than seven authors, list the first seven followed by et al.

Examples of references are given below. The use of »gray literature« is strongly discouraged.

Authors can use the Zotero and Endnote AGS Style templates, which are available in the Article submission section on the https://ags.zrc-sazu.si.

4.1 Articles

Last Name1, A. B., Last Name, C. D. Year: Title. *Journal Name* Volume-Issue. https://doi.org/…

- Breg Valjavec, M., Janža, M., Smrekar, A. 2018: Environmental risk resulting from historical land degradation in alluvial plains considered for dam planning. *Land Degradation & Development* 29-11. https://doi.org/10.1002/ldr.3168
- Kladnik, D., Kruse, A., Komac, B. 2017a: Terraced landscapes: An increasingly prominent cultural landscape type. *Acta geographica Slovenica* 57-2. https://doi.org/10.3986/AGS.4770
- Kladnik, D., Šmid Hribar, M., Geršič, M. 2017b: Terraced landscapes as protected cultural heritage sites. *Acta geographica Slovenica* 57-2. https://doi.org/10.3986/AGS.4628
- Ni, J., Jin, J., Wang, Y., Li, B., Wu, Q., Chen, Y., Du, S. et al. 2024: Surface ozone in global cities: A synthesis of basic features, exposure risk, and leading meteorological driving factors. *Geography and Sustainability* 5-1. https://doi.org/10.1016/j.geosus.2023.09.008
- Unangst, M. 2023: (De)Colonial historical geography and historical GIS. *Journal of Historical Geography* 79. https://doi.org/10.1016/j.jhg.2022.12.003
- Van de Kerk, G., Manuel, A. R. 2008: A comprehensive index for a sustainable society: The SSI – The Sustainable Society Index. *Ecological Economics* 66-2,3. https://doi.org/10.1016/j.ecolecon.2008.01.029
- Yang, D.-H., Goerge, R., Mullner, R. 2006: Comparing GIS-based methods of measuring spatial accessibility to health services. *Journal of Medical Systems* 30-1. https://doi.org/10.1007/s10916-006-7400-5

4.2 Books

Last Name1, A. B., Last Name2, C. D. Year: Book title. *Book Series Title* with Number. Publisher. https://doi.org/…

If the book is edited by editors, add '(eds.)' before the year of publication.

- Achino, K. F., Velušček, A. 2022: The lake-dwelling phenomenon. *E-Monographiae Instituti Archaeologici Sloveniae* 13. Založba ZRC. https://doi.org/10.3986/9789610506560
- Gams, I. 2004: Kras v Sloveniji v prostoru in času. Založba ZRC.
- Hall, T., Barrett, H. 2018: Urban geography. Routledge. https://doi.org/10.4324/9781315652597
- Knox, P., Marston, S. 2015: Human geography: Places and regions in global context. Pearson.
- Luc, M., Somorowska, U., Szmańda, J. B. (eds.) 2015: Landscape analysis and planning. *Springer Geography*. Springer. https://doi.org/10.1007/978-3-319-13527-4
- Marshall, T. 2016: Prisoners of geography: Ten maps that explain everything about the World. *Politics of Place*. Scribner.
- Mihelič Pulsipher, L., Pulsipher, A., Johansson, O. 2019: World regional geography: Global patterns, local lives. W. H. Freeman.

4.3 Chapters of books or proceedings

Last Name1, A. B., Last Name2, C. D. Year: Chapter title. In: Book Title. *Book Series Title* with Number. Publisher. https://doi.org/…

- Griffin, A. L. 2018: Cartography, visual perception and cognitive psychology. In: The Routledge Handbook of Mapping and Cartography. Routledge. https://doi.org/10.4324/9781315736822
- Solem, M., Boehm, R. 2015: A research coordination network for geography education. In: EUGEO Budapest 2015: Congress Programme and Abstracts. Hungarian Geographical Society.
- Stethem, C. 2013: Avalanches. In: Encyclopedia of Natural Hazards. Springer. https://doi.org/10.1007/978-1-4020-4399-4_7
- Zorn, M., Ferk, M., Lipar, M., Komac, B., Tičar, J., Hrvatin, M. 2020: Landforms of Slovenia. In: The Geography of Slovenia: Small But Diverse. *World Regional Geography Book Series*. Springer. https://doi.org/10.1007/978-3-030-14066-3_3

4.4 Reports, theses, dissertations, and other materials with authors

Last Name1, A. B., Last Name2, C. D. Year: Title. *Type of document*. Publisher. https://doi.org/…

- Davies, G. 2017: The place of data papers: Producing data for geography and the geography of data production. *Blog post*. Geo: Geography and Environment.
- Easterbrook, D. J. 1976: Geologic map of western Whatcom County, Washington (1-854-B). *1:62,500 map*. United States Geological Survey.
- Fležar, U., Hočevar, L., Sindičić, M., Gomerčić, T., Konec, M., Slijepčević, V., Bartol, M. et al. 2022: Surveillance of the reinforcement process of the Dinaric - SE Alpine lynx population in the lynx-monitoring year 2020–2021. *Technical report*. LIFE Lynx.
- Hawking, S. 1966: Properties of expanding universes. *Ph.D. thesis*. University of Cambridge. https://doi.org/10.17863/CAM.11283
- Hrvatin, M. 2016: Morfometrične značilnosti površja na različnih kamninah v Sloveniji. *Ph.D. thesis*. Univerza na Primorskem.
- Šifrer, M. 1997: Površje v Sloveniji. *Technical report*. Geografski inštitut Antona Melika ZRC SAZU.

4.5 Sources without authors

Use in-text citations (see Chapter 3). If sources need to be listed in the references use the following style: Publisher/Institution Year: Title. *Type of document*. https://doi.org/…

- Geodetska uprava Republike Slovenije 1998: Državna topografska karta Republike Slovenije 1 : 25.000 (Brežice). *1:25,000 map*.
- Royal Australian Survey Corps 1988: Australia 1:50 000 topographic survey (Tamborine, Queensland). *1:50,000 map*.
- United Nations 1987: Report of the World Commission on Environment and Development: Our common future. *Report*.
- European Space Agency 2022: Copernicus Sentinel-2 MSI Level-1C TOA Reflectance. *Dataset*. https://doi.org/10.5270/S2_-742ikth

5 Tables

Number all tables in the article uniformly and provide their own titles. The number and the title text are separated by a colon, and the title ends with a period. A table title is located above the corresponding table. Examples:

- Table 1: Number of inhabitants of Ljubljana.
- Table 2: Changes in average air temperature in Ljubljana (Velkavrh 2009).

Tables must be indicated in the main text in parentheses, for example: (Table 1), or as a part of the sentence, for example »… as can be seen in Table 1.« Tables should contain no formatting and must be inserted in the article file.

6 Figures

Figures encompass different graphic presentations used in the article: photography, graphs, illustrations, maps, etc.

Number all figures in the article uniformly and provide their own titles. The number and the title text are separated by a colon, and the title ends with a period. A figure title is located below the corresponding figure. Example:

- Figure 1: Location of measurement points along the glacier.

Figures must be indicated in the main text in parentheses, for example: (Figure 1), or as a part of the sentence, for example »… as can be seen in Figure 1.«

Figures should be exactly 134 mm wide (one page) or 64 mm wide (half page, one column), and up to 200 mm high.

Titles should appear in a caption only. Save colors in CMYK. Use Times New Roman font with a minimum size of 6.

Figures must be submitted as separate files. Multiple graphic files should be uploaded in one zip file. Figures should also be inserted in the main text file in order to ease the review process.

Regardless of the graphic/cartographic software used, save or export figures to the following formats:

- jpg or tiff file for regular photos (use a minimum of 300 dpi),
- xlsx file for graphs made with MS Office Excel,
- pdf or similar common files for maps and illustrations with vector drawings and/or text (embed the font if possible). See chapter 6.3 for details.

If the graphic files cannot be uploaded according to the guidelines, consult the editorial board (ags@zrc-sazu.si) in advance.

To make anonymous peer review possible, the authorship of figures can be added by authors at a later (copyediting) stage, after the review has been completed.

6.1 Photos

Photos must be in raster format with a resolution of at least 300 dpi, preferably in jpg or tiff format.

Figures containing a screenshot should be prepared at the highest possible screen resolution. A figure can be made using Print Screen, and the captured screen is pasted to the selected graphic program (e.g., Paint) and saved as a tiff or jpg file. The size of the image or its resolution must not be changed.

6.2 Graphs

Graphs should be made using MS Excel on separate sheets and accompanied by data.

6.3 Maps and illustrations

Maps should be informative and prepared according to the journal size limitations (see general guidelines defined in chapter 6). Use Times New Roman for the legend (size 8) and colophon (size 6). List scale, source, and copyright in the colophon. List the authors of the content and authors of the maps if needed. Write the colophon in English. Use a graphic scale if possible.

Example of the colophon structure:
Content by: Name Surname
Map by: Name Surname
Source: Institution Year
© Year, Copyright holder

Maps should be submitted in an editable form if possible so that minor errors can be corrected even in the final stages of article production. **The preferred submission file is pdf**. As an exception, maps can be produced in digital raster form with at least 300 dpi resolution, preferably in jpg or tiff format.

Please, pay attention when exporting maps from these software packages:

- if using QGIS, ESRI ArcGIS Pro or similar, maps should be exported as a pdf file,
- if using Gimp, Inkscape, CorelDraw, Adobe Illustrator or similar, two separate files should be prepared: the original software file (e.g. cdr if using CorelDraw) and a pdf file,
- if using ESRI ArcGIS Desktop (ArcMap) with raster layers and vector layers (e.g., a geotiff file for shaded relief and a shp file for roads), three files should be exported and submitted: a pdf or an ai file with all the vector content without transparency (polygons, lines, points, legend, colophon, labels, etc.), a tiff file with a raster background, and a jpg file with all of the content (vector and raster elements) together showing the final version of the map; see an example of the correct file structure (available at https://ojs.zrc-sazu.si/ags/libraryFiles/downloadPublic/14) for submitting a map created with ESRI ArcGIS Desktop.

Illustrations should be prepared according to the journal size limitations (see general guidelines defined in chapter 8). Use Times New Roman font size 8. **The preferred submission file is pdf**. As an exception, illustrations can be produced in digital raster form with at least 300 dpi resolution, preferably in jpg or tiff format.

7 Research data

Authors have to make the research data used in the article published in *Acta geographica Slovenica* publicly available in a recognized online repository and provide the editorial board with a link.

The publication of the data in the repository must indicate that the data are part of the published article. The article must be properly cited when using the data.

See detailed information on our research data management web page.

SUBMISSION PREPARATION CHECKLIST

As part of the submission process, authors are required to check off their submission's compliance with all of the following items, and submissions may be returned to authors who do not adhere to these guidelines.

- I, the corresponding author, declare that this manuscript is original and is therefore based on original research, done exclusively by the authors. All information and data used in the manuscript were prepared by the authors or the authors have properly acknowledged other sources of ideas, materials, methods, and results. The authors followed the ZRC SAZU guidelines for responsible use of AI.
- Authors confirm that they are the authors of the submitting article, which is under consideration to be published (print and online) in the journal *Acta geographica Slovenica* by Založba ZRC, ZRC SAZU.
- All authors have seen and approved the article being submitted.
- The submission has not been previously published, nor it is under consideration in another journal (or an explanation has been provided in Comments to the Editor). Authors have disclosed any prior posting, publication or distribution of all or part of the manuscript to the Editor.
- Upon publishing an article in the journal, the authors agree to license non-exclusive copyrights to ZRC SAZU (Založba ZRC): they retain the copyright in the scope that enables them to continue to use their work, even by publishing it in one of the personal or institutional repositories.
- Authors consent to the publication of their works under Creative Commons Attribution-ShareAlike 4.0 International (CC BY-SA 4.0).
- Permission has been obtained for the use (in printed and electronic format) of copyrighted material from other sources, including online sources. Restrictions on the transfer of copyright on this material have been clearly indicated.
- All the necessary permits to work with people have been obtained in the research related to the article (in accordance with the applicable laws and institutional guidelines and approved by the relevant institutions).
- The journal policies and guidelines have been reviewed and followed.
- The metadata (title, abstract, keywords, authors, affiliation, ORCiD, etc.) are provided in English (Slovenian authors must also provide the metadata in Slovenian).
- The list of authors is complete. Failure to do so may result in co-authors not being listed on the article at publication.
- The submission is in Microsoft Word format and the document template was used (single-spaced text, 10-point font, no formatting except italics and bold).
- The article has been checked for spelling and grammar.
- Figures are provided as separate graphic files: editable vector format (e.g., cdr, ai, pdf) for maps and illustrations; jpg or tiff for photographs; xlsx for graphs.
- Tables are placed in the Word file with text in the appropriate place.
- The reference list was prepared following the guidelines.
- All references in the reference list are cited in the text.
- Where available, URLs and DOI numbers for references are provided.
- Graphic files are in one zip file.
- Authors agree that any costs of English proofreading are borne by the author(s). No additional costs are associated with the submission.
- The instructions for ensuring a double-blind review have been followed.
- If the article is accepted, the authors will provide unique information (e.g., a DOI) about the online repository where the research data underlying the article is located. This information must be provided before the article is published. Metadata of the data in the repository must indicate that the data are part of the published article in the journal Acta geographica Slovenica. The article must be properly cited when using the data.

ACTA GEOGRAPHICA SLOVENICA EDITORIAL REVIEW FORM

This is the review form for editorial review (version 15) of an article submitted to the AGS journal.

This is an original scientific article.
(The article is original and the first presentation of research results with the focus on methods, theoretical aspects or a case study.)

- Yes
- No

The article follows the standard IMRAD/ILRAD scheme.

- Yes
- No

The article's content is suitable for reviewing in the AGS journal.
(The article is from the field of geography or related fields of interest, the presented topic is interesting for the readers of *Acta geographica Slovenica* and well presented. In case of a negative answer, add comments below.)

- Yes
- No

Editorial notes regarding the article's content.

The reference list is suitable (the author cites previously published articles with similar topics from other relevant geographic scientific journals).

- Yes, the author cited previously published articles on a similar topic.
- No, the author did not cite previously published articles on a similar topic.

Notes to the editor-in-chief regarding previously published scientific work.

Is the language of the article appropriate and understandable?

RECOMMENDATION OF THE EDITOR

- The article is accepted and can be sent to the review process.
- Reconsider after a major revision (see notes).
- The article is rejected.

ACTA GEOGRAPHICA SLOVENICA REVIEW FORM

This is the *Acta geographica Slovenica* review form (version 8).

1 RELEVANCE

Are the findings original and is the article therefore a significant one?

- yes
- no
- partly

Is the article suitable for the subject focus of the AGS journal?

- yes
- no

2 SIGNIFICANCE

Does the article discuss an important problem in geography or related fields?

- yes
- no
- partly

Does it bring relevant results for contemporary geography?

- yes
- no
- partly

What is the level of the novelty of the research presented in the article?

- high
- middle
- low

3 ORIGINALITY

Has the article already been published or is it too similar to already published work?

- yes
- no

Does the article discuss a new issue?

- yes
- no

Are the presented methods sound and adequate?

- yes
- no
- partly

Do the presented data support the conclusions?

- yes
- no
- partly

4 CLARITY

Is the article clear, logical, and understandable?

- yes
- no

If necessary, add comments and recommendations to improve the clarity of the title, abstract, keywords, introduction, methods or conclusion:

5 QUALITY

Is the article technically sound? (If not, the author should discuss with the Editorial Board [ags@zrc-sazu.si] for assistance.)

- yes
- no

Does the article take into account relevant current and past research on the topic?

- yes
- no

Propose amendments if no is selected:

Is the references list at the end of the article adequate?

- yes
- no

Propose amendments if no is selected:

Is the quoting in the text appropriate?

- yes
- no
- partly

Propose amendments if no is selected:
Which tables are not necessary?
Which figures are not necessary?

COMMENTS OF THE REVIEWER

Comments of the reviewer on the contents of the article:
Comments of the reviewer on the methods used in the article:

RECOMMENDATION OF THE REVIEWER TO THE EDITOR-IN-CHIEF

Please rate the article from 1 [low] to 100 [high] (this will NOT be presented to the author):
Personal notes of the reviewer to the editor-in-chief (this will NOT be presented to the authors):

Would you like to review the article again after corrections (in case the article needs them and is not declined)? The second review is expected to be done in 14 days.

- yes
- no

COPYRIGHT NOTICE

Authors that publish with this journal agree to the following terms:

- The authors confirm that they are the sole authors of the article submitted for publication (print and online) in the journal *Acta geographica Slovenica* of ZRC SAZU, Založba ZRC. The names of the authors will be evident in the article in the journal. All decisions regarding the layout and distribution of the article are in the hands of ZRC SAZU.
- The authors guarantee that the work is their own original creation and that it does not violate any legal or common-law copyright or property rights of third parties. In the case of any third-party claims, the authors agree to defend the interests of the publisher and to pay any costs.
- The copyright of the work published in this publication remains with the authors. The author licenses ZRC SAZU the right to publish, reproduce, and distribute the article in print and electronic form in various formats in the ZRC SAZU journal. The authors agree that, if the article is reused, ZRC SAZU obtains attribution to the original publisher, and the article shall be made available to the public under Creative Commons Attribution-ShareAlike 4.0 International (CC BY-SA 4.0). Users may access and use all journal archives and individual articles published therein under the terms of this license. This does not apply to third-party materials published in the articles.
- The same applies to some (older) articles, in which the indications »© authors and ZRC SAZU« or »© ZRC SAZU« are used: the authors are the sole copyright holders.
- Authors may enter into separate, additional contractual arrangements for the nonexclusive distribution of the version of their work that appears in the journal (e.g., place it in an institutional repository or publish it in a book), provided that they acknowledge that the initial publication was made in this journal.
- Authors may and are encouraged to post the final pdf version of their article online (e.g., in institutional repositories or on their websites) because this may lead to productive sharing and earlier and greater citation of the published work.
- Authors grant permission to the publisher to modify the article to comply with the publisher's guidelines. No honoraria are paid for articles in *Acta geographica Slovenica* or for reviews.

PRIVACY STATEMENT

By submitting their articles or other contributions the authors and reviewers consent to the collection and processing of their personal data (e.g., name, surname and email address) for the purposes of effective communication, editing, and publication of articles or other contributions.

The names and e-mail addresses provided to this journal site will be used exclusively for the stated purposes of this journal and will not be made available for any other purpose or to any other party.

PUBLISHER

Anton Melik Geographical Institute
Research Centre of the Slovenian Academy of Sciences and Arts
PO Box 306
SI–1001 Ljubljana
Slovenia

SOURCES OF SUPPORT

The journal is subsidized by the Slovenian Research and Innovation Agency (B6-7614) and is issued in the framework of the Geography of Slovenia long-term core research programme (P6-0101). The journal is also supported by the Slovenian Academy of Sciences and Arts.

JOURNAL HISTORY

Acta geographica Slovenica (print version: ISSN: 1581-6613, digital version: ISSN: 1581-8314) was founded in 1952. It was originally named *Geografski zbornik / Acta geographica* (print ISSN 0373-4498, digital ISSN: 1408-8711). Altogether, 42 volumes were published. In 2002 *Geographica Slovenica* (ISSN 0351-1731, founded in 1971, 35 volumes) was merged with the journal.

Since 2003 (from Volume 43 onward), the name of the joint journal has been *Acta geographica Slovenica*. The journal continues the numbering system of the journal *Geografski zbornik / Acta geographica*.

Until 1976, the journal was published periodically, then once a year, twice a year from 2003, and three times a year since 2019.

The online version of the journal has been available since 1995. In 2013, all volumes of the magazine were digitized from the beginning of its publication to including 1994.

All articles of the journal are available free of charge in digital form on the journal website http://ags.zrc-sazu.si**.**

Those interested in the history of the journal are invited to read the article »The History of *Acta geographica Slovenica*« in volume 50-1.

ISSN: 1581-6613
UDC – UDK: 91
ACTA GEOGRAPHICA SLOVENICA
GEOGRAFSKI ZBORNIK

66-1
2026

2026, ZRC SAZU, Geografski inštitut Antona Melika
Print/tisk: CICERO, Begunje, d. o. o.

Ljubljana 2026

ACTA GEOGRAPHICA SLOVENICA
GEOGRAFSKI ZBORNIK
66-1 • 2026

Contents

Hasan BASRI, Tuti MUTIA, Abdul RASYAD, Ahmad TOHRI, Hanapi HANAPI, Muhamad ALI
The impacts of tourism on shifting mountain climbing ritual tradition in geopark Rinjani, Indonesia 7

Rok TURNIŠKI, Helena GRČMAN
Soils of the Dinaric karst in Slovenia: properties, pedogenesis and land use 21

Klemen COF, Uroš STEPIŠNIK, Manja ŽEBRE, Matej LIPAR
Hierarchical cluster classification and analysis of cirques in Slovenian Alps 39

Danijel DAVIDOVIĆ, Jure ČUŠ, Danijel IVAJNŠIČ
Land-use dynamics and grassland succession challenges in the Natura 2000 site Kras: The socioeconomic perspective 61

Zoltán BÁTORI, Kata FREI, Gábor LI, Orsolya VALKÓ, András VOJTKÓ, Csaba TÖLGYESI, Tünde FARKAS, Alida Anna HÁBENCZYUS, Ágnes TÓTH, László ERDŐS, Zsófia KRIVÁCS, Balázs DEÁK
Karstic microrefugia reflect diverse biogeographic affinities of vascular plant species 81

Boudjemline FOUZIA
Mapping and assessing forest fire severity using remote sensing indices: A case study of Tizi Ouzou, Algeria 99

Peter FRANTAR, Frank HERRMANN, Mišo ANDJELOV
National-scale water balance in Slovenia (1972–2024): Long-term trends and variability in water balance components 121

Juš GAŠPARIČ, Ana POTOČNIK BUHVALD, Dušan PETROVIČ
Satellite-based analysis of light pollution in Slovenia for the period 2013–2022 147

Entin HIDAYAH, Mokhammad Farid MARUF, Siti Norafida JUSOH, Joko WIDODO, Afif AMILUDDIN
Machine learning-based landslide susceptibility assessment for shallow landslide mitigation in the Gumitir Mountain Area, Indonesia 179

ISSN 1581-6613